A mechanistic assessment of novel anticancer drugs targeting the metastatic cascade and tumour vascularisation

Dissertation

von

Katharina Mahal

UNIVERSITÄT
BAYREUTH

- Lehrstuhl für Organische Chemie -

Fakultät für Biologie, Chemie und Geowissenschaften

Universität Bayreuth

A mechanistic assessment of novel anticancer drugs targeting the metastatic cascade and tumour vascularisation

–

Mechanistische Studien neuartiger Krebstherapeutika mit antiinvasiver, antimetastatischer und antivaskulärer Wirkung

Dissertation

zur Erlangung des akademischen Grades

Doktor der Naturwissenschaften

(Dr. rer. nat.)

vorgelegt von

Katharina Mahal

Bayreuth 2015

Die vorliegende Arbeit wurde in der Zeit von November 2010 bis Juni 2014 in Bayreuth am Lehrstuhl für Organische Chemie I (OC I) unter der Betreuung von Prof. Dr. Rainer Schobert angefertigt.

Vollständiger Abdruck der von der Fakultät für Biologie, Chemie und Geowissenschaften der Universität Bayreuth genehmigten Dissertation zur Erlangung des akademischen Grades eines Doktors der Naturwissenschaften (Dr. rer. nat.).

Dissertation eingereicht am:	18.02.2015
Zulassung durch die Promotionskommission:	25.02.2015
Wissenschaftliches Kolloquium:	08.05.2015

Amtierender Dekan: Prof. Dr. Rhett Kempe

Prüfungsausschuss:

Prof. Dr. Rainer Schobert	(Erstgutachter)
Prof. Dr. Matthias Ocker	(Zweitgutachter)
Prof. Dr. Matthias Ullmann	(Vorsitz)
Prof. Dr. Klaus Ersfeld	

INHALTSVERZEICHNIS

Abkürzungsverzeichnis

ABC-Transporter	*ATP-binding cassette*-(Efflux-)Transporter
Akt	Proteinkinase B
Azixa	vgl. auch Verubulin
CA-4, CA-1-P, CA-4-P	Combretastatin A-4, Combretastatin A-1-Phosphat, Combretastatin A-4-Phosphat
Cdc42	*Cell division control protein 42 homolog*, Vertreter der kleinen GTPasen der Rho-Familie
DAPI	4',6-Diamidin-2-phenylindol (Fluoreszenzfarbstoff zur Zellkernfärbung)
E-Cadherin	*Epithelial Cadherin*, Vermittler von Zell-Zell-Adhäsionen (Cadherin-Catenin-Komplexe)
ECM	*Extracellular* matrix, Extrazelluläre Matrix
EGF / EGFR	*Epithelial growth factor-Receptor*
EMT	*Epithelial-to-Mesenchymal-Transition*
F-Aktin	filamentöses Aktin, Aktin-Filamente
FAK	*Focal adhesion kinase*
FGF	*Fibroblast growth factor*
Fosbretabulin	Markenname der Firma OxiGene für Combretastatin A-4-Phosphat
GTPasen	Proteinfamilie kleiner GTPasen, GTP-Hydrolasen
HDAC	Histondeacetylase
HDACi	Histondeacetylase-Inhibitor
HE-Färbung	Hämatoxylin-Eosin-Färbung (DNA- und Membran/Bindegewebe-Färbung)
HUVEC	*Human umbilical vein endothelial cells*
HIF-1alpha	*Hypoxia-inducible factor-1alpha*
IGF-1	*Insulin-like growth factor 1*
MDR	*Multidrug resistance,* Mehrfachresistenz gegen Wirkstoffe
MMP	Matrix-Metalloproteinase
MPC-6827	vgl. auch Verubulin
MRP1	*Multidrug resistance-related protein 1*
NSCLC	*Non-small cell lung cancer,* nicht-kleinzelliges Lungenkarzinom

Target	*hier*: Angriffsziel niedermolekularer Wirkstoffe
PDGF	*Platelet-derived growth factor*
PI3K	Phosphoinositid-3-Kinase
P-gp	P-Glycoprotein
Rac1	*Ras-related C3 botulinum toxin substrate 1*; Rho-Familie kleiner GTPasen
RhoA	*Ras homolog gene familiy, member A*; Rho-Familie kleiner GTPasen
Rho-GTPasen	vgl. GTPasen
ROCK	*Rho-associated coiled-coil-containing protein kinase*; Effektor von RhoA
RTK	Rezeptor-Tyrosinkinase
SAHA	*Suberoyl anilide hydroxamic acid*; HDAC-Inhibitor
TKi	Tyrosinkinase-Inhibitor
VDA	Vaskular-disruptives Agens (*Vascular-disruptive agent*), vermittelt die Zerstörung bestehender Blutgefäße
VE-Cadherin	*Vascular endothelial cadherin*; Extrazellulärer/ Transmembran-Vermittlung endothelialer Zell-Zell-Adhäsion
VEGF / VEGFR	V*ascular endothelial growth factor-Receptor*
Verubulin	Azixa, MPC-6827: Mikrotubuli-destabilisierendes *Quinazolin*-Derivat der Firma Myriad Pharmaceuticals (Myrexis).
Zybrestat	Markenname der Firma OxiGene für CA-4-P

Summary

Angiogenesis, the process of induced blood vessel sprouting and vascularisation are essential for the growth and progression of solid tumours. Recruitment of blood vessels is also an important step of the metastatic cascade that enables development of macrometastasis and growth to secondary tumours. Thus, intratumoral blood vessels represent an important target for anticancer drugs. The two classes of antivascular chemotherapeutics are vascular-disrupting agents (VDA) that target already established tumour blood vessels, and compounds with antiangiogenic acitivity that interfere with processes during the formation of new blood vessels.

Most vascular-disrupting agents bind to tubulin and mediate blood vessel destruction by secondary effects ensuing microtubule destabilisation. These include or are based on actin cytoskeleton reorganisation, cellular contractility and endothelial permeability. Eventually, the loss of the tightly-organised monolayer integrity of the endothelium results in blood vessel disruption and intratumoral haemorrhages.

The tubulin-binding agents discussed in this thesis are derived from the synthetic quinazoline derivate Verubulin or the natural drug Combretastatin A-4 (CA-4). Their preclinical evaluation includes the determination of their *in vitro* cytotoxicity profile against a panel of different tumour cells lines and various biochemical and immunological methods to clarify their molecular and cellular mechanism of action. Both antimetastatic and antivascular activity of the best derivatives were assessed *in vitro* by using endothelial or tumour cell-based assays or *in vivo* by analyses of developing blood vessels within in the chorioallantois membrane (CAM) of chicken embryos.

CA-4-derived oxazole and imidazole analogues that were synthesised and developed at the Chair of Organic Chemistry of the University of Bayreuth were able to overcome typical drawbacks of clinical CA-4 phosphate prodrugs including their short plasma half-life and metabolic instability as well as the induction of multidrug resistance (MDR)-mediating overexpression of efflux transporters. Unlike CA-4, imidazoles are chemically stable and do not undergo isomerisation into the inactive *trans*-configuration of the CA-4 stilbene motiv. Additionally, they are not recognised by MDR-transporters of cancer cell lines that are refractory to CA-4. In *in vitro* experiments, active derivatives led to extensive microtubule depolymerisation which we could correlate to their cytotoxicty and vascular-disrupting activity. The latter is a consequence of typical effects such as actin cytoskeleton remodelling

and defective cellular adhesion dynamics. In addition, these drug-induced cytoskeletal alterations are also the origin of decreased tumour cell motility and reduced invasive behaviour. One of the most promising derivatives which is designated with its short name Brimamin, was shown to mediate perturbation of nuclear NF-kappaB signalling. Interference with this resistance mediator has not been described for CA-4 and is different from the mode of action of other antiangiogenic agents.

A second generation of CA-4-derived imidazoles with acrylic hydroxamic acid appendages were shown to combine histone deacetylase (HDAC) inhibition with synergistic effects of the 4,5-diarylimidazole residue. Some of the derivatives proved a greater cytotoxicity against a panel of resistant cell lines and a higher specificity for cancer over non-malignant cells then the clinical approved HDAC inhibitor Vorinostat. The imidazoles also exceeded the antimetastatic *in vitro* acitivity and the antiangiogenic *in vivo* activity of Vorinostat. Like the latter, the best derivatives were shown to act as so called pan-HDAC inhibitors with unspecific inhibition of all Zn(II)-dependent HDAC isoenzymes, but a higer specificity for the tubulin deacetylase HDAC6. As a consequence, treatment with the best performing derivative with the short name Etacrox led not only to hyperacetylation of microtubules but also induced severe alterations in cytoskeletal and focal adhesion dynamics. An additional mode of action unique for the new imidazole-based HDAC inhibitors is the direct inhibition of matrix metalloproteinases (MMPs) which are known to promote angiogeneses and metastasis. The latter of pleiotropic effects together with HDAC inhibition-mediated perturbation of pro-angiogenic signalling cascades apparently mediates the strong antiangiogenic and antimetastatic effects. Altogether, the high tolerance of large doses in mice and their multitargeted anticancer effects make the 4,5-diarylimidazole HDAC inhibitors a promising class of new drug candidates for clinical applications.

Zusammenfassung

Die Ausbildung von intratumoralen Blutgefäßen und die Vaskularisierung solider Tumore ist ein essentieller Prozess für Tumorwachstum, Tumorprogression und Metastasierung und stellt somit ein wichtiges *Target* für Chemotherapeutika dar. Man unterscheidet dabei zwischen vaskular-disruptiven Wirkstoffen, die in der Lage sind, bereits bestehende Blutgefäße zu zerstören, und antiangiogenen Wirkstoffen, die in verschiedene Prozesse der Angiogenese, der Neubildung von Blutgefäßstrukturen, eingreifen können.

Im ersten Teil der vorliegenden Arbeit wurden Verbindungen aus der Klasse Tubulin-bindender Substanzen untersucht, die den größten Anteil an heute bekannten vaskular-disruptiven Agenzien (VDA) darstellen. Ihr primäres *Target* ist das Zytoskelett von Endothelzellen, die in Tumorumgebung aufgrund der kontinuierlichen Wachstumsfaktor-Stimulation oft fehlstrukturierte und entartete Blutgefäße bilden. Sie sind daher besonders anfällig für die zellulären Sekundäreffekte in Folge depolymerisierter Mikrotubuli. Diese beinhalten die erhöhte endotheliale Permeabilität und die vermehrte Kontraktilität einzelner Zellen innerhalb der hoch organisierten Endothelzellschicht und führen letztlich zum Verlust von Endothelintegrität und der Zerstörung der Blutgefäßstruktur.
Die präklinische Evaluation von Mikrotubuli-destabilisierenden Derivaten beschäftigte sich dabei zunächst mit der Bestimmung der *in vitro*-Toxizität der hier gezeigten Referenzsubstanzen und deren Analoga an kultivierten Krebszelllinien verschiedenster Entitäten sowie mit der zellbiologischen und biochemischen Untersuchung ihrer Wirkmechanismen und daran beteiligter Signaltransduktionswege. Das antimetastatische und antivaskuläre Potential ausgewählter Derivate wurde *in vitro* an verschiedenen Zelltypen und *in vivo* anhand des sich entwickelnden Blutgefäßsystems innerhalb der Chorioallantoismembran von Hühnerembryos untersucht (CAM-Assay).
Bei weiteren, hier gezeigten Mikrotubuli-destabilisierenden Substanzen handelt es sich neben einer Serie von bizyklischen Heteroaryl-Anloga von Verubulin, einem synthetischen Quinazolin-Derivat, ausschließlich um Oxazol- und Imidazol-Analoga des Naturstoffs Combretastatin A-4 (CA-4). Phosphat-*Prodrugs* von verschiedenen Combretastatinen sind aktuell in klinischen Studien oder bereits für klinische Anwendungen zugelassen, besitzen aber neben ihrer geringen Plasma-Halbwertszeit und Tendenz zu metabolischer Isomerisierung in inaktive Konformationen oft weitere Nachteile wie die Vermittlung von Multiresistenzen gegen verschiedene Zytostatika während der ersten Behandlungszyklen. Die

am Lehrstuhl für Organische Chemie I der Universität Bayreuth entwickelten, zum Teil halogenierten Oxazol- und Imidazol-Derivate umgehen diese Nachteile durch Stabilisierung der bioaktiven Konfiguration und strukturelle Veränderungen der CA-4-Leitstruktur, die eine Erkennung durch *Multidrug Resistance*-Effluxtransporter und somit die Detoxifizierung der Zelle verhindern. Die effektivsten Derivate vermitteln die Störung der Zytoskelett-Dynamik, im Einzelnen die vermehrte Mikrotubuli-Depolymerisation, die Induktion der Aktin-Zytoskelett-Stressantwort und die Beeinflussung der zellulären Fokaladhäsionsdynamik. Diese Effekte haben nicht nur vaskular-disruptive und antiangiogene Wirkung, sondern auch eine erheblichen Beeinträchtigung der Migrationfähigkeit von Tumorzellen zur Folge. Aktuelle *in vitro*-Studien mit einem der effektivsten Imidazol-Analoga (Brimamin) an Endothelzellen zeigten zudem eine für CA-4 bislang nicht beschriebene Inhibition des Resistenz-vermittelten NF-kappaB-Signalwegs. Diese Modulation von Resistenz-Regulatoren ist ein Mechanismus, in dem sich Brimamin deutlich von anderen antiangiogenen Substanzen unterscheidet und unterstreicht somit das enorme Potential dieser CA-4-abgeleiteten Wirkstoffklasse für die klinische Anwendung als Chemotherapeutika mit verbesserter antivaskulärer und antimetastatischer Wirkung.

Der zweite Teil dieser Arbeit beschäftigt sich mit der Charakterisierung von Substanzen, die eine Weiterentwicklung dieser ersten Generation von CA-4-abgeleiteten Imidazolen darstellt. Die Erweiterung des ursprünglichen CA-4-Phenolrings um Acrylhydroxamsäure-Reste führte zu einer neuen Klasse hoch effizienter 4,5-Diarylimidazol-baiserter Histondeacetylase-Inhibitoren (HDACi), die die Wirkung von bereits klinisch etablierten Hydroxamsäure-Analoga wie Vorinostat vor allem im Hinblick auf ihre antimetastatischen und antiangiogenen Aktivität übertrifft. Beide Substanzen vermitteln die unspezifische Inhibition von Histondeacetylase (HDAC)-Isoformen, während die effektivsten, hier gezeigten Derivate im Vergleich zu den typischen HDACs höhere Selektivität für die zytoplasmatische Tubulin-Deacetylase HDAC6 besitzten. Anders als viele Hydroxamsäure-HDACi sind die Imidazol-Derivate zudem in der Lage, pro-metastatische und pro-angiogene Matrix-Metalloproteinasen zu inhibieren. Die Induktion einer Vielzahl von zellulären Effekten wie der Fehlregulation von Zytoskelettdynamik, der Hemmung von proliferations- und differenzierungsrelevanten Signalkaskaden und der direkten Inhibition von Metastase-vermittelnden Proteinasen scheinen zu den vielversprechenden antimetastatischen und antiangiogenen Effekten dieser neuartigen Verbindungen beizutragen.

1 Einleitung

1.1 „The Hallmarks of Cancer“: Die Charakteristika maligner Krebserkrankungen

Die im Jahr 2000 erschienene Veröffentlichung mit dem Titel „*The Hallmarks of Cancer*“ ist einer der gegenwärtig meist-zitierten Artikel auf dem Gebiet der Krebsforschung.[1] Hier postulieren die Autoren *Hanahan* und *Weinberg* erstmals, dass die zellulären und biochemischen Eigenschaften maligner Krebserkrankungen auf sechs grundlegende Merkmale zu reduzieren sind. Diese setzen sich zusammen aus (1) konstitutiv-aktiver, pro-proliferativer Signaltransduktion, (2) geringer Sensitivität gegenüber natürlichen biologischen, wachstumshemmenden Stimuli (Wachstumssuppressoren), (3) Resistenzmechanismen gegen Apoptose-Induktion, (4) der Fähigkeit zu replikativer Immortaliät bzw. potentiell unendlicher, unkontrollierter Teilungsfähigkeit, (5) der Induktion von Blutgefäßneubildung (Angiogenese) sowie (6) dem Potential einzelner Tumorzellen, in umliegende Gewebe vorzudringen und dort Kolonien auszubilden (Tumorinvasion und Metastasierung).[1] Aufgrund neuer Kenntnisse der Komplexität genetischer, zellulärer und biologischer Vorgänge, die für die Tumor-Entstehung (Tumorigenese, Carcinogenese), das Wachstum von Tumoren sowie deren metastatische Verbreitung eine zentrale Rolle spielen, wurde dieses stark vereinfachte Konzept im Jahr 2011 um einige, inzwischen relevante Faktoren erweitert.[2] Auch die zentrale Rolle der direkten Tumorumgebung, der Interaktion mit als Tumor-*Microenvironment* bezeichneten Zellverbänden und Komponenten der extrazellulären Matrix, wurde hier weiter in den Vordergrund gestellt.[2] Eine Übersicht der genannten Faktoren ist in Abbildung 1 nach dem Vorbild der in *Cell* beschriebenen *Hallmarks of Cancer* dargestellt.[1,2] Trotz der Tatsache, dass Krebsentstehung und -wachstum einem weit komplexeren Zusammenspiel dieser und weiterer Einzelfaktoren folgen,[2,3] bildet das Konzept nach wie vor eine wichtige Grundlage für die aktuelle Krebs- und Wirkstoffforschung. Da Metastasierung bei 90% aller Krebspatienten die hauptsächliche Todesursache darstellt, rücken bei der Entwicklung neuer Wirkstoffe die Teilaspekte der Tumor-Angiogenese und Metastasierung immer mehr in den Fokus.

Im Folgenden sollen die Merkmale der Angiogenese-Stimulation, der tumoralen Ausbreitung durch Metastasierung und die damit in Zusammenhang stehende Interaktion von Tumorzellen mit der umgebenden, extrazellulären Matrix (*extracellular matrix,* ECM) sowie dafür relevante Signaltransduktionswege genauer betrachtet werden.

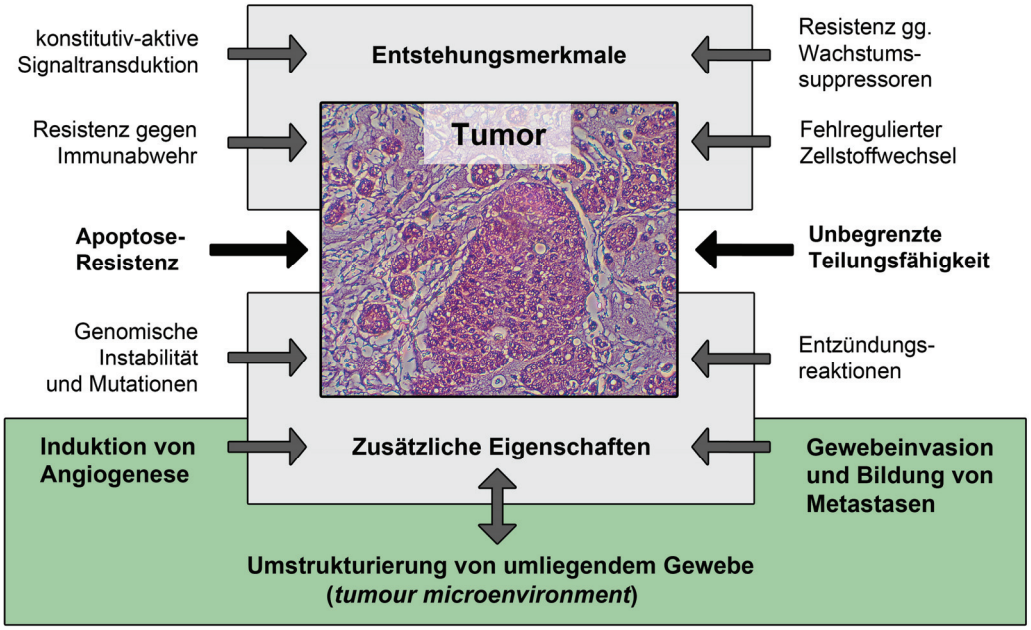

Abbildung 1 – Übersicht der wichtigsten Kennzeichen von Krebserkrankungen. Freie Interpretation und Darstellung des Konzepts der „*Hallmarks of Cancer – The Next Generation*“ nach *Hanahan* und *Weinberg* (*Cell* 2011).[2] Charakteristika von soliden Tumoren [(Tumor: HE-Färbung eines Gewebedünnschnitts eines HT-29-Kolonkarzinom-Mikro-Xenografts)] und Tumorentstehung sowie zusätzliche Faktoren, die zu Tumorwachstum und Tumorausbreitung führen: Angiogenese, Metastasierung und Umstrukturierung des umliegenden Gewebes.

1.2 Tumor-Angiogenese

Grundsätzlich spielt die Neubildung von Blutgefäßen eine wichtige Rolle während der Embryonalentwicklung und später bei Wundheilungsprozessen und gewährleistet die Versorgung des durchbluteten Gewebes mit Nährstoffen und Sauerstoff.[4,5] Die Ausbildung neuer Gefäßstrukturen wird induziert durch die Stimulation zirkulierender, endothelialer Vorläuferzellen oder durch Sprossungs- und Auswuchsprozesse bestehender Blutgefäße.[5–7] Letzteres setzt die Migration einzelner Endothelzellen von der die Blutgefäße auskleidenden, straff organisierten Endothelzell-Einzelschicht (Endothel) durch Wachstumsfaktor-Stimulation sowie die proteolytische Umstrukturierung der extrazellulären Matrix und die Lumenbildung durch diese Endothelzellverbände voraus.[5,6,8] Die Ausbildung neuer primärer Gefäßstrukturen wird durch die Verschiebung eines Wachstumsfaktor-Wachstumssuppressor-Gleichgewichts von anti-angiogenen hin zu pro-angiogenen Signalmolekülen induziert. Zu den pro-angiogenen Wachstumsfaktoren zählen VEGF (*vascular endothelial growth factor*),

FGF (*fibroblast growth factor*), PDGF (*platelet-derived growth factor*) und EGF (*epithelial growth factor*).[5,6,9,10] In erwachsenen Menschen findet Angiogenese fast ausschließlich in reproduktiven Organen und im Rahmen der Wundheilung statt, wobei neu gebildete Blutgefäße einem Reifungsprozess unterliegen, in dem primäre Endothelzell-Kanäle (Kapillaren) meist von einer stabilisierenden Schicht aus Perizyten und glatten Muskelzellen umhüllt werden (perivaskuläre Zellen, vaskuläre Gefäßwand).[5,6,9,11] Progressive, solide Tumore benötigen ab einer bestimmten Größe selbst die Versorgung durch Blutgefäße.[9,11,12] Abhängig von der Art des Tumors und seiner Mikroumgebung sind Tumorzellansammlungen in der Lage, durch Überproduktion und Sekretion enormer Mengen an pro-angiogenen Wachstumsfaktoren den so genannten *angiogenic switch* zu induzieren.[5,6,11] Dieser Vorgang dient der Rekrutierung umliegender Blutgefäße und führt neben dem Auswuchern bereits bestehender Blutgefäße in Richtung der Tumormasse letztlich zur Vaskularisierung des vorhandenen Tumorgewebes.[6,9,11] Aufgrund der ständigen Überproduktion von pro-angiogenen Wachstumsfaktoren und der damit verbundenen Entartung tumor-assoziierter Endothelzellen, unterscheiden sich Blutgefäße innerhalb des Tumors in ihrer Architektur jedoch stark von den physiologisch relevanten, regulär gebildeten.[6,11] Aus Endothelzellen mit abnormer Morphologie und Teilungsrate sowie fehlerhafter Zell-Zell-Adhäsion (*adherens junctions*) entstehen somit unregelmäßig-verzweigte und oft undichte Blutgefäßsysteme, für die ungleichmäßiger Blutfluss, Ausblutungen und das Fehlen der umgebenden Perizytenschicht charakteristisch sind.[2,6,11,13–15] Neuere Studien ergaben, dass solche Tumor-Endothelzellen innerhalb der Tumorumgebung dauerhaft umprogrammiert und diese Signaltransduktionsmodifikationen auch nach Explantation in *ex vivo*-Kultivierung beibehalten werden.[6,16–18] Die Heterogenität von Tumor-Endothelzellen beinhaltet vor allem hohe Expressionslevel der VEGF-Rezeptoren 1 und 2, des pro-angiogenen *hypoxia-inducible factor-1alpha* (HIF-1alpha) und von Migration-regulierenden Proteinen der RhoGTPase-Superfamilie. Diese gehören über den Phosphatidylinositol-3-Kinase (PI3K) -und Proteinkinase B (Akt)-Signalweg (PI3K/Akt-*Signalling*) zu den wichtigsten *downstream*-Effektoren der konstitutiv-aktiven VEGF-Stimulierung.[6,19]

Da die Ausbildung eines Tumor-Blutgefäßsystems für Tumorprogression und Metastasierung essentiell ist, stellen neben VEGF-VEGFR (*vascular endothelial growth factor receptor*)-*Signalling* die entarteten Tumor-Blutgefäße selbst einen wichtigen Angriffspunkt (*Target*) für antitumorale Wirkstoffe dar.[5,9]

1.3 Metastasierung

Bei der Bildung von Metastasen tragen sowohl Tumor- als auch nicht entartete Blut- und Lymphgefäße zur anatomischen Verbreitung und Verteilung (Tumor-Dissemination) von Krebszellen bei. Als zentrale Prozesse bei der Metastasierung können hierbei die Dissoziation einzelner Tumorzellen oder Tumorzellverbände vom Primärtumor und die Penetration (Invasion) des umliegenden Gewebes angesehen werden, gefolgt vom Eindringen dieser Tumorzellansammlungen in neu gebildete oder bereits bestehende Blutgefäße (*Intravasation*) und ihrem Transport mittels Blutstrom oder Lymphsystem sowie dem erneuten Durchdringen von Gefäßwänden (*Extravasation*) und dem Anwachsen von neuen Tumorkolonien nach erfolgreicher Anpassung an das Milieu des infiltrierten Gewebes (Abbildung 2).[10,20] An Entstehung und Wachstums eines sekundären Tumors aus diesen so genannten Mikro-Metastasen können wiederum Tumor-Angiogenese und proteolytischer ECM-Abbau beteiligt sein.[10,21]

Epithelial-to-Mesenchymal-Transition

Der Metastasierung eines malignen, soliden Primärtumors liegt meist ein Prozess zugrunde, der als *Epithelial-to-Mesenchymal-Transition* (EMT) bezeichnet wird.[10,20,22,23] Hierbei verlieren Epithelzellen einige ihrer epithelialen Merkmale und nehmen bezüglich ihrer Morphologie und Proteinexpression Eigenschaften an, die für Zellen mesenchymalen Ursprungs charakteristisch sind. Epithelgewebe stellt den häufigsten Ursprung solider Tumore dar und zeichnet sich durch seine apikal-basolaterale Polarität und die straffe Organisation von Epithelzell-Einzelschichten durch eine hohe Anzahl stabilisierender Zell-Zell-Adhäsionskomplexe aus.[10,22] Im Gegensatz dazu bilden mesenchymale Zellen nur wenig Zell-Zell-Kontakte aus, besitzen jedoch höhere Motilität und in Zellkultur eine oft spindel-förmige, Fibroblasten-ähnliche Morphologie, als Folge ihrer hohen Migrationsrate.[22] EMT-Charakteristika sind zunächst der Verlust der Epithelzell-typischen Polarität und das Ablösen transformierter, maligner Epithelzellen vom übrigen Epithel aufgrund des Verlusts intakter Zell-Zell-Adhäsionen (*adherens junctions*, vgl. auch Abbildung 2).

Diese werden in Epithelzellschichten hauptsächlich aus interzellulären E-Cadherin-beta-Catenin-Komplexen gebildet und über beta-Catenin mit dem Aktin-Zytoskelett verbunden.[24,25] Da die E-Cadherin-Expression im Verlauf des EMT fast vollständig verringert wird, wird beta-Catenin aus den Cadherin-Catenin-Komplexen freigesetzt und transloziert in den Zellkern, wo es als Transkriptionsfaktor andere Proliferations-relevante Signalwege

aktiviert.[10,23] Gleichzeitig wird die Expression typischer mesenchymaler Proteine wie N-Cadherin, Vimentin und verschiedener Zytokeratine induziert, die die Zellmotilität fördern und Interaktion mit der ECM ermöglichen.[22]

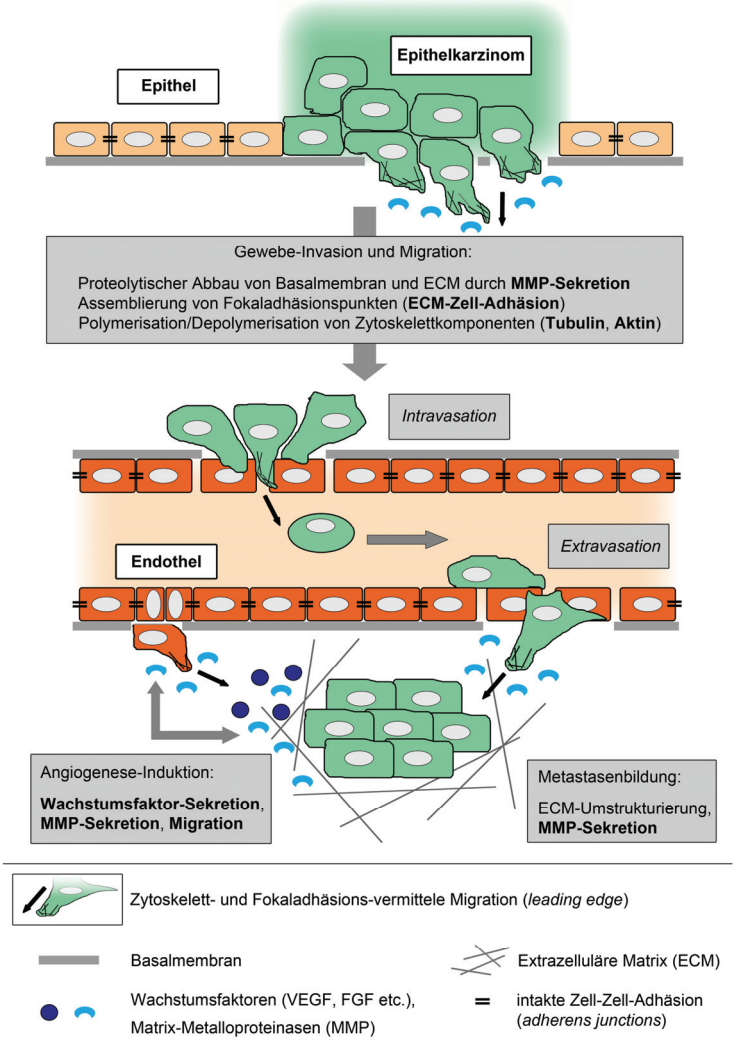

Abbildung 2 – Schematische Darstellung der Bildung von Metastasen am Beispiel eines Epithelkarzinoms und zentraler Vorgänge während der Metastasierung. Transformierte, maligne Epithelzellen infiltrieren umliegendes Gewebe (Gewebe-Invasion) und Blutgefäße (*Intravasation*) durch gerichtete Migration und Überwindung physiologischer Barrieren (Basalmembran, ECM, Endothel). Anheftung an die Gefäßwand und erneute Überwindung der Endothelschicht (*Extravasation*) führt zur Bildung von Mikro-Metastasen und deren Wachstum durch Umbau der ECM (MMP-Sekretion) bis hin zur Rekrutierung neuer Blutgefäße durch Wachstumsfaktor-Ausschüttung und Stimulierung von Endothelzell-Proliferation und -Migration (Tumor-Angiogenese). Migration wird dabei durch dynamische Zytoskelettkomponenten (Tubulin, Aktin) und Fokaladhäsionen (ECM-Zell-Adhäsion) vermittelt. [Eigene Darstellung nach *Bacac and Stamenkovic* 2008 (*Metastatic Cancer Cell*) und *Geiger and Peeper* 2011, (*Metastasis Mechanism*).[10,20]]

Erhöhte Expression und Sekretion von Matrix-Metalloproteinasen (MMPs) ist ein weiteres Charakteristikum des EMT. Diese gewährleisten während Migration und Wachstum von Mikro-Metastasen nicht nur den für die Lumenbildung benötigten Abbau von ECM-Komponenten wie Kollagen und Fibronectin, sondern auch die proteolytische Freisetzung von ECM-gebundenen Wachstums- und Pro-Angiogenesefaktoren (Abbildung 2).[10,21]

Induziert werden diese und weitere EMT-vermittelte, zelluläre Veränderungen durch zahlreiche, extrazelluläre Signalmoleküle der TGF-β (*Transforming Growth Factor*- β)-

Familie, NF-kappaB, FGF, EGF und die damit verbundene, konstitutive Aktivierung von Rezeptor-Tyrosinkinase (RTK)-Signaltransduktionswegen.[10]

Tumorzell-Invasion und Migration

Zur Metastasierung trägt letztlich vor allem die gerichtete Migration transformierter Tumorzellen bei, die sich dabei aktiv durch die ECM benachbarten Gewebes bis hin zu bereits bestehenden Blut- oder Lymphgefäßen bewegen (*Intravasation*, Abbildung 2). Tumorzellen können dabei einzeln oder als multizelluläre Tumorzellkolonien wandern.[26] Tumorzell-Migration und Migration von Zellen im Allgemeinen beinhaltet grundlegende mechanische und biochemische Prozesse, die zu einer polarisierten Ausdehnung der Zelle, der Bildung von Aktin-Zytoskelett- und Membran-Ausläufern in Migrationsrichtung, den so genannten Invapodien oder Lamellipodien (*Leading Edge, Membrane Protrusions*), und der Anheftung an die ECM mittels Fokaladhäsionen führt.[26] Der dynamische Auf- und Abbau dieser Fokaladhäsionen während Aktin-Myosin-vermittelter Kontraktion der Zelle ermöglicht letztlich das gerichtete Vorwärtsgleiten der Zelle durch die umgebende Extrazellulärmatrix aus einem dichten Netzwerk mit Gewebe-spezifischem Anteil an Kollagen-, Laminin und Fibronektin-Fasern und Proteoglykanen.

Tumorzell-Invasion und Migration: Die Rolle von Matrix-Metalloproteinasen

Hier spielt die Sekretion von Matrix-Metalloproteinasen eine wichtige Rolle, die am Leitsaum der Zelle konzentriert und sekretiert werden und die vorwärts-gerichtete Invasion ermöglichen.[21,26] Dabei schaffen die Matrix-Proteasen eine Art chemotaktische Umgebung durch Proteolyse von ECM-Fragmenten und Bildung spezifischer Integrin-Bindestellen. Die proteolytische Freisetzung pro-migratorischer Faktoren wie EGF oder IGF-1 (*Insulin-like growth factor-1*) aus der ECM treibt die Migration durch die intrazelluläre Aktivierung pro-migrativer Signalwege wie PI3K- und Rho-*Signalling* zusätzlich voran.[26] MMP-Expression und Sekretion ist nicht zuletzt aufgrund von EMT-induzierter Änderung des Expressionsprofils in vielen malignen Tumoren hochreguliert, insbesondere werden hier die Isoformen MMP-2 und MMP-9 als prognostischer Marker angesehen.[10,21,27]

Tumorzell-Invasion und Migration: Dynamik von Aktin-Filamenten und Fokaladhäsionen

Zellkontraktion und Bewegung entlang von Fokaladhäsionen werden hauptsächlich durch das Aktin-Zytoskelett vermittelt. Gerichtete Aktin-Polymerisation in Aktin-Filamente (F-Aktin)

und die Ausbildung des *Leading Edge* ist der erste essentielle Schritt der Zellmigration. Ein dynamisches Netzwerk aus kortikalem F-Aktin unterhalb der Plasmamembran ermöglicht dabei die mechanische Ausbuchtung und Streckung der Zelle. Dem zugrunde liegt ein kontinuierlicher Aktin-Polymerisationsprozess in Migrationsrichtung und die Bildung neuer Aktin-Zellmembran-Ankerpunkte. Erste Zell-Matrix-Verbindungen erfolgen durch Integrine, eine Proteinfamilie verschiedener Transmembran-Rezeptoren, deren extrazelluläre Domänen mit entsprechenden Bindestellen an ECM-Makromolekülen interagieren. Diese fokalen Komplexe rekrutieren im Laufe ihrer Reifung zur komplexen Fokaladhäsion weitere Adaptor- und Signalproteine wie Vinculin, Paxillin, PI3K und FAK (*Focal adhesion kinase*). Auch MMPs werden an die Fokaladhäsionspunkte dirigiert und sekretiert. Reguliert wird die Lamellipodium-gerichtete Aktin-Polymerisation und die Bildung neuer Fokalkomplexe hauptsächlich durch die Vertreter Rac1 und Cdc42 der Rho-Familie der kleinen GTPasen (*small GTPases*), was letztlich zur Bildung von Pseudopodien, den Vorstufen von Lamellipodien und Invapodien führt (Abbildung 3a).[26,28–30]

Aktinfilamente werden während der Fokaladhäsionsassemblierung kontinuierlich gebildet und liegen zusätzlich zum Aktin-Netzwerk im Lamellipodium als zytoplasmatische Aktin-*Stress fibres* vor. Dabei handelt es sich um dicke, parallele Fasern aus quervernetzten Aktin-Filamenten und Myosin-Motorproteinen, die Zytoplasma und Fokaladhäsionen miteinander verbinden.[15,26,30] Nach der Ausbildung stabiler Zell-Matrix-Verbindungen kommt es zum Zusammenziehen der Zelle über Actinomyosin-Kontraktion und Deassemblierung von Fokaladhäsionen im hinteren Teil der Zelle, beides vermittelt durch RhoA und Rho-Kinase (ROCK).[30] Die funktionierende, hoch-dynamische und regulierte Fluktuation von Aktin-Filamenten und Fokaladhäsionen ist somit entscheidend für die gerichtete Zellmigration (vgl. Abbildung 3a).

Aktuellen Studien zufolge ist die Aktin-Zytoskelett-vermittelte Ausbildung von Invapodien ein zentraler Schritt bei der *Extravasation*, dem Durchdringen der endothelialen Gefäßwand an endothelialen Zell-Zell-Adähsionen, das die Voraussetzung für die Bildung von Metastasen darstellt.[31] Bei vielen Krebsarten, z. B. malignem Melanom, sind zudem einige Mutationen bekannt, die die Zell-Motilität und Invapodia-Formation erhöhen. Dazu gehören unter anderem aktivierende Mutation von PI3K sowie die Überexpression der PI3K-Effektorkinase Akt oder Mutationen der Migration-regulierenden Rho-GTPase Rac1.[32–35]

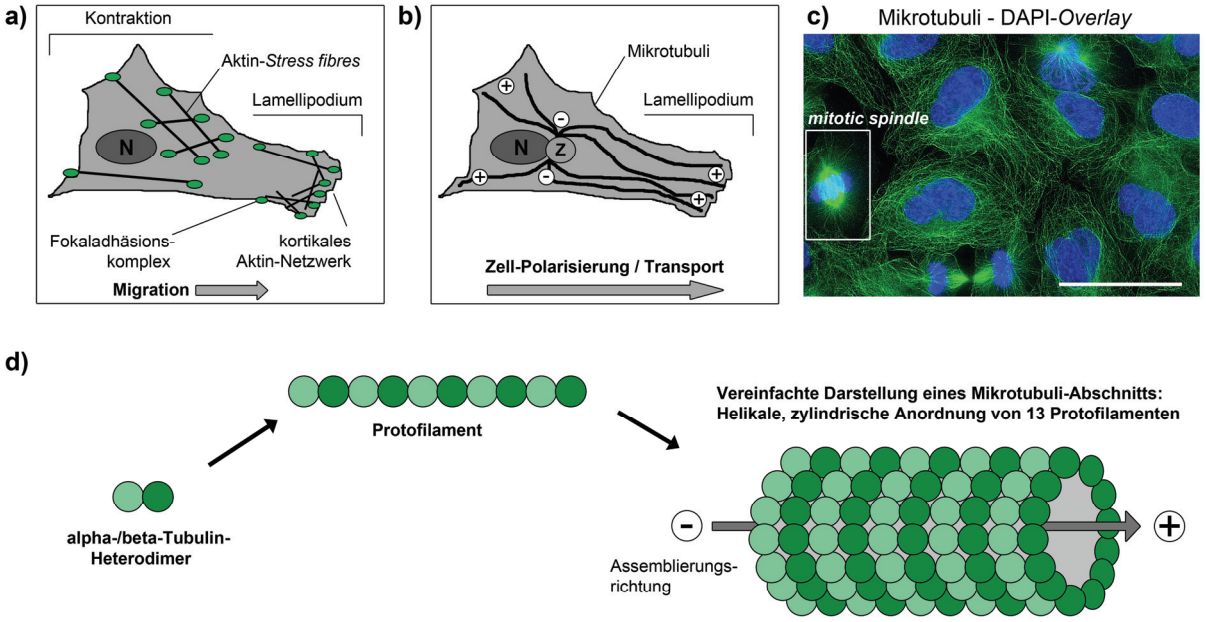

Abbildung 3 – Schematische Darstellung von Zytoskelett- und Zelladhäsions-Komponenten. **a)** Schematische Darstellung von Aktin-Filamenten und Fokaladhäsionen in migrierenden Zellen. Ein Netzwerk aus kortikalem Aktin vermittelt die Bildung von Lamellipodien/Invapodien, die Vorwärtsbewegung ermöglichen die Kontraktion der Zelle über Aktin-*Stress fibres* und die Dynamik von Fokaladhäsionskomplexen. **b)** Die Polymerisation (Minus-/Pluspol) der Mikrotubuli ausgehend vom Zentrosom (Z) und ihre Orientierung in Migrationsrichtung ermöglichen gerichteten Transport und Signaltransduktion. N = Nucleus. **c)** Typische Anordung von Mikrotubuli in konfluenten Interphase-Zellen und ihre Spindel-Funktion (*mitotic spindle*) bei der Chromosomensegregation während der Mitose. **d)** Schematischer Aufbau der Mikrotubuli aus alpha- und beta-Tubulin-Heterodimeren und Tubulin-Protofilamenten. [**a-b**: Eigene Darstellung nach *Etienne-Manneville* 2013 und *Akhshi et al.* 2014.[38,39] **d**: Eigene Darstellung nach *Akhmanova and Steinmetz* 2008.[37]]

Tumorzell-Invasion und Migration: Beitrag der Mikrotubuli

Neben Intermediärfilamenten und Aktin-Filamenten bilden die Mikrotubuli den Hauptbestandteil des Zytoskeletts und sind essentiell für die Erhaltung von Zellmorphologie- und Integrität.[36,37] In Interphase-Zellen werden Mikrotubuli ausgehend von *Microtubule organisation centres* (MTOCs) wie beispielsweise dem Zellkern-assoziierten Zentrosom aus Protofilamenten gebildet. Deren Assemblierung und GTP-abhängige Polymerisation in eine asymmetrische, helikale und hohlzylindrische Anordnung verleiht den Mikrotubuli ihre Polarität und typische Orientierung innerhalb der Zelle (vgl. Abbildung 3b-d).[37–39]

Während der Mitose sind Mikrotubuli essentiell für die Chromosomensegregation, indem die aus Mikrotubuli aufgebaute mitotische Spindel die mechanische Trennung der Chromosomenpaare vermittelt (vgl. Abbildung 3c).[40]

Die charakteristische Lokalisierung und Verteilung der bisher beschriebenen Zytoskelett- und Fokaladhäsions-Komponenten in verschiedenen Zelltypen ist in Abbildung 4 nochmals vergleichend dargestellt.

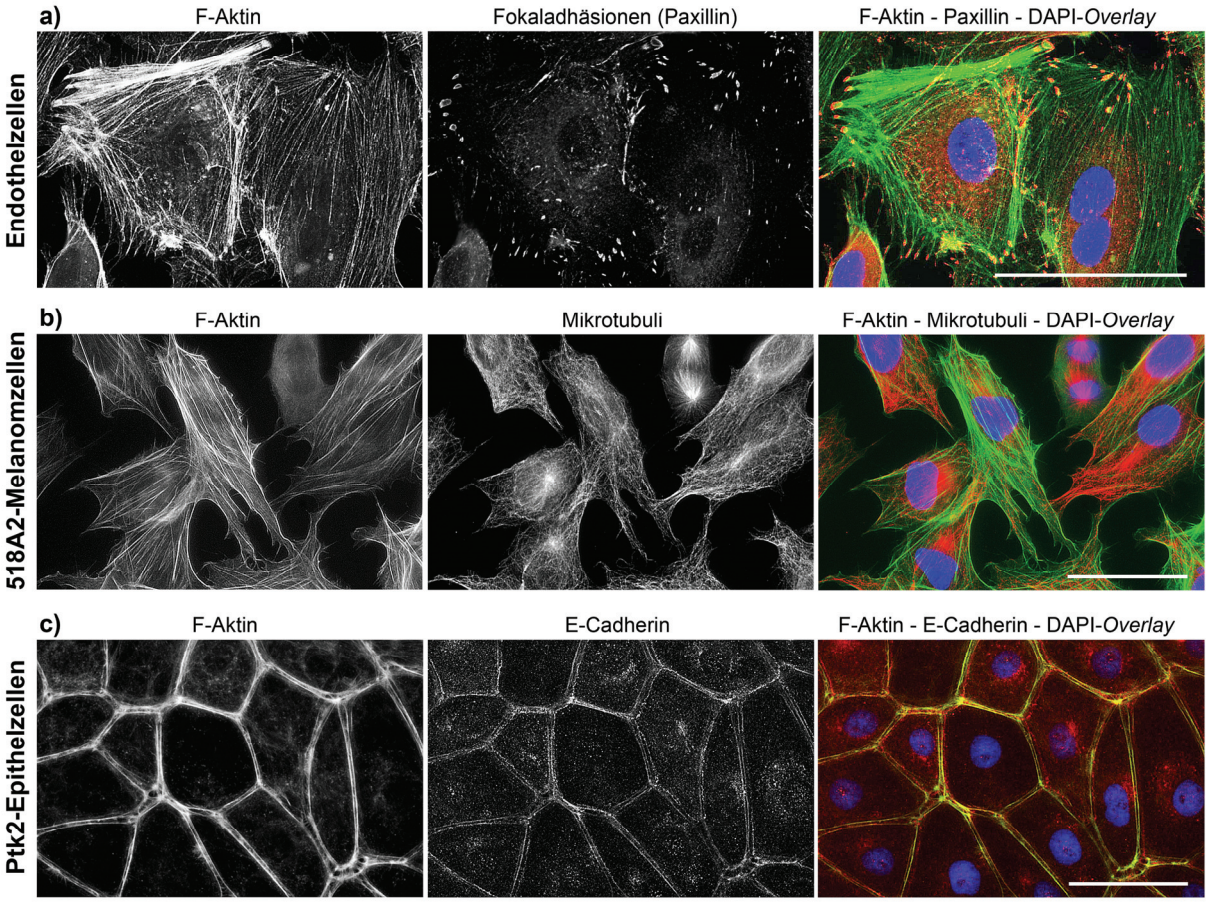

Abbildung 4 – Charakeristische Lokalisierung und Verteilung von Zytoskelett- und Zelladhäsions-Komponenten bei verschiedenen Zelltypen in 2D-Kultur. Fluoreszenzmikroskopische Aufnahmen verschiedener Zytoskelett-Komponenten in **a)** primären Endothelzellen: Aktin-Zytoskelett (filamentöses Aktin = F-Aktin, grün) und Fokaladhäsionen (Paxillin, rot), **b)** 518A2-Melanomzellen: F-Aktin (grün) und Mikrotubuli (rot), **c)** Ptk2-Epithelzellen mit charakteristischer Einzelschicht-Organisation (Aktin-Orientierung entlang der Zell-Peripherie, F-Aktin, grün) und hohem Anteil an epithelialen Zell-Zell-Kontakten (E-Cadherin, rot). Visualisierung mittels Immuno- oder Phalloidin-Fluoreszenzfärbung, Überlagerung der Einzelfärbungen (*Overlay*) mit Zellkern-Gegenfärbung (DAPI), 630- oder 400-fache Vergrößerung, Maßstabsbalken = 50 µm.

Mikrotubuli unterliegen ähnlich den Aktin-Filamenten einem kontinuierlichen Polymerisations-Depolymerisationsgleichgewicht. Eine Vielzahl von Proteinen nimmt durch Beeinflussung dieses Prozesses und durch post-translationale Modifikation von alpha- oder beta-Tubulin-Untereinheiten an der Regulation von Mikrotubuli-Stabilität -und Funktion

teil.[37,41–44] Ihre Asymmetrie ermöglicht zudem den Plus- oder Minuspol gerichteten Vesikeltransport über Mikrotubuli-assoziierte Motorproteine wie Kinesin und Dynein.[39] Hierin liegt auch der Anteil der Mikrotubuli an der mesenchymalen Migration, bei der der Transport entlang Lamellipodium-ausgerichteter Mikrotubuli zum *Leading edge* die Versorgung mit dort essentiellen Faktoren gewährleistet. Dazu gehören neben Membranbestandteilen zur Erweiterung der Plasmamembran auch die kleinen GTPasen Rac und Cdc42, die dort Aktin-Polymerisation und Fokaladhäsionsausbildung induzieren. (RTK-)Signaltransduktion wird ebenfalls durch den Transport von Endosomen und Membran-assoziierten Signalmolekülen entlang der Mikrotubuli vermittelt.[38,45,46] Zusätzlich sind die Regulation von Aktin- und Tubulin-Zytoskelett-Komponenten über Rho-*Signalling* aneinander gekoppelt, weshalb Veränderungen der Stabilität bzw. der Polymerisation-Depolymerisations-Dynamik von Interphase-Mikrotubuli zur Aktivierung von Rac1 oder RhoA führen und damit entweder die Bildung von Lamellipodien oder die Bildung von Aktin-*Stress fibres* induzieren können.[15,39,47]

Da die Mikrotubuli an der Aufrechterhaltung der Zell-Morphologie und Integrität von organisierten Zellschichten wie Epithel oder Endothel, aber auch an Zellteilung, Zellmigration und Vermittlung einer Vielzahl von Signaltransduktionswegen beiteiligt sind, stellen sie eins der wichtigsten *Targets* für antitumorale Wirkstoffe dar. Die wichtigsten zellulären Effekte, die durch Mikrotubuli-aktive Substanzen induziert werden, sollen im Folgenden im Kontext antivaskulärer Zytostatika genauer betrachtet werden.

1.4 Antimetastatische Chemotherapie: Etablierte vaskular-disruptive und antiangiogene Therapeutika

Chemotherapeutika, die aktuell Anwendung in der Krebstherapie finden, zielen meist auf die Zerstörung des Primärtumors ab und blockieren wichtige zelluläre Vorgänge bei der Zellproliferation.[48] Beispiele hierfür sind Alkylantien wie Cisplatin und Carboplatin oder DNA-interkalierende Topo-Isomerase-Inhibitoren wie das Anthrazyklin Doxorubicin, die hauptsächlich über Hemmung von DNA-Replikation und DNA-Schädigung zur Induktion von Apoptose führen.[49–52] Bei stark-metastasierenden Tumoren des nicht-kleinzelligen Lungenkarzinoms (*non-small cell lung cancer,* NSCLC) werden heute hauptsächlich EGFR-Inhibitoren bzw. EGFR-Tyrosinkinase-Inhibitoren (EGFR-TKi) wie beispielsweise Gefitinib oder Erlotinib eingesetzt und oft mit weiteren Zytostatika kombiniert.[53–58] Trotz vielversprechender klinischer Studien stellen abgesehen von Nebenwirkungen die intrinsische Tumorheterogenität sowie die Entwicklung von Mehrfachresistenzen gegenüber Arzneimitteln und Wirkstoffen und die Entwicklung spezieller Wirkstoff-Resistenzen in Folge einer Chemotherapie nach wie vor ein Problem dar.[52,59–62] In Folge sterben etwa 90% aller Krebspatienten aufgrund von Metastasenbildung und anatomischer Tumorstreuung. Die Entwicklung von Therapeutika, die vermehrt in den Metastasierungsprozess selbst eingreifen, stehen daher aktuell im Fokus der Zytostatika-/antitumoralen Wirkstoffforschung.[48,63]

Als Angriffspunkte für so genannte antimetastatische Substanzen können hierbei unter anderem die bisher beschriebenen Vorgänge während der Tumorzell-Dissemination (EMT, Invasion, Migration, *Intra*- und *Extravasation*, Interaktion mit der Tumorumgebung) dienen, vor allem aber auch bestehende Tumorblutgefäße sowie die zellulären Prozesse der Tumor-Angiogenese selbst, da diese zu Etablierung und Wachstum von Mikro- und Makrometastasen und letztlich zur Tumorprogression beitragen (vgl. Abbildung 1-2).

Ein wichtiger Fortschritt bei der Tumor-Angiogenese-orientierten Krebstherapie in den letzten Jahren war die Entwicklung von Bevacizumab, einem therapeutischen VEGF-Antikörper.[64–66] Seine Wirkung beruht hauptsächlich auf dem Abfangen von Tumorzell-sekretiertem VEGF und dem Blockieren der VEGF/VEGFR-induzierten Tumorvaskularisierung.[66,67] Eine länger andauernde Blockade der VEGF-Signaltransduktion durch VEGF-Antikörper oder niedermolekulare VEGFR-TKi wie Sunitinib führte jedoch aktuellen Studien zufolge vermehrt zu aggressiver, maligner Progression, Invasion und Metastasierung nach Abschluss der Behandlung.[68–70]

Auch für Matrix-Metalloproteinasen, die durch proteolytische Freisetzung von pro- und antiangiogenen Faktoren direkt in die Regulation des *Angiogenic switch* involviert sind, wurde im Rahmen antivaskulärer und antimetastatischer Therapieansätze eine Vielzahl an Inhibitoren entwickelt, von denen bis heute keiner erfolgreich klinische Studien durchlief.[21,71,72] In den letzten Jahren lag der Fokus vermehrt auf MMP-Isoform-spezifischen Wirkstoffen, um die Komplexität MMP-regulierter Prozesse und den Anteil einzelner Vertreter der MMP-Familie an der Regulation von Zellwachstum und Angiogenese besser verstehen und untersuchen zu können.[21,73]

Vaskular-disruptive Agenzien (VDAs) bilden neben Substanzen mit antiangiogener Wirkung den wichtigsten Anteil an antivaskulären Tumortherapeutika. Im Gegensatz zum antiangiogenen Ansatz greifen sie nicht ausschließlich in die Blutgefäßneubildung ein, sondern zerstören vor allem bereits bestehende Tumor-Blutgefäße. Die Wirkstoffklasse der VDAs setzt sich hauptsächlich aus verschiedenen Tubulin-bindenden Substanzen (Tubulin-Binder) zusammen.[74–80]

1.4.1 Tubulin-bindende Wirkstoffe als vaskular-disruptive Zytostatika

Diese binden je nach Wirkstoffklasse an spezifische Bindestellen in der beta-Tubulin-Unterheit der Tubulin-Heterodimere und beeinflussen die Dynamik der kontinuierlich stattfindenden Tubulin-Polymerisation.[74,81] Man unterscheidet dabei zwischen Mikrotubuli-stabilisierenden und destabilisierenden Substanzen. Einige ihrer wichtigsten Vertreter sind in Abbildung 5 dargestellt und kommen aus unterschiedlichsten Naturstoffklassen oder stellen synthetische Derivate dar.

Ein bekannter stabilisierender Tubulin-Binder ist Paclitaxel (Taxol) aus der Wirkstoffklasse der Taxane, das mit der so genannten Taxan-Bindestelle in der beta-Tubulin-Untereinheit im inneren Hohlraum der Mikrotubuli interagiert und dort über Konformationsänderungen den Einbau weiterer Tubulin-Heterodimere induziert. Dies führt letztlich zur Zunahme von Interphase-Mikrotubuli und einem geringeren Anteil löslicher Tubulin-Dimere in behandelten Zellen (Abbildung 6b).[81,82] Im Gegensatz dazu binden Mikrotubuli-destabilisierende Verbindungen aus der Klasse der Vinca-Alkaloide oder Colchicin-Analoga jeweils an spezifische Bindestellen der beta-Tubulin-Untereinheit – der Vinca-Domäne oder der Colchicin-Bindestelle - und verhindern so die Tubulinpolymerisation (Abbildung 5).

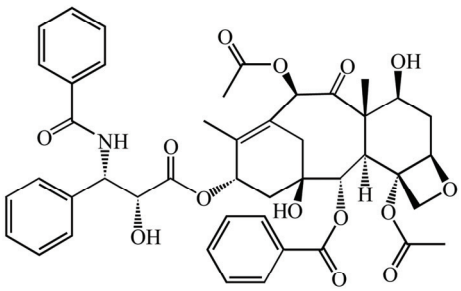

Paclitaxel (Taxol)

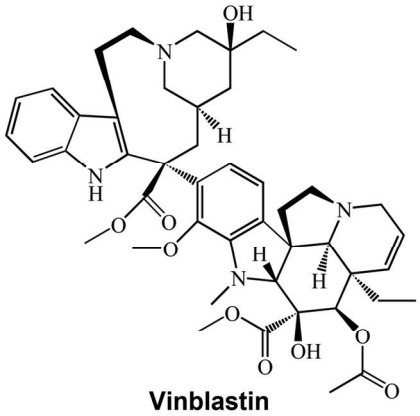

Vinblastin

Bindung an:	Taxan-Bindestelle, stabilisierend	Vinca-Domäne, destabilisierend

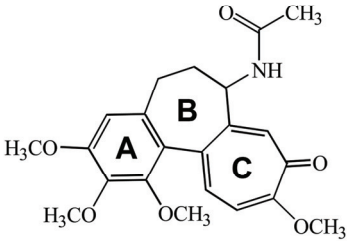

Colchicin

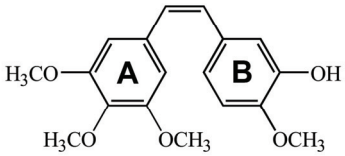

Combretastatin A-4 (CA-4)

Bindung an:	Colchicin-Bindestelle, destabilisierend

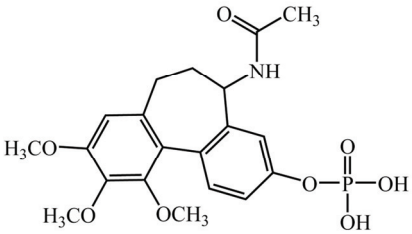

ZD6126
(Colchicin-Analogon)

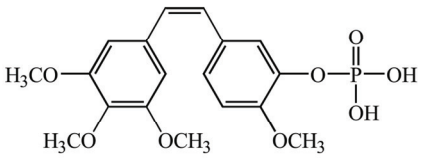

CA-4-Phosphat (CA-4-P)
(CA-4-*Prodrug*)

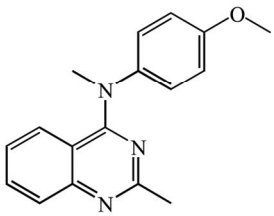

MPC-6827 (Azixa, Verubulin)

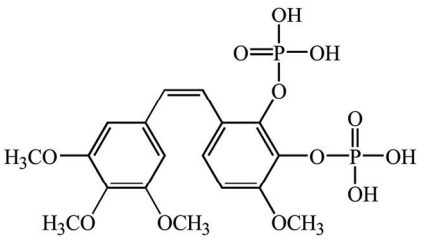

CA-1-Phosphat (CA-1-P, Oxi4503)
(CA-1-*Prodrug*)

Abbildung 5 – Beispiele für Tubulin-bindende Agenzien aus verschiedenen Substanzklassen und ihre Interaktion mit der beta-Tubulin-Untereinheit in alpha-/beta-Tubulin-Heterodimeren. Paclitaxel (Taxol) aus der Klasse der Taxane bindet an die Taxan-Bindestelle und wirkt sich stabilisierend auf die Tubulinpolymere aus. Vinca-Alkaloide wie Vinblastin interagieren mit der Vinca-Domäne und destabilisieren Mikrotubuli durch Inhibition der Tubulinpolymerisation. Colchicin bindet wie das strukturverwandte Combretastatin A-4 (CA-4) an die Colchicin-Bindestelle und wirkt destabilisierend auf die Mikrotubuli. Charakteristisch ist das Trimethoxy-Motiv des sog. A-Rings. Weitere bekannte Mikrotubuli-destabilisierende Agenzien: ZD6126, Combretastatin-Phosphat-*Prodrugs* (CA-4-P/ Fosbretabulin, CA-1-P/Oxi4503) und das synthetische Chinazolin-Derivat MPC-6827 (Azixa/Verubulin). Entwicklung der Derivate durch die Firmen AstraZeneca, OxiGene und Myriad Pharmaceuticals.

Colchicin, das Gift der Herbstzeitlosen (*Colchicum autumnale L.*), ist namensgebend für die Bindestelle an der Grenzfläche zwischen alpha- und beta-Tubulin-Heterodimeren (Abbildung 6a) und ist die erste beschriebene, Tubulin-bindende Substanz.[83] Die verschiedenen Ringsysteme des Naturstoffs sowie das charakteristische Trimethoxy-Motiv des A-Rings (vgl. Abbildung 5) ermöglichen die Interaktion mit der hydrophoben Bindetasche und verschiedenen Protein-Seitenketten (vg. Abbildung 6a).[84,85] Ein chemotherapeutischer Einsatz von Colchicin ist aufgrund seiner enormen Toxizität und starken Nebenwirkungen jedoch nicht möglich. Auch klinische Studien mit dem wasserlöslichen Phosphat-*Prodrug* des *N*-Acetylcolchinol-Analogons ZD6126 wurden aufgrund hoher Kardiotoxizität bei pharmakologisch-relevanter Dosierung eingestellt.[81,83,86]
Das strukturverwandte Combretastatin A-4 (CA-4) stellt einen weiteren Naturstoff dar, der an die Colchicin-Bindestelle der beta-Tubulin-Unterheit bindet. Es wurde 1987 erstmals aus der Rinde der afrikanischen Buschweide (*Combretum caffrum*) isoliert.[87] Im Gegensatz zu Colchicin und ZD6126 zeigten verschiedene, wasserlösliche Phosphat-*Prodrugs* von Combretastatin A-4, vor allem Combretastatin A-4-Phosphat (CA-4-P, Zybrestat oder Fosbretabulin) vielversprechende Wirkung in zahlreichen klinischen Studien.[77,81,88–92] Daneben existiert eine Vielzahl von Naturstoff-abgeleiteten und synthetischen *Colchicin Site*-Inhibitoren, von denen mit dem Chinazolin-Derivat Verubulin (MPC-6827, Azixa) der Firma Myriad Pharmaceuticals nur einer genannt werden soll (vgl. Abbildung 5).
Hohe Konzentrationen dieser Substanzen verschieben das Gleichgewicht von polymerisierten Tubulin-Heterodimeren auf die Seite löslicher, unstrukturierter Tubulin-Heterodimere und ziehen somit eine vollständige Destabilisierung von Interphase-Mikrotubuli nach sich.[82,83] Charakteristische Effekte auf die Tubulin-Organisation in Melanomzellen nach Inkubation mit dem typischen Mikrotubuli-Stabilisator Taxol oder dem Mikrotubuli-destabilisierenden CA-4 *in vitro* sind in Abbildung 6b dargestellt.
Da Tubulin-Binder auch den Aufbau der mitotischen Spindel hemmen, induzieren sie zudem Zellzyklusarrest beim Eintritt der Zelle in die Mitose oder während der Mitose. Fehlregulation bei der Polymerisation, die dadurch ausgelöste Aktivierung von Signalwegen und nachfolgende Arretierung vor Zellzyklus-relevanten *Checkpoints* aufgrund fehlerhafter Spindel-Dynamik sind die Ursachen dafür, dass Zellzyklus und Zellteilung nicht vollständig ablaufen können. Man spricht in diesem Zusammenhang von der antimitotischen Wirkung der Tubulin-Binder, die letztlich auch die Induktion von Apoptose nach länger-andauerndem Zellzyklusarrest nach sich ziehen kann.[93,94]

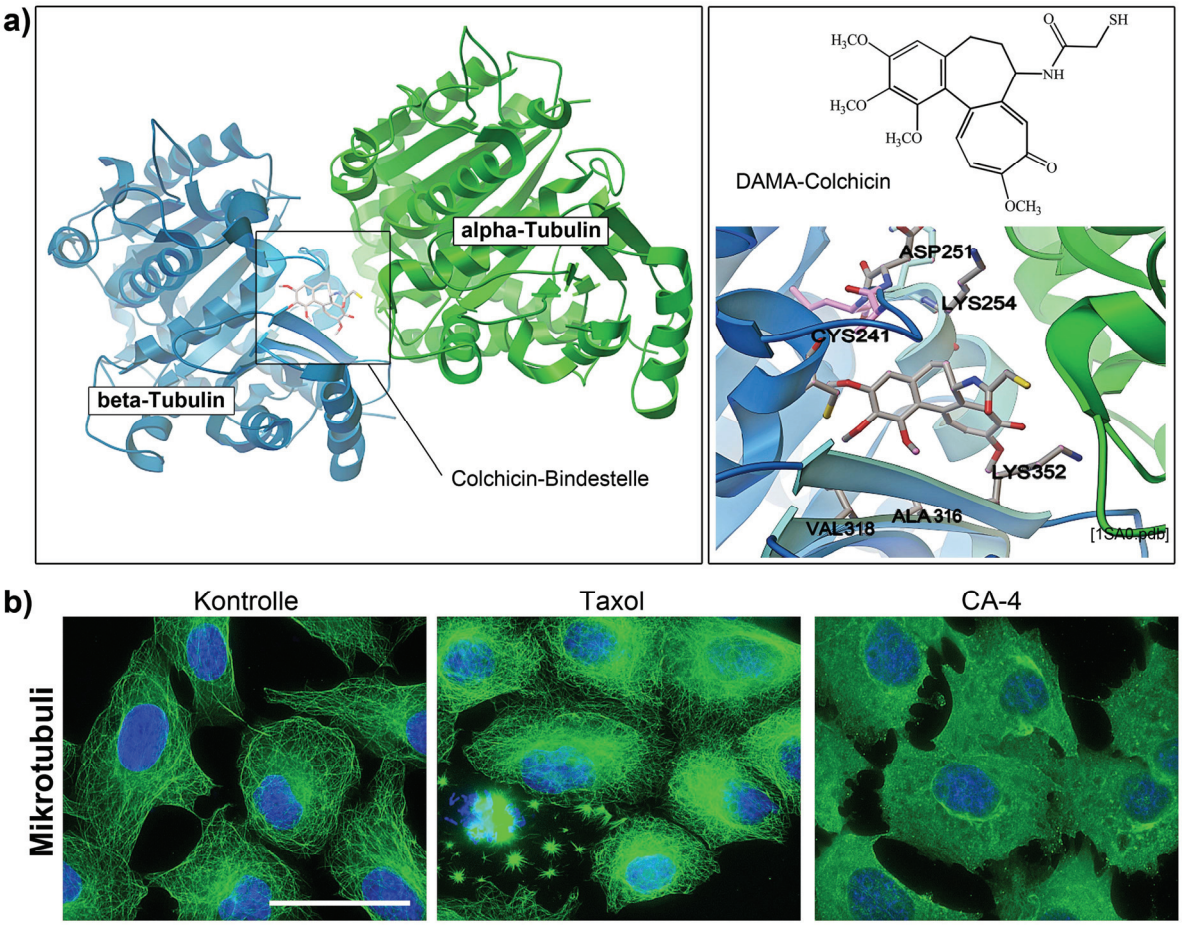

Abbildung 6 – Die Colchicin-Bindestelle an der Grenzfläche zwischen alpha-/beta-Tubulin-Heterodimeren und die Auswirkung von Tubulin-bindenden Substanzen auf die zelluläre Tubulin-Organisation. a) Colchicin-Bindestelle zwischen alpha-(grün) und beta-Tubulin (blau)-Untereinheit. Darstellung mit gebundenem *N*-Deacetyl-*N*-(2-Mercaptoacetyl)-Colchicin (DAMA-Colchicin) in der Bindetasche, die schematisch mit ihren wichtigsten Protein-Seitenketten (beta-Tubulin: CYS241, ASP251, LYS254, VAL316, ALA318, LYS352) und Sekundärstrukturelementen (hell markiert) dargestellt ist. pdb-Code: 1SA0.[84] **b)** Charakteristische Organisation von Interphase-Mikrotubuli in Melanomzellen (Kontrolle) nach Inkubation mit hohen Konzentration von Taxol (Mikrotubuli-stabilisierend) und Combretastatin A-4 (CA-4, Mikrotubuli-destabilisierend). Fluoreszenzmikroskopische Visualisierung nach Immunofluoreszenzfärbung der Mikrotubuli (grün) und Zellkerngegenfärbung mit DAPI (blau), 400-fache Vergrößerung, Maßstabsbalken = 50 µm.

Der Wirkmechanismus eines VDA am Beispiel von Combretastatin-Analoga

Die vaskular-disruptive Wirkung von Combretastatinen und anderen VDAs beruht hauptsächlich auf der Schädigung und Umstrukturierung des Zytoskeletts von Endothelzellen, insbesondere von Tumor-assoziierten Endothelzellen, die die Tumor-Blutgefäße bilden. Zytoskelett-vermittelte Effekte tragen letztlich zur Zerstörung der Endothel-Integrität bei. Dazu gehört neben der Mikrotubuli-Destabilisierung und dem Verlust der Mikrotubuli-Stabilitätsfunktion in einzelnen Zellen vor allem die Aktivierung der kleinen GTPase RhoA

und Rho-Kinase (ROCK), die als Folge der Behandlung mit CA-4-P sowohl *in vitro* als auch *in vivo* beobachtet werden kann und eine entsprechende Remodellierung des Aktin-Zytoskeletts induziert.[75,95] Es kommt somit zu vermehrter Aktin-Polymerisation und Aktinfilament-Stabilisierung in Form von Aktin-*Stress fibre*-Bildung und ebenfalls zu vermehrter Assemblierung von Fokaladhäsionen. *Myosin light chain* (MLC)-Phosphorylierung durch ROCK trägt letztlich zur CA-4-P-induzierten Aktinomyosin-Kontraktion und erhöhter Zellkontraktilität bei. In die typischen zellulären *in-vitro*-Effekte sind zudem verschiedene MAP-Kinasen (*Mitogen-activated protein kinases*, MAPK) involviert. So spielt vermehrte Aktivierung von SAPK2 (*Stress-activated protein kinase 2*, p38) und reduzierte ERK1/2 (*Extracellular signal-stimulated kinase* 1/2)-Aktivität eine wichtige Rolle für die Ausbildung einer als *Membrane Blebbing* bezeichneten, endothelialen Morphologie mit zahlreichen Aktin-vermittelten Membraneinschnürungen.[75,96–98] All diese Effekte erhöhen nicht nur die Endothelzell-Permeabilität, sondern führen auch zur Fehlassemblierung oder Zerstörung bereits assemblierter, endothelspezifischer interzellulärer VE-Cadherin-beta-Catenin-Verbindungen im Endothel.[99] Vermehrte Endothelzell-Permeabilität und Kontraktilität einzelner Endothelzellen im hoch-organisierten Endothelverbund sind letztlich CA-4-P-vermittelte Sekundäreffekte, die für den Zusammenbruch von Kapillaren und Gefäßsystemen im Tumor verantwortlich sind.[77,95,97,100] Die Zerstörung der Endothel-Integrität tritt in VDA-behandelten Tumoren für gewöhnlich äußerst schnell auf und führt bestenfalls zum vollständigen Kollabieren der tumoralen Blutversorgung, was von Tumor-Einblutungen und Nekrose des Tumorgewebes begleitet wird.[78,80,88] Aufgrund ihrer anomalen Strukturierung und unausgereifter Stabilisierung sind Tumor-Blutgefäße (vgl. Abschnitt *1.2 Tumorangiogenese*) im Vergleich zu den regulären, hoch-organisierten Blutgefäßen besonders anfällig für die VDA-induzierte Zytoskelett- und Fokaladhäsions-Fehlorganisation. Zudem wird vermutet, dass Tumor-Endothelzellen selbst eine erhöhte Sensitivität gegenüber VDAs aufweisen.[101] Da auch für die Prozesse während der Neoangiogenese und Tumor-Vaskularisierung wie beispielsweise der Endothelzell-Migration, funktionierende Zytoskelett-Komponenten essentiell sind, besitzen VDAs oft auch antiangiogene Wirkung.[77]

Aktuelle Probleme bei der Chemotherapie mit VDAs

Vor allem aufgrund der antimitotischen Effekte Tubulin-bindender VDAs ist ihre Toxizität nicht nur auf Endothelzellen beschränkt. Ihre Auswirkungen auf die Bildung der mitotischen

Spindel und die damit verbundene Hemmung von Mitose und Zellproliferation sind vor allem für schnell-proliferierende Tumorzellen enorm toxisch. Im Falle von CA-4-P, das *in vivo* nur eine geringe Plasma-Halbwertszeit aufweist,[102] wurde direkte Tumorzelltoxizität nur bei wiederholter Verabreichung und bestimmten Krebstypen gefunden.[75] Es stellt somit ein VDA dar, dessen antitumorale Aktivität meist vollständig auf den antivaskulären Effekten beruht.[100] Zudem tritt die VDA-induzierte Tumornekrose generell nur im Inneren des soliden Tumors auf, wobei meist eine äußere, noch hoch-vaskularisierte Tumorrinde (*viable tumour rim*) zurückbleibt. Hiervon geht meist erneutes Tumorwachstum aus, weshalb VDAs wie CA-4-P hauptsächlich in Kombination mit anderen etablierten Zytostatika verabreicht werden.[88,89,100]
Ein weiteres Problem, das nach CA-4-P-Behandlung auftreten kann, ist die Ausbildung von Multiresistenzen (*multidrug resistance*, MDR) durch erhöhte Expression von Efflux-Transportern. Diese als Transmembranpumpen fungierende ABC (*ATP-binding cassette*)-Transporter schleusen unter ATP-Verbrauch xenobiotische Substanzen über die Zellmembran und verhindern so die Akkumulation von Wirkstoffen im Zellinneren.[59,103] CA-4-P wird als Substrat unter anderem von MRP1 (*Multidrug resistance-associated protein 1*)-Transportern erkannt und stimuliert die Überexpression weiterer MDR-Transporter wie P-gp (*P-Glycoprotein*). Dies kann nicht nur zur Resistenz verbliebener Tumorzellen gegen erneute CA-4-P-Verabreichung führen, sondern auch Resistenzen gegen eine Sekundärbehandlung mit weiteren Zytostatika vermitteln.[59,100,103]
Die Etablierung neuer, effektiverer CA-4-Derivate mit verbesserter metabolischer Stabilität und für MDR-Proteine nicht erkennbaren strukturellen Motiven ist daher nach wie vor von großem Interesse.
Erste Erfolge auf diesem Gebiet beschreibt eine Publikation von *Wang et al.*, die sich mit der chemischen Stabilisierung der *cis*-Konfiguration des Naturstoffs CA-4 beschäftigte.[104] Die Einbindung der *cis*-Doppelbindung in Heterozyklen verhindert dabei die Isomerisierung in das inaktive *trans*-Stilben und stabilisiert die bioaktive, Tubulin-bindende Konfiguration der Phenylringsysteme (vgl. Abbildung 5). Eine weitere Naturstoffoptimierung konnte bereits durch Halogensubstitution von einer der Methoxygruppen des A-Ring-Trimethoxymotivs erreicht werden, die die Affinität für die Colchicinbindestelle deutlich erhöht. Gleichzeitige Substitution der B-Ring-Hydroxygruppe, die die CA-4-Resistenz durch die strukturelle Ähnlichkeit zu Phenolsubstraten von MRP1 vermittelt, führte zur Resensitivierung von MRP1-positiven Tumorzelllinien. Bei diesen 2011 am Lehrstuhl für Organische Chemie der Universität Bayreuth entwickelten und patentierten Derivaten handelt es sich zudem um gut-

wasserlösliche Imidazolium-Hydrochlorid-Salze mit erstaunlicher antitumoraler *in vivo*-Aktivität.[105,106]

1.4.2 Histondeacetylase-Inhibitoren als potentielle antiangiogene und antimetastatische Chemotherapeutika

Eine weitere Wirkstoffklasse, die sich über die letzten Jahre als Chemotherapeutikum etabliert hat, sind die bisher noch nicht erwähnten Histondeacetylase-Inhibitoren (HDACi). Ihre aktuell noch nicht vollständig verstandene antiangiogene Wirkungsweise unterscheidet sich stark von der bei aktuell eingesetzten therapeutischen Antikörpern und TKis und bietet deshalb einen vielversprechenden neuen Ansatz zur chemotherapeutischen Hemmung von Metastasierung und Tumorangiogenese.[107,108]

Histondeacetylasen als Target für antitumorale Wirkstoffe

Die Proteinfamilie der humanen Histondeacetylasen vermittelt prinzipiell post-translationale Modifizierung durch katalytische Deacetylierung von Lysin-Seitenketten in ihren jeweiligen Zielproteinen.[109,110] Zu diesen gehören nicht nur die namensgebenden Histone, sondern auch zahlreiche andere Proteine, deren Stabilität, Funktion und Lokalisierung in der Zelle durch ein Zusammenspiel von HDAC-vermittelter Deacetylierung und Histon-Acetyltransferase (HAT)-Aktivität beeinflusst und reguliert werden.[110–113] Zink-abhängige Histondeacetylasen nehmen somit an einer Vielzahl zellulärer Prozesse teil und werden aktuell in verschiedene Unterklassen eingeteilt. Je nach struktureller Ähnlichkeit unterscheidet man dabei zwischen den Klasse I-Isoenzymen HDAC1, HDAC2, HDAC3 und HDAC8, Klasse IIa-Isoenzymen HDAC4, HDAC5, HDAC7 und HDAC9 und den Klasse IIb-Vertretern HDAC6 und HDAC10. HDAC11 wird aufgrund seiner Proteinstruktur einer eigenen Klasse IV zugeordnet. Klasse III-Sirtuine (Sirt1-7) besitzen Deacetylasefunktion über einen NAD-abhängigen Mechanismus und werden im Weiteren nicht als *Targets* für antitumorale Wirkstoffe behandelt. Die einzelnen HDAC-Isoenzyme mit Zn^{2+} im aktiven Zentrum unterscheiden sich sowohl in ihrer Substratprotein-Spezifität, als auch in ihrer zellulären Lokalisierung (Abbildung 7).[107,114–116]

Ihre Aktivität in der klassischen Deacetylierung von Histonproteinen als Bestandteil der Nucleosomen ist essentiell für die epigenetische Regulation von Genexpression oder Gen-*Silencing*.[117,118] Dabei ist der Proteinkern der Nucleosomen aus Histon-Octameren aufgebaut,

jeweils zwei Kopien der Histone H2A, H2B, H3 und H4. Der jeweilige Acetylierungsstatus ihrer Lysin-reichen, N-terminalen Region beeinflusst dabei die Konformation der Chromatinstruktur.[114,119,120] Vereinfacht dargestellt erhöhen HDACs durch Deacetylierung von Lysin-Seitenketten die kompakte Chromatin-Kondensation, was die Interaktion mit den Multiproteinkomplexen der Transkriptionsmaschinerie erschwert und letztlich zur Repression der Genexpression führt.[121,122] Tatsächlich interagieren die verschiedenen, Zellkern-lokalisierten HDAC-Isoformen auch mit einer großen Anzahl Transkriptionsaktivatoren –und Repressoren.[114,120,121] Zielgene- und DNA-Promotorregionen, die einer epigenetischen Regulation durch HDACs unterliegen, stehen zudem oft in Verbindung mit Zellzyklusregulatoren, Tumorsuppressoren sowie Differenzierungs- oder pro-apoptotischen Faktoren. HDAC-Fehlregulierung und Überexpression werden daher häufig mit Tumorentstehung in Verbindung gebracht.[120,121]

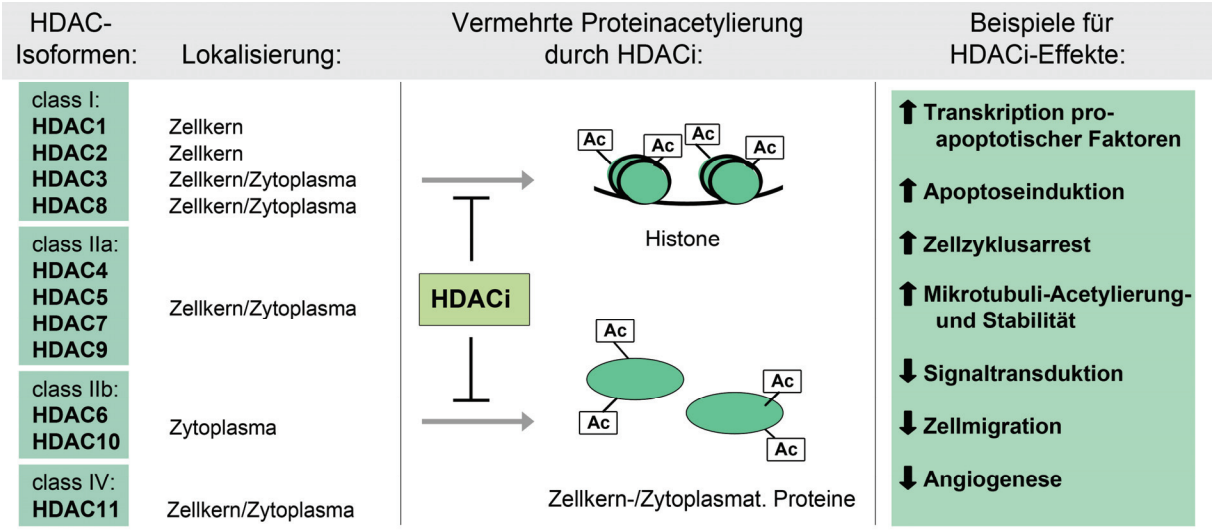

Abbildung 7 – Klassifizierung und Lokalisierung von humanen, Metall-abhängigen Histon-deacetylasen (HDACs) und mögliche Effekte von Histondeacetylase-Inhibitoren (HDACi). Einordnung der 11 humanen HDACs in die Klassen I-IV (class I, IIa, IIb, IV, nicht gezeigt: class III = NAD^+-abhängige Sirtuine) und die zelluläre Lokalisierung einzelner HDAC-Isoformen. Einzelne Isoformen verändern ihre Lokalisierung aufgrund spezifischer Stimuli (Zellkern/Zytoplasma). HDACi hemmen die Deacetylierung von Histon- und Nicht-Histonproteinen (Zellkern-/zytoplasmatische Proteine). In Folge vermehrter Proteinacetylierung (Hyperacetylierung) kommt es zur Induktion oder Inhibition verschiedener zellulärer Effekte (HDACi-Effekte). [Eigene Darstellung nach *Kanzantsev and Thompson* 2008.[115]]

Zu den zahlreichen Nicht-Histon-Substraten von sowohl Zellkern-lokalisierten und zytoplasmatischen HDACs zählen beispielsweise der EGF-Rezeptor, der Transkriptionsfaktor

und Bestandteil des Cadherin-Adhäsionskomplexes beta-Catenin, Transkriptionsfaktoren der STAT-Familie (STAT1/3, *Signal transducers and activators of transcription*), das Tumorsuppressorprotein p53, und viele Angiogenese-relevante Proteine wie VEGFR, HIF-1alpha oder Cortactin.[60,123–129] Die zytoplasmatische Klasse IIb-Isoform HDAC6 ist unter anderem für die Deacetylierung von alpha-Tubulin in den Mikrotubuli verantwortlich und somit an der Regulation von Mikrotubuli-Stabilität und Mikrotubuli-vermitteltem Vesikeltransport sowie Signaltransduktion beteiligt.[123,130–132] Durch Substratproteine wie Cortactin (von *cortical actin-binding protein*) ist HDAC6 auch essentiell für die Koordination der Aktin-Polymerisation. Proteinacetylierung spielt somit nicht nur im Rahmen der epigenetischen Genregulation durch Histon-Modifikation oder Transkriptionsfaktor-Interaktion, sondern auch für Wachstumfaktor-vermittelte Signaltransduktion und für Zytoskelett-vermittelte Adhäsion und Migration eine zentrale Rolle.[122,131] Es erscheint daher nicht überraschend, dass HDAC-Inhibitoren ein breites Spektrum an Tumor-relevanten *Targets* und Signaltransduktionswegen beeinflussen können (vgl. Abbildung 7).

Hydroxamsäure-Derivate als Beispiel für antiangiogene Histondeacetylase-Inhibitoren

Typische niedermolekulare HDACi besitzen charakteristische Strukturelemente wie Hydroxamsäuren, aliphatische Säuren oder Benzamide.[120,133,134] Neben HDAC-Isoform-unspezifischen Inhibitoren (pan-HDACi) wie den Hydroxamsäure-Derivaten Vorinostat (Suberoylanilide hydroxamic acid, SAHA), Belinostat (PXD101) und Panobinostat (LBH589) befinden sich HDAC-Klasse I-spezifische Benzamide wie Entinostat (MS-275) oder das zyklische Peptid Romidepsin in klinischen Studien, ebenso wie die kurzkettigen, aliphatischen Fettsäuren Valproinsäure oder Butyrat, die beide Selektivität für HDAC-Isoformen der Klasse I und IIa besitzen (Abbildung 8).[113,120,122] Im Folgenden soll ausschließlich auf Hydroxamsäure-basierte HDACi mit Breitspektrum-Wirkung auf Metall-abhängige HDAC-Isoformen eingegangen werden.

Ihre inhibitorische Wirkung basiert grundsätzlich auf der Chelatisierung der zweiwertigen Zinkionen im aktiven Zentrum durch ihre Hydroxamsäure-Einheit, deren strukturelle Ähnlichkeit zum natürlichen Acetyl-Lysin-Substrat die Anlagerung in die Bindetasche ermöglicht.[114,135] Hydroxamsäuren wie Vorinostat besitzen *in vitro* eine enorme antitumorale Wirkung bei gleichzeitiger hoher Selektivität gegenüber nicht-malignen Zellen und Gewebe. Diese beruht hauptsächlich auf der Induktion von Apoptose, Zellzyklusarrest, einer Vielzahl an Stress-induzierten Signaltransduktionswegen und der Störung epigenetischer

Regulationsmechanismen, für die Krebszellen grundsätzlich anfälliger sind.[113] Vor allem die Vielzahl der von pan-HDACi beeinflussten zellulären Vorgänge scheint verantwortlich für ihren Therapieerfolg zu sein.[113,120]

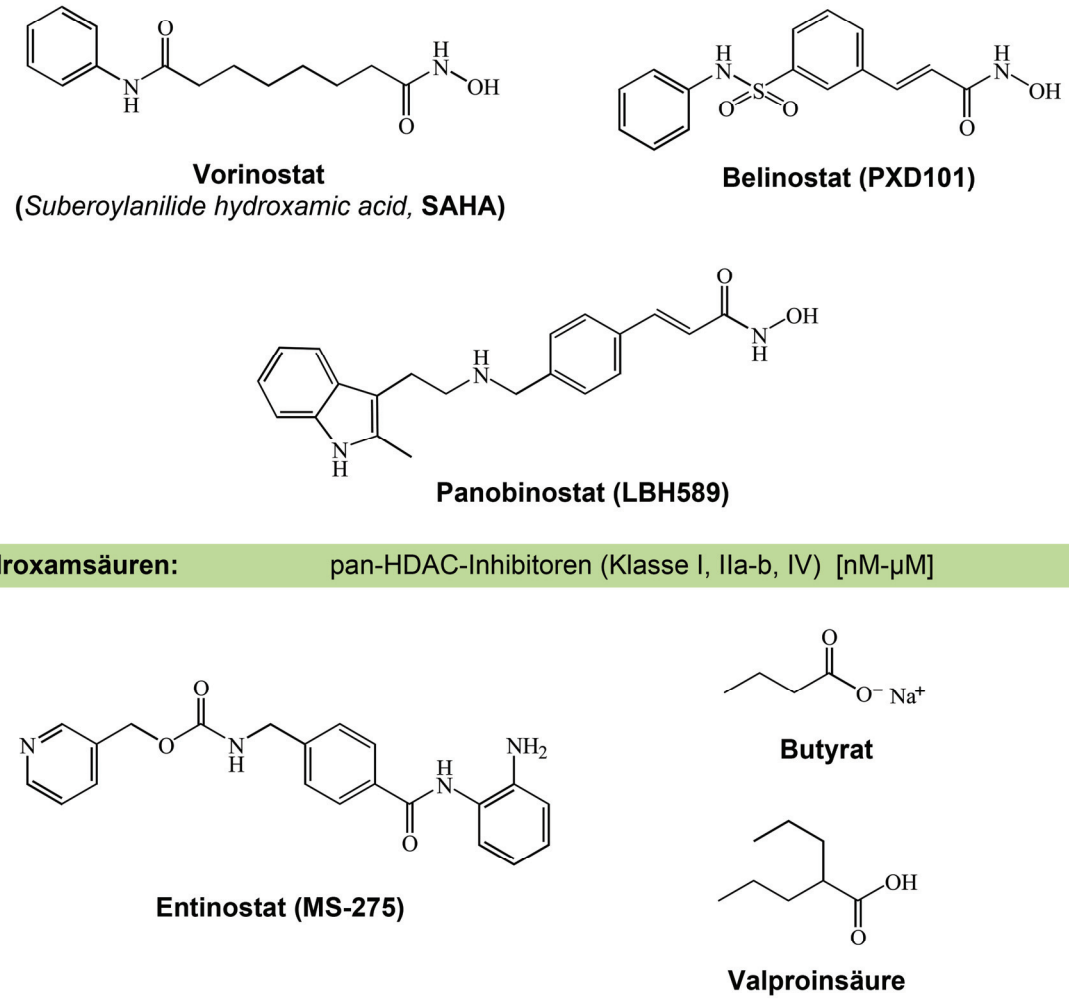

Abbildung 8 – Beispiele für Histondeacetylase-Inhibitoren (HDACi) mit unterschiedlicher Selektivität für HDAC-Isoformen der Klassen I, II und IV. Hydroxamsäure-basierte HDACi vermitteln meist unspezifische HDAC-Inhibition (pan-HDACi) in nanomolaren und micromolaren Konzentrationsbereichen: Vorinostat (*Suberoylanilide hydroxamic acid*, SAHA), Belinostat und Panobinostat. Entinostat (MS-275) als Beispiel für Benzamid-HDACi mit Spezifität für Klasse I-HDAC-Isoformen, Aktivität im micromolaren Bereich. Die kurzkettigen Fettsäuren Butyrat und Valproinsäure als HDACi mit Spezifität für Klasse I- und Klasse IIa-HDAC-Isoformen, Aktivität im millimolaren Bereich. [Eigene Darstellung von Angaben in *K. Ververis et al.* 2013.[122]]

Zahlreiche Studien belegen die antiangiogenen Eigenschaften von Hydroxamsäure-HDACi. Die antiangiogenen Effekte basieren auf reduzierter Expression von Angiogenese-relevanten Proteinen wie VEGF, VEGFR oder MMP-9, die für die Migration und Differenzierung von Endothelzellen in hoch-organisierte Kapillarstrukturen essentiell sind, sowie auf der Hemmung von VEGFR *downstream-Signalling* über den PI3K/Akt-Signalweg und der HDAC6-vermittelten Destabilisierung von HIF-1alpha.[126,128,136–139] Die Inhibition der HDAC6-Aktivität scheint zudem über Substrate wie Cortactin die Motilität und Fokaladhäsionsdynamik von Endothelzellen zu hemmen/verringern.[129,140–143]

Trotz vielversprechender Ergebnisse in einigen Phase I-Mono- und Kombinationstherapien, wurde auch für den zugelassenen HDACi Vorinostat das Auftreten von MDR nachgewiesen, insbesondere durch vermehrte Expression von ABC-Transportern wie P-gp.[144] Auch bei guter Verträglichkeit von Vorinostat konnte in weiterführenden Studien nur geringe Effektivität gegen verschiedene Tumorerkrankungen mit soliden Tumoren nachgewiesen werden, was die Kombination mit anderen Zytostatika erfordert.[122,145,146] Die Umgehung von Wirkstoffresistenzen und die Entwicklung effektiverer, metabolisch-stabiler HDACi stellen somit nach wie vor eine Herausforderung für die Wirkstoffentwicklung dar.[113,122]

2 Zielsetzung

Wirkstoffe, die nicht nur Tumorzell-Toxizität besitzen, sondern auch für die Tumorprogression essentielle zelluläre und biologische Vorgänge hemmen können, gehören zum Ansatz der antivaskulären und antimetastatischen Chemotherapie.[48] Heutzutage ist es vor allem die Kombination effektiver Wirkstoffe, die je nach Art der Krebserkrankung in der Lage sein sollen, auftretende Wirkstoffresistenzen zu umgehen und nach operativen Eingriffen oder vorangegangener Chemotherapie einen Rückfall durch Metastasenbildung und Wachstum von Sekundärtumoren zu verhindern. Der Bedarf an neuen Verbindungen mit verbesserter antitumoraler Wirkung und nachgewiesenen anti-metastatischen oder antiangiogenen Eigenschaften ist daher enorm.

In der vorliegenden Arbeit sollte die Evaluation neuer potentieller Wirkstoffe im Rahmen präklinischer Untersuchungen durchgeführt werden. Bei den hier untersuchten Verbindungen handelt es sich hauptsächlich um **Mikrotubuli-destabilisierende Agenzien** und **Histondeacetylase-Inhibitoren**, die sich an der Leitstruktur des vaskular-disruptiven Naturstoffs Combretastatin A-4 orientieren und am Lehrstuhl für Organische Chemie der Universität Bayreuth entwickelt wurden. Zur Abschätzung ihrer **antitumoralen Effektivität** und **Tumorselektivität** sowie zur Aufklärung ihres Wirkmechanismus sollten unter anderem Experimente an kultivierten, humanen Zelllinien unterschiedlicher Entitäten durchgeführt werden. Die Charakterisierung ihrer **antimetastatischen und antivaskulären Wirkung** erfolgte dabei über verschiedene *in vitro*- und *in vivo*-Modellsysteme. Im Fokus der hier gezeigten Experimente standen vor allem Wirkstoff-Effekte auf die Zytoskelett-Komponenten von Krebszellen, da diese essentiell an den Vorgängen während Metastasierung und Angiogenese sowie wie an der Aufrechterhaltung der Tumorblutgefäß-Integrität beteiligt sind. Auf der Grundlage dieser biologischen und pharmakologischen Evaluation soll letztlich die Optimierung potentieller Wirkstoffkandidaten für die Krebstherapie ermöglicht werden.

3 Zusammenfassung der Ergebnisse (Synopsis)

3.1 Übersicht der Teilprojekte

Die vorliegende kumulative Dissertation enthält sechs Publikationen bzw. Manuskripte, die die zellbiologische Charakterisierung des Wirkmechanismus von neuen niedermolekularen, zytotoxischen Substanzen beinhalten. Dazu gehören neben heterozyklischen Derivaten des synthetischen Chinazolin-Derivates Verubulin (Azixa, MPC-6827) neuartige, Combretastatin A-4-abgeleitete Oxazol- und Imidazol-Derivate mit Tubulin-bindenden und vaskular-disruptiven Eigenschaften. Die hier untersuchten Diarylimidazole stellen metabolisch-stabile Derivate der Naturstoff-Leitstruktur dar und gehören zu einer patentierten Serie von Halogen-substituierten Stilbenen (Patent no. WO 2011/138409 A1).[105,106] Zudem wird die Weiterentwicklung des 4,5-Diarylimidazol-Motivs zu einer neuen Klasse von Hydroxamsäure-basierten Histondeacetylase-Inhibitoren gezeigt, die sowohl antiangiogene als auch antimetastatische Aktivität aufweisen. Eine Zuordnung der einzelnen Arbeiten zu den jeweiligen Wirkstoffklassen und zu den gefundenen, für Chemotherapeutika-etablierten *Targets* ist in Abbildung 9 schematisch dargestellt.

Alle hier untersuchten Testsubstanzen wurden am Lehrstuhl für Organische Chemie I der Universität Bayreuth hergestellt. Untersuchungen zum Wirkmechanismus der Verbindungen wurden zum Teil in Kooperation mit dem Institut für Innere Medizin, Onkologie/Hämatologie der Martin Luther-Universität Halle-Wittenberg, dem Institut für Molekulare Strukturbiologie der Georg August-Universität Göttingen, dem Institut für Pathologie an der *Wayne State University School of Medicine* und dem *Karmanos Cancer Institute* der *Wayne State University* in Detroit (Michigan, USA), dem Institut für Physiologie der Charité-Universitätsmedizin Berlin und dem Lehrstuhl für Genetik der Universität Bayreuth durchgeführt.

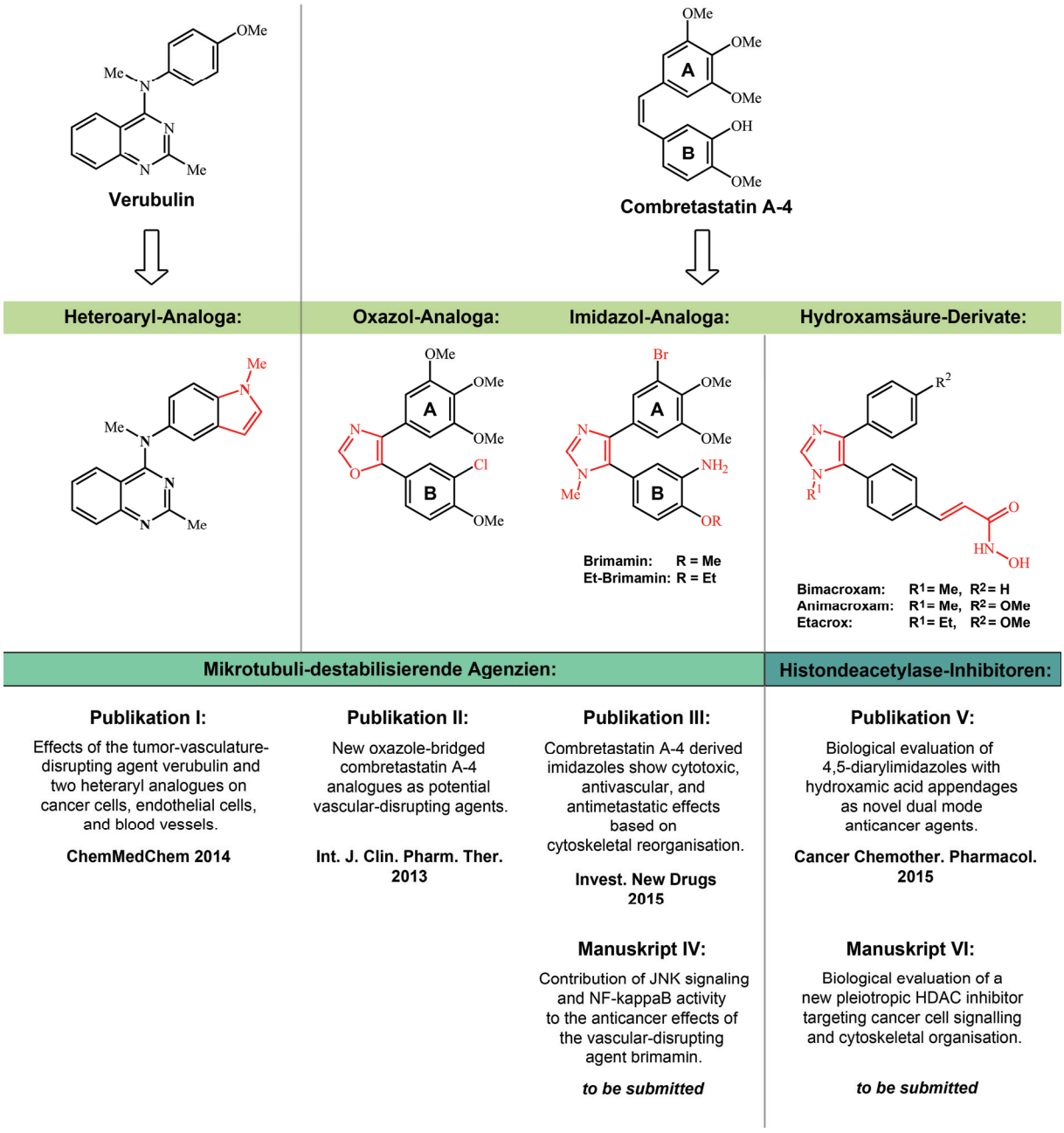

Abbildung 9 – Schematische Darstellung der verwendeten Wirkstoffklassen und Wirkstoff-*Targets* und Übersicht über die Zuordnung der jeweiligen Einzelarbeiten. Reihe oben: Als Leitstrukturen für die hier untersuchten Verbindungen dienten das synthetische, vaskular-disruptive Agens Verubulin (Azixa) und der vaskular-disruptive Naturstoff Combretastatin A-4 (CA-4). **Reihe Mitte:** Strukturen der jeweiligen effektivsten Derivate der Verubulin-abgeleiteten Heteroaryl-Analoga und der CA-4-abgeleiteten Oxazol- und Imidazol-Analoga sowie 4,5-Diarylimidazole mit Cinnamylhydroxamsäure-Resten. **Unten:** Zuordnung der untersuchten Derivate zu ihren jeweiligen Protein-*Targets* und ihren jeweiligen Wirkmechanismen (Mikrotubuli-destabilisierende Agenzien oder Histondeacetylase-Inhibitoren) und Übersicht der zugehörigen, hier vorgelegten Publikation und Manuskripte (Titel, Fachjournal, Jahr der Publikation; *to be submitted*: Manuskriptentwurf).

3.2 Biologische Evaluation von Mikrotubuli-destabilisierenden Agenzien mit antivaskulärer Wirkung

Tubulin-Binder bilden den größten Anteil an heute bekannten Wirkstoffen der Klasse vaskular-disruptiver Agenzien (VDAs). Vor allem Mikrotubuli-destabilisierende *Colchicine site*-Inhibitoren der Polymerisation von Tubulin, die möglichst selektiv zur Zerstörung entarteter Tumor-Blutgefäße beitragen könnten, stellen eine vielversprechende Verbindungsklasse dar.

3.2.1 *In vitro*- und *in vivo*-Effekte von zwei Heteroaryl-Analoga des antitumoralen VDA Verubulin auf Tumorzellen, Endothelzellen und Blutgefäßorganisation

Der erste Artikel zu vaskular-disruptiven Agenzien behandelt eine Serie von Analoga des synthetischen Tubulin-Binders Verubulin (Markenname: Azixa). Das *para*-Methoxyanilin-substituierte Aminoquinazolin-Derivat wurde ursprünglich von der Firma Myrexis (früher: Myriad Pharmaceuticals, USA) entwickelt und als Tubulin-bindendes Agens identifiziert. Verubulin zeigte enorme Toxizität und Apoptose-induzierende Wirkung gegen eine Reihe von Krebszelllinien *in vitro* und *in vivo*. Eine Abhängigkeit oder Einschränkung dieser Wirkung durch typische MDR-Transporter konnte nicht nachgewiesen werden, weshalb nach dem Einstellen weiterer Untersuchungen durch Myrexis aus wirtschaftlichen Gründen im Jahr 2011 eine Weiterentwicklung bzw. Wirkoptimierung dieses Strukturmotivs vielversprechend erschien.

Anstelle des Anisyl-Rests wurden in den Quinazolin-Pharmakophor (4-(Methyl-amino)-2-methylquinazolin) bizyklische Substituenten wie Benzodioxan, Benzodioxolan, Benzofuran und Methylindol eingeführt. Die hohe *in vitro*-Toxizität von Azixa und den Heteroaryl-Derivaten spiegelt sich in den IC_{50}-Werten (halbmaximale, inhibitorische Konzentration; Maß für Wachstumsinhibition oder Toxizität von Wirkstoffen) wieder, die an allen verwendeten Zelllinien im einstelligen, nanomolaren oder sogar picomolaren Bereich lagen. Nicht-maligne Endothelzellen und Fibroblasten zeigten jedoch geringere Sensitivität. Die beiden effektivsten Derivate mit Benzodioxan- und Methylindol-Substituenten [**5a** und **10** in **Publikation I**] konnten in behandelten Endothelzellen den für Tubulin-bindende Substanzen typischen G2/M-Zellzyklusarrest induzieren, der auf der Hemmung des Aufbaus der mitotischen Spindel basiert. Neben der Zerstörung der endothelialen Mikrotubuli-Organisation konnte mittels Immunofluoreszenz-mikroskopie die Bildung von Aktin-*Stress fibres* gezeigt werden (Abbildung 10).

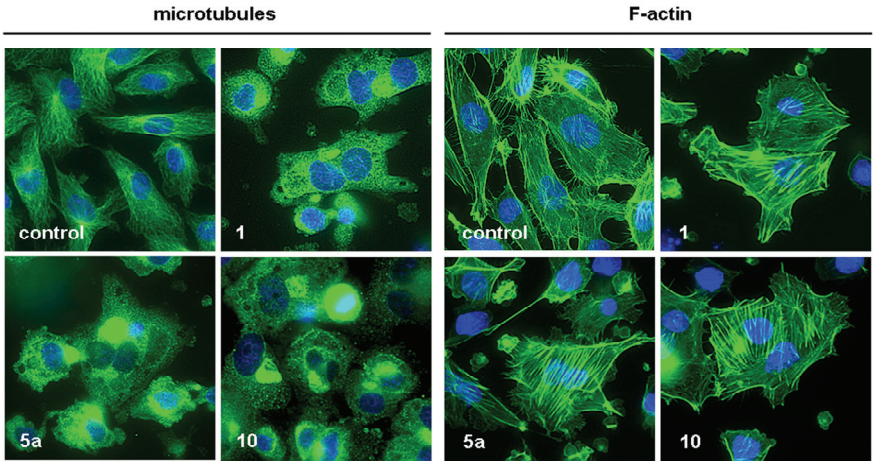

Abbildung 10 – Effekte von Verubulin und Analoga (5a, 10) auf die Zytoskelett-Organisation von Mikrotubuli (links) und F-Aktin (rechts) in Endothelzellen. [Reprinted with permission from K. Mahal, M. Resch, *et al.* ChemMedChem *9(4)*, 847-854, doi 10.1002/cmdc. 201300531. Copyright 2014, Wiley-VCH Verlag GmbH & Co. KGaA, Weinheim.]

In ersten *in vivo*-Studien an Mäusen mit hoch-vaskularisierten Xenograft-Tumoren konnten für das Indol-Derivat VDA-typische Verfärbungen des Tumors aufgrund von intratumoralen Einblutungen bei relativ niedriger Dosierung beobachtet werden. Histologische Untersuchungen von Tumorgewebeschnitten zeigten die ebenfalls VDA-typische Nekrose im Inneren des Xenografts und die verbleibende Tumorrinde mit intakten Blutgefäßen (Abbildung 11).

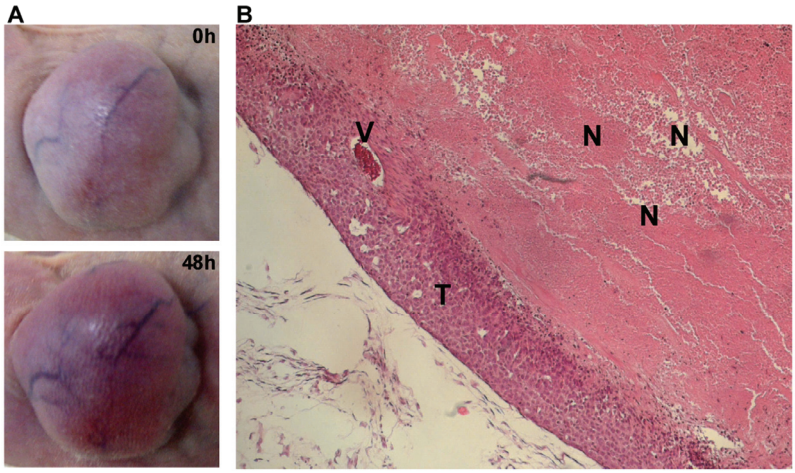

Abbildung 11 – Effekte des Methylindol-Analogs von Verubulin in Xenograft-Tumoren. Dokumentation eines Tumors (A) und von HE-Tumorgewebeschnitten (B), die intratumorale Nekrose (N) und die intakte äußere Tumorrinde (T) mit intakten Blutgefäßen (V) zeigen. [Reprinted with permission from K. Mahal, M. Resch, *et al.* ChemMedChem *9 (4)*, 847-854, doi: 10.1002/cmdc.201300531. Copyright 2014, Wiley-VCH Verlag GmbH & Co. KGaA, Weinheim.]

Bei den durchgeführten *in vivo*-Untersuchungen am Blutgefäßsystem der Chorioallantois-membran (CAM) in fertilisierten Hühnereiern, führte die enorme Toxizität von Verubulin zu einer hohen Letalität der behandelten Hühnerembryos. Eine Stoffmenge von 1.0 nmol des VDA Verubulin war aufgrund der fast vollständigen Zerstörung der Blutgefäße innerhalb von

CAM und Embryo nach etwa sechs Stunden zu 100% letal. Die beiden effektivsten Derivate zeigten bei vergleichbaren vaskular-disruptiven Effekten nicht nur bessere Verträglichkeit (bis zu 10-fach höhere Wirkstoffkonzentrationen), sondern führten auch zu keiner weiteren Beeinträchtigung des embryonalen Wachstums.

Am Beispiel der Verubulin-Derivate ist daher zu sehen, dass Wirkoptimierung nicht ausschließlich mit der Steigerung der Toxizität einhergehen muss, sondern wie in diesem Fall reduzierte apparente VDA-Effekte der Derivate von einer deutlich höheren Wirkstofftoleranz und geringeren Nebenwirkungen profitieren können.

Weitere Details in: K. Mahal, M. Resch, R. Ficner, R. Schobert, B. Biersack, T. Mueller. ***Effects of the tumor-vasculature-disrupting agent Verubulin and two heteroaryl analogues on Cancer Cells, Endothelial Cells, and Blood Vessels.*** ChemMedChem **2014** *9*, 847-854.
[**Publikation I**]

3.2.2 Neue Combretastatin A-4-abgeleitete Oxazole als potentielle, vaskular-disruptive Agenzien

Ähnlich den Azixa-Derivaten besitzen auch CA-4-abgeleitete Oxazole *in vitro*-Zytotoxizität gegen Krebszellen im ein- bis zweistelligen nanomolaren Bereich. Bei den hier untersuchten Oxazolen handelt es sich um eine kleine Serie mit dem ursprünglichen A-Ring-Trimethoxyphenyl-Motiv und Chloro-Substituenten anstelle der Hydroxygruppe in *meta*-Position sowie verschiedenen funktionellen Resten (OMe, OEt, SMe) am B-Ringsystem. Im Gegensatz zu CA-4 selbst zeigten die Oxazol-Analoga hohe Toxizität gegenüber der Darmkrebszelllinie HT-29, die aufgrund hoher Expression von ABC-Transportern des MRP1-Typs Resistenz gegen CA-4 besitzen (IC_{50}-Wert für CA-4 > 1.000 nM, IC_{50}-Wert für bestes Derivat = 6 ± 1 nM). Die Einführung der B-Ring-Chlor-Substitution reicht dabei als strukturelle Veränderung aus, um nicht mehr von MRP1-Effluxproteinen als xenobiotisches Phenol erkannt und ausgeschleust zu werden. Die Oxazole induzierten zudem in Endothelzellen einen für Tubulin-Binder typischen Zellzyklusarrest in der G2/M-Phase.

In diesem *Extended Abstract* sollte erstmals der Effekt von Oxazolen auf die Differenzierung von Endothelzellen zu Blutgefäßvorstufen *in vitro* untersucht werden. Der so genannte *Tube formation*-Assay beinhaltet die Kultivierung von Endothelzellen auf einer mit Wachstumsfaktoren angereicherten Basalmembranmatrix-Mischung (Matrigel), die die natürliche ECM imitiert und Endothelzellen zur Ausbildung multizellulärer, verzweigter Netzwerke stimuliert. Diese Eigenschaft ist typisch für Endothelzellen und stellt aufgrund ihrer enormen Morphologieveränderung und dreidimensionalen Organisation prinzipiell einen initialen angiogenen Prozess dar.[147,148]

Die zwei besten Oxazole der Serie zeigten in nanomolaren Konzentrationen deutliche destruktive Effekte auf bereits ausgebildete, Blutgefäß-ähnliche endotheliale Netzwerke und besitzen so nachweislich vaskular-disruptive Eigenschaften in *in vitro*-Modellsystemen.

Weitere Details in: K. Mahal, B. Biersack, R. Schobert.
New oxazole-bridged combretastatin A-4 analogues as potential vascular-disrupting agents.
Int. J. Clin. Pharmacol. Ther. **2013** *51*, 41-43.
[**Publikation II**]

3.2.3 Zytotoxische, antivaskuläre und antimetastatische Effekte von CA-4-abgeleiteten Imidazol-Derivaten basierend auf aberrativer Zytoskelett-Dynamik

Im Rahmen einer früheren Publikation zu Synthese und biologischen Effekten von den am Lehrstuhl für Organische Chemie I der Universität Bayreuth entwickelten azazyklischen und halogenierten CA-4-Analoga wurden zwei Derivate als besonders effektiv im Hinblick auf ihr *in vitro*-Toxizitätsprofil und ihre Aktivität in Xenograft-Studien identifiziert.[105] Dabei handelt es sich um Imidazole mit 3-Chloro- oder 3-Bromo-4,5-dimethoxy-substituiertem A-Ring und 3-Amino-4-methoxy-substituiertem B-Ringsystem, die von Bernhard Biersack synthetisiert und benannt wurden: Aufgrund ihres Substituentenmusters wurden die Substanzen mit den Abkürzungen bzw. Trivialnamen Climamin und Brimamin versehen, die im Folgenden anstelle der korrekten Bezeichnung nach IUPAC (1-*N*-Methyl-5-(3"-amino-4"-methoxyphenyl)-4-(3'-bromo-4',5'-dimethoxyphenyl)-Imidazol) verwendet werden sollen.

Die erste hier gezeigte Publikation beschäftigt sich mit der biologischen Evaluation von fünf neuen, halogenierten Imidazol-Derivaten mit *meta*-substituiertem A-Ring, verschiedenen B-Ring-Modifikationen der *meta*-Substituenten und Einführung einer Ethoxygruppe in *para*-Position des B-Rings (Abbildung 12). Diese Serie wurde bezüglich ihrer Zytotoxizität und Tubulin-Affinität mit den entsprechenden Methoxy-Analoga verglichen. Generell führte die Ethoxy-Substitution zu einer höheren Toxizität gegen die ausgewählten Krebszelllinien. Alle Derivate zeigten hohe Zytotoxizität gegen CA-4-resistente HT-29-Darmkrebszellen. Diese Resensitivierung ließ sich auch auf Xenograft-Studien übertragen, in denen HT-29-Tumore deutlich auf Brimamin oder Et-Brimamin ansprachen. Zudem zeigte das Derivat Et-Brimamin (vgl. Abbildung 12) mit den niedrigsten IC_{50}-Werten gegen Tumorzellen in zellbasierten und zellfreien Tubulinpolymerisationsassays gleichzeitig den größten Einfluss auf die Tubulinpolymerisation. Die *in vitro*-Toxizität korreliert demnach direkt mit der Affinität der Substanzen für Tubulin. Die chemische Manipulation und Einstellung von Tubulin-Imidazol-Wechselwirkungen scheint zudem zur erhöhten Selektivität der Imidazole für Tumorzellen

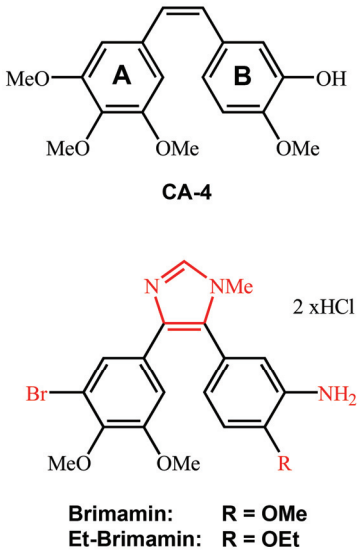

Abbildung 12 – Strukturen von CA-4, Brimamin und Et-Brimamin. Namensgebend sind A-Ring-Brom-Substitution des Imidazol-Analogs und B-Ring-Amino-Substitution.

beizutragen. Nicht-maligne Zellen (Endothelzellen, Fibroblasten) tolerierten im direkten Vergleich zu CA-4 meist die doppelte Konzentration an Brimamin oder Et-Brimamin bei gleichbleibender oder verbesserter Tumorzelltoxizität. Zudem zeigten Brimamin und Et-Brimamin alle typischen Tubulin-Binder-Eigenschaften wie die Arretierung von behandelten Krebszellen in der Mitose und endotheliale Aktin-Zytoskelett-Umstrukturierung. Sowohl die Aktin-*Stress fibre*-Induktion sowie die vermehrte Bildung von Fokaladhäsionen sind dabei auf Aktivierung von Rho-*Signalling* aufgrund fehlerhafter Mikrotubuli-Dynamik zurückzuführen und vermitteln typische VDA-Effekte, die mit Hilfe von *in vitro-Tube formation*-Assays und *in vivo*-Tests an den Blutgefäßen der CAM in fertilisierten Hühnereiern nachgewiesen werden konnten (Abbildung 13).

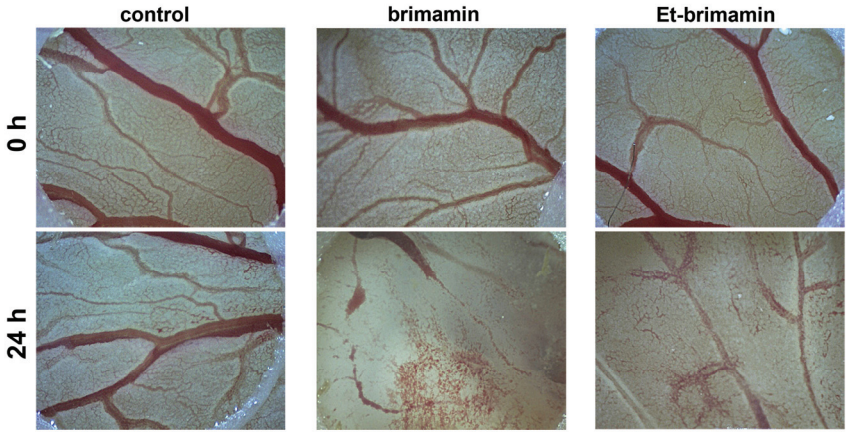

Abbildung 13 – Effekte auf das Blutgefäßsystem der Chorioallantois-membran (CAM) in fertilisierten Hühner-eiern durch Brimamin und Et-Brimamin. [Reprinted from Springer Invest. New Drugs doi: 10.1007/s10637-015-0215-9. K. Mahal, B. Biersack, *et al.* with kind permission from Springer Science and Business Media.]

Dass die durch Et-Brimamin beeinflusste Mikrotubuli-, Aktinfilament- und Fokaladhäsionsdynamik nicht nur für die Integrität des Endothels, sondern auch für die funktionierende Zellmigration essentiell ist, konnte in verschiedenen dreidimensionalen (3D) Migrationsassays gezeigt werden. In diesen *in vitro*-Modellsystemen folgen kultivierte Tumorzellen einem Nährstoffgradienten und überwinden dabei entweder aktiv eine Matrix aus Fibronectin und Kollagen ähnlich der natürlichen ECM (Matrigel; Transwell-Migrations-assay) oder eine konfluente Endothelzellschicht, was die Penetration von Blutgefäßen (*Intravasation/Extravasation*, vgl. *Kapitel 1.3* und Abbildung 2) simuliert. Nicht toxische Konzentrationen von Et-Brimamin reichten in diesen Assays aus, um die Motilität von Zellen einer metastasierenden Melanomzelllinie deutlich zu reduzieren. Die effektivsten Imidazole der Serie stellen somit nicht nur eine Verbindungsklasse mit verbesserter Toxizität und

Selektivität dar, sondern besitzen neben ihren vaskular-disruptiven Eigenschaften auch das Potential, in Zytoskelett-vermittelte Metastasierungsprozesse und die Invasion von Tumorzellen einzugreifen.

Aufgrund der verbesserten Wasserlöslichkeit und metabolischen Stabilität der Imidazol-Analoga im Vergleich zur CA-4-Leitstruktur, erscheinen weitere *in vivo*-Studien zur antimetastatischen Wirkung der besten Derivate Et-Brimamin und Brimamin sinnvoll. Auch die Bestimmung der Plasma-Halbwertszeit von Brimamin- und seinen Derivaten im Vergleich zu der von CA-4-P steht noch aus, könnte aber erste Rückschlüsse auf eine generell höhere, antitumorale *in vivo*-Effizienz der Imidazole durch höhere Plasmakonzentrationen zulassen.

Weitere Details in: K. Mahal, B. Biersack, H. Caysa, R. Schobert, T. Mueller.
Combretastatin A-4 derived imidazoles show cytotoxic, antivascular, and antimetastatic effects based on cytoskeletal reorganisation.
Invest. New Drugs **2015** *33*, 541-554.
[**Publikation III**]

3.2.4 Die Rolle von verschiedenen Kinasen und NF-kappaB-Aktivität für die antivaskuläre und antitumorale Wirkung des CA-4-abgeleiteten VDA Brimamin

Der exakte Wirkmechanismus und der Grund für die hohe Selektivität der neuen Imidazol-basierten VDAs sollte auch im Hinblick auf seine klinische Relevanz und im Vergleich zu den für CA-4-P bereits publizierten Effekten untersucht werden. Wie in Studien von *Kanthou* und *Tozer et al.* für CA-4-P beschrieben, spielen neben Rho-*Signalling* auch MAP-Kinasen eine wichtige Rolle für den vaskular-disruptiven Effekt des *Prodrugs*.[95,97] Im ersten Teil der hier vorliegenden Studie wird der Einfluss selektiver Kinase-Inhibitoren auf die Brimamin-vermittelte Endothelzell-Toxizität, Apoptose-Induktion und Störung der endothelialen Differenzierung untersucht. In Toxizitätstests (MTT-Assays) und durchflusszytometrischer Analyse apoptotischer Zellen wurden synergistische Effekte für Brimamin und Inhibitoren von PI3K und ERK1/2 gefunden. Die gleichzeitige Inhibition von ERK1/2, die als pro-proliferativer Regulator gilt und PI3K, die gerade in Endothelzellen als *downstream*-Mediator der VEGFR-Signaltransduktion für Migrationsverhalten und Regulation von Aktin-Zytoskelett- und Fokaladhäsionsdynamik ist, scheint nicht nur die Endothelzell-Toxizität von Brimamin zu erhöhen, sondern auch dessen antivaskulären Effekt zu verstärken. Die Inhibition der *c-Jun N-terminalen Kinase* (JNK) wirkte sich dagegen negativ auf die Brimamin-Effekte in Endothelzellen aus: Gleichzeitige Behandlung mit einem JNK-Inhibitor reduzierte sowohl Zytotoxizität und Apoptoserate, als auch die Anfälligkeit endothelialer Netzwerke in *Tube formation*-Assays für die sonst disruptiven Eigenschaften von Brimamin gegen diese multizellulären Verzweigungen aufgrund von Zytoskelett-Fehlorganisation. Beides scheint auf Funktionen von JNK in mitotischen oder Interphase-Zellen zu beruhen. So wurde bereits durch andere Arbeitsgruppen nachgewiesen, dass JNK in mitotischen Zellen grundsätzlich aktiviert ist und verlängerter mitotischer Arrest durch Inkubation mit antimitotischen Substanzen wie Tubulin-Bindern, letztlich zum Auslösen von Apoptose führt. JNK-vermittelte Apoptose stellt somit einen wichtigen Sekundäreffekt für die Toxizität von Brimamin dar, der durch Inhibition der Kinase unterbunden werden kann. In Interphase-Zellen ist JNK zudem über Phosphorylierung von Stathmin, dem natürlichen Stabilisatorprotein der Tubulin-Heterodimere, an der Regulation von Mikrotubuli-Stabilität beteiligt. Die Inhibition von JNK kann somit der Mikrotubuli-destabilisierenden Wirkung von Brimamin entgegenwirken. Weiterhin wurde gefunden, dass bei Brimamin wie im Falle von CA-4-P die Bildung von Aktin-*Stress fibres* einem Rho/ROCK-abhängigen Mechanismus zuzuordnen ist. Diese Kombinationstests aus Brimamin und Kinase-Inhibitoren erlauben

somit weitere Einblicke in den molekularen Wirkmechanismus und das Zusammenspiel von Proteinen, die an den vaskular-disruptiven Sekundäreffekten beteiligt sein könnten. Sie sollen später auch als Grundlage für weitere geplante Untersuchungen des Zusammenspiels von Rho-, JNK- und NF-kappaB-Signaltransduktion dienen. Der Transkriptionsfaktor NF-kappaB stellt eine der Hauptursachen für die MDR in einigen hoch-resistenten Brust- und Pankreaskarzinomen dar. Diese bilden einen der Forschungsschwerpunkte unserer Kooperationspartner an der *Wayne State University School of Medicine* in Detroit. Ihre Untersuchungen an den klinischen relevanten Zelllinien MDA-MB-231 und BxPC-3 zeigten nicht nur eine verbesserte *in vitro*-Zytotoxizität und Apoptose-induzierende Wirkung für Brimamin im Vergleich zu CA-4, sondern auch reduzierte NF-kappaB-Proteinlevel in Xenograft-Tumoren, die über einen Zeitraum von 30 Tagen mit Brimamin behandelt wurden. Es ist literaturbekannt, dass für NF-kappaB-Translokalisation in den Zellkern, wo es als Transkriptionsfaktor die Expression Resistenz-vermittelnder Gene induziert, intakte Mikrotubuli als Mediator von Vesikeltransport nötig sind. In Endothelzellen konnten wir zeigen, dass diese Translokalisierung durch Brimamin unterbunden wird. Da bekannt ist, dass die Expressionprodukte von NF-kappaB-Zielgenen die JNK-Aktivität hemmen können, erscheint der Brimamin-Effekt auf diesen Signalweg besonders wichtig. Ähnliche Effekte wurden für CA-4 oder CA-4-P bislang nicht beschrieben. Die Untersuchungen zu diesem Anti-MDR-Effekt von Brimamin stehen zwar erst am Anfang und sollen in weiterführenden Studien im Detail untersucht werden, liefern aber jetzt schon erste Einblicke in das Potential von Brimamin für die Behandlung von multiresistenten Tumoren.

Weitere Details in: K. Mahal, A. Ahmad, M. Resch, R. Ficner, F. H. Sarkar, R. Schobert, B. Biersack.
Contribution of JNK signaling and NF-kappaB activity to the anticancer effects of the vascular-disrupting agent Brimamin.
- to be submitted -
[**Manuskript IV**]

3.3 Biologische Evaluation von Histondeacetylase-Inhibitoren

Histondeacetylase-Inhibitoren (HDACi) stellen eine weitere vielversprechende Klasse von Chemotherapeutika dar, wie nicht zuletzt die Vielzahl von HDACi in aktuellen klinischen Studien zeigt (vgl. *Kapitel 1.4.2*). Darunter nehmen den größten Anteil Hydroxamsäure-basierte HDACi ein.

3.3.1 Biologische Evaluation von Hydroxamsäure-basierten Histondeacetylase-Inhibitoren (HDACi) mit neuartigem 4,5-Diarylimidazol-Strukturmotiv als bimodale Wirkstoffe mit antitumoraler und antiangiogener Wirkung

Die Erweiterung unseres Imidazol-Motivs um Hydroxamsäure-Reste, die typischerweise HDAC-Inhibition vermitteln, zielte ursprünglich auf die Generierung bimodaler Wirkstoffe ab, die sowohl Tubulin-Binder-Eigenschaften als auch HDAC-Inhibition in sich vereinen. Die hier vorgestellte, erste Serie setzt sich aus einer Reihe von 4,5-Diarylimidazolen und -oxazolen mit Variationen des ursprünglich CA-4-abgeleiteten Trimethoxyphenyl-Motivs und der Erweiterung des B-Rings um Cinnamylhydroxamsäure-Reste zusammen. Die beiden Derivate mit der generell höchsten Toxizität gegen eine Auswahl an Krebszelllinien sind in Abbildung 14 dargestellt [Substanz **3a** und **3c** in **Publikation V**]. Sie zeigten im direkten Vergleich mit dem klinisch eingesetzten HDACi Vorinostat nicht nur eine verbesserte zytotoxische Wirkung, sondern auch eine verbesserte Selektivität für Krebszellen. Im Gegensatz zu den ursprünglichen Imidazolen besitzen die Derivate des neuen Imidazol-Cinnamylhydroxamsäure-Typs keine Tubulin-bindenden Eigenschaften mehr. Stattdessen führte die Behandlung von Zellen der stark metastasierenden Zelllinie 518A2 mit den Derivaten zur Hyperacetylierung verschiedener HDAC-Substrate wie der Histonkomplex-Untereinheit Histon-H2B und alpha-Tubulin. Die neuen Derivate inhibieren demnach nicht nur Zellkern-assozierte HDACs, sondern auch die zytoplasmatische Tubulin-Deacetylase HDAC6. Sie sind somit aufgrund ihrer unspezifischen Breitband-Inhibierung von HDAC-Isoformen, wie auch Vorinostat den so genannten *pan*-HDAC-Inhibitoren zuzuordnen. Neben der Acetylierung der Mikrotubuli führt die Inkubation mit den Derivaten *in vitro* zur Bildung von Aktin-*Stress fibres* und reduziert das invasive Verhalten der Melanomzellen in 3D-Migrationsassays

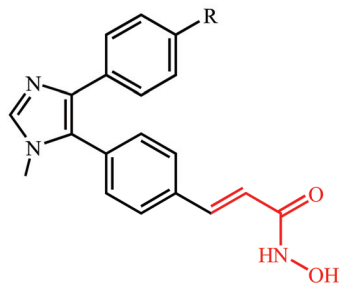

Bimacroxam: R = H
Animacroxam: R = OMe

Abbildung 14 – Struktur der zwei effektivsten *N*-Methyl-4,5-diarylimidazole mit Hydroxamsäure-Rest.

deutlich effektiver als der HDACi Vorinostat. Erste *in vivo*-Untersuchungen im CAM-Assay-Modell zur potentiellen antiangiogenen Wirkung zeigten zudem enormen Einfluss auf Ausbildung und Morphologie des Blutgefäßsystems durch das Derivat Bimacroxam. Neben dem Ausdünnen bereits bestehender Blutgefäße konnte eine deutliche Reduktion neugebildeter Kapillaren beobachtet werden. Die Inhibition des Angiogeneseprozesses ist ein literaturbekannter Effekt für viele HDACi und könnte auch im Falle der neuen Imidazol-HDACi auf Fehlregulation der Genexpression, Veränderung der Proteinstabilität pro-angiogener Faktoren durch Hyperacetylierung oder auf die Inhibition Angiogenese-relevanter Signaltransduktionswege zurückzuführen sein. Die weitere Charakterisierung der hier vorgestellten, neuen Wirkstoffklasse 4,5-Diphenylimidazol-basierter HDACi mit Acrylhydroxamsäure-Resten ist der Inhalt nachfolgender, weiterführender Studien, die sich im Detail mit dem molekularen und biochemischen Wirkmechanismus der Derivate beschäftigen.

Weitere Details in: K. Mahal, S. Schruefer, G. Steinemann, F. Rausch, R. Schobert, B. Biersack, M. Höpfner.
Biological Evaluation of 4,5-diarylimidazoles with hydroxamic acid appendages as novel dual mode anticancer agents.
Cancer Chemother. Pharmacol. **2015** *75,* 691-700.
[**Publikation V**]

3.3.2 Tumorwachstum-relevante Signaltransduktion und Zytoskelett-Organisation als *Target* neuer pleiotroper Histondeacetylase-Inhibitoren des 4,5-Diarylimidazol-Typs mit Zimtsäure-Hydroxamat-Resten

Detailliertere Einblicke in den Wirkmechanismus der Imidazol-basierten HDACi wurden anhand von zellbiologischen Experimenten zur Aktivität eines neuen, weiter optimierten *N*-Ethyl-Imidazol-Analogs [Substanz **3** in **Manuskript VI**] gewonnen. Im Vergleich zu klinisch etablierten Hydroxamsäure-Derivaten wie Vorinostat und den wirksamsten *N*-Methyl-Analoga der vorherigen Serie [Substanz **1** und **2** in **Manuskript VI**], zeigte das neue, mit dem Kurznamen Etacrox bezeichnete Derivat ein weiter verbessertes Zytotoxizitätsprofil gegen resistente Krebszelllinien bei Erhalt der geringen Toxizität gegen nicht-maligne Fibroblasten (Strukturen relevanter Derivate, vgl. Abbildung 15).

Die Inkubation mit Etacrox führte zur effektiven Acetylierung von alpha-Tubulin (Abbildung 16). Western Blot-Analysen der Acetyl-Tubulin-Level in Etacrox-behandelten Zellen zeigten zudem eine schnellere, effizientere Mikrotubuli-Acetylierung im direkten Vergleich mit Vorinostat. Wie Aktivitätstests an den rekombinanten, humanen HDAC-Isoenzymen HDAC1 und HDAC6 vermuten lassen, ist dies auf eine höhere Spezifität der Imidazol-HDACi für die Tubulin-Deacetylase HDAC6 zurückzuführen. Wie bereits in einigen Publikationen über HDACi beschrieben, wirkt sich die vermehrte Acetylierung der Mikrotubuli auch auf deren Stabilität aus. Für Etacrox konnte in 518A2-Melanomzellen eine Verschiebung des Gleichgewichts von löslichen zu polymersierten Tubulin-Heterodimeren und somit eine Stabilisierung von Interphase-Mikrotubuli nachgewiesen werden. Übermäßigs Wachstum der Mikrotubuli und ihre vermehrte Stabilität sind die Konsequenz einer Fehlregulation der Mikrotubuli-Dynamik und ziehen die Aktivierung einiger, wahrscheinlich Rho-vermittelter Signalwege nach sich, die auch zu Veränderungen in der Fokaladhäsionsdynamik führen. Eine wichtige Konsequenz für diese Dynamik nach Behandlung von Melanom- aber auch Endothelzellen mit Etacrox war die Verdickung gebildeter Fokaladhäsionen und die vermutlich daraus resultierende, eingeschränkte Migrationsfähigkeit. Auch die verstärkte Einbindung von beta-Catenin in interzelluläre Cadherin-Catenin-Adhäsionskomplexe und die augenscheinliche Inhibition der

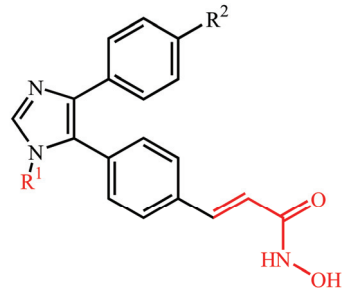

Bimacroxam:	R^1 = Me,	R^2 = H
Animacroxam:	R^1 = Me,	R^2 = OMe
Etacrox:	R^1 = Et,	R^2 = OMe

Abbildung 15 – Strukturen der effektivsten *N*-Methyl-4,5-Diarylimidazole mit Hydroxamsäure-Resten und ihre Trivialnamen.

Translokation von beta-Catenin in den Zellkern, wo es als Transkriptionsfaktor für die Expression proliferations-relevanter Zielgene verantwortlich ist, sind vermutlich Effekte vermehrter Proteinacetylierung. Zudem zeigten sowohl Etacrox als auch Bimacroxam im Vergleich zu Vorinostat verbesserte inhibitorische Wirkung auf die Migrations-relevante Proteinkinase Akt. Dieser Effekt scheint auf die höhere Spezifiät der Imidazol-Derivate für die zytoplasmatische HDAC6 oder zytoplasmatische HDAC-Isoformen im Allgemeinen zurückzuführen sein.

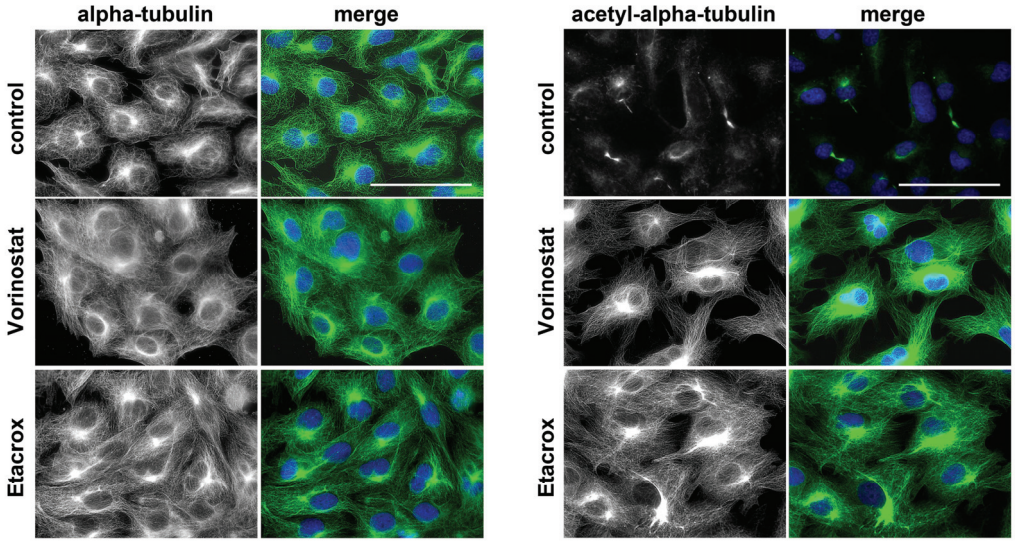

Abbildung 16 – Inkubation mit Vorinostat und Etacrox führen zu vermehrter Mikrotubuli-Acetylierung in Melanomzellen. Fluoreszenzmikroskopische Visualisierung der Mikrotubuli (links, alpha-Tubulin) und ihres Acetylierungsstatus (rechts, acetyl-alpha-tubulin) in unbehandelten (control), Vorinostat (5 µM)- oder Etacrox (2.5 µM)-behandelten Zellen nach 24 h, merge = Überlagerung von Immunofluoreszenz-markierten Mikrotubuli (grün) und Zellkerngegenfärbung (blau) mit DAPI. 400-fache Vergrößerung, Maßstabsbalken = 100 µm.

Einige in der Literatur beschriebene Hydroxamsäure-Derivate werden zudem als Inhibitoren der pro-angiogenen und pro-metastatischen Matrix-Metalloproteinasen (MMPs) eingesetzt. Jedoch besitzen entsprechende Hydroxamsäure-Analoga meist hohe Selektivität für diese eine Klasse von Metall-abhängigen Enzymen. Auch Hydroxamsäure-basierte HDACi wie Vorinostat zeigen meiste eine hohe Spezifität für HDACs, aber trotz ihrer Metall-bindenden Funktion nur geringe Aktivität gegenüber MMPs.[149] Interessanterweise ist Etacrox aber in der Lage, die Aktivität der pro-angiogenen und pro-metastatischen MMP-2 und MMP-9 direkt zu inhibieren. Es besitzt somit nicht nur HDAC-inhibitorische Wirkung, sondern auch Breitbandwirkung gegen andere Metalloenzyme wie MMPs. Da diese nicht nur für gerichtete Tumorzell-Migration, sondern auch für Angiogenese und Wachstumsfaktor-Freisetzung aus

der ECM essentiell sind, könnte dieser zusätzliche Effekt für die im Vergleich zu Vorinostat verstärkte, antimetastatische und antiangiogene Wirkung von Etacrox verantwortlich sein.
Beides wurde in der vorliegenden Arbeit anhand von 3D-Migrationsstudien *in vitro* und mit Hilfe des CAM-Assays *in vivo* untersucht: In den *in vitro*-Studien reichten nicht- oder nur geringfügig toxische Konzentrationen an Etacrox aus, die Invasion und Überwindung simulierter ECM-Barrieren durch Tumorzellen zu hemmen. Zudem konnte gezeigt werden, dass Wachstum und Reifung von Blutgefäßen innerhalb der CAM fertilisierter Hühnereier nach topischer Behandlung mit Etacrox deutlich beeinflusst werden (Abbildung 17).

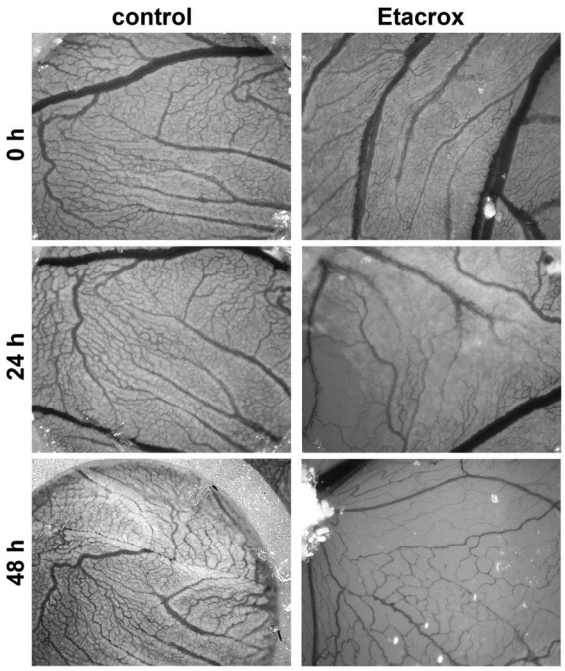

Abbildung 17 – Anti-angiogene Effekte auf das Blutgefäßsystem der Chorioallantoismembran (CAM) in fertilisierten Hühnereiern durch den HDACi Etacrox.

Die Vielzahl der von Etacrox-induzierten Effekte wie die Störung der Mikrotubuli- und Fokaladhäsions-Dynamik, die Inhibition wichtiger Signalkaskaden und die direkte Inhibition von MMPs, scheinen verantwortlich für die erhebliche Einschränkung von Tumorzell-Motilität und angiogenen Prozessen zu sein. Aufgrund seiner guten Verträglichkeit und Applizierbarkeit in ersten Tests an Mäusen werden aktuell weitere *in vivo*-Studien durchgeführt, die detailliertere Einblicke in das Potential dieser neuen Wirkstoffklasse ermöglichen sollten.

Weitere Details in: K. Mahal, P. Kahlen, B. Biersack, R. Schobert.
A new pleiotropic HDAC inhibitor targeting cancer cell signalling and cytoskeletal organisation.
- to be submitted - [**Manuskript VI**]

4 Literaturverzeichnis

(1) Hanahan, D., and Weinberg, R. A. (2000) The hallmarks of cancer. C*ell 100*, 57–70.

(2) Hanahan, D., and Weinberg, R. A. (2011) Hallmarks of Cancer: The Next Generation. *Cell 144*, 646–674.

(3) Lazebnik, Y. (2010) What are the hallmarks of cancer? *Nat. Rev. Cancer 10*, 232–233.

(4) Ribatti, D. (2014) Introduction, in *Angiogenesis and Anti-Angiogenesis in Hematological Malignancies*, pp 1–5. Springer Netherlands, Dordrecht.

(5) Carmeliet, P. (2005) Angiogenesis in life, disease and medicine. *Nature 438*, 932–936.

(6) Kushner, E. J., and Bautch, V. L. (2013) Building blood vessels in development and disease: *Curr. Opin. Hematol. 20,* 231-236.

(7) Ribatti, D. (2006) Genetic and epigenetic mechanisms in the early development of the vascular system. *J. Anat. 208*, 139–152.

(8) Gomes, F. G., Nedel, F., Alves, A. M., Nör, J. E., and Tarquinio, S. B. C. (2013) Tumor angiogenesis and lymphangiogenesis: Tumor/endothelial crosstalk and cellular/microenvironmental signaling mechanisms. *Life Sci. 92*, 101–107.

(9) Folkman, J. (1971) Tumor angiogenesis: therapeutic implications. *N. Engl. J. Med. 285*, 1182–1186.

(10) Geiger, T. R., and Peeper, D. S. (2009) Metastasis mechanisms. *Biochim. Biophys. Acta 1796*, 293–308.

(11) Hanahan, D., and Folkman, J. (1996) Patterns and emerging mechanisms of the angiogenic switch during tumorigenesis. *Cell 86*, 353–364.

(12) Bergers, G., and Benjamin, L. E. (2003) Tumorigenesis and the angiogenic switch. *Nat. Rev. Cancer 3*, 401–410.

(13) De Bock, K., Cauwenberghs, S., and Carmeliet, P. (2011) Vessel abnormalization: another hallmark of cancer? Molecular mechanisms and therapeutic implications. *Curr. Opin. Genet. Dev. 21*, 73–79.

(14) Liu, W., Ahmad, S. A., Reinmuth, N., Shaheen, R. M., Jung, Y. D., Fan, F., and Ellis, L. M. (2000) Endothelial cell survival and apoptosis in the tumor vasculature. *Apoptosis Int. J. Program. Cell Death 5*, 323–328.

(15) Chrzanowska-Wodnicka, M., and Burridge, K. (1996) Rho-stimulated contractility drives the formation of stress fibers and focal adhesions. *J. Cell Biol. 133*, 1403–1415.

(16) Ghosh, K., Thodeti, C. K., Dudley, A. C., Mammoto, A., Klagsbrun, M., and Ingber, D. E. (2008) Tumor-derived endothelial cells exhibit aberrant Rho-mediated mechanosensing and abnormal angiogenesis in vitro. *Proc. Natl. Acad. Sci. 105*, 11305–11310.

(17) Fiorio Pla, A., Ong, H. L., Cheng, K. T., Brossa, A., Bussolati, B., Lockwich, T., Paria, B., Munaron, L., and Ambudkar, I. S. (2012) TRPV4 mediates tumor-derived endothelial cell migration via arachidonic acid-activated actin remodeling. *Oncogene 31*, 200–212.

(18) Matsuda, K., Ohga, N., Hida, Y., Muraki, C., Tsuchiya, K., Kurosu, T., Akino, T., Shih, S.-C., Totsuka, Y., Klagsbrun, M., Shindoh, M., and Hida, K. (2010) Isolated tumor endothelial cells maintain specific character during long-term culture. *Biochem. Biophys. Res. Commun. 394*, 947–954.

(19) Ohga, N., Ishikawa, S., Maishi, N., Akiyama, K., Hida, Y., Kawamoto, T., Sadamoto, Y., Osawa, T., Yamamoto, K., Kondoh, M., Ohmura, H., Shinohara, N., Nonomura, K., Shindoh, M., and Hida, K. (2012) Heterogeneity of tumor endothelial cells. *Am. J. Pathol. 180*, 1294–1307.

(20) Bacac, M., and Stamenkovic, I. (2008) Metastatic cancer cell. *Annu. Rev. Pathol. Mech. Dis. 3*, 221–247.

(21) Deryugina, E. I., and Quigley, J. P. (2006) Matrix metalloproteinases and tumor metastasis. *Cancer Metastasis Rev. 25*, 9–34.

(22) Thiery, J. P., and Sleeman, J. P. (2006) Complex networks orchestrate epithelial–mesenchymal transitions. *Nat. Rev. Mol. Cell Biol. 7*, 131–142.
(23) Polyak, K., and Weinberg, R. A. (2009) Transitions between epithelial and mesenchymal states: acquisition of malignant and stem cell traits. *Nat. Rev. Cancer 9*, 265–273.
(24) Conacci-Sorrell, M., Zhurinsky, J., and Ben-Ze'ev, A. (2002) The cadherin-catenin adhesion system in signaling and cancer. *J. Clin. Invest. 109*, 987–991.
(25) Wheelock, M. J., and Johnson, K. R. (2003) Cadherins as modulators of cellular phenotype. *Annu. Rev. Cell Dev. Biol. 19*, 207–235.
(26) Friedl, P., and Wolf, K. (2003) Tumour-cell invasion and migration: diversity and escape mechanisms. *Nat. Rev. Cancer 3*, 362–374.
(27) Orgaz, J. L., and Sanz-Moreno, V. (2013) Emerging molecular targets in melanoma invasion and metastasis. *Pigment Cell Melanoma Res. 26*, 39–57.
(28) Van Nieuw Amerongen, G. P., and van Hinsbergh, V. W. M. (2001) Cytoskeletal effects of Rho-like small guanine nucleotide-binding proteins in the vascular system. *Arterioscler. Thromb. Vasc. Biol. 21*, 300–311.
(29) Zamir, E., and Geiger, B. (2001) Molecular complexity and dynamics of cell-matrix adhesions. *J. Cell Sci. 114*, 3583–3590.
(30) Wozniak, M. A., Modzelewska, K., Kwong, L., and Keely, P. J. (2004) Focal adhesion regulation of cell behavior. *Biochim. Biophys. Acta BBA - Mol. Cell Res. 1692*, 103–119.
(31) Leong, H. S., Robertson, A. E., Stoletov, K., Leith, S. J., Chin, C. A., Chien, A. E., Hague, M. N., Ablack, A., Carmine-Simmen, K., McPherson, V. A., Postenka, C. O., Turley, E. A., Courtneidge, S. A., Chambers, A. F., and Lewis, J. D. (2014) Invadopodia are required for cancer cell extravasation and are a therapeutic target for metastasis. *Cell Rep. 8*, 1558–1570.
(32) Wu, H., Goel, V., and Haluska, F. G. (2003) PTEN signaling pathways in melanoma. *Oncogene 22*, 3113–3122.
(33) Stahl, J. M., Sharma, A., Cheung, M., Zimmerman, M., Cheng, J. Q., Bosenberg, M. W., Kester, M., Sandirasegarane, L., and Robertson, G. P. (2004) Deregulated Akt3 activity promotes development of malignant melanoma. *Cancer Res. 64*, 7002–7010.
(34) Krauthammer, M., Kong, Y., Ha, B. H., Evans, P., Bacchiocchi, A., McCusker, J. P., Cheng, E., Davis, M. J., Goh, G., Choi, M., Ariyan, S., Narayan, D., Dutton-Regester, K., Capatana, A., Holman, E. C., Bosenberg, M., Sznol, M., Kluger, H. M., Brash, D. E., Stern, D. F., Materin, M. A., Lo, R. S., Mane, S., Ma, S., Kidd, K. K., Hayward, N. K., Lifton, R. P., Schlessinger, J., Boggon, T. J., and Halaban, R. (2012) Exome sequencing identifies recurrent somatic RAC1 mutations in melanoma. *Nat. Genet. 44*, 1006–1014.
(35) Hodis, E., Watson, I. R., Kryukov, G. V., Arold, S. T., Imielinski, M., Theurillat, J.-P., Nickerson, E., Auclair, D., Li, L., Place, C., DiCara, D., Ramos, A. H., Lawrence, M. S., Cibulskis, K., Sivachenko, A., Voet, D., Saksena, G., Stransky, N., Onofrio, R. C., Winckler, W., Ardlie, K., Wagle, N., Wargo, J., Chong, K., Morton, D. L., Stemke-Hale, K., Chen, G., Noble, M., Meyerson, M., Ladbury, J. E., Davies, M. A., Gershenwald, J. E., Wagner, S. N., Hoon, D. S. B., Schadendorf, D., Lander, E. S., Gabriel, S. B., Getz, G., Garraway, L. A., and Chin, L. (2012) A landscape of driver mutations in melanoma. *Cell 150*, 251–263.
(36) Dráber, P., Sulimenko, V., and Dráberová, E. (2012) Cytoskeleton in mast cell signaling. *Front. Immunol. 3*, 130.
(37) Akhmanova, A., and Steinmetz, M. O. (2008) Tracking the ends: a dynamic protein network controls the fate of microtubule tips. *Nat. Rev. Mol. Cell Biol. 9*, 309–322.
(38) Etienne-Manneville, S. (2013) Microtubules in cell migration. *Annu. Rev. Cell Dev. Biol. 29*, 471–499.
(39) Akhshi, T. K., Wernike, D., and Piekny, A. (2014) Microtubules and actin crosstalk in cell migration and division. *Cytoskeleton 71*, 1–23.

(40) Yamada, H. Y., and Gorbsky, G. J. (2006) Spindle checkpoint function and cellular sensitivity to antimitotic drugs. *Mol. Cancer Ther. 5*, 2963–2969.
(41) Ng, D. C. H., Zhao, T. T., Yeap, Y. Y. C., Ngoei, K. R., and Bogoyevitch, M. A. (2010) c-Jun N-terminal kinase phosphorylation of stathmin confers protection against cellular stress. *J. Biol. Chem. 285*, 29001–29013.
(42) Lieuvin, A., Labbé, J.-C., Dorée, M., and Job, D. (1994) Intrinsic microtubule stability in interphase cells. *J. Cell Biol. 124*, 985–996.
(43) Akisaka, T., Yoshida, H., and Takigawa, T. (2011) Differential distribution of posttranslationally modified microtubules in osteoclasts. *J. Histochem. Cytochem. 59*, 630–638.
(44) Westermann, S., and Weber, K. (2003) Post-translational modifications regulate microtubule function. *Nat. Rev. Mol. Cell Biol. 4*, 938–948.
(45) Ballestrem, C., Wehrle-Haller, B., Hinz, B., and Imhof, B. A. (2000) Actin-dependent lamellipodia formation and microtubule-dependent tail retraction control-directed cell migration. *Mol. Biol. Cell 11*, 2999–3012.
(46) Reed, N. A., Cai, D., Blasius, T. L., Jih, G. T., Meyhofer, E., Gaertig, J., and Verhey, K. J. (2006) Microtubule acetylation promotes Kinesin-1 binding and transport. *Curr. Biol. 16*, 2166–2172.
(47) Kaverina, I., and Straube, A. (2011) Regulation of cell migration by dynamic microtubules. *Semin. Cell Dev. Biol. 22*, 968–974.
(48) Lu, D.-Y., Lu, T.-R., and Wu, H.-Y. (2013) New insights into individualized antimetastatic therapy. *Adv. Tech. Biol. Med. 1*, 106-109.
(49) Marques, M. P. M., Gianolio, D., Cibin, G., Tomkinson, J., Parker, S. F., Valero, R., Pedro Lopes, R., and Batista de Carvalho, L. A. E. (2015) A molecular view of cisplatin's mode of action: interplay with DNA bases and acquired resistance. *Phys Chem Chem Phys*. *17*, 5155-5171.
(50) Okuma, Y., Saito, M., Hosomi, Y., Sakuyama, T., and Okamura, T. (2015) Key components of chemotherapy for thymic malignancies: a systematic review and pooled analysis for anthracycline-, carboplatin- or cisplatin-based chemotherapy. *J. Cancer Res. Clin. Oncol. 141*, 323–331.
(51) Rossi, A., Chiodini, P., Sun, J.-M., O'Brien, M. E. R., von Plessen, C., Barata, F., Park, K., Popat, S., Bergman, B., Parente, B., Gallo, C., Gridelli, C., Perrone, F., and Di Maio, M. (2014) Six versus fewer planned cycles of first-line platinum-based chemotherapy for non-small-cell lung cancer: a systematic review and meta-analysis of individual patient data. *Lancet Oncol. 15*, 1254–1262.
(52) Minotti, G. (2004) Anthracyclines: Molecular advances and pharmacologic developments in antitumor activity and cardiotoxicity. *Pharmacol. Rev. 56*, 185–229.
(53) Singh, N. (2014) Erlotinib usage after prior treatment with gefitinib in advanced non-small cell lung cancer: A clinical perspective and review of published literature. *World J. Clin. Oncol. 5*, 858-864.
(54) Tartarone, A., Lerose, R., Lazzari, C., Gregorc, V., and Aieta, M. (2014) Which tyrosine kinase inhibitor should be recommended as initial treatment for non-small cell lung cancer patients with EGFR mutations? *Med. Oncol. 31*, 78.
(55) Zhang, J., Yu, J., Sun, X., and Meng, X. (2014) Epidermal growth factor receptor tyrosine kinase inhibitors in the treatment of central nerve system metastases from non-small cell lung cancer. *Cancer Lett. 351*, 6–12.
(56) Spaans, J. N., and Goss, G. D. (2015) Epidermal growth factor receptor tyrosine kinase inhibitors in early-stage nonsmall cell lung cancer. *Curr. Opin. Oncol. 27*, 102-107.
(57) Sun, L., Ma, J.-T., Zhang, S.-L., Zou, H.-W., and Han, C.-B. (2015) Efficacy and safety of chemotherapy or tyrosine kinase inhibitors combined with bevacizumab versus chemotherapy or tyrosine kinase inhibitors alone in the treatment of non-small cell lung

cancer: a systematic review and meta-analysis. *Med. Oncol. Northwood Lond. Engl. 32*, 473.

(58) Spigel, D. R., Patel, J. D., Reynolds, C. H., Garon, E. B., Hermann, R. C., Govindan, R., Olsen, M. R., Winfree, K. B., Chen, J., Liu, J., Guba, S. C., Socinski, M. A., and Bonomi, P. (2015) Quality of life analyses from the randomized, open-label, phase III point break study of pemetrexed-carboplatin-bevacizumab followed by maintenance pemetrexed-bevacizumab versus paclitaxel-carboplatin-bevacizumab followed by maintenance bevacizumab in patients with stage IIIB or IV nonsquamous non-small-cell lung cancer. *J. Thorac. Oncol. Off. Publ. Int. Assoc. Study Lung Cancer 10*, 353–359.

(59) Eckford, P. D. W., and Sharom, F. J. (2009) ABC efflux pump-based resistance to chemotherapy drugs. *Chem. Rev. 109*, 2989–3011.

(60) Song, H., Li, C.-W., Labaff, A. M., Lim, S.-O., Li, L.-Y., Kan, S.-F., Chen, Y., Zhang, K., Lang, J., Xie, X., Wang, Y., Huo, L.-F., Hsu, S.-C., Chen, X., Zhao, Y., and Hung, M.-C. (2011) Acetylation of EGF receptor contributes to tumor cell resistance to histone deacetylase inhibitors. *Biochem. Biophys. Res. Commun. 404*, 68–73.

(61) Sacher, A. G., Jänne, P. A., and Oxnard, G. R. (2014) Management of acquired resistance to epidermal growth factor receptor kinase inhibitors in patients with advanced non-small cell lung cancer: Acquired resistance to EGFR kinase inhibitors. *Cancer 120*, 2289–2298.

(62) Lavi, O., Greene, J. M., Levy, D., and Gottesman, M. M. (2013) The role of cell density and intratumoral heterogeneity in multidrug resistance. *Cancer Res. 73*, 7168–7175.

(63) Mina, L. A., and Sledge, G. W. (2011) Rethinking the metastatic cascade as a therapeutic target. *Nat. Rev. Clin. Oncol. 8*, 325-332.

(64) Trédan, O., Lacroix-Triki, M., Guiu, S., Mouret-Reynier, M.-A., Barrière, J., Bidard, F.-C., Braccini, A.-L., Mir, O., Villanueva, C., and Barthélémy, P. (2014) Angiogenesis and tumor microenvironment: bevacizumab in the breast cancer model. *Target. Oncol. Epub ahead of print/in press.*

(65) Gutierrez, M., and Giaccone, G. (2008) Antiangiogenic therapy in nonsmall cell lung cancer. *Curr. Opin. Oncol. 20*, 176–182.

(66) Willett, C. G., Boucher, Y., di Tomaso, E., Duda, D. G., Munn, L. L., Tong, R. T., Chung, D. C., Sahani, D. V., Kalva, S. P., Kozin, S. V., Mino, M., Cohen, K. S., Scadden, D. T., Hartford, A. C., Fischman, A. J., Clark, J. W., Ryan, D. P., Zhu, A. X., Blaszkowsky, L. S., Chen, H. X., Shellito, P. C., Lauwers, G. Y., and Jain, R. K. (2004) Direct evidence that the VEGF-specific antibody bevacizumab has antivascular effects in human rectal cancer. *Nat. Med. 10*, 145–147.

(67) Ellis, L. M., and Hicklin, D. J. (2008) VEGF-targeted therapy: mechanisms of anti-tumour activity. *Nat. Rev. Cancer 8*, 579–591.

(68) Weis, S. M., and Cheresh, D. A. (2011) Tumor angiogenesis: molecular pathways and therapeutic targets. *Nat. Med. 17*, 1359–1370.

(69) Pàez-Ribes, M., Allen, E., Hudock, J., Takeda, T., Okuyama, H., Viñals, F., Inoue, M., Bergers, G., Hanahan, D., and Casanovas, O. (2009) Antiangiogenic therapy elicits malignant progression of tumors to increased local invasion and distant metastasis. *Cancer Cell 15*, 220–231.

(70) Ebos, J. M. L., Lee, C. R., Cruz-Munoz, W., Bjarnason, G. A., Christensen, J. G., and Kerbel, R. S. (2009) Accelerated metastasis after short-term treatment with a potent inhibitor of tumor angiogenesis. *Cancer Cell 15*, 232–239.

(71) Overall, C. M., and López-Otín, C. (2002) Strategies for MMP inhibition in cancer: innovations for the post-trial era. *Nat. Rev. Cancer 2*, 657–672.

(72) Vandenbroucke, R. E., and Libert, C. (2014) Is there new hope for therapeutic matrix metalloproteinase inhibition? *Nat. Rev. Drug Discov. 13*, 904–927.

(73) Verma, R. P. (2012) Hydroxamic acids as matrix metalloproteinase inhibitors, in *Matrix Metalloproteinase Inhibitors* (Gupta, S. P., Ed.), pp 137–176. Springer Basel, Basel.

(74) Schwartz, E. L. (2009) Antivascular actions of microtubule-binding drugs. *Clin. Cancer Res. 15*, 2594–2601.
(75) Tozer, G. M., Kanthou, C., and Baguley, B. C. (2005) Disrupting tumour blood vessels. *Nat. Rev. Cancer 5*, 423–435.
(76) Kanthou, C., and Tozer, G. M. (2007) Tumour targeting by microtubule-depolymerising vascular disrupting agents. *Expert Opin. Ther. Targets 11*, 1443–1457.
(77) Kanthou, C., and Tozer, G. M. (2009) Microtubule depolymerizing vascular disrupting agents: novel therapeutic agents for oncology and other pathologies. *Int. J. Exp. Pathol. 90*, 284–294.
(78) Lippert, J. W. (2007) Vascular disrupting agents. *Bioorg. Med. Chem. 15*, 605–615.
(79) Mason, R. P., Zhao, D., Liu, L., Trawick, M. L., and Pinney, K. G. (2011) A perspective on vascular disrupting agents that interact with tubulin: preclinical tumor imaging and biological assessment. *Integr. Biol. 3*, 375.
(80) Meyer, T. (Ed.). (2010) Vascular disruptive agents for the treatment of cancer. Springer, New York.
(81) Jordan, M. A., and Wilson, L. (2004) Microtubules as a target for anticancer drugs. *Nat. Rev. Cancer 4*, 253–265.
(82) Stanton, R. A., Gernert, K. M., Nettles, J. H., and Aneja, R. (2011) Drugs that target dynamic microtubules: A new molecular perspective. *Med. Res. Rev. 31*, 443–481.
(83) Lu, Y., Chen, J., Xiao, M., Li, W., and Miller, D. D. (2012) An overview of tubulin inhibitors that interact with the colchicine binding site. *Pharm. Res. 29*, 2943–2971.
(84) Ravelli, R. B. G., Gigant, B., Curmi, P. A., Jourdain, I., Lachkar, S., Sobel, A., and Knossow, M. (2004) Insight into tubulin regulation from a complex with colchicine and a stathmin-like domain. *Nature 428*, 198–202.
(85) Nguyen, T. L., McGrath, C., Hermone, A. R., Burnett, J. C., Zaharevitz, D. W., Day, B. W., Wipf, P., Hamel, E., and Gussio, R. (2005) A common pharmacophore for a diverse set of colchicine site inhibitors using a structure-based approach. *J. Med. Chem. 48*, 6107–6116.
(86) Goto, H., Yano, S., Zhang, H., Matsumori, Y., Ogawa, H., Blakey, D. C., and Sone, S. (2002) Activity of a new vascular targeting agent, ZD6126, in pulmonary metastases by human lung adenocarcinoma in nude mice. *Cancer Res. 62*, 3711–3715.
(87) Pettit, G., Singh, S., Hamel, E., Lin, C., Alberts, D., and Garcia-Kendall, D. (1989) Isolation and structure of the strong cell growth and tubulin inhibitor combretastatin A-4. *Experientia 45*, 209–211.
(88) Siemann, D. W., Chaplin, D. J., and Walicke, P. A. (2009) A review and update of the current status of the vasculature-disabling agent combretastatin-A4 phosphate (CA4P). *Expert Opin. Investig. Drugs 18*, 189–197.
(89) Rustin, G. J., Shreeves, G., Nathan, P. D., Gaya, A., Ganesan, T. S., Wang, D., Boxall, J., Poupard, L., Chaplin, D. J., Stratford, M. R. L., Balkissoon, J., and Zweifel, M. (2010) A Phase Ib trial of CA4P (combretastatin A-4 phosphate), carboplatin, and paclitaxel in patients with advanced cancer. *Br. J. Cancer 102*, 1355–1360.
(90) Nathan, P., Zweifel, M., Padhani, A. R., Koh, D.-M., Ng, M., Collins, D. J., Harris, A., Carden, C., Smythe, J., Fisher, N., Taylor, N. J., Stirling, J. J., Lu, S.-P., Leach, M. O., Rustin, G. J. S., and Judson, I. (2012) Phase I trial of combretastatin A4 phosphate (CA4P) in combination with bevacizumab in patients with advanced cancer. *Clin. Cancer Res. 18*, 3428–3439.
(91) Ibrahim, M. A., Do, D. V., Sepah, Y. J., Shah, S. M., Van Anden, E., Hafiz, G., Donahue, J. K., Rivers, R., Balkissoon, J., Handa, J. T., Campochiaro, P. A., and Nguyen, Q. D. (2013) Vascular disrupting agent for neovascular age related macular degeneration: a pilot study of the safety and efficacy of intravenous combretastatin A-4 phosphate. *BMC Pharmacol. Toxicol. 14*, 7.

(92) Ng, Q.-S., Goh, V., Carnell, D., Meer, K., Padhani, A. R., Saunders, M. I., and Hoskin, P. J. (2007) Tumor antivascular effects of radiotherapy combined with combretastatin a4 phosphate in human non-small-cell lung cancer. *Int. J. Radiat. Oncol. Biol. Phys. 67*, 1375–1380.

(93) Bhalla, K. N. (2003) Microtubule-targeted anticancer agents and apoptosis. *Oncogene 22*, 9075–9086.

(94) Yamada, H. Y., and Gorbsky, G. J. (2006) Spindle checkpoint function and cellular sensitivity to antimitotic drugs. *Mol. Cancer Ther. 5*, 2963–2969.

(95) Williams, L. J., Mukherjee, D., Fisher, M., Reyes-Aldasoro, C. C., Akerman, S., Kanthou, C., and Tozer, G. M. (2014) An *in vivo* role for Rho kinase activation in the tumour vascular disrupting activity of combretastatin A-4 3- *O* -phosphate: Rho kinase and tumour vascular targeting. *Br. J. Pharmacol. 171*, 4902–4913.

(96) Tron, G. C., Pirali, T., Sorba, G., Pagliai, F., Busacca, S., and Genazzani, A. A. (2006) Medicinal chemistry of combretastatin A4: Present and future directions. *J. Med. Chem. 49*, 3033–3044.

(97) Kanthou, C. (2002) The tumor vascular targeting agent combretastatin A-4-phosphate induces reorganization of the actin cytoskeleton and early membrane blebbing in human endothelial cells. *Blood 99*, 2060–2069.

(98) Quan, H., Xu, Y., and Lou, L. (2007) p38 MAPK, but not ERK1/2, is critically involved in the cytotoxicity of the novel vascular disrupting agent combretastatin A4. *Int. J. Cancer 122*, 1730–1737.

(99) Vincent, L. (2005) Combretastatin A4 phosphate induces rapid regression of tumor neovessels and growth through interference with vascular endothelial-cadherin signaling. *J. Clin. Invest. 115*, 2992–3006.

(100) Jane Lunt, S., Akerman, S., Hill, S. A., Fisher, M., Wright, V. J., Reyes-Aldasoro, C. C., Tozer, G. M., and Kanthou, C. (2011) Vascular effects dominate solid tumor response to treatment with combretastatin A-4-phosphate. *Int. J. Cancer 129*, 1979–1989.

(101) Honore, S., Pasquier, E., and Braguer, D. (2005) Understanding microtubule dynamics for improved cancer therapy. *Cell. Mol. Life Sci. CMLS 62*, 3039–3056.

(102) Kirwan, I. G., Loadman, P. M., Swaine, D. J., Anthoney, D. A., Pettit, G. R., Lippert, J. W., Shnyder, S. D., Cooper, P. A., and Bibby, M. C. (2004) Comparative preclinical pharmacokinetic and metabolic studies of the combretastatin prodrugs combretastatin A4 phosphate and A1 phosphate. *Clin. Cancer Res. Off. J. Am. Assoc. Cancer Res. 10*, 1446–1453.

(103) Choi, Y., and Yu, A.-M. (2014) ABC Transporters in Multidrug Resistance and Pharmacokinetics, and Strategies for Drug Development. *Curr. Pharm. Des. 20*, 793–807.

(104) Wang, L., Woods, K. W., Li, Q., Barr, K. J., McCroskey, R. W., Hannick, S. M., Gherke, L., Credo, R. B., Hui, Y.-H., Marsh, K., Warner, R., Lee, J. Y., Zielinski-Mozng, N., Frost, D., Rosenberg, S. H., and Sham, H. L. (2002) Potent, orally active heterocycle-based combretastatin A-4 analogues: Synthesis, structure-activity relationship, pharmacokinetics, and in vivo antitumor activity evaluation. *J. Med. Chem. 45*, 1697–1711.

(105) Schobert, R., Biersack, B., Dietrich, A., Effenberger, K., Knauer, S., and Mueller, T. (2010) 4-(3-Halo/amino-4,5-dimethoxyphenyl)-5-aryloxazoles and -*N*-methylimidazoles that are cytotoxic against combretastatin A-4 resistant tumor cells and vascular disrupting in a cisplatin resistant germ cell tumor model. *J. Med. Chem. 53*, 6595–6602.

(106) Schobert, R., Biersack, B., and Mueller, T. (2011) Combretastatin analogs for use in the treatment of cancer. *Patent application*. PCT Int. Appl. WO 2011/138409 A1.

(107) Dokmanovic, M., Clarke, C., and Marks, P. A. (2007) Histone deacetylase inhibitors: Overview and perspectives. *Mol. Cancer Res. 5*, 981–989.

(108) Kim, H.-J., and Bae, S.-C. (2011) Histone deacetylase inhibitors: Molecular mechanisms of action and clinical trials as anti-cancer drugs. *Am. J. Transl. Res. 3*, 166-179.
(109) Phillips, D. M. P. (1963) The presence of acetyl groups in histones. *Biochem. J. 87*, 258-263.
(110) Sadoul, K., Boyault, C., Pabion, M., and Khochbin, S. (2008) Regulation of protein turnover by acetyltransferases and deacetylases. *Biochimie 90*, 306–312.
(111) Sadoul, K., Wang, J., Diagouraga, B., and Khochbin, S. (2011) The tale of protein lysine acetylation in the cytoplasm. *J. Biomed. Biotechnol. 2011*, 1–15.
(112) Kim, S. C., Sprung, R., Chen, Y., Xu, Y., Ball, H., Pei, J., Cheng, T., Kho, Y., Xiao, H., and Xiao, L. (2006) Substrate and functional diversity of lysine acetylation revealed by a proteomics survey. *Mol. Cell 23*, 607–618.
(113) Ocker, M. (2010) Deacetylase inhibitors - focus on non-histone targets and effects. *World J. Biol. Chem. 1*, 55-61.
(114) Marks, P. A., Rifkind, R. A., Richon, V. M., Breslow, R., Miller, T., and Kelly, W. K. (2001) Histone deacetylases and cancer: causes and therapies. *Nat. Rev. Cancer 1*, 194–202.
(115) Kazantsev, A. G., and Thompson, L. M. (2008) Therapeutic application of histone deacetylase inhibitors for central nervous system disorders. *Nat. Rev. Drug Discov. 7*, 854–868.
(116) Lee, J.-H., and Marks, P. A. (2010) Histone deacetylase inhibitors in the therapy of cancer: much to learn. *Epigenomics 2*, 723–725.
(117) Glaser, K. B., Staver, M. J., Waring, J. F., Stender, J., Ulrich, R. G., and Davidsen, S. K. (2003) Gene expression profiling of multiple histone deacetylase (HDAC) inhibitors: defining a common gene set produced by HDAC inhibition in T24 and MDA carcinoma cell lines. *Mol. Cancer Ther. 2*, 151–163.
(118) Minucci, S., and Pelicci, P. G. (2006) Histone deacetylase inhibitors and the promise of epigenetic (and more) treatments for cancer. *Nat. Rev. Cancer 6*, 38–51.
(119) Khan, O., and La Thangue, N. B. (2012) HDAC inhibitors in cancer biology: emerging mechanisms and clinical applications. *Immunol. Cell Biol. 90*, 85–94.
(120) New, M., Olzscha, H., and La Thangue, N. B. (2012) HDAC inhibitor-based therapies: Can we interpret the code? *Mol. Oncol. 6*, 637–656.
(121) Glozak, M. A., and Seto, E. (2007) Histone deacetylases and cancer. *Oncogene 26*, 5420–5432.
(122) Licciardi, P., Ververis, Hiong, and Karagiannis. (2013) Histone deacetylase inhibitors (HDACIs): multitargeted anticancer agents. *Biol. Targets Ther.* 47.
(123) Gao, Y. s., Hubbert, C. C., and Yao, T. P. (2010) The microtubule-associated histone deacetylase 6 (HDAC6) regulates epidermal growth factor receptor (EGFR) endocytic trafficking and degradation. *J. Biol. Chem. 285*, 11219–11226.
(124) Li, Y., Zhang, X., Polakiewicz, R. D., Yao, T.-P., and Comb, M. J. (2008) HDAC6 is required for epidermal growth factor-induced beta-catenin nuclear localization. *J. Biol. Chem. 283*, 12686–12690.
(125) Wang, R., Cherukuri, P., and Luo, J. (2005) Activation of Stat3 sequence-specific DNA binding and transcription by p300/CREB-binding protein-mediated acetylation. *J. Biol. Chem. 280*, 11528–11534.
(126) Deroanne, C. F., Bonjean, C., Servotte, S., Devy, L., Colige, A., Clausse, N., Blacher, S., Verdin, E., Foidart, J.-M., Nusgens, B. V., and Castronovo, V. (2002) Histone deacetylases inhibitors as anti-angiogenic agents altering vascular endothelial growth factor signaling. *Oncogene 21*, 427–436.
(127) Jeong, J.-W., Bae, M.-K., Ahn, M.-Y., Kim, S.-H., Sohn, T.-K., Bae, M.-H., Yoo, M., Song, E. J., Lee, K.-J., and Kim, K.-W. (2002) Regulation and destabilization of HIF-1α by ARD1-mediated acetylation. *Cell 111*, 709–720.

(128) Kaluza, D., Kroll, J., Gesierich, S., Yao, T.-P., Boon, R. A., Hergenreider, E., Tjwa, M., Rössig, L., Seto, E., Augustin, H. G., and others. (2011) Class IIb HDAC6 regulates endothelial cell migration and angiogenesis by deacetylation of cortactin. *EMBO J. 30*, 4142–4156.

(129) Zhang, X., Yuan, Z., Zhang, Y., Yong, S., Salas-Burgos, A., Koomen, J., Olashaw, N., Parsons, J. T., Yang, X.-J., Dent, S. R., Yao, T.-P., Lane, W. S., and Seto, E. (2007) HDAC6 modulates cell motility by altering the acetylation level of cortactin. *Mol. Cell 27*, 197–213.

(130) Hubbert, C., Guardiola, A., Shao, R., Kawaguchi, Y., Ito, A., Nixon, A., Yoshida, M., Wang, X.-F., and Yao, T.-P. (2002) HDAC6 is a microtubule-associated deacetylase. *Nature 417*, 455–458.

(131) Aldana-Masangkay, G. I., and Sakamoto, K. M. (2011) The role of HDAC6 in cancer. *J. Biomed. Biotechnol. 2011*, 1–10.

(132) Matsuyama, A., Shimazu, T., Sumida, Y., Saito, A., Yoshimatsu, Y., Seigneurin-Berny, D., Osada, H., Komatsu, Y., Nishino, N., and Khochbin, S. (2002) In vivo destabilization of dynamic microtubules by HDAC6-mediated deacetylation. *EMBO J. 21*, 6820–6831.

(133) Xu, W. S., Parmigiani, R. B., and Marks, P. A. (2007) Histone deacetylase inhibitors: molecular mechanisms of action. *Oncogene 26*, 5541–5552.

(134) Paris, M., Porcelloni, M., Binaschi, M., and Fattori, D. (2008) Histone deacetylase inhibitors: From bench to clinic. *J. Med. Chem. 51*, 1505–1529.

(135) Marks, P. A. (2007) Discovery and development of SAHA as an anticancer agent. *Oncogene 26*, 1351–1356.

(136) Kuljaca, S., Liu, T., Tee, A. E., Haber, M., Norris, M. D., Dwarte, T., and Marshall, G. M. (2007) Enhancing the anti-angiogenic action of histone deacetylase inhibitors. *Mol. Cancer 6*, 68.

(137) Qian, D. Z. (2006) Targeting tumor angiogenesis with histone deacetylase inhibitors: the hydroxamic acid derivative LBH589. *Clin. Cancer Res. 12*, 634–642.

(138) Wozniak, M. B., Villuendas, R., Bischoff, J. R., Aparicio, C. B., Martínez Leal, J. F., de La Cueva, P., Rodriguez, M. E., Herreros, B., Martin-Perez, D., Longo, M. I., Herrera, M., Piris, M. A., and Ortiz-Romero, P. L. (2010) Vorinostat interferes with the signaling transduction pathway of T-cell receptor and synergizes with phosphoinositide-3 kinase inhibitors in cutaneous T-cell lymphoma. *Haematologica 95*, 613–621.

(139) Heider, U., Kaiser, M., Sterz, J., Zavrski, I., Jakob, C., Fleissner, C., Eucker, J., Possinger, K., and Sezer, O. (2006) Histone deacetylase inhibitors reduce VEGF production and induce growth suppression and apoptosis in human mantle cell lymphoma. *Eur. J. Haematol. 76*, 42–50.

(140) Ellis, L., Hammers, H., and Pili, R. (2009) Targeting tumor angiogenesis with histone deacetylase inhibitors. *Cancer Lett. 280*, 145–153.

(141) Iordache, F., Buzila, C., Constantinescu, A., Andrei, E., and Maniu, H. (2012) Histone deacetylase (HDAC) inhibitors down-regulate endothelial lineage commitment of umbilical cord blood derived endothelial progenitor cells. *Int. J. Mol. Sci. 13*, 15074–15085.

(142) Kaluza, D., Kroll, J., Gesierich, S., Yao, T.-P., Boon, R. A., Hergenreider, E., Tjwa, M., Rössig, L., Seto, E., Augustin, H. G., and others. (2011) Class IIb HDAC6 regulates endothelial cell migration and angiogenesis by deacetylation of cortactin. *EMBO J. 30*, 4142–4156.

(143) Tran, A. D.-A., Marmo, T. P., Salam, A. A., Che, S., Finkelstein, E., Kabarriti, R., Xenias, H. S., Mazitschek, R., Hubbert, C., Kawaguchi, Y., Sheetz, M. P., Yao, T.-P., and Bulinski, J. C. (2007) HDAC6 deacetylation of tubulin modulates dynamics of cellular adhesions. *J. Cell Sci. 120*, 1469–1479.

(144) Ni, X., Li, L., and Pan, G. (2015) HDAC inhibitor-induced drug resistance involving ATP-binding cassette transporters (Review). *Oncol. Lett. 9*, 515-521.

(145) Vansteenkiste, J., Van Cutsem, E., Dumez, H., Chen, C., Ricker, J. L., Randolph, S. S., and Schöffski, P. (2008) Early phase II trial of oral vorinostat in relapsed or refractory breast, colorectal, or non-small cell lung cancer. *Invest. New Drugs 26*, 483–488.

(146) Luu, T. H., Morgan, R. J., Leong, L., Lim, D., McNamara, M., Portnow, J., Frankel, P., Smith, D. D., Doroshow, J. H., Wong, C., Aparicio, A., Gandara, D. R., and Somlo, G. (2008) A phase II trial of vorinostat (suberoylanilide hydroxamic acid) in metastatic breast cancer: a california cancer consortium study. *Clin. Cancer Res. Off. J. Am. Assoc. Cancer Res. 14*, 7138–7142.

(147) Aranda, E., and Owen, G. I. (2009) A semi-quantitative assay to screen for angiogenic compounds and compounds with angiogenic potential using the EA. hy926 endothelial cell line. *Biol. Res. 42*, 377–389.

(148) Bauer, J., Margolis, M., Schreiner, C., Edgell, C.-J., Azizkhan, J., Lazarowski, E., and Juliano, R. L. (1992) In vitro model of angiogenesis using a human endothelium-derived permanent cell line: Contributions of induced gene expression, G-proteins, and integrins. *J. Cell. Physiol. 153*, 437–449.

(149) Day, J. A., and Cohen, S. M. (2013) Investigating the selectivity of metalloenzyme inhibitors. *J. Med. Chem. 56*, 7997–8007.

5 Publikationen und Manuskripte

5.1 Darstellung des Eigenanteils

Die in dieser Dissertation gezeigten Publikationen und Manuskripte wurden hauptsächlich in Kooperation mit anderen Arbeitsgruppen erarbeitet. Dazu gehören das Institut für Innere Medizin, Onkologie/Hämatologie der Martin Luther-Universität Halle-Wittenberg, das Institut für Molekulare Strukturbiologie der Georg August-Universität Göttingen, das Institut für Pathologie an der *Wayne State University School of Medicine* und das *Karmanos Cancer Institute* der *Wayne State University* in Detroit (Michigan, USA), das Institut für Physiologie der Charité-Universitätsmedizin Berlin und der Lehrstuhl für Genetik der Universität Bayreuth.

Der Beitrag aller Ko-Autoren zu den jeweiligen Publikationen und Manuskripten soll im Folgenden detailliert dargestellt werden.

5.1.1 Biologische Evaluation von Mikrotubuli-destabilisierenden Agenzien mit antivaskulärer Wirkung

Publikation I:

***In vitro*- und *in vivo*-Effekte von zwei Heteroaryl-Analoga des antitumoralen VDA Verubulin auf Tumorzellen, Endothelzellen und Blutgefäßorganisation**

(vgl. Kapitel 3.2.1)

Ergebnisse zu diesem Thema wurden im Journal ***ChemMedChem*** veröffentlicht unter dem Titel

"Effects of the tumor-vasculature-disrupting agent Verubulin and two heteroaryl analogues on Cancer Cells, Endothelial Cells, and Blood Vessels"

von den Autoren

Katharina Mahal, Marcus Resch, Ralf Ficner, Rainer Schobert, Bernhard Biersack und Thomas Mueller.

Die Arbeit wurde in Kooperation mit dem Institut für Molekulare Strukturbiologie der Georg August-Universität Göttingen und dem Institut für Innere Medizin IV, Onkologie/Hämatologie der Martin Luther-Universität Halle-Wittenberg durchgeführt.

Eigenanteil:

Konzeption, Durchführung und Auswertung biologischer Assays:

Zellkultivierung, Zytotoxizitätsbestimmungen (MTT-Assay), Zellzyklusanalysen, Zytoskelettfärbungen und Fluoreszenzmikroskopie, *Tube formation*- und Chorioallantoismembran (CAM)-Assays.

Verfassen entsprechender Manuskriptpassagen inkl. Diskussion und Interpretation der Ergebnisse sowie Korrektur und Revision des Manuskripts; Beteiligung an der Manuskript-Konzeption; graphische Repräsentation und Bearbeitung der Abbildungen.

Bernhard Biersack:	Synthese, Aufreinigung und Charakterisierung aller getesteten Verbindungen; Manuskript-Konzeption.
Thomas Müller:	Durchführung von Tubulin-Polymerisationsassays, Durchführung und Dokumentation der Xenograft-Studien an Mäusen sowie histologische Untersuchung der Tumorgewebeschnitte und ihre graphische Darstellung.
Marcus Resch:	Durchführung, Analyse und graphische Darstellung der Docking-Studien.
Rainer Schobert:	Manuskriptkonzeption, Diskussion und Korrektur des Manuskripts.
Ralf Ficner:	Diskussion des Manuskripts.

Alle aufgeführten Autoren trugen zum Verfassen entsprechender Manuskriptpassagen bei und waren an Diskussionen über die Inhalte sowie an Korrekturen und Überarbeitungen beteiligt.

Geschätzter Eigenanteil: ca. 60-70%

Publikation II:

Neue Combretastatin A-4-abgeleitete Oxazole als potentielle, vascular-disruptive Agenzien (vgl. Kapitel 3.2.2)

Ergebnisse zu diesem Thema wurden als *Extended Abstract* in der Fachzeitschrift

International Journal of Clinical Pharmacology and Therapeutics

veröffentlicht unter dem Titel

"New oxazole-bridged combretastatin A-4 analogues as potential vascular-disrupting agents"

von den Autoren

Katharina Mahal, Bernhard Biersack und Rainer Schobert.

Eigenanteil:

Konzeption, Durchführung und Auswertung biologischer Assays:

Zellkultuvierung, Zytotoxizitätsbestimmungen (MTT-Assay), Zellzyklusanalysen, *Tube formation*-Assays.

Konzeption und Verfassen des *Abstracts* inkl. Interpretation und Abbildung der Ergebnisse sowie Korrektur und Revision des Textes.

Bernhard Biersack:	Synthese, Aufreinigung und Charakterisierung der getesteten Verbindungen.
Rainer Schobert:	Diskussion und Korrektur des *Abstracts*.

Geschätzter Eigenanteil: ca. 90%

Publikation III:

Zytotoxische, antivaskuläre und antimetastatische Effekte von CA-4-abgeleiteten Imidazol-Derivaten basierend auf aberrativer Zytoskelett-Dynamik (vgl. Kapitel 3.2.3)

Ergebnisse zu diesem Thema wurden im Journal ***Investigational New Drugs*** veröffentlicht unter dem Titel

"Combretastatin A-4 derived imidazoles show cytotoxic, antivascular, and antimetastatic effects based on cytoskeletal reorganisation"

von den Autoren

Katharina Mahal, Bernhard Biersack, Henrike Caysa, Rainer Schobert und Thomas Mueller.

Die Arbeit wurde in Kooperation mit dem Institut für Innere Medizin IV, Onkologie/Hämatologie der Martin Luther-Universität Halle-Wittenberg durchgeführt.

Eigenanteil:

Konzeption, Durchführung und Auswertung biologischer Assays:

Zellkultuvierung und Isolierung von primären Fibroblasten aus Hühnerembryos, Zytotoxizitätsbestimmungen (MTT-Assay), Zellzyklusanalysen, Zytoskelettfärbungen und Fluoreszenzmikroskopie, Tubulin-Fraktionierung und Western Blot-Analysen, *Tube formation*- und Chorioallantoismembran (CAM)-Assays, Transwell-Migrations- und Transendothelmigrations-Assays.

Verfassen des Manuskripts inkl. Diskussion und Interpretation der Ergebnisse sowie Korrektur und Revision des Manuskripts; Manuskript-Konzeption; graphische Repräsentation und Bearbeitung der Abbildungen.

Bernhard Biersack: Synthese, Aufreinigung und Charakterisierung aller getesteten Verbindungen.

Henrike Caysa und Thomas Müller:

Durchführung und Dokumentation von Xenograft-Experimenten an Mäusen sowie histologische Untersuchung der Tumorgewebeschnitte und ihre graphische Darstellung.

Rainer Schobert: Diskussion und Korrektur des Manuskripts.

Alle aufgeführten Autoren trugen zum Verfassen entsprechender Manuskriptpassagen bei und waren an Diskussionen über die Inhalte sowie an Korrekturen und Überarbeitungen beteiligt.

Geschätzter Eigenanteil: ca. 80%

Manuskript IV:

Die Rolle von verschiedenen Kinasen und NF-kappaB-Aktivität für die antivaskuläre und antitumorale Wirkung des CA-4-abgeleiteten VDA Brimamin (vgl. Kapitel 3.2.4)

Ergebnisse zu diesem Thema wurden zur Publikation vorbereitet, unter dem Titel

"Contribution of JNK signaling and NF-kappaB activity to the anticancer effects of the vascular-disrupting agent Brimamin"

von den Autoren

Katharina Mahal, Aamir Ahmad, Marcus Resch, Ralf Ficner, Fazlul Sarkar, Rainer Schobert und Bernhard Biersack.

Die Arbeit wurde in Kooperation mit dem Institut für Pathologie und dem *Karmanos Cancer Institute* an der *Wayne State University School of Medicine* in Detroit (Michigan, USA) sowie dem Institut für Molekulare Strukturbiologie der Georg August-Universität Göttingen durchgeführt.

Eigenanteil:

Konzeption, Durchführung und Auswertung biologischer Assays:

Zellkultivierung, Zytotoxizitätsbestimmungen (MTT-Assay), Zellzyklusanalysen, Zytoskelettfärbungen und Fluoreszenzmikroskopie, *Tube formation*-Assays, Herstellung von Zelllysatfraktionen und Western Blot-Analysen.

Verfassen entsprechender Manuskriptpassagen inkl. Diskussion und Interpretation der Ergebnisse sowie Korrektur und Revision des Manuskripts; Beteiligung an der Manuskript-Konzeption; graphische Repräsentation und Bearbeitung der Abbildungen.

Aamir Ahmad: Durchführung und Auswertung biologischer Assays: Apoptose-Nachweis mittels ELISA, NF-kappaB-*Electrophoretic mobility shift assays* (EMSA), Durchführung und Dokumentation von Xenograft-Studien in Mäusen sowie Analyse von Tumorgewebe mittels Western Blot-Analyse; Graphische Darstellung und Bearbeitung von Abbildungen.

Marcus Resch: Durchführung, Analyse und graphische Darstellung der Docking-Studien.

Bernhard Biersack:	Manuskript- und Assay-Konzeption; Synthese und Charakterisierung von Brimamin; Verfassen und Diskussion sowie Überarbeitung und Korrektur des Manuskripts.
Rainer Schobert:	Diskussion, Überarbeitung und Korrektur des Manuskripts.
Ralf Ficner:	Diskussion des Manuskripts.
Fazlul H. Sarkar:	Diskussion des Manuskripts.

Alle aufgeführten Autoren trugen zum Verfassen entsprechender Manuskriptpassagen bei und waren an Diskussionen über die Inhalte sowie an Korrekturen und Überarbeitungen beteiligt.

Geschätzter Eigenanteil: ca. 50%

5.1.2 Biologische Evaluation von Histondeacetylase-Inhibitoren

Publikation V:

Biologische Evaluation von Hydroxamsäure-basierten Histondeacetylase-Inhibitoren (HDACi) mit neuartigem 4,5-Diarylimidazol-Strukturmotiv als bimodale Wirkstoffe mit antitumoraler und antiangiogener Wirkung (vgl. Kapitel 3.3.1)

Ergebnisse zu diesem Thema wurden im Journal ***Cancer Chemotherapy and Pharmacology*** veröffentlicht unter dem Titel

"Biological evaluation of 4,5-diarylimidazoles with hydroxamic acid appendages as novel dual mode anticancer agents"

von den Autoren

Katharina Mahal, Sebastian Schruefer, Gustav Steinemann, Franziska Rausch, Rainer Schobert, Bernhard Biersack und Michael Höpfner.

Die Arbeit wurde in Kooperation mit dem Institut für Physiologie der Charité-Universitätsmedizin Berlin durchgeführt.

Eigenanteil:

Konzeption, Durchführung und Auswertung biologischer Assays:

Zellkultivierung und Isolierung von primären Fibroblasten aus Hühnerembryos, Zytotoxizitätsbestimmungen (MTT-Assay), HDAC-Aktivitätstests und Western Blot-Analysen acetylierter Proteine, Transwell-Invasion-Assays, Zytoskelettfärbungen und Fluoreszenzmikroskopie, CAM-Assays.

Verfassen des Manuskripts inkl. Diskussion und Interpretation der Ergebnisse sowie Korrektur und Revision des Manuskripts; Manuskript-Konzeption; graphische Repräsentation und Bearbeitung der Abbildungen.

Sebastian Schrüfer: Durchführung von Western Blot-Analysen acetylierter Proteine, Zytoskelettfärbungen und Fluoreszenzmikroskopie im Rahmen der Bachelorarbeit (Betreut von K. Mahal und R. Schobert)

Gustav Steinemann und Franziska Rausch:	
	Zellkultivierung, Zytotoxizitätsbestimmungen, Durchführung und Auswertung von Caspase-Aktivitätsassays und Apoptose-nachweisen.
Bernhard Biersack:	Beteiligung an der Manuskript-Konzeption; Synthese, Aufreinigung und Charakterisierung aller Testsubstanzen; Diskussion, Überarbeitung und Korrektur des Manuskripts.
Rainer Schobert:	Diskussion, Überarbeitung und Korrektur des Manuskripts.
Michael Höpfner:	Beteiligung an der Manuskript-Konzeption; Diskussion, Überarbeitung und Korrektur des Manuskripts.

Alle aufgeführten Autoren trugen zum Verfassen entsprechender Manuskriptpassagen bei und waren an Diskussionen über die Inhalte sowie an Korrekturen und Überarbeitungen beteiligt.

Geschätzter Eigenanteil: ca. 60-70%

Manuskript VI:

Tumorwachstum-relevante Signaltransduktion und Zytoskelett-Organisation als *Target* neuer pleiotroper Histondeacetylase-Inhibitoren des 4,5-Diarylimidazol-Typs mit Cinnamylhydroxamat-Resten (vgl. Kapitel 3.3.2)

Ergebnisse zu diesem Thema wurden zur Veröffentlichung vorbereitet unter dem Titel

"4-(1-Ethyl-4-anisyl-imidazol-5-yl)-N-hydroxycinnamide - A new pleiotropic HDAC inhibitor targeting cancer cell signalling and cytoskeletal organisation."

von den Autoren

Katharina Mahal, Philip Kahlen, Bernhard Biersack und Rainer Schobert.

Die Arbeit wurde in Kooperation mit dem Lehrstuhl für Genetik der Universität Bayreuth durchgeführt

Eigenanteil:

Konzeption, Durchführung und Auswertung biologischer Assays:

Zellkultivierung, Zytotoxizitätsbestimmungen (MTT-Assay), HDAC- und MMP-Aktivitätstests, Western Blot-Analysen, FITC-Gelatine-*Labelling* und Gelatine-Zymographie, Transwell-Invasion-Assays, Zytoskelettfärbungen und Fluoreszenz-mikroskopie, CAM-Assays.

Verfassen des Manuskripts inkl. Diskussion und Interpretation der Ergebnisse sowie Korrektur und Revision des Manuskripts; Manuskript-Konzeption; graphische Repräsentation und Bearbeitung der Abbildungen; Densitometrie- und Signifikanz-Analyse.

Philip Kahlen:	Expression, Aufreinigung und Charakterisierung aktiver rekombinanter HDAC1, HDAC-Aktivitätstests, Herstellung und Western Blot-Charakterisierung von Zelllysaten.
Bernhard Biersack:	Synthese und Charakterisierung aller Testsubstanzen.
Rainer Schobert:	Diskussion, Überarbeitung und Korrektur des Manuskripts.

Alle aufgeführten Autoren trugen zum Verfassen entsprechender Manuskriptpassagen bei und waren an Diskussionen über die Inhalte sowie an Korrekturen und Überarbeitungen beteiligt.

Geschätzter Eigenanteil: ca. 80%

Publikationen und Manuskripte zur biologischen Evaluation von Mikrotubuli-destabilisierenden Agenzien mit antivaskulärer Wirkung:

Publikationen I-III und Manuskript IV

PUBLIKATION I

Effects of the Tumor-Vasculature-Disrupting Agent Verubulin and Two Heteroaryl Analogues on Cancer Cells, Endothelial Cells, and Blood Vessels.

Katharina Mahal,[a] Marcus Resch,[b] Ralf Ficner,[b] Rainer Schobert,[a] Bernhard Biersack,*[a] Thomas Mueller*[c]

[a] *Organic Chemistry Laboratory, University of Bayreuth, Universitätsstraße 30, 95440 Bayreuth (Germany)*

[b] *Department of Molecular Structural Biology, Georg August University Göttingen, Justus-von-Liebig-Weg 11, 37077 Göttingen (Germany)*

[c] *Department of Internal Medicine IV, Oncology/Hematology, Martin Luther University Halle-Wittenberg, Ernst-Grube-Straße 40, 06120 Halle (Germany)*

* email: bernhard.biersack@uni-bayreuth.de; thomas.mueller@medizin.uni-halle.de

ChemMedChem **2014**, *9 (4)*, 847-854.

ChemPubSoc Europe

DOI: 10.1002/cmdc.201300531

Effects of the Tumor-Vasculature-Disrupting Agent Verubulin and Two Heteroaryl Analogues on Cancer Cells, Endothelial Cells, and Blood Vessels

Katharina Mahal,[a] Marcus Resch,[b] Ralf Ficner,[b] Rainer Schobert,[a] Bernhard Biersack,*[a] and Thomas Mueller*[c]

Two analogues of the discontinued tumor vascular-disrupting agent verubulin (Azixa®, MPC-6827, **1**) featuring benzo-1,4-dioxan-6-yl (compound **5a**) and *N*-methylindol-5-yl (compound **10**) residues instead of the *para*-anisyl group on the 4-(methylamino)-2-methylquinazoline pharmacophore, were prepared and found to exceed the antitumor efficacy of the lead compound. They were antiproliferative with single-digit nanomolar IC_{50} values against a panel of nine tumor cell lines, while not affecting nonmalignant fibroblasts. Indole **10** surpassed verubulin in seven tumor cell lines including colon, breast, ovarian, and germ cell cancer cell lines. In line with docking studies indicating that compound **10** may bind the colchicine binding site of tubulin more tightly ($E_{bind} = -9.8$ kcal mol^{-1}) than verubulin ($E_{bind} = -8.3$ kcal mol^{-1}), **10** suppressed the formation of vessel-like tubes in endothelial cells and destroyed the blood vessels in the chorioallantoic membrane of fertilized chicken eggs at nanomolar concentrations. When applied to nude mice bearing a highly vascularized 1411HP germ cell xenograft tumor, compound **10** displayed pronounced vascular-disrupting effects that led to hemorrhages and extensive central necrosis in the tumor.

Introduction

Tumor blood vessels are a therapeutic target as they are fundamentally different from normal vasculature.[1,2] Vascular-targeting agents may belong to either of two groups: antiangiogenic compounds[3,4] which address factors that regulate the neo-formation of blood vessels or vascular-disrupting agents (VDA)[5,6] that destroy irregular tumor blood vessels. VDA are particularly interesting, as they often exhibit an immediate impact on the vasculature of tumors provoking their collapse after only a few applications. Most VDA are small molecules derived from natural lead compounds such as the combretastatins A,[7] plantal stilbene metabolites that bind to the colchicine binding site of tubulin and cause extensive cytoskeletal rearrangements of the microtubule and the actin backbones of endothelial cells.[8] Examples of this type are fosbretabulin[9,10] and AVE8062,[11,12] a phosphate and a serinyl prodrug of combretastatin A-4, respectively, and the combretastatin A-1 derivative OXi4503.[13] More recently, combretastatin A derivatives with imidazole, oxazole, or related heterocycles were developed that retain the vascular-disrupting effect of the lead compound while showing an enhanced cytotoxicity.[14–17] Other heterocyclic VDA, structurally remote from the archetypal natural VDA blueprints, were also identified. Verubulin (Azixa®, MPC-6827, **1**), a *para*-anisidyl-substituted quinazoline, exhibits vascular-disrupting effects coupled with strong apoptosis induction in tumor cells, including multidrug resistant cells. It is also capable of penetrating the blood brain barrier. Although it had successfully passed a phase IIb clinical trial for glioblastoma multiforme[18–20] the proprietor, Myrexis Inc., decided in 2011 to suspend any further development of **1** for economic reasons, only. As earlier competition assays with **1** and proven tubulin binders had suggested that it might bind to the colchicine or a nearby binding site, we now prepared and studied a series of analogues of **1** that bore benzoxacycles and indoles, heterocycles that figure prominently in other synthetic antimitotic agents.[21–23] Herein we report on the effects of **1** and of two derivatives with superior efficacy against tumor cells on the propensity of endothelial cells to form blood vessel-like tubular structures and on real blood vessels in hen egg models and xenograft tumors. The affinity of these three compounds to tubulin and the cytoskeleton of nonmalignant and cancer cells was ascertained by docking studies, in vitro binding assays, and immunofluorescent cell staining.

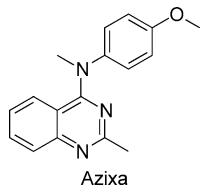

Azixa

[a] K. Mahal, Prof. Dr. R. Schobert, Dr. B. Biersack
Organic Chemistry Laboratory, University of Bayreuth
Universitätsstraße 30, 95440 Bayreuth (Germany)
E-mail: bernhard.biersack@uni-bayreuth.de

[b] Dr. M. Resch, Prof. Dr. R. Ficner
Department of Molecular Structural Biology
Georg August University Göttingen
Justus-von-Liebig-Weg 11, 37077 Göttingen (Germany)

[c] Dr. T. Mueller
Department of Internal Medicine IV, Oncology/Hematology
Martin Luther University, Halle-Wittenberg, 06120 Halle (Germany)
E-mail: thomas.mueller@medizin.uni-halle.de

Supporting information for this article is available on the WWW under http://dx.doi.org/10.1002/cmdc.201300531.

Results and Discussion

Chemistry

A series of 4-aminoquinazolines with benzo-1,4-dioxan-6-yl (**5a**), benzo-1,3-dioxolan-5-yl (**5b**), and benzofuran-5-yl (**5c**) residues were prepared by alkylation of the respective methyl aryl amines **4a–c** with 4-hydroxy-2-methylquinazoline in the presence of BOP[24] and DBU (Scheme 1). The amines **4**[25–27]

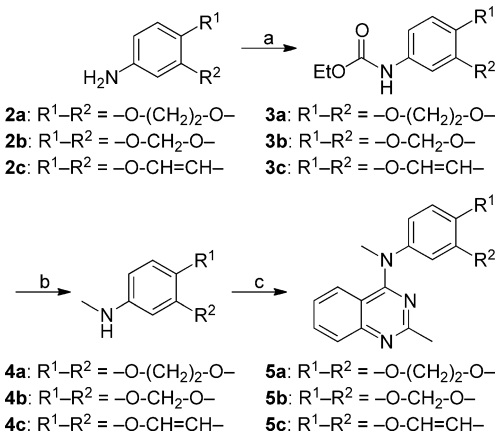

Scheme 1. Synthesis of quinazoline derivatives **5**. *Reagents and conditions*: a) EtOCOCl, Et_3N, THF, RT, 4 h, 78–95%; b) $LiAlH_4$, THF, reflux, 1 h, 79–94%; c) 2-methyl-4-hydroxyquinazoline, BOP, PhOPh, DBU, MeCN, RT, 16 h, 21–31%.

were obtained by conversion of the primary amines **2** to the carbamates **3** with ethyl chloroformate and reduction of **3** with $LiAlH_4$.

Scheme 2 depicts the synthesis of 2-methyl-4-[*N*-methyl-*N*-(1-methylindol-5-yl)]aminoquinazoline **10**. *N*-Methyl-5-nitroindole **6** was protected at C3 by chlorination with NCS to give compound **7**. Reduction of the nitro group with Zn/HCl and acylation of the resulting amine with ethyl chloroformate afforded carbamate **8**. This was reduced to methyl amine **9** by $LiAlH_4$. Analogous to compounds **4**, the amine **9** was coupled with 4-hydroxy-2-methylquinazoline in the presence of BOP and then dechlorinated via Pd-catalyzed hydrogenation to yield compound **10**.

Biological evaluation

The antiproliferative activities of compounds **5a–c** and **10** were evaluated first by MTT assays[28] with cells of highly proliferative 518A2 melanoma, chemosensitive HCT-116 colon, and multidrug resistant MCF-7/Topo breast carcinomas, as well as with hybrid Ea.hy926 endothelial cells and nonmalignant human foreskin fibroblasts (HF). The benzo-1,4-dioxane **5a** and the *N*-methylindole **10** were highly efficacious against all cancer cell lines with IC_{50} (72 h) values ranging from 0.4 to 1.0 nM, values not significantly

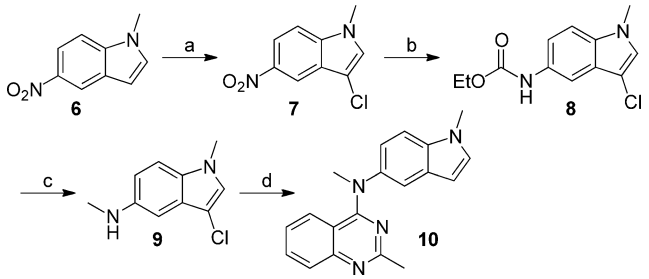

Scheme 2. Synthesis of *N*-(methylindolyl)aminoquinazoline **10**. *Reagents and conditions*: a) NCS, MeCN, RT, 4 h, 60%; b) Zn/HCl, THF, RT, 10 min, then EtOCOCl, Et_3N, THF, RT, 4 h, 61%; c) $LiAlH_4$, THF, reflux, 1 h, 87%; d) 2-methyl-4-hydroxyquinazoline, BOP, PhOPh, DBU, MeCN, RT, 16 h, then H_2, 10% Pd/C, MeOH, RT, 2 h, 32%.

different from **1**. Endothelial Ea.hy926 cells were also affected at nanomolar concentrations (72 h) whereas normal fibroblasts were not affected by compounds **5a** and **10** at concentrations of up to 10 μM. The derivatives **5b** and **5c** were less antiproliferative by one order of magnitude in all cells tested (Table 1). Next, the most active compounds **1**, **5a**, and **10** were tested against a second panel comprising two related testicular germ cell tumor cell lines,[29] the chemosensitive H12.1 and the drug-resistant 1411HP, as well as the colon cancer cell lines HT-29, DLD-1, and HCT-8, and the ovarian cancer cell line A2780.[30] Generally, indole **10** was marginally more antiproliferative against all six cancer cell lines than **1**. For the sensitive A2780 ovarian cancer cell line it even reached a sub-nanomolar IC_{50} (96 h) value. Compound **5a** exhibited a lower, though still impressive, activity with IC_{50} (96 h) values <6 nM for all cancer cell lines tested.

For an assessment of the effects of the new verubulin analogues on endothelial cells we used the hybrid endothelial cell

Table 1. Inhibitory concentrations of compounds **1**, **5a–c**, and **10** when applied to human foreskin fibroblasts (HF), Ea.hy926 hybrid endothelial cells, and various cancer cells.

Cell Line	IC_{50} [nM][a]				
	1	**10**	**5a**	**5b**	**5c**
HF[b]	>10000	>10000	>10000	–	–
Ea.hy926[c]	>1000	>1000	>1000	–	–
Ea.hy926[b]	30±10	27±5	43±8	–	–
518A2[b]	0.3±0.1	0.4±0.1	0.9±0.1	7.6±3.7	30±9
HCT-116[b]	0.2±0.0	1.0±0.0	0.8±0.1	9.0±0.6	11±1
MCF-7/Topo[b]	1.3±0.6	1.0±0.0	1.0±0.0	51±17	29±2
H12.1[d]	1.8±0.1	1.7±0.1	4.3±0.6	–	–
1411HP[d]	2.6±0.5	2.0±0.2	5.8±0.2	–	–
HT-29[d]	1.7±0.1	1.4±0.1	3.4±1.1	–	–
HCT-8[d]	1.8±0.1	1.6±0.1	4.2±1.1	–	–
DLD-1[d]	1.8±0.1	1.7±0.1	4.7±0.6	–	–
A2780[d]	1.4±0.1	0.9±0.2	1.8±0.1	–	–

[a] Values are derived from dose–response curves obtained by measuring the percentage of viable cells relative to untreated controls after exposure to test compounds using: [b] MTT (72 h exposure), [c] MTT (24 h exposure), or [d] SRB (96 h exposure) assays. Values represent the mean±SD of four independent experiments (–: not measured). Human cancer cell lines: 518A2 melanoma, HCT-116 colon, HT-29 colon, HCT-8 colon, DLD-1 colon, MCF-7/Topo breast, A2780 ovarian carcinoma, H12.1, and 1411HP germ cell tumors.

line Ea.hy926, which is easier to passage and cultivate than primary endothelial cells such as human umbilical vein endothelial cells (HUVEC). The flow cytometric analysis revealed a two- to threefold increase of cells in the G2/M phase following incubation for 24 h with 10 nM of **1**, **5a**, or **10** (Figure 1, Table 2). Compared with **1** and **5a** the onset of this effect was somewhat retarded in the case of **10**. The fact that only 10% of the cells were apoptotic after 24 h, as assessed from the sub-G1 events, suggests that the pronounced growth inhibition observed in the MTT and SRB assays after 96 h is owed not to a direct induction of apoptosis but to this G2/M cell-cycle arrest. Other tubulin-targeting agents such as taxol, vinblastine, and combretastatin A-4 are known to cause such a mitotic arrest in primary cells as a result of an aberrant or impaired development of functional spindle microtubules and the disruption of the normal chromosome attachment to the mitotic spindle apparatus.[31] A prolonged mitotic arrest can eventually lead to the induction of apoptosis, or alternatively, cells may also exit from mitosis by dividing into daughter cells with polyploid or other abnormal genome content.[31]

To determine how the microtubule dynamics of Ea.hy926 endothelial cells respond to treatment with compounds **1**, **5a**, or **10**, their microtubule cytoskeleton was visualized by immunofluorescent staining (Figure 2). Exposure for 24 h to 10 nM of the compounds caused a complete disruption of the highly organized tubulin filaments and a diffuse distribution of the stained microtubule subunits throughout the whole of the cytosol. The cells also showed an aberrant cell morphology and a distinct membrane blebbing. In principal, this blebbing could be the result of an actin-mediated cellular stress response as in the case of endothelial cells treated with combretastatin A-4.[32] Alternatively, it could be "apoptotic blebbing", as a consequence of apoptosis induction. Here, in the case of Ea.hy926 cells treated with **1**, **5a**, or **10** the morphological changes are indicative of alterations in the actin cytoskeleton. As a proof we stained their actin filaments with a fluorescent phalloidin conjugate and analyzed the subcellular distribution of filamentous actin (F-actin, Figure 2). Although most actin filaments in untreated control cells were of the cortical type, concentrated near the plasma membrane fringe, the F-actin in cells exposed to 10 nM of **1**, **5a**, or **10** was organized in trusses of stress fibers, scattered all over the cell body. The majority of treated cells also featured a markedly increased cytosolic volume and two contiguous or separated nuclei. We therefore assume that the mechanism by which verubulin (**1**) and its analogues **5a** and **10** induce growth inhibition is at least partially mediated by inhibiting cell division due to the loss of a func-

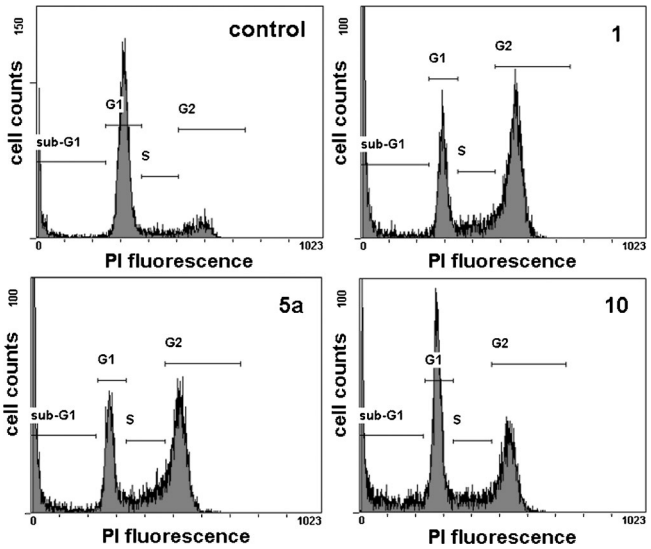

Figure 1. Effect of **1**, **5a**, and **10** (10 nM, 24 h) on the cell cycle of Ea.hy926 cells. Typical cell-cycle profiles and percentage of treated cells in G1, S, and G2 phases as well as sub-G1 events (apoptotic cells) as obtained by flow cytometry after DNA staining with propidium iodide; control: DMSO.

Table 2. Percentage of Ea.hy926 endothelial cells in G1, S, and G2/M cell-cycle phases and the proportion of apoptotic cells (sub-G1) after treatment with compounds **1**, **5a**, or **10**.

Phase	Cell Count [%][a]			
	Control	**1**	**5a**	**10**
sub-G1	14.5 ± 0.1	24.1 ± 2.4	24.9 ± 0.7	21.1 ± 3.4
G1	66.2 ± 0.8	22.4 ± 0.7	22.3 ± 1.7	41.3 ± 3.0
S	6.8 ± 0.3	9.5 ± 1.0	10.6 ± 2.3	10.7 ± 0.5
G2/M	12.6 ± 0.3	44.0 ± 1.6	42.2 ± 4.6	26.9 ± 1.0

[a] Determined by flow cytometry. Cells were treated with the test compound at 10 nM for 24 h; control cells were treated with DMSO only. Values represent the mean ± SD of $n = 3$ independent experiments.

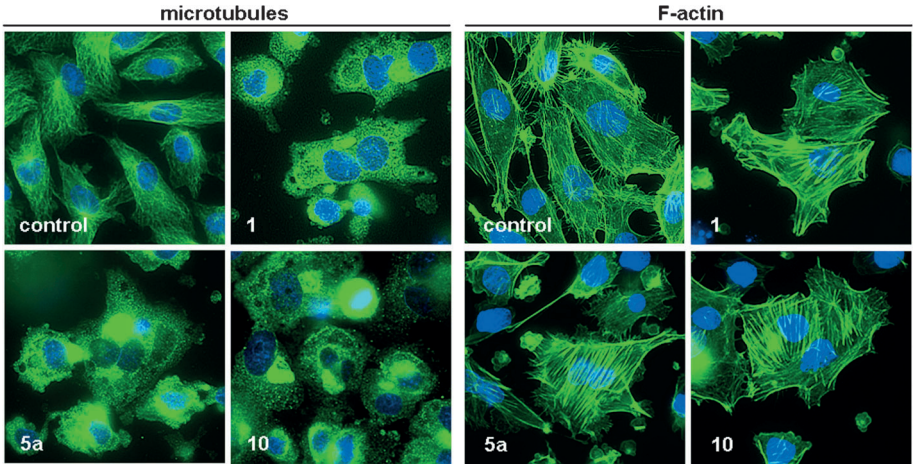

Figure 2. Effect of **1**, **5a**, and **10** (10 nM, 24 h) on the cytoskeletal organization of microtubules (left panels) and F-actin (right panels) in Ea.hy926 endothelial cells. Nuclei (blue) were counterstained with DAPI (400× magnification).

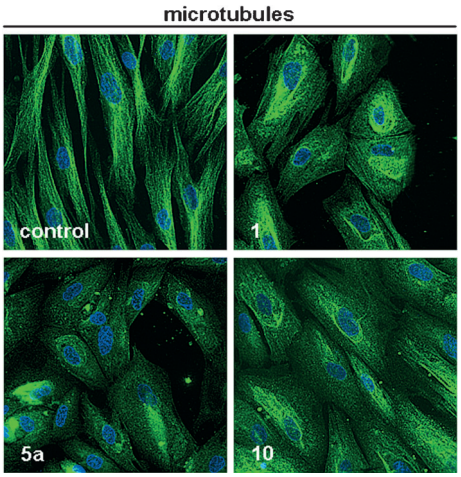

Figure 3. Effect of **1**, **5a**, and **10** (100 nM, 24 h) on the microtubule cytoskeleton of human fibroblasts (HF). Nuclei (blue) were stained with DAPI (400× magnification).

tional cytoskeletal organization.[31] Immunofluorescent staining of microtubules in nonmalignant fibroblasts (HF cells) treated with 100 nM of **1**, **5a**, or **10** revealed a pronounced disruption of the microtubule cytoskeleton, yet no dinucleated cells (Figure 3). Thus, the test compounds predominantly affect rapidly proliferating cells.

As mentioned in the introductory section, the molecular mechanism of action of verubulin **1** is still largely unknown. This includes the precise mode of its interaction with tubulin which is believed to take place near the colchicine binding site at the α-/β-tubulin heterodimeric interface.[20] We now studied the molecular interaction of compounds **1**, **5a**, and **10** with tubulin in two different ways: first, kinetically, with purified tubulin and the tubulin polymerization assay kit by Cytoskeleton, and then by in silico prediction, via molecular docking. Figure 4 shows the time dependency of tubulin polymerization in samples containing 3 μM of the test compounds. Interestingly, indole **10** was a less effective polymerization inhibitor than **1** and **5a**, despite its stronger growth inhibitory effect in most of the tested cancer cell lines and its pronounced effect

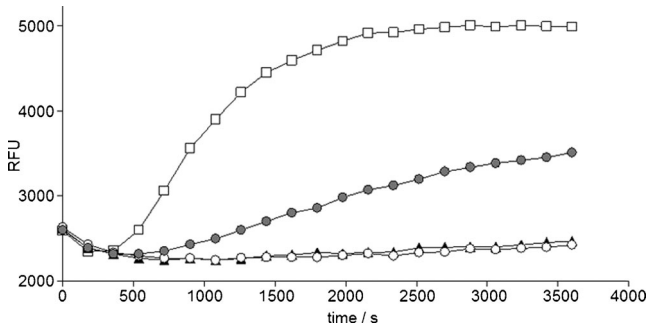

Figure 4. Effects of **1** (▲), **5a** (○), or **10** (●), each at 3 μM, on the polymerization of tubulin as ascertained with a fluorescence-based assay kit from Cytoskeleton (control, □). Data are representative of four independent experiments; RFU: relative fluorescence units as a measure of the degree of polymerization.

on the cytoskeleton. Tubulin interaction seems to be just one of many factors that contribute to the overall impact on the cell and it is probably not decisive for the viability of cells that can exit mitotic arrest without immediate death.

Next, molecular docking studies were conducted to gain insight into the possible tubulin binding mode and to gauge the binding energy of the quinazolines **1**, **5a**, and **10**. The crystal structure of bovine dimeric tubulin (PDB ID: 1SA0, 100% sequence identity to human tubulin) complexed with colchicine and Mg^{2+}-coordinated GDP and GTP was used to dock the quinazolines in the colchicine binding site.[33] Docking studies with the suite AutoDock Vina[34] predicted them to bind in an orientation analogous to colchicine with the aryl ring, that is, anisyl (**1**), benzo-1,4-dioxanyl (**5a**), or *N*-methylindolyl ring (**10**), proximal to Cys-β241 (Figure 5) and its respective heteroatom,

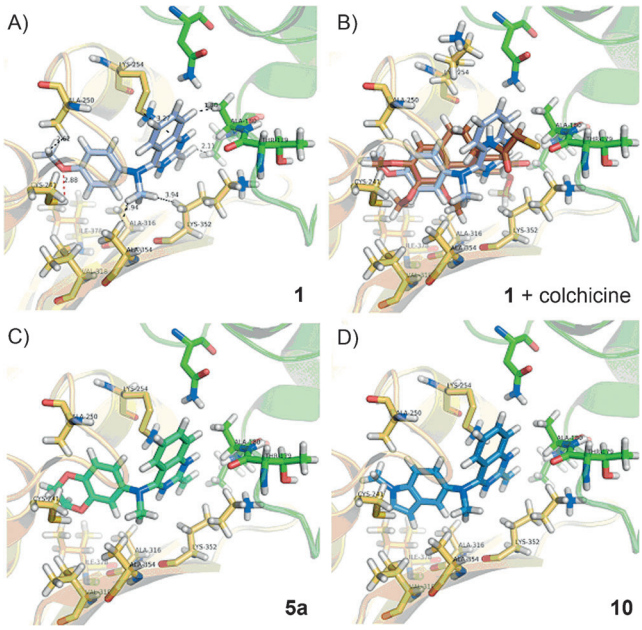

Figure 5. Docking of verubulin (**1**) (A, B), **5a** (C), and **10** (D) into the crystal structure of bovine tubulin (PDB ID: 1SA0) with α-tubulin shown in green and β-tubulin in ochre. Important amino acid residues are depicted as sticks and labeled accordingly. Secondary structure elements are semitransparent. A) Putative hydrogen bonding (red dashed lines) and van der Waals interactions (black dashed lines) of **1** to bovine tubulin. B) Overlay of the docking positions of **1** (calculated) and of colchicine (from X-ray crystal structure; brown). C) Optimized docking position of **5a**. D) Optimized docking position of **10**.

O or N, within typical hydrogen bond distance from the SH-group of Cys-β241 (Figure 5 A,C). A similar binding situation was previously found for combretastatin A-4 analogues.[35,36] In addition, the A ring including the *para*-methoxy group of **1**, the dioxane and phenyl rings of **5a**, and the *N*-methylindole moiety of **10** are stabilized by van der Waals interactions within the hydrophobic pocket made up by the side chains of Leu-β248, Ala-β250, Ala-β316, Val-β318, Ala-β354, and Ile-β378 (Figure 5 A,C,D). This hydrophobic network mimics that of colchicine's trimethoxyphenyl ring (Figure 5 B).[33] Furthermore, the methyl group at the bridging exocyclic amino nitrogen

Table 3. Calculated binding energies of colchicine and quinazolines **1**, **5a**, and **10** to the colchicine binding site of tubulin.

Ligand	E_{bind} [kcal mol^{-1}][a]
colchicine	−9.0
1	−8.3
5a	−9.0
10	−9.8

[a] Values calculated by AutoDock Vina.[31]

atom favorably interacts with the Lys-β352 β-methylene and the side chains of Ala-β316 and Ala-β354. Remarkably, the ammonium residue of Lys-β254 can enter into a cation–π interaction with the quinazoline rings of **1**, **5a**, and **10**.[37,38] Table 3 summarizes the calculated binding energies. Compounds **5a** and **10** are predicted to bind more strongly to tubulin than **1**, and indole **10** even more strongly than the lead compound colchicine. However, given a standard error of 2.8 kcal mol^{-1} for AutoDock Vina calculations,[31] these binding enthalpies should not be over interpreted. A permissible conclusion from these studies is that the new compounds are able to bind in a similar orientation and at least as strongly to tubulin as the known verubulin (**1**).

We further assessed the antivascular properties in vitro using tube formation assays[39,40] which are based on the propensity of endothelial cells to form complex cord- or tube-like networks when grown on a basement membrane matrix (matrigel). Relative to untreated control cells which undergo a continuous migration and differentiation into highly ordered structures, cultures of hybrid endothelial Ea.hy926 cells exposed to 25 nM of **1**, **5a**, or **10** showed a retraction of the stretched intercellular connections after only 6 h (Figure 6). After 24 h there were clusters of vital cells without tubular outgrowth indicating that the essential morphological alterations, migrations, and differentiation processes were severely hindered because of cytoskeletal damage and reorganization induced by **1**, **5a**, or, most distinctly, by **10**.

These effects were reproducible in vivo when **1**, **5a**, or **10** were applied topically to the vascularized chorioallantoic membrane (CAM) of fertilized chicken eggs.[41] Disruption of small blood vessels as well as hemorrhages as a result of leaking or broken vessels were observed within the first 6 h (Figure 7). Even after 24 h hours there was no sign of regeneration or neo-formation of blood vessels within the silicon ring that confined the area of application.

Finally, we investigated the vascular-disrupting effect of compound **10** on established tumor vessels in vivo using our model of the highly vascularized 1411HP nude mouse xeno-

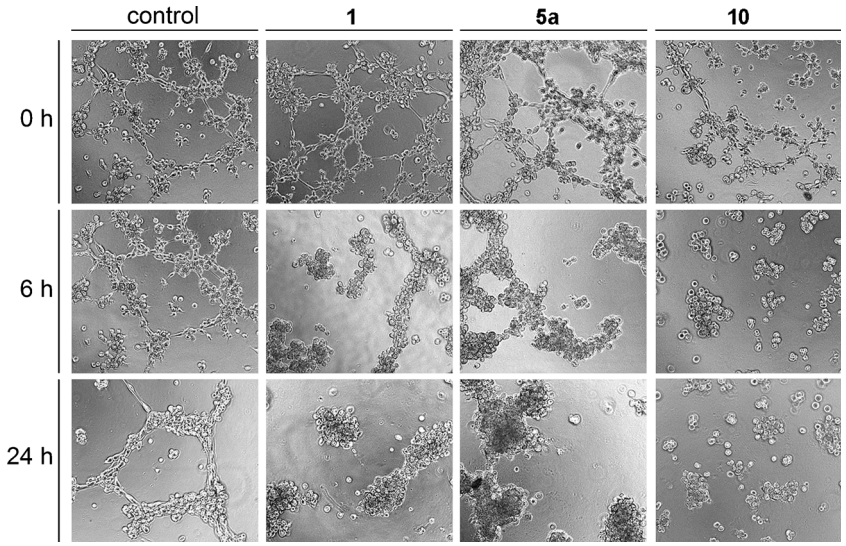

Figure 6. Formation or destruction of tubular networks in Ea.hy926 endothelial cells grown on thin matrigel layers when treated with compound **1**, **5a**, **10** (each at 25 nM), or with DMSO (control) for the indicated incubation times. Images were taken with a light microscope (100× magnification).

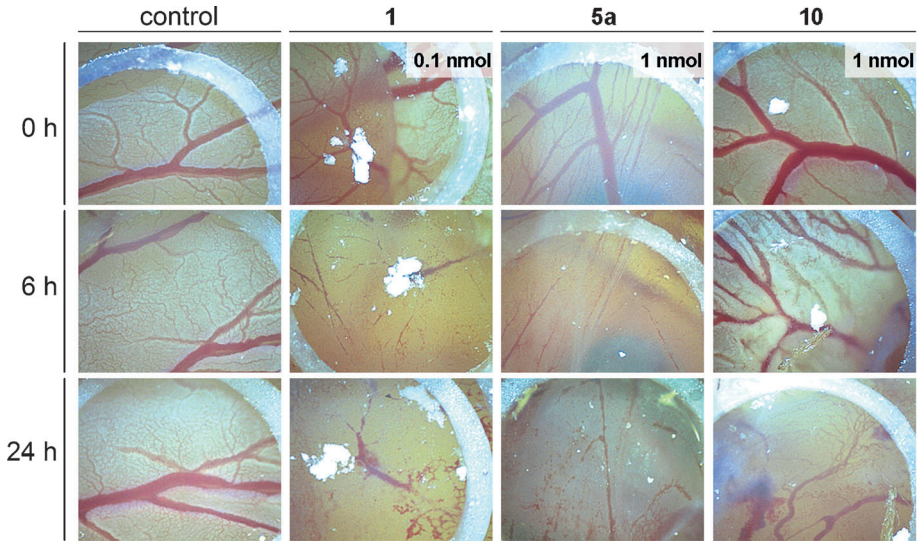

Figure 7. Effects of compounds **1** (0.1 nmol), **5a** (1.0 nmol), and **10** (1.0 nmol) on the blood vessels of the CAM of fertilized chicken eggs inside a ring of silicon foil (5 mm diameter) after 0, 6, and 24 h; control: DMSO. Images are representative of three independent assays (60× magnification).

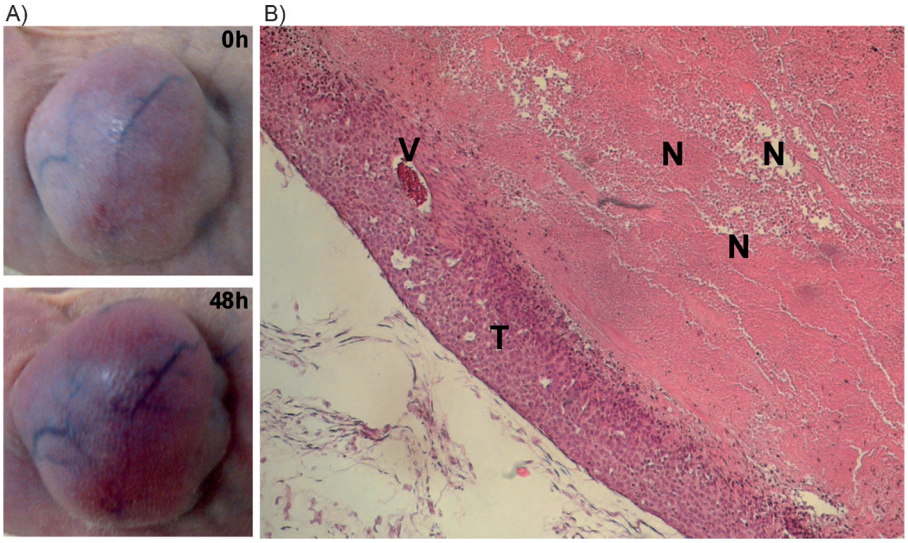

Figure 8. Vascular disrupting effect of **10** in a 1411HP xenograft tumor. A) Discoloration of the tumor due to intratumoral hemorrhage. B) Lateral section of the tumor shown in A (bottom) after HE staining featuring a large necrotic core area (**N**) surrounded by a cortical layer of vital tumor cells (**T**) which encompasses intact blood vessels (**V**).

graft tumor.[17] As shown in Figure 8 A, a single intraperitoneal dose of 5 mg kg^{-1} of **10** induced a strong discoloration of the entire tumor because of substantial intratumoral hemorrhage. A histological examination of the treated tumor revealed an extensive central necrosis and a persistent rim of surviving tumor cells, features that are usually observed upon treatment with VDA. No internal bleeding could be detected in the sacrificed mice.

Conclusions

We identified the microtubule and actin cytoskeletons as the main cellular targets of the discontinued antitumor drug candidate verubulin (**1**). The rapid and pronounced depolymerization of the microtubules of cancer cells by **1** and the formation of actin stress fiber networks in these led to a G2/M cell-cycle arrest and eventual cell death. These effects are similar to those described for other vascular-disrupting agents such as CA-4.[8,32,42] On a molecular level the strong affinity of **1** for tubulin could be demonstrated by in vitro polymerization assays with purified tubulin and by in silico docking experiments. The propensity of endothelial cells to form vasculature-like tubular networks was markedly attenuated by **1** and existing blood vessels in the chorioallantoic membrane (CAM) of fertilized hen eggs were destroyed by it.

Out of a series of new derivatives of **1** with heterocyclic appendages other than *para*-anisyl, two compounds **5 a** and **10** stuck out. While addressing the same molecular targets, the cytotoxic effect of **10** in malignant cells was greater than that of **1**. More importantly, its vascular-disrupting effect in the tube formation assay was more distinct as was its tolerance by chicken embryos in the CAM assay. Application of doses higher than 0.5 nmol was lethal after 6 h only in the case of **1**. Treatment with the same amount of **5 a** or **10** was far better tolerated by the chicken embryo and did not prevent it from growing and developing normally (Supporting Information, Table S1). In in vivo studies with mice bearing strongly vascularized 1411HP germ cell tumor xenografts, indole **10** caused extensive intratumoral hemorrhages and eventually necrosis due to long-lasting vascular occlusion (ischemia). The resulting necrotic core of the tumor was surrounded by a rim of persistent viable tumor cells as is typical of VDA in general.[42] Internal bleeding in the mice was not detected.

Experimental Section

Chemistry

2-Methyl-4-(*N*-benzodioxan-3-yl-*N*-methylamino)quinazoline (5 a): 2-Methyl-4-hydroxyquinazoline (100 mg, 0.62 mmol) and BOP (393 mg, 0.89 mmol) were dissolved in acetonitrile (5 mL) and treated with diphenyl ether (108 μL, 0.68 mmol) and DBU (205 μL, 1.37 mmol). The solution was stirred at RT for 5 min before compound **4 a** (370 mg, 2.24 mmol) was added. The reaction mixture was stirred at RT for 16 h. The solvent was evaporated and purification by column chromatography (silica gel 60; EtOAc/*n*-hexane, 1:1) gave **5 a** as a colorless solid (40 mg, 21 %): mp: 200 °C; R_f = 0.15 (EtOAc/*n*-hexane, 1:1); ^{1}H NMR (300 MHz, $CDCl_3$): δ = 2.69 (s, 3 H), 3.54 (s, 3 H), 4.2–4.3 (m, 4 H), 6.60 (dd, ^3J = 8.6 Hz, ^4J = 2.6 Hz, 1 H), 6.70 (d, ^4J = 2.6 Hz, 1 H), 6.81 (d, ^3J 8.6 Hz, 1 H), 6.9–7.0 (m, 1 H), 7.10 (dd, ^3J = 7.7 Hz, ^4J = 2.0 Hz, 1 H), 7.5–7.6 (m, 1 H), 7.72 (dd, ^3J = 7.7 Hz, ^4J = 1.8 Hz, 1 H); ^{13}C NMR (75.5 MHz, $CDCl_3$): δ = 26.4, 42.5, 64.3, 114.8, 115.0, 118.2, 119.2, 124.0, 126.2, 127.6, 131.7, 142.1, 144.3, 152.0, 161.6, 163.3 ppm; ATR-IR (neat): $\tilde{\nu}_{max}$ = 2968, 2928, 2875, 1614, 1587, 1564, 1547, 1492, 1464, 1448, 1434, 1381, 1352, 1308, 1278, 1245, 1229, 1180, 1155, 1125, 1099, 1063, 1049, 1035, 1007, 989, 937, 911, 885, 862, 827, 766, 748, 726, 687 cm^{-1}; MS (EI, 70 eV): *m/z* (%): 307 (100) $[M]^+$, 306 (73), 250 (14), 222 (28), 164 (44), 143 (42), 102 (43).

2-Methyl-4-(*N*-methyl-*N*-1-methylindol-5-ylamino)quinazoline (10): A solution of 2-methyl-4-hydroxyquinazoline (100 mg, 0.62 mmol) and BOP (393 mg, 0.89 mmol) in acetonitrile (5 mL) was treated with diphenyl ether (108 μL, 0.68 mmol) and DBU (205 μL, 1.37 mmol), stirred at RT for 5 min, and then treated with **9** (130 mg, 0.67 mmol). The reaction mixture was stirred at RT for 16 h. The solvent was evaporated and the residue was purified by column chromatography (silica gel 60; EtOAc/MeOH, 95:5). The obtained 3-chloroindol-5-ylaminoquinazoline (R_f 0.29, EtOAc) was separated from adhering benzotriazole impurities by extraction of the solid mixture with minute amounts of ethyl acetate. The yellow ethyl acetate phase was separated from the less soluble benzotriazole and concentrated in vacuo to leave the 3-chloroindol-5-ylaminoquinazoline. This was dissolved in methanol (10 mL), treated with 10 % Pd/C (70 mg), and stirred at RT under hydrogen gas (1 atm) for 2 h. The resulting black suspension was filtered over Celite and the filtrate was concentrated in vacuo to afford the title com-

pound **10** as a yellow solid (60 mg, 32%): mp: 248 °C; ^{1}H NMR (300 MHz, MeOD): $\delta = 2.71$ (s, 3H), 3.79 (s, 3H), 3.86 (s, 3H), 6.48 (d, $^3J = 3.1$ Hz, 1H), 6.74 (d, $^3J = 8.6$ Hz, 1H), 6.9–7.0 (m, 1H), 7.14 (dd, $^3J = 8.6$ Hz, $^4J = 2.2$ Hz, 1H), 7.30 (d, $^3J = 3.1$ Hz, 1H), 7.5–7.6 ppm (m, 4H); ^{13}C NMR (75.5 MHz, MeOD): $\delta = 23.8$, 33.3, 45.0, 102.7, 112.6, 119.3, 120.4, 122.5, 126.7, 128.7, 131.0, 132.7, 135.1, 137.5, 139.3, 158.2, 162.7 ppm; ATR-IR (neat): $\tilde{\nu}_{max} = 3639$, 3343, 2948, 1623, 1608, 1588, 1569, 1528, 1488, 1424, 1389, 1366, 1338, 1271, 1242, 1196, 1162, 1108, 1084, 996, 829, 761, 737, 686 cm^{-1}; MS (EI, 70 eV): *m/z* (%): 302 (100) $[M]^+$, 301 (89), 286 (10), 159 (37), 144 (45), 130 (22), 102 (38), 77 (14).

Molecular docking studies

Coordinate files of the ligand structures were generated by the GlycoBioChem PRODRG2 Server (http://davapc1.bioch.dundee.ac.uk/prodrg/submit.html).[43] Molecular docking calculations were carried out with the AutoDock Vina software.[34] and Gasteiger partial charges[44] were calculated on ligand atoms using AutoDock Tools. The X-ray structure of the crystallized tubulin–colchicine complex (PDB ID: 1SA0) was downloaded from the Protein Data Bank (http://www.rcsb.org). Polar hydrogen atoms were added to the protein and Gasteiger partial charges were calculated. Water molecules, heteroatoms, and ligands were removed from the structure prior to docking calculations. Residues Lys-β254, Lys-β352, Asn-α101, Val-β318, and Ile-β378 were treated as flexible residues. Simulation boxes were centered on the originally crystallized ligand colchicine. A 17×23×19 Å simulation box and an exhaustiveness option of 1,000 were used in the docking calculations. Figures were prepared with the program PyMOL.[45]

Biological studies

Cell-cycle analyses: Ea.hy926 cells (1×10^5 mL) grown on six-well plates were treated with DMSO (control), **1**, **5a**, or **10** (10 nM, 24 h), fixed (70% EtOH, 1 h, 4 °C) and incubated with propidium iodide (PI; Carl Roth) staining solution (50 μg mL^{-1} PI, 0.1% sodium citrate, 50 μg mL^{-1} RNase A in PBS) for 30 min at 37 °C. The fluorescence intensity of 10,000 single cells at $\lambda_{em} = 620$ nm ($\lambda_{ex} = 488$ nm laser source) was recorded with a Beckman Coulter Cytomics FC 500 flow cytometer and analyzed for the distribution of single cells (%) to G1, S, or G2/M phases as well as for the content of sub-G1 (apoptotic) events (CXP software, Beckman Coulter).

Fluorescence labeling of microtubules and actin filaments: Ea.hy926 cells (1×10^5 mL) were grown on glass coverslips in 24-well plates, treated with DMSO (control), **1**, **5a**, or **10** (10 nM) for 24 h, fixed with 4% formaldehyde in PBS for 20 min at RT, and permeabilized with 1% BSA, 0.1% Triton X-100 (in PBS) for 30 min. Nonmalignant HF were treated with 100 nM of **1**, **5a**, or **10**. To visualize F-actin, coverslips were incubated with 1 U AlexaFluor®-488-conjugated phalloidin (Invitrogen) for 1 h at 37 °C. For microtubule staining, fixed and permeabilized cells were treated with a primary antibody against α-tubulin (anti-α-tubulin, mouse mAb, Invitrogen; 5 μg mL^{-1}) for 1 h (37 °C, 5% CO_2, 95% humidity) followed by incubation with the secondary antibody conjugated to the fluorescent AlexaFluor®-488 dye (goat anti-mouse IgG-AlexaFluor-488 conjugate, Invitrogen; 4 μg mL^{-1}) for 1 h at RT in the dark. The coverslips were then mounted in Mowiol 4-88-based mounting medium containing 2.5% (*w/v*) DABCO and 1 μg mL^{-1} DAPI (4′,6-diamidino-2-phenylindole) for counterstaining the nuclei. Fluorescence microscopic analysis of the effects on both cytoskeletal components was performed using the ZEISS Axio Imager.A1 microscope.

Tube formation assays:[39,40] The effect of **1**, **5a**, and **10** on the propensity of stimulated Ea.hy926 cells to form vascular-like tubular networks in vitro was assessed by growing the cells (0.5×10^6 mL) on thin matrigel (BD Biosciences) layers for 12 h and then treating them with DMSO (control) or 25 nM of the test compounds. Documentation by light microscopy after 6 h and 24 h (10× magnification, Axiovert 135, AxioCam MRc 5, ZEISS). MTT was additionally added to each well after 24 h to ensure that more than 80% of the remaining cells are vital.

Chorioallantoic membrane (CAM) assays:[41] Fertilized white leg horn chicken eggs (SPF eggs, VALO Biomedia) were incubated (37 °C, 50–60% humidity) and opened on day six by cutting a window of 2–3 cm diameter into the eggshell at the more rounded pole. Rings of silicon foil (Ø 5 mm) were placed on the developing CAM vessels, the windows were sealed with tape and the eggs were incubated for a further 12–18 h. 1 nmol or 0.1 nmol (10 μL of a 100 μM or 10 μM solution in ddH_2O) of **1**, **5a**, **10**, or vehicle (DMSO) were pipetted inside the silicon ring. The effects were documented after 0 h, 6 h, and 24 h post application with a microscope (60× magnification, Traveller).

Animal studies: The vascular-disrupting activity of **10** was studied on the established model of highly vascularized 1411HP xenograft tumors previously described.[17] This study was approved by the Laboratory Animal Care Committee of Sachsen-Anhalt, Germany. Nude mice (Harlan and Winkelmann, Borchen, Germany) received 5 mg kg^{-1} body weight of compound **10** by intraperitoneal injection and tumor discoloration was documented immediately and after 48 h with a Canon IXUS 50. For histological examination the tumors were explanted, fixed in 4% formalin, and embedded in paraffin. Hematoxylin/eosin staining of the tissue slices was performed according to standard protocols.

Supporting Information

Instruments used; syntheses, microanalytical and spectroscopic data of all new compounds; MTT and SRB assays; tubulin polymerization assays.

Abbreviations

BOP, benzotriazol-1-yloxy-tris(dimethylamino)phosphonium hexafluorophosphate; CA-4, combretastatin A-4; CAM, chorioallantoic membrane; DAPI, 4′,6-diamidino-2-phenylindole; DBU, 1,8-diazabicyclo[5.4.0]undec-7-ene; HE, hematoxylin-eosin; MTT, 3-(4,5-dimethylthiazol-2-yl)-2,5-diphenyltetrazolium bromide; PI, propidium iodide; SRB, sulforhodamine-B; VDA, vascular-disrupting agent.

Keywords: angiogenesis · antitumor agents · quinazolines · vascular-disrupting agents · verubulin

[1] D. McDonald, P. Choyke, *Nat. Med.* **2003**, *9*, 713–725.
[2] D. J. Chaplin, G. J. Dougherty, *Br. J. Cancer* **1999**, *80 (Suppl. 1)*, 57–64.
[3] N. Ferrara, R. S. Kerbel, *Nature* **2005**, *438*, 967–974.
[4] P. Carmeliet, R. K. Jain, *Nature* **2000**, *407*, 249–257.
[5] D. W. Siemann, *Cancer Treat. Rev.* **2011**, *37*, 63–74.
[6] J. W. Lippert III, *Bioorg. Med. Chem.* **2007**, *15*, 605–615.
[7] G. R. Pettit, S. B. Singh, E. Hamel, C. M. Lin, D. S. Alberts, D. Garcia-Kendall, *Experientia* **1989**, *45*, 209–211.
[8] C. Kanthou, G. M. Tozer, *Expert Opin. Ther. Targets* **2007**, *11*, 1443–1457.
[9] D. J. Chaplin, S. Hill, *Int. J. Radiat. Oncol. Biol. Phys.* **2002**, *54*, 1491–1496.

[10] C. J. Mooney, G. Nagaiah, P. Fu, J. K. Wasman, M. M. Cooney, P. S. Savvides, J. A. Bokar, A. Dowlati, D. Wang, S. S. Agarwala, S. M. Flick, P. H. Hartman, J. D. Ortiz, P. N. Lavertu, S. C. Remick, *Thyroid* **2009**, *19*, 233 – 240.
[11] A. Delmonte, C. Sessa, *Expert Opin. Invest. Drugs* **2009**, *18*, 1541 – 1548.
[12] G. Del Conte, R. Bahleda, V. Moreno, S. Damian, A. Perotti, N. Lassau, F. Farace, M. Ong, S. J. Stimpson, N. Tunariu, S. Micallef, B. Demers, C. Oprea, G. Capri, J.-C. Soria, C. Sessa, L. R. Molife, *J. Clin. Oncol.* **2012**, *30 (Suppl. Abstr.)*, 3080.
[13] H. W. Salmon, D. W. Siemann, *Clin. Cancer Res.* **2006**, *12*, 4090 – 4094.
[14] G. C. Tron, T. Pirali, G. Sorba, F. Pagliai, S. Busacca, A. A. Genazzani, *J. Med. Chem.* **2006**, *49*, 3033 – 3044.
[15] L. Wang, K. W. Woods, Q. Li, K. J. Barr, R. W. McCroskey, S. M. Hannick, L. Gherke, R. B. Credo, Y.-H. Hui, K. Marsh, R. Warner, J. Y. Lee, N. Zielinski-Mozng, D. Frost, S. H. Rosenberg, H. L. Sham, *J. Med. Chem.* **2002**, *45*, 1697 – 1711.
[16] K. Bonezzi, G. Taraboletti, P. Borsotti, F. Bellina, R. Rossi, R. Giavazzi, *J. Med. Chem.* **2009**, *52*, 7906 – 7910.
[17] R. Schobert, B. Biersack, A. Dietrich, K. Effenberger-Neidnicht, S. Knauer, T. Mueller, *J. Med. Chem.* **2010**, *53*, 6595 – 6602.
[18] N. Sirisoma, A. Pervin, H. Zhang, S. Jiang, J. A. Willardsen, M. B. Anderson, G. Mather, C. M. Pleiman, S. Kasibhatla, B. Tseng, J. Drewe, S. X. Cai, *J. Med. Chem.* **2009**, *52*, 2341 – 2351.
[19] N. Sirisoma, A. Pervin, H. Zhang, S. Jiang, J. A. Willardsen, M. B. Anderson, G. Mather, C. M. Pleiman, S. Kasibhatla, B. Tseng, J. Drewe, S. X. Cai, *Bioorg. Med. Chem. Lett.* **2010**, *20*, 2330 – 2334.
[20] S. Kasibhatla, V. Baichwal, S. X. Cai, B. Roth, I. Skvortsova, S. Skvortsov, P. Lukas, N. M. English, N. Sirisoma, J. Drewe, A. Pervin, B. Tseng, R. O. Carlson, C. M. Pleiman, *Cancer Res.* **2007**, *67*, 5865 – 5871.
[21] S. Arora, X. I. Wang, S. M. Keenan, C. Andaya, Q. Zhang, Y. Peng, W. J. Welsh, *Cancer Res.* **2009**, *69*, 1910 – 1915.
[22] S. Ahn, C. B. Duke III, C. M. Barrett, D. J. Hwang, C.-M. Li, D. D. Miller, J. T. Dalton, *Mol. Cancer Ther.* **2010**, *9*, 2859 – 2868.
[23] G. La Regina, R. Bai, W. Rensen, A. Coluccia, F. Piscitelli, V. Gatti, A. Bolognesi, A. Lavecchia, I. Granata, A. Porta, B. Maresca, A. Soriani, M. L. Iannitto, M. Mariani, A. Santoni, A. Brancale, C. Ferlini, G. Dondio, M. Varasi, C. Mercurio, E. Hamel, P. Lavia, E. Novellino, R. Silvestri, *J. Med. Chem.* **2011**, *54*, 8394 – 8406.
[24] Z.-K. Wan, S. Wacharasindhu, C. G. Levins, M. Lin, K. Tabei, T. S. Mansour, *J. Org. Chem.* **2007**, *72*, 10194 – 10210.
[25] M. Mateu, A. S. Capilla, Y. Harrak, M. D. Pujol, *Tetrahedron* **2002**, *58*, 5241 – 5250.
[26] W. J. Houlihan, G. Cooke, M. Denzer, J. Nicoletti, *J. Heterocycl. Chem.* **1982**, *19*, 1453 – 1456.
[27] S. Ghosh, M. Lobera, D. Schmidt, E. Baloglu (Tempero Pharmaceuticals, Cambridge, MA, USA), Int. PCT Pub. No. WO 2013/006408A1, **2013**.
[28] T. Mosmann, *J. Immunol. Methods* **1983**, *65*, 55 – 63.
[29] T. Müller, W. Voigt, H. Simon, A. Frühauf, A. Bulankin, A. Grothey, H.-J. Schmoll, *Cancer Res.* **2003**, *63*, 513 – 521.
[30] K. T. Papazisis, G. D. Geromichalos, K. A. Dimitriadis, A. H. Kortsaris, *J. Immunol. Methods* **1997**, *208*, 151 – 158.
[31] H. Y. Yamada, G. J. Gorbsky, *Mol. Cancer Ther.* **2006**, *5*, 2963 – 2963.
[32] C. Kanthou, G. M. Tozer, *Blood* **2002**, *99*, 2060 – 2069.
[33] R. B. Ravelli, B. Gigant, P. A. Curmi, I. Jourdain, S. Lachkar, A. Sobel, M. Knossow, *Nature* **2004**, *428*, 198 – 202.
[34] O. Trott, A. J. Olson, *J. Comput. Chem.* **2010**, *31*, 455 – 461.
[35] F. Bellina, S. Cauteruccio, S. Monti, R. Rossi, *Bioorg. Med. Chem. Lett.* **2006**, *16*, 5757 – 5762.
[36] M. Botta, S. Forli, M. Magnani, F. Manetti, in *Topics in Current Chemistry, Vol. 286* (Eds.: T. Carlomagno, K.-H. Altmann), Springer-Verlag, Berlin Heidelberg, **2009**, pp. 279 – 328.
[37] J. P. Gallivan, D. A. Dougherty, *Proc. Natl. Acad. Sci. USA* **1999**, *96*, 9459 – 9464.
[38] D. A. Dougherty, *J. Nutr.* **2007**, *137*, 1504S – 1508S.
[39] E. Aranda, G. I. Owen, *Biol. Res.* **2009**, *42*, 377 – 389.
[40] J. Bauer, M. Margolis, C. Schreiner, C. J. Edgell, J. Azizkhan, R. L. Juliano, *J. Cell. Physiol.* **1992**, *153*, 437 – 449.
[41] B. Nitzsche, C. Gloesenkamp, M. Schrader, M. Ocker, R. Preissner, M. Lein, A. Zakrzewicz, B. Hoffmann, M. Höpfner, *Br. J. Cancer* **2010**, *103*, 18 – 28.
[42] S. J. Lunt, S. Akerman, S. A. Hill, M. Fisher, V. J. Wright, C. C. Reyes-Aldasoro, G. M. Tozer, C. Kanthou, *Int. J. Cancer* **2011**, *129*, 1979 – 1989.
[43] PRODRG: A tool for high-throughput crystallography of protein – ligand complexes. A. W. Schüttelkopf, D. M. F. van Aalten, *Acta Crystallogr. Sect. D* **2004**, *60*, 1355 – 1363.
[44] J. Gasteiger, M. Marsili, *Tetrahedron* **1980**, *36*, 3219 – 3228.
[45] W. DeLano, The PyMOL Molecular Graphics System, DeLano Scientific LLC, San Carlos, CA (USA), **2003**.

Received: December 16, 2013
Published online on February 23, 2014

CHEMMEDCHEM
Chemistry & Drug Discovery

Supporting Information

Effects of the Tumor-Vasculature-Disrupting Agent Verubulin and Two Heteroaryl Analogues on Cancer Cells, Endothelial Cells, and Blood Vessels

Katharina Mahal,[a] Marcus Resch,[b] Ralf Ficner,[b] Rainer Schobert,[a] Bernhard Biersack,*[a] and Thomas Mueller*[c]

cmdc_201300531_sm_miscellaneous_information.pdf

Supporting Information

Table S1. Lethality of 7/8-day-old chicken embryos in the CAM assay model (within 24 h after application) after single treatment of the CAM with 1 nmol, 0.5 nmol or 0.1 nmol dilutions of verubulin **1** or its derivatives **5a** and **10**. At least 10 fertilised chicken eggs were treated with the indicated amount of substance.

lethality	1 nmol	0.5 nmol	0.1 nmol
1	100 %	70 %	10 %
5a	90 %	-	-
10	80 %	-	-

General remarks and instruments used

Column chromatography: silica gel 60 (230-400 mesh). Melting points (uncorrected), Electrothermal 9100; IR spectra, Perkin-Elmer Spectrum One FT-IR spectrophotometer with ATR sampling unit; NMR spectra, Bruker Avance 300 spectrometer; chemical shifts are given in parts per million (δ) downfield from tetramethylsilane as internal standard; Mass spectra, Thermo Finnigan MAT 8500 (EI); Microanalyses, Perkin-Elmer 2400 CHN elemental analyzer. All tested compounds are > 98% pure by LC-MS (Varian 1200 L) or GC-MC (Finnigan MAT 95) analysis. All starting compounds were purchased from the usual retailers and used without further purification.

Syntheses and characterization of compounds 3a-c, 4a-c,[25-27] 5b-c, 7-9

5-Ethoxycarbonylaminobenzodioxane (3a). A mixture of 5-aminobenzodioxane **2a** (500 mg, 3.31 mmol), THF (10 mL), triethylamine (554 µL, 4.0 mmol) and ethyl chloroformate (349 µL, 3.67 mmol) was stirred at room temperature for 4 h, diluted with 1M HCl and then extracted with ethyl acetate. The organic phase was washed with water and brine, dried over Na_2SO_4, filtered and concentrated in vacuum. The oily residue was purified by column

chromatography (silica gel 60). Yield, 700 mg (95%); yellow gum; R_f 0.63 (ethyl acetate/*n*-hexane 1:1); ν_{max} (ATR)/cm^{-1} 3327, 2986, 2942, 1697, 1608, 1542, 1507, 1478, 1462, 1433, 1330, 1273, 1231, 1206, 1177, 1062, 972, 922, 895, 863, 815, 789, 767, 738, 679; ^{1}H NMR (300 MHz, $CDCl_3$): δ 1.25 (3 H, t, *J* 7.1 Hz), 4.1-4.2 (6 H, m), 6.64 (1 H, s), 6.7-6.8 (2 H, m), 6.96 (1 H, s); ^{13}C NMR (75.5 MHz, $CDCl_3$): δ 14.5, 61.0, 64.2, 64.4, 108.7, 112.5, 117.1, 131.7, 139.7, 143.5, 153.8; m/z (EI, %) 223 (100) [M$^+$], 195 (32), 177 (42), 150 (81), 95 (79).

5-Ethoxycarbonylaminobenzodioxolane (3b). A mixture of 5-aminobenzodioxolane **2b** (500 mg, 3.65 mmol), THF (10 mL), triethylamine (554 µL, 4.0 mmol) and ethyl chloroformate (349 µL, 3.67 mmol) was stirred at room temperature for 4 h, diluted with 1M HCl and extracted with ethyl acetate. The organic phase was washed with water and brine, dried over Na_2SO_4, filtered and concentrated in vacuum. The oily residue was purified by column chromatography (silica gel 60). Yield, 650 mg (85%); yellow gum; R_f 0.70 (ethyl acetate/*n*-hexane 1:1); ν_{max} (ATR)/cm^{-1} 3321, 2991, 2907, 1694, 1637, 1551, 1501, 1491, 1480, 1455, 1370, 1337, 1274, 1227, 1212, 1188, 1145, 1105, 1059, 1035, 953, 924, 891, 855, 818, 803, 788, 765, 753, 675; ^{1}H NMR (300 MHz, $CDCl_3$): δ 1.22 (3 H, t, *J* 7.2 Hz), 4.15 (2 H, q, *J* 7.2 Hz), 5.84 (2 H, s), 6.6-6.7 (2 H, m), 7.03 (1 H, s), 7.11 (1 H, s); ^{13}C NMR (75.5 MHz, $CDCl_3$): δ 14.3, 60.8, 100.9, 101.8, 107.8, 111.9, 132.3, 143.4, 147.6, 154.0; m/z (EI, %) 209 (85) [M$^+$], 181 (18), 163 (37), 136 (100), 106 (27), 80 (37), 53 (30).

5-Ethoxycarbonylaminobenzofurane (3c). A mixture of 5-aminobenzofurane **2c** (250 mg, 1.88 mmol), THF (10 mL), triethylamine (316 µL, 2.28 mmol), and ethyl chloroformate (200 µL, 2.10 mmol) was stirred at room temperature for 4 h, diluted with 1M HCl and extracted with ethyl acetate. The organic phase was washed with water and brine, dried over Na_2SO_4, filtered and concentrated in vacuum. The oily residue was purified by column chromatography (silica gel 60). Yield, 300 mg (78%); yellow gum; R_f 0.50 (ethyl acetate/*n*-hexane 1:2); ^{1}H

NMR (300 MHz, $CDCl_3$): δ 1.25 (3 H, t, *J* 7.2 Hz), 4.20 (2 H, q, *J* 7.2 Hz), 6.61 (1 H, d, *J* 2.2 Hz), 7.1-7.3 (2 H, m), 7.33 (1 H, d, *J* 8.8 Hz), 7.53 (1 H, d, *J* 2.2 Hz), 7.72 (1 H, s); ^{13}C NMR (75.5 MHz, $CDCl_3$): δ 14.4, 60.9, 106.5, 111.1, 111.6, 116.8, 127.6, 133.2, 145.5, 151.4, 154.2; m/z (EI, %) 205 (100) [M^+], 177 (14), 146 (36), 133 (71).

5-Methylaminobenzodioxane (4a). Carbamate **3a** (630 mg, 2.83 mmol) was treated with $LiAlH_4$ (1M solution in THF, 7.5 mL, 7.5 mmol) and stirred under reflux for 1 h. After cooling to room temperature water was added dropwise and the resulting mixture was extracted with ethyl acetate. The organic phase was dried over Na_2SO_4, filtered and concentrated in vacuum. The residue was purified by column chromatography (silica gel 60). Yield, 370 mg (79%); yellow oil; R_f 0.60 (ethyl acetate/*n*-hexane 1:1); ν_{max} (ATR)/cm^{-1} 3405, 2977, 2925, 2873, 2803, 1627, 1594, 1507, 1473, 1453, 1431, 1328, 1300, 1277, 1240, 1205, 1176, 1151, 1119, 1067, 1041, 913, 883, 827, 794, 746, 734; ^1H NMR (300 MHz, $CDCl_3$): δ 2.72 (3 H, s), 3.5-3.6 (1 H, m), 4.1-4.2 (4 H, m), 6.1-6.2 (2 H, m), 6.71 (1 H, d, *J* 8.5 Hz); ^{13}C NMR (75.5 MHz, $CDCl_3$): δ 31.0, 63.8, 64.4, 98.2, 100.6, 106.0, 117.2, 135.1, 143.8, 144.3; m/z (EI, %) 165 (100) [M^+], 109 (86), 80 (20).

5-Methylaminobenzodioxolane (4b). Carbamate **3b** (630 mg, 3.01 mmol) was treated with $LiAlH_4$ (1M solution in THF, 7.5 mL, 7.5 mmol) and stirred under reflux for 1 h. After cooling to room temperature water was added dropwise and carefully and the mixture was extracted with ethyl acetate. The organic phase was dried over Na_2SO_4, filtered and concentrated in vacuum. The residue was purified by column chromatography (silica gel 60). Yield, 370 mg (81%); brown oil; R_f 0.60 (ethyl acetate/*n*-hexane 1:1); ν_{max} (ATR)/cm^{-1}: 3410, 2879, 2809, 1634, 1609, 1501, 1485, 1448, 1293, 1242, 1196, 1151, 1140, 1095, 1033, 935, 913, 810, 786; ^1H NMR (300 MHz, $CDCl_3$): δ 2.75 (3 H, s), 3.5-3.6 (1 H, m), 5.83 (2 H, s), 6.03 (1 H, dd, *J* 8.3 Hz, *J* 2.4 Hz), 6.24 (1 H, d, *J* 2.4 Hz), 6.69 (1 H, d, *J* 8.4 Hz); ^{13}C NMR (75.5 MHz,

$CDCl_3$): δ 31.2, 60.1, 95.3, 100.3, 103.4, 108.3, 139.2, 145.1, 148.1; m/z (EI, %) 151 (100) [M^+], 122 (26), 93 (57), 78 (86), 63 (35), 51 (42).

5-Methylaminobenzofurane (4c). Carbamate **3c** (280 mg, 1.37 mmol) was treated with $LiAlH_4$ (1M solution in THF, 5 mL, 5 mmol) and stirred under reflux for 1 h. After cooling to room temperature water was added dropwise and carefully and the mixture was extracted with ethyl acetate. The organic phase was dried over Na_2SO_4, filtered and concentrated in vacuum. The residue was purified by column chromatography (silica gel 60). Yield, 190 mg (94%); yellow oil; R_f 0.67 (ethyl acetate/*n*-hexane 1:1); ^{1}H NMR (300 MHz, $CDCl_3$): δ 2.86 (3 H, s), 3.6-3.7 (1 H, m), 6.6-6.7 (2 H, m), 6.80 (1 H, d, *J* 2.3 Hz), 7.39 (1 H, d, *J* 8.8 Hz), 7.59 (1 H, d, *J* 2.3 Hz); ^{13}C NMR (75.5 MHz, $CDCl_3$): δ 31.4, 101.8, 106.2, 111.4, 112.0, 128.1, 145.0, 145.6, 148.7; m/z (EI, %) 147 (100) [M^+], 146 (97), 132 (16), 118 (28).

2-Methyl-4-(*N*-benzodioxolan-3-yl-*N*-methyl-amino)quinazoline (5b). 2-Methyl-4-hydroxy-quinazoline (100 mg, 0.62 mmol) and BOP (393 mg, 0.89 mmol) were dissolved in acetonitrile (5 mL) and treated with diphenylether (108 µL, 0.68 mmol) and DBU (205 µL, 1.37 mmol). The solution was stirred at room temperature for 5 min before compound **4b** (370 mg, 2.45 mmol) was added. The reaction mixture was stirred at room temperature for 16 h. The solvent was evaporated and the residue was purified by column chromatography (silica gel 60, ethyl acetate/*n*-hexane 1:1). Yield, 55 mg (31%); off-white solid of mp: 161 °C; R_f 0.15 (ethyl acetate/*n*-hexane 1:1); ν_{max} (ATR)/cm^{-1} 3016, 1613, 1565, 1546, 1488, 1474, 1447, 1383, 1355, 1343, 1221, 1182, 1162, 1126, 1111, 1089, 1031, 989, 931, 913, 877, 863, 811, 797, 761, 729, 684; ^{1}H NMR (300 MHz, $CDCl_3$): δ 2.69 (3 H, s), 3.53 (3 H, s), 5.99 (2 H, s), 6.59 (1 H, dd, *J* 8.2 Hz, *J* 2.2 Hz), 6.67 (1 H, d, *J* 2.2 Hz), 6.73 (1 H, d, *J* 8.2 Hz), 6.9-7.0 (1 H, m), 7.10 (1 H, d, *J* 9.0 Hz), 7.5-7.6 (1 H, m), 7.72 (1 H, d, *J* 9.0 Hz), 7.5-7.6 (4 H, m); ^{13}C NMR (75.5 MHz, $CDCl_3$): δ 26.4, 42.6, 57.9, 101.6, 107.3, 108.9, 114.7, 119.4, 124.1, 126.1, 127.6,

131.7, 142.8, 146.0, 148.7, 152.0, 161.6, 163.3; m/z (%) 293 (100) [M^+], 292 (81), 143 (51), 102 (72), 65 (29).

2-Methyl-4-(*N*-benzofuran-5-yl-*N*-methyl-amino)-quinazoline (5c). 2-Methyl-4-hydroxy-quinazoline (90 mg, 0.56 mmol) and BOP (393 mg, 0.89 mmol) were dissolved in acetonitrile (20 mL) and treated with diphenylether (108 µL, 0.68 mmol) and DBU (205 µL, 1.37 mmol). The solution was stirred at room temperature for 5 min before compound **4c** (190 mg, 1.29 mmol) was added. The reaction mixture was stirred at room temperature for 16 h. The solvent was evaporated and the residue was purified by column chromatography (silica gel 60, gradient elution from ethyl acetate/*n*-hexane 1:1 to pure ethyl acetate). Yield, 40 mg (25%); colorless gum; R_f 0.08 (ethyl acetate/*n*-hexane 1:1); ^{1}H NMR (300 MHz, $CDCl_3$): δ 2.67 (3 H, s), 3.68 (3 H, s), 6.85 (1 H, d, *J* 2.2 Hz), 6.9-7.0 (1 H, m), 7.5-7.7 (4 H, m), 7.85 (1 H, d, *J* 2.2 Hz); ^{13}C NMR (75.5 MHz, $CDCl_3$): δ 25.8, 43.8, 108.1, 114.0, 120.3, 124.2, 125.5, 127.1, 127.8, 133.6, 148.5; m/z (%) 289 (99) [M^+], 288 (100) [M^+], 146 (71), 102 (41).

3-Chloro-1-methyl-5-nitroindole (7). 1-Methyl-5-nitroindole (570 mg, 3.24 mmol) was dissolved in acetonitrile (25 mL) and treated with *N*-chlorosuccinimide (518 mg, 3.9 mmol). The reaction mixture was stirred at room temperature for 4 h and the resulting yellow precipitate was collected and dried in vacuum. Yield, 410 mg (60%); yellow solid; v_{max} (ATR)/cm^{-1} 3115, 2940, 1611, 1576, 1515, 1481, 1460, 1427, 1390, 1320, 1276, 1237, 1184, 1145, 1113, 1081, 1034, 977, 890, 876, 805, 784, 770, 749, 731; ^{1}H NMR (300 MHz, $CDCl_3$): δ 3.82 (3 H, s), 7.16 (1 H, s), 7.32 (1 H, d, ^3J 9.1 Hz), 8.13 (1 H, dd, *J* 9.0 Hz, *J* 2.2 Hz), 8.55 (1 H, d, *J* 2.2 Hz); ^{13}C NMR (75.5 MHz, $CDCl_3$): δ 33.5, 107.4, 109.7, 116.0, 118.1, 125.2, 128.4, 138.4, 142.0; m/z (%) 212 (33) [M^+], 210 (100) [M^+], 166 (17), 164 (60), 152 (21), 129 (27), 128 (49), 102 (35), 101 (42).

3-Chloro-5-ethoxycarbonylamino-1-methyl-indole (8). A solution of **7** (410 mg, 1.95 mmol)

in THF (10 mL) was cooled in an ice-bath and treated with Zn powder (808 mg, 12.4 mmol) and conc. HCl (1.74 mL). After stirring for 10 min the reaction mixture was poured into water and basified (pH 8) with saturated aqueous $NaHCO_3$ solution. After extraction with ethyl acetate the organic phase was dried over Na_2SO_4, filtered and concentrated in vacuum. The residue was purified by column chromatography (silica gel 60, ethyl acetate/methanol 95:5) giving the amine as a yellow oil (270 mg, 1.5 mmol, 77%). The amine was dissolved in THF (p.a.), treated with triethylamine (250 µL) and ethyl chloroformate (160 µL, 1.68 mmol) and stirred at room temperature for 4 h. The reaction mixture was diluted with 1M HCl and extracted with ethyl acetate. The organic phase was washed with water and brine, dried over Na_2SO_4, filtered and concentrated in vacuum. The oily residue was purified by column chromatography (silica gel 60). Yield, 230 mg (0.91 mmol, 61%); yellow gum; R_f 0.53 (ethyl acetate/*n*-hexane 1:1); v_{max} (ATR)/cm^{-1} 3321, 3115, 2979, 2928, 1695, 1581, 1526, 1496, 1473, 1444, 1365, 1287, 1235, 1213, 1169, 1142, 1114, 1062, 987, 925, 855, 791, 774, 752; ^{1}H NMR (300 MHz, $CDCl_3$): δ 1.28 (3 H, t, *J* 7.0 Hz), 3.63 (3 H, s), 4.22 (2 H, q, *J* 7.0 Hz), 6.84 (1 H, s), 6.91 (1 H, s), 7.1-7.3 (2 H, m), 7.60 (1 H, s); ^{13}C NMR (75.5 MHz, $CDCl_3$): δ 14.4, 32.8, 61.0, 103.9, 108.5, 109.7, 116.3, 125.7, 125.9, 127.5, 130.9, 132.8, 154.2; m/z (%) 254 (32) [M$^+$], 252 (100) [M$^+$], 224 (18), 206 (27), 179 (73), 152 (25).

3-Chloro-1-methyl-5-methylaminoindole (9). Carbamate **8** (210 mg, 0.83 mmol) was treated with $LiAlH_4$ (1 M solution in THF, 4.5 mL, 4.5 mmol) and stirred under reflux for 1 h. After cooling to room temperature water was added dropwise and the mixture was extracted with ethyl acetate. The organic phase was dried over Na_2SO_4, filtered and concentrated in vacuum. The residue was purified by column chromatography (silica gel 60). Yield, 140 mg (87%); yellow oil; R_f 0.51 (ethyl acetate/*n*-hexane 1:1); v_{max} (ATR)/cm^{-1}: 3403, 3118, 2880, 2806, 1627, 1575, 1500, 1446, 1418, 1362, 1348, 1314, 1281, 1238, 1169, 1148, 1112, 1047, 973, 874, 826, 781, 771, 715; ^{1}H NMR (300 MHz, $CDCl_3$): δ 2.92 (3 H, s), 3.5-3.6 (1 H, m),

3.65 (3 H, s), 6.69 (1 H, dd, *J* 8.8 Hz, *J* 2.2 Hz), 6.79 (1 H, d, *J* 2.2 Hz), 6.91 (1 H, s), 7.13 (1 H, d, *J* 8.8 Hz); m/z (%) 194 (100) [M^+], 193 (40), 179 (37), 152 (14), 97 (10).

Cell Lines and Culture Conditions. The human 518A2 melanoma cell line was a gift from the Department of Radiotherapy and Radiobiology, University Hospital Vienna, the MCF-7/Topo cells were obtained from the Institute of Pharmacy of the University of Regensburg, Germany, and the colon HCT-116 cells from the University Hospital Erlangen, Germany. The HUVEC-derived endothelial hybrid cell line Ea.hy926 (ATCC no. CRL-2922) was a gift from the Institute of Physiology, Charité Berlin, Germany, the human foreskin fibroblasts (HF) were a gift from the Institut für Chirurgische Forschung, Philipps-Universität Marburg, Germany. The 518A2, MCF-7/Topo, HCT-116 as well as the Ea.hy926 endothelial and HF cells were cultured in Dulbecco's Modified Eagle Medium (DMEM, Gibco) containing 10% FBS, 100 IU/mL penicillin G, 100 µg/mL streptomycin sulfate, 0,25 µg/mL amphotericin B and 250 µg/mL gentamycine. The origin and culture conditions of H12.1 and 1411HP cells were as previously described.[S2] The A2780, HCT-8, HT-29 and DLD-1 cells were obtained from the American Type Culture Collection (ATCC), Rockville, MD, and from the German National Resource Centre for Biological Material (DSMZ), Braunschweig. Cell lines were maintained as monolayer cultures in RPMI 1640 supplemented with 10% heat inactivated fetal bovine serum (Biochrom KG Seromed, Germany) and streptomycin/penicillin (GIBCO, Germany). Cultures were grown at 37 °C in a humidified atmosphere of 5% CO_2.

Cell Proliferation Assay (MTT Assay).[S1] MTT [3-(4,5-dimethylthiazol-2-yl)-2,5-diphenyl-tetrazolium bromide] was used to identify viable cells that reduce it to a violet formazan. 518A2 melanoma, HCT-1116 colon carcinoma, MCF-7 breast carcinoma (5×10^4 cells/mL), Ea.hy926 endothelial cells and non-malignant human foreskin fibroblasts (HF, $1\text{x}10^5$ cell/mL) were seeded and cultured for 24 h on 96-well microplates. Incubation (5% CO_2, 95% humidity, 37 °C) of cells following treatment with the test compounds (dilution series of 10 mM

stock solutions in DMSO ranging from 0.0001 to 100 μM in ddH_2O) was continued for 72 h. Blanks and solvent controls were treated identically. The MTT assay was performed as previously described[1]. Briefly, a 5 mg/mL stock solution of MTT in PBS was added to a final MTT concentration of 0.05%. After 2 h incubation, the microplates were centrifuged at 300 g for 5 min, the medium was discarded and the precipitate of formazan crystals was redissolved in a SDS-DMSO solution (10% SDS (w/v), 0.6% acetic acid in DMSO). The absorbance at wavelengths 570 and 630 nm (background) was measured using an automatic ELISA microplate reader (Tecan). All experiments were carried out at least in triplicate, the percentage of viable cells quoted was calculated as the mean ± S.D. with respect to the controls set to 100%.

Cell Proliferation Assay (SRB Assay). Dose-response curves of the cell lines exposed to drug concentrations of 0.0001-10 μM were established using the sulforhodamine-B (SRB) microculture colorimetric assay[S3] which was performed as previously described.[S2] Briefly, cells were seeded into 96-well plates on day 0, at cell densities previously determined to ensure exponential cell growth during the period of the experiment. On day 1, cells were treated with the drugs dissolved in DMSO to give the appropriate concentrations for indicated times and the percentage of surviving cells relative to untreated controls was determined on day 5.

Tubulin polymerization assay. Analysis of tubulin polymerization was performed using the tubulin polymerization assay kit (Cytoskeleton) according to manufactures instructions. The assay is fluorescence-based, and tubulin polymerization was followed by measuring RFU (relative fluorescence units) on the SpectraFluorPlus (Tecan, Switzerland) using the following filters: excitation 360 nm, emission 465 nm.

References

[S1] Mosmann T.; Rapid colorimetric assay for cellular growth and survival: application to proliferation and cytotoxicity assays. *J. Immunol. Methods* **1983**, *65*, 55–63.

[S2] Müller, T.; Voigt, W.; Simon, H.; Frühauf, A.; Bulankin, A.; Grothey, A.; Schmoll, H.-J. Failure of activation of caspase-9 induces a higher threshold for apoptosis and cisplatin resistance in testicular cancer. *Cancer Res.* **2003**, *63*, 513–521.

[S3] Papazisis, K. T.; Geromichalos, G. D.; Dimitriadis, K. A.; Kortsaris, A. H. Optimization of the sulforhodamine B colorimetric assay. *J. Immunol. Methods* **1997**, *208*, 151–158.

PUBLIKATION II

New oxazole-bridged Combretastatin A-4 analogues as potential vascular-disrupting agents (*Extended Abstract*)

Katharina Mahal*, Bernhard Biersack, Rainer Schobert

Organic Chemistry Laboratory, University of Bayreuth, Universitätsstraße 30, 95440 Bayreuth (Germany)

* email: katharina.mahal@uni-bayreuth.de

Int. J. Clin. Pharmacol. Ther. **2013**, *51*, 41-43.

International Journal of Clinical Pharmacology and Therapeutics, Vol. 51 – No. 1/2013 (41-43)

Extended Abstract

ISSN 0946-1965

DOI 10.5414/CPP51041
e-pub: December 21, 2012

New oxazole-bridged combretastatin A-4 analogues as potential vascular-disrupting agents

Katharina Mahal, Bernhard Biersack and Rainer Schobert

Chair of Organic Chemistry, University Bayreuth, Bayreuth, Germany

Key words
antivascular agents – combretastatin A-4 – oxazoles – Ea.hy926 tube formation

Correspondence to
Katharina Mahal
University Bayreuth,
Universitaetsstr. 30,
NW I, 95440 Bayreuth,
Germany
katharina.mahal@uni-bayreuth.de

Introduction

The *cis*-stilbene combretastatin A-4 (CA-4) is a metabolite of the South-African bush willow *Combretum caffrum* with remarkable antitumoral properties. Its mode of action is based on its high affinity for the colchicine binding site of β-tubulin and the resulting destabilization of the microtubule cytoskeleton [1]. CA-4 is also known to target the vasculature of solid tumors and to induce blood vessel shutdown leading to secondary tumor cell death [2]. The metabolic conversion of CA-4 to its inactive *trans*-isomer and its poor solubility are drawbacks that limit its applicability in anticancer therapy. Recent efforts to stabilize the *cis*-configuration by integration into heterocycles led to CA-4 derivatives with imidazole and oxazole rings the activity of which is dependent on the pattern of substituents in the phenyl rings [3, 4, 5, 6]. Some halogen-substituted oxazoles of this type showed enhanced efficacy against resistant cancer cell lines and also exhibited anti-vascular properties [6]. The cytotoxicity and inhibition of tube formation, as well as the ability to interfere with the cell cycle of a second generation of *chloro*-substituted oxazoles with additional functional groups int the B-ring (1: -OMe, 2: -OEt, 3: -SMe) (Figure 1) has now been investigated using human endothelial cells.

Materials and methods

The synthesis of compounds 1 – 3 has been published or will be published elsewhere [6].

Cell culture conditions

Cells of resistant human HT-29 colon carcinoma, human 518A2 melanoma, and Ea.hy926 endothelial hybrid cells were cultivated in RPMI or DMEM (supplemented with 10% FBS, 1% Pen/Strep, 100X, Gibco) and incubated at 37 °C, 5% CO_2 and 95% humidity. The cells were harvested by trypsination and grown for 24 h prior to treatment with the compounds 1 – 3 (in DMSO).

MTT assay

The cytotoxic effect on the three cell lines upon exposure to the oxazoles 1 – 3 for 72 hours was determined by a standard MTT assay with 3(4,5-dimethylthiazol-2-yl)-2,5-diphenyltetrazolium bromide, 0.05% in 1X PBS acc. to ref. [6].

Cell cycle analysis

Ea.hy926 cells (0.1×10^6 cells/ml) grown on 6-well plates were treated with DMSO (control) or 1 – 3 (1 µM, 24 h), fixed (70% EtOH) and incubated with propidium iodide (PI, Carl Roth) staining solution (50 µg/ml PI, 0.1% sodium citrate, 1 µg/ml RNase A in 1X PBS) for 30 min at 37 °C. The fluorescence intensity of 10,000 single cells at λ_{em} = 570 nm (λ_{ex} = 488 nm) was recorded by a Beckman Coulter Cytomics FC 500 flow cytometer and analyzed (CXP software, Beckman Coulter) to render the percentage of cells in G1, S- and G2/M-phase of the cell cycle. Apoptotic cells were assessed from sub-G1-peaks.

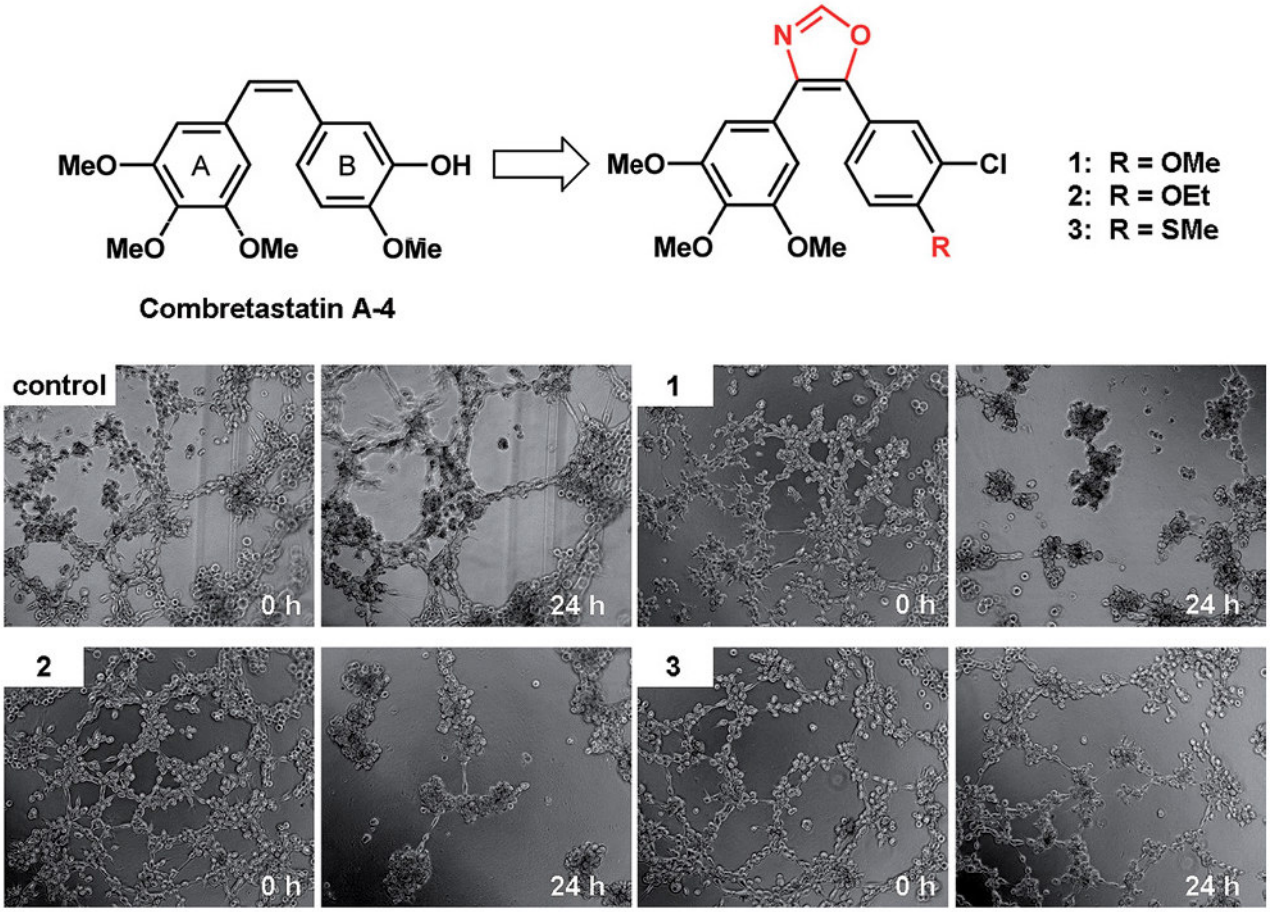

Figure1. Tube formation by Ea.hy926 endothelial cells grown on thin Matrigel layers and treated with 100 nM of compound 1 – 3 for 24 hours compared with untreated cells that form blood vessel-like networks (10-fold magnification).

Tube formation assay

The effect of oxazoles 1 – 3 on the propensity of stimulated Ea.hy926 cells to form vascular-like tubular networks in vitro was assessed by growing the cells (0.5×10^6 cells/ml) on thin Matrigel (BD Biosciences) layers for 12 hours and then treating them with DMSO (control) or 100 nM of 1 – 3 for additional 24 hours. It was documented by light microscopy (10-fold magnification).

Results and conclusions

In growth inhibition MTT assays, the new oxazoles 1 – 3 were active with nanomolar IC_{50}(72h) against drug sensitive 518A2 melanoma cells (1: 3 ± 2; 2: 2 ± 1; 3: 50 ± 15 nM), CA-4 resistant HT-29 colon carcinoma cells (1: 6 ± 1; 2: 11 ± 1; 3: 76 ± 3 nM), and the endothelial hybrid cell line Ea.hy926 (1: 9 ± 1; 2: 31 ± 3; 3: 77 ± 4 nM). CA-4 itself was efficacious against melanoma and endothelial cells while not affecting the growth of HT-29 cells (IC_{50}(72 h) > 1,000 nM), which feature MRP-1 transporters that expel xenobiotic phenols [5, 7]. Previous studies had already shown that the replacement or removal of the B-ring *meta*-hydroxy group resulted in a distinct increase of the cytotoxicity against HT-29 cells [5]. Likewise, the oxazoles 1 – 3 bearing a *meta*-chloro residue on the B-ring were much more efficacious against these resistant cells when compared with CA-4. Furthermore, the cytotoxicity of the oxazoles varied with the *para*-substituents. Compound 1 featuring a methoxy group was the most active one, either because of a higher affinity to the colchicine binding site at the tubulin heterodimer interface or due to an improved uptake via endocytosis. Docking studies lend some support to the first assumption (unpublished results).

By quantifying the DNA fragmentation after drug treatment, it could be shown that the cytotoxic effect of 1 – 3 was mediated by induction of apoptosis as assessed from slightly increased sub-G1-peaks of 10 – 15% when compared to untreated cells. The cell cycle profiles of Ea.hy926 cells treated with 1 µM of 1 – 3 (24 h) revealed an accumulation at the G2/M interphase which is typical of inhibitors of tubulin polymerization. Apparently, the compounds 1 – 3 prevent or delay cell division by disturbing the microtubule organization.

Next, we evaluated the antivascular effect of oxazoles 1 – 3 on the endothelial cells [8]. Ea.hy926 cells when grown on thin basement membrane matrix layers (Matrigel) soon start to form tubular networks which are regarded to be suitable surrogates or mimics for blood vessels. These were significantly diminished and a neo-formation was inhibited by incubation with 100 nM of 1 – 3 for 24 hours (Figure 1) – a concentration that the cells tolerated well for at least 24 hours. This effect was most evident when cells were treated with the methoxy derivative 1 or the para-ethoxy congener 2. The methyl thioether 3 had a weaker inhibitory effect on tube formation, in line with its lower cytotoxicity. However, all new chloro oxazoles displayed antivascular activities without signs of toxicity. Taken together, the new chloro oxazoles 1 – 3 are interesting multi-modal drugs that combine vascular disrupting/antiangiogenic effects and strong cytotoxicity. Further investigations and in vivo studies are currently underway.

References

[1] *Tron GC, Pirali T, Sorba G, Pagliai F, Busacca S, Genazzani AA*. Medicinal chemistry of combretastatin A4: present and future directions. J Med Chem. 2006; *49:* 3033-3044. doi:10.1021/jm0512903 PubMed

[2] *Tozer GM, Prise VE, Wilson J, Cemazar M, Shan S, Dewhirst MW, Barber PR, Vojnovic B, Chaplin DJ*. Mechanisms associated with tumor vascular shut-down induced by combretastatin A-4 phosphate: intravital microscopy and measurement of vascular permeability. Cancer Res. 2001; *61:* 6413-6422. PubMed

[3] *Wang L, Woods KW, Li Q, Barr KJ, McCroskey RW, Hannick SM, Gherke L, Credo RB, Hui Y-H, Marsh K, Warner R, Lee JY, Zielinski-Mozng N, Frost D, Rosenberg SH, Sham HL*. Potent, orally active heterocycle-based combretastatin A-4 analogues: synthesis, structure-activity relationship, pharmacokinetics, and in vivo antitumor activity evaluation. J Med Chem. 2002; *45:* 1697-1711. doi:10.1021/jm010523x PubMed

[4] *Biersack B, Effenberger K, Schobert R, Ocker M*. Oxazole-bridged combretastatin A analogues with improved anticancer properties. ChemMedChem. 2010; *5:* 420-427. doi:10.1002/cmdc.200900477 PubMed

[5] *Schobert R, Effenberger-Neidnicht K, Biersack B*. Stable combretastatin A-4 analogues with sub-nanomolar efficacy against chemoresistant HT-29 cells. Int J Clin Pharmacol Ther. 2011; *49:* 71-72. PubMed

[6] *Schobert R, Biersack B, Dietrich A, Effenberger K, Knauer S, Mueller T*. 4-(3-Halo/amino-4,5-dimethoxyphenyl)-5-aryloxazoles and -N-methylimidazoles that are cytotoxic against combretastatin A resistant tumor cells and vascular disrupting in a cisplatin resistant germ cell tumor model. J Med Chem. 2010; *53:* 6595-6602. doi:10.1021/jm100345r PubMed

[7] *Cummings J, Zelcer N, Allen JD, Yao D, Boyd G, Maliepaard M, Friedberg TH, Smyth JF, Jodrell DI*. Glucuronidation as a mechanism of intrinsic drug resistance in colon cancer cells: contribution of drug transport proteins. Biochem Pharmacol. 2004; *67:* 31-39. doi:10.1016/j.bcp.2003.07.019 PubMed

[8] *Hinnen P, Eskens FALM*. Vascular disrupting agents in clinical development. Br J Cancer. 2007; *96:* 1159-1165. doi:10.1038/sj.bjc.6603694 PubMed

PUBLIKATION III

Combretastatin A-4 derived imidazoles show cytotoxic, antivascular, and antimetastatic effects based on cytoskeletal reorganisation.

Katharina Mahal,[a] Bernhard Biersack,[a] Henrike Caysa,[b] Rainer Schobert,*[a], Thomas Müller*[b]

[a] *Organic Chemistry Laboratory, University of Bayreuth, Universitätsstraße 30, 95440 Bayreuth (Germany)*

[b] *Department of Internal Medicine IV, Oncology/Hematology, Martin Luther University Halle-Wittenberg, Ernst-Grube-Straße 40, 06120 Halle (Germany)*

* email: rainer.schobert@uni-bayreuth.de; thomas.mueller@medizin.uni-halle.de

Invest. New Drugs **2015**, *33 (3)*, 541-554.

doi: 10.1007/s10637-015-0215-9

Invest New Drugs
DOI 10.1007/s10637-015-0215-9

PRECLINICAL STUDIES

Combretastatin A-4 derived imidazoles show cytotoxic, antivascular, and antimetastatic effects based on cytoskeletal reorganisation

Katharina Mahal · Bernhard Biersack · Henrike Caysa · Rainer Schobert · Thomas Mueller

Received: 5 January 2015 / Accepted: 1 February 2015

Summary *Introduction* Combretastatin A-4 (CA-4) is a natural *cis*-stilbene which interferes with the cellular tubulin dynamics and which selectively destroys tumour blood vessels. Its pharmacological shortcomings such as insufficient chemical stability, water solubility, and cytotoxicity can be remedied by employing its imidazole derivatives. *Methods* We studied 11 halogenated imidazole derivatives of CA-4 for their effects on the microtubule and actin cytoskeletons of cancer and endothelial cells and on the propensity of these cells to migrate across tissue barriers or to form blood vessel-like tubular structures. *Results* A series of *N*-methyl-4-aryl-5-(4-ethoxyphenyl)-imidazoles proved far more efficacious than the lead CA-4 in growth inhibition assays against CA-4-resistant HT-29 colon carcinoma cells and generally more selective for cancer over nonmalignant cells. Et-brimamin (**6**), the most active compound, inhibited the growth of various cancer cell lines with IC_{50} (72 h) values in the low nanomolar range. Active imidazoles such as **6** reduced the motility and invasiveness of cancer cells by initiating the formation of actin stress fibres and focal adhesions as a response to the extensive microtubule disruption. The antimetastatic properties were ascertained in 3D-transwell migration assays which simulated the transgression of highly invasive melanoma cells through the extracellular matrix of solid tumours and through the endothelium of blood vessels. The studied imidazoles exhibited vascular-disrupting effects also against tumour xenografts that are refractory to CA-4. They were also less toxic and better tolerated by mice. *Conclusions* We deem the new imidazoles promising drug candidates for combination regimens with antiangiogenic VEGFR inhibitors.

Keywords Combretastatin A-4 · Imidazoles · Vascular-disrupting agents (VDA) · Antimetastatic activity · Transwell invasion assay · Trans-endothelium migration assay · CAM assay

Electronic supplementary material The online version of this article (doi:10.1007/s10637-015-0215-9) contains supplementary material, which is available to authorized users.

K. Mahal · B. Biersack · R. Schobert (✉)
Organic Chemistry Laboratory, University Bayreuth, Universitaetsstrasse 30, 95440 Bayreuth, Germany
e-mail: rainer.schobert@uni-bayreuth.de

H. Caysa · T. Mueller
Department of Internal Medicine IV, Oncology/Hematology, Martin-Luther-University Halle-Wittenberg, 06120 Halle-Saale, Germany

Introduction

The *cis*-stilbene combretastatin A-4 (CA-4; Fig. 1a) which was first isolated from the South-African bushwillow *Combretum caffrum* shows a remarkable antivascular activity [1, 2]. CA-4 and its clinically investigated phosphate prodrug fosbretabulin (CA-4P) are vascular-disrupting agents (VDA) which selectively target the blood vessels of solid tumours [3–5]. CA-4 binds primarily to the colchicine binding site of beta-tubulin and impedes the polymerisation of heterodimeric tubulin subunits to give microtubules [2, 6]. Its antiproliferative effect is based mainly on this disruption of the highly organised microtubule cytoskeleton. Cells affected in this way are hindered to develop mitotic spindles leading to mitotic arrest and eventually to apoptosis [4, 7–9]. In contrast, the disruption of blood vessels by CA-4 or CA-4P is an immediate effect originating from a rapid change of the morphology of individual endothelial cells and a perturbation of the integrity of endothelial cell monolayers. Investigations into the signalling pathways involved in the cellular response to inhibitors of microtubule formation showed the small GTPase Rho, Rho-associated kinase (Rho-kinase) and various mitogen-

Published online: 14 February 2015

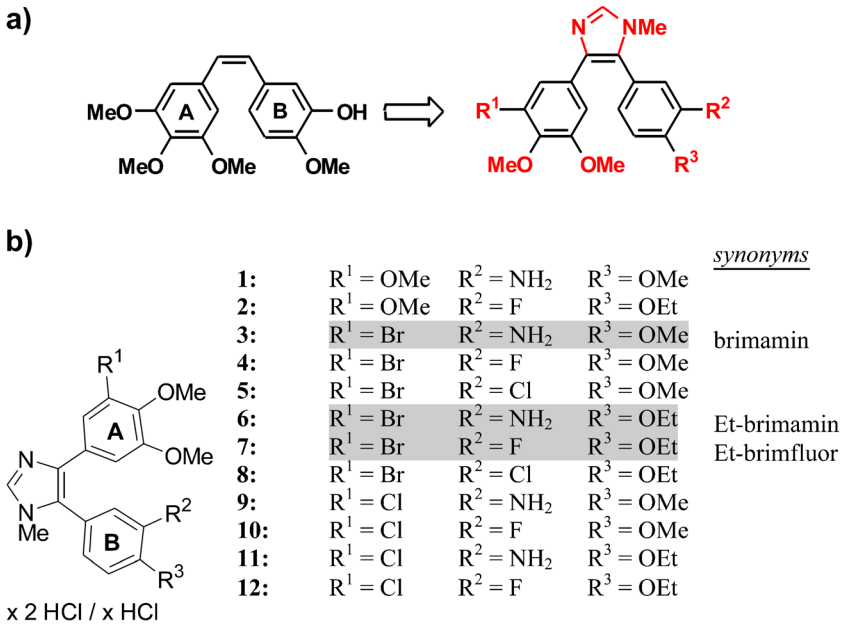

Fig. 1 Structures of combretastatin A-4 (CA-4) and imidazole analogues. **a**) Structure of CA-4 with A- and B-ring denotation and of imidazole analogues with various substitution sites. **b**) Structures of N-methyl-4-(4,5-dimethoxyphenyl)-5-phenyl-imidazolium hydrochlorides **1**–**12** with variation in residues R^1, R^2, and R^3 as specified. Important compounds highlighted and assigned short names

activated protein kinases (MAPKs) to play an essential role. Typical effects of CA-4 are the assembly of actin stress fibres, an increase in cell contractility, a loss of cell-cell contacts and the induction of apoptosis [10–12]. They are responsible for the disruption of the tight cellular organisation of the endothelium, the increase in endothelial permeability, and the leaking or disruption of tumour blood vessels. The consequences visible in solid tumours are haemorrhages and necrosis [3, 4, 13]. Unfortunately, CA-4 is not suitable for clinical application because of its metabolic conversion to the inactive *trans*-isomer and its insufficient solubilty and cytotoxicity [2, 5]. Although the irregular vasculature of solid tumours is a promising drug target the number of clinically tested antivascular drugs is still rather small. Examples are the CA-4 serinyl prodrug AVE8062 [14, 15] and the CA-1 diphosphate prodrug OXi4503 [16]. More recently, combretastatin A derivatives with imidazole, oxazole or other heterocycles bridging the alkene bond were developed that retain the vascular-disrupting effect while showing an enhanced chemical stability and cytotoxicity [17–20]. Lately, we developed a series of *N*-methylimidazole-brigded CA-4 derivatives bearing *meta*-halogen substituents at the A- or B-ring (Fig. 1b) and optimised their antitumoural and antivascular properties both in vitro and in vivo [18, 19].

The current paper presents a new series of five halogenated imidazole analogues of CA-4 (**6**–**8**,**11**,**12**) which share a *meta*-halogen substituted A-ring and a B-ring with *meta*-halogen/NH_2 and *para*-OEt substitution. With both series of imidazoles in hand we could now study the influence of various substituent constellations on their cytotoxicity, vascular-disrupting activity in vitro and in vivo, their cancer selectivity, and the underlying cellular mechanisms, also in comparison to the lead compound CA-4. Particularly insightful was a comparison of imidazole couples that differ only in the *para*-substituent on the B-ring, being either the original methoxy group of CA-4 or an ethoxy group, i.e., **3**/**6**, **4**/**7**, **5**/**8**, **9**/**11**, and **10**/**12**.

Materials and methods

Imidazoles, stock solutions and dilution series

CA-4 was purchased from Sigma Aldrich. The known imidazoles **1**–**4** were prepared as published [17–19], the new derivatives **5**–**8**,**11**,**12** were synthesised analogously (cf. Electronic supplementary material). Stock solutions were prepared by dissolving CA-4 and the purified imidazolium hydrochlorides **2**–**12** in DMSO to a final concentration of 10 mM. All dilution series were prepared in 1 × PBS or ddH_2O.

Cell lines and culture conditions

The human carcinoma cell lines HT-29 (colon), HCT-116 (colon), and MCF-7 (breast) were purchased from The German Collection of Microorganisms and Cell Culture (DSMZ, Braunschweig). MCF-7 cells were rendered multidrug-resistant, indicated as MCF-7/Topo, by repeated application of topotecan. Primary human umbilical vein endothelial cells (HUVEC) were obtained from DSMZ and the HUVEC-derived endothelial hybrid cell line Ea.hy926 from The American Type Culture Collection (ATCC no. CRL-2922). The human melanoma cell line 518A2 was a gift from the Department of Radiotherapy and Radiobiology, University Hospital Vienna. It is not available from cell banks, yet easily identified by its large size and its flat, spread-out morphology. Cells of

cell lines 518A2, HT-29, HCT-116, MCF-7/Topo, and Ea.hy926 were grown in DMEM or RPMI (HT-29) medium, supplemented with 10 % fetal bovine serum (FBS), 1 % Antibiotic-Antimycotic solution (both from Gibco) and 250 μg/mL gentamycin (SERVA). Experiments with HUVEC were conducted at the Helmholtz Centre for Infection Research (Braunschweig, Germany). HUVEC were cultured in EGM-2 medium (Lonza). Primary chicken heart fibroblasts (CHF) were explanted from 10 day-old chicken embryos and separated from other cell types for several weeks. The established cell line based on single fibroblasts was finally grown in DMEM (10 % FBS, 1 % Anti-Anti, 250 μg/mL gentamycin) and used before the 20th passage. All cells were incubated at 37 °C, 5 % CO_2, 95 % humidified atmosphere. Only mycoplasm-free cell cultures were used.

Cell cycle analyses

CA-4-sensitive 518A2 melanoma cells (2×10^5 cells/well) grown on 6-well cell culture plates were treated with DMSO (control), CA-4 (5 nM) or the imidazole derivatives **3** (25 nM) and **6** (10 nM). HT-29 colon carcinoma cells (2×10^5 cells/well) were treated with vehicle or compounds **3** or **6** (100 nM). Since HT-29 are resistant to CA-4 [21, 22], a higher concentration of CA-4 (10 μM) was used to observe comparable effects on the cell cycle. After incubation for 24 h, cells were harvested by trypsination, fixed (ice-cold 70 % EtOH, 1 h, 4 °C), and incubated with propidium iodide (PI, Carl Roth) staining solution (50 μg/mL PI, 0.1 % sodium citrate, 50 μg/mL RNase A in PBS) for 30 min at 37 °C. The fluorescence intensity of 10,000 single cells at an emission wavelength of 620 nm (exCitation with a 488 nm laser source) was recorded with a Beckman Coulter Cytomics FC500 flow cytometer and analysed for the distribution of single cells (%) to G1, S and G2-M phase of the cell cycle as well as for the content of sub-G1 events (apoptotic cells) by using the CXP software (Beckman Coulter).

Determination of the mitotic index

518A2 or HT-29 cells (1×10^4 cells/well) grown on glass coverslips were allowed to adhere for 24 h and then exposed to CA-4 (518A2: 5 nM CA-4, HT-29: 5 μM CA-4) or to imidazoles **3** and **6** for 6 h. After fixation with 4 % formaldehyde in PBS for 20 min, coverslips were washed twice with PBS and mounted in Mowiol 4-88-based mounting medium containing 1 μg/mL DAPI (4′,6-diamidino-2-phenylindole) overnight at 4 °C. Pictures of DAPI-stained nuclei in random fields of the slides were recorded with a ZEISS Axiovert 135 fluorescence microscope (AxioCam MRc5, 400-fold magnification). For each concentration a minimum of 800 cells from at least four pictures were counted (AxioVision software) and the percentage of mitotic cells was calculated from the ratio of mitotic cells to the total number of counted cells (mitotic index±S.D.) [23].

Quantification of polymeric and depolymerised tubulin fractions

To assess early effects on the microtubule cytoskeleton, 518A2 cells cultured for 24 h in 24-well plates (5×10^4 cells/well) were exposed to DMSO (control), CA-4 as a positive control (1 μM), or increasing concentrations of the imidazoles **3** and **6** (50, 100, 250, 500, 1000 nM) for 6 h. The cells were then harvested by trypsination and centrifuged at 400 g for 5 min at room temperature. The resulting cell pellet was resuspended in 100 μL hypotonic cell lysis buffer (20 mM Tris-HCl, 1 mM $MgCl_2$, 2 mM EGTA, 0.5 % Triton X-100, pH 6.8) supplemented with protease inhibitor (protease inhibitor cocktail Set III, EDTA-free, Calbiochem) for 10 min at room temperature. After centrifugation at 12,000 g (10 min, room temperature), the supernatant containing soluble, depolymerised tubulin was separated from the pellet fraction representing detergent-insoluble, polymeric microtubules [23, 24]. Cell lysate and the pellet fractions were mixed with 100 μL 2× SDS-sample buffer (4 % SDS, 20 % glycerol, 20 mM DTT, 0.005 % bromophenol blue in 125 mM Tris-HCl, pH 6.8) and boiled at 95 °C for 10 min. Equal volumes of the samples were subjected to 10 % SDS-polyacrylamide gel electrophoresis followed by a standard Western blotting procedure and chemiluminescent detection (anti-alpha-tubulin mouse monoclonal antibody, clone no. TU-01, ca. One microgram per milliliter; goat anti-mouse IgG-HRP conjugate, Cell Signaling Technology) of the alpha-tubulin content. ImageJ software was used for graphical work and densitometric analyses.

Fluorescence labelling of microtubules, actin filaments and focal adhesions

Cells were seeded on glass coverslips (5×10^4 518A2 cells/well, 1×10^5 HUVECs/well) and allowed to adhere for 24 h and then treated with vehicle (DMSO) or various concentrations of CA-4 or the imidazoles **3**, **6**, or **7**. After 24 h of incubation cells were fixed with 4 % formaldehyde in PBS for 20 min at room temperature followed by blocking and permeabilisation (1 % BSA, 0.1 % Triton X-100 in PBS) for 30 min. For visualisation of filamentous actin (F-actin) coverslips were incubated with 1 U AlexaFluor®-488-conjugated phalloidin (Invitrogen) for 1 h at 37 °C. For immunostaining of microtubules and paxillin-associated focal adhesions fixed and permeabilised cells were treated with a primary antibody against alpha-tubulin (anti-alpha-tubulin, mouse monoclonal antibody, clone no. TU-01, ca. 10 μg/mL) or against paxillin (anti-paxillin, mouse monoclonal antibody, clone no. 177/Paxillin, 0.5 μg/mL, BD Transduction Laboratories) followed

by incubation with a secondary antibody conjugated to AlexaFluor®-488 (goat anti-mouse IgG-AlexaFluor®-488 conjugate, Cell Signaling Technology) for 1 h in the dark. Coverslips were mounted in Mowiol 4-88-based mounting medium containing 2.5 % (w/v) DABCO and 1 μg/mL DAPI for counterstaining the nuclei. Cytoskeletal components were documented by fluorescence microscopy (ZEISS Axio Imager.A1; 400× magnification for microtubule and microfilament staining, 630× for paxillin staining).

Tube formation assay with endothelial cells

The ability of permanent Ea.hy926 endothelial hybrid cells to form vascular-like networks upon growth factor stimulation was used to assess the vascular-disruptive activity of CA-4, **3** and **6** in vitro. Ea.hy926 cells retain essential endothelial characteristics and are an appropriate, often used model for angiogenesis studies [25, 26]. In the so-called tube formation assay Ea.hy926 cells (5×10^4/well) were grown for 12 h on thin Matrigel™ (basement membrane matrix, high concentration, with growth factors, BD Biosciences) layers pre-gelled in the wells of a black 96-well cell culture plate (20 μL of pure matrigel solution, 30 min at 37 °C) and then treated with vehicle (DMSO), CA-4 or the compounds **3** or **6** (50 nM). Tubular networks were documented by light microscopy (100× magnification, Axiovert 135, AxioCam MRc 5, ZEISS) after a further 12 h incubation. To exclude false-positive effects of contractile cells and tubule disruption as a consequence of the cytotoxicity of the compounds rather than early cytoskeletal rearrangements, MTT was additionally added to each well (25 μL 0.5 % MTT solution in PBS). After incubation for 2 h at 37 °C the plates were centrifuged (300 g, 4 °C, 5 min) and the supernatant was carefully aspirated. The cells were lysed and the precipitated formazan was redissolved by adding 100 μL of an SDS-DMSO solution (10 % SDS, 0.6 % acetic acid in DMSO) to each well. The absorbance at wavelengths 570 and 630 nm (background) was measured using an automatic ELISA microplate reader (Tecan) and the percentage of viable cells was calculated relative to controls.

Chorioallantoic membrane (CAM) assay with fertilised chicken eggs [27]

Chicken eggs (SPF eggs, VALO Biomedia) were incubated (37 °C, 50–60 % humidity) until day 7 after fertilisation and opened by cutting a window of 2–3 cm diameter into the pole end of the eggshell. Rings of silicon foil (5 mm diameter) were placed on the developing vessels within the CAM and the windows were sealed with tape followed by further incubation for 24 h. Dilutions of DMSO (control) and the imidazoles **3** and **6** in PBS were pipetted inside the silicon ring (10 μL of a 25 or 50 μM dilution) and alterations in the blood vessel organisation were documented after 0 and 24 h post application with a stereomicroscope (60× magnification, Traveller).

Animal studies

The vascular-disrupting activity of **6** was studied on the established model of highly vascularised 1411HP xenograft tumours previously described [18]. This study was approved by the Laboratory Animal Care Committee of Sachsen-Anhalt, Germany. Nude mice (Harlan and Winkelmann, Borchen, Germany) received 30 mg/kg body weight of compound **6** by intraperitoneal injection and tumour discoloration was documented after 24 h with a Canon IXUS 50. For histological examination the tumours were explanted, fixed in 4 % formalin, and embedded in paraffin. Hematoxylin/eosin (HE) staining of the tissue slices was performed according to standard protocols. HE images shown are representative of three independent in vivo observations.

Matrigel-based transwell migration assay

This assay provides a realistic three-dimensional model for tumour cell invasion stimulated by a chemoattractant. It takes into account both degradation and active movement of cells through a basement membrane matrix [28, 29]. The migration chambers were set up using ThinCert™ cell culture inserts with porous membranes (translucent PET membrane, 8 μm pore size, Greiner bio-one) for 24-well plates. The procedure for quantification of invasive cells was adapted from the manufacturer's application manual (ThinCert™ application notes, Greiner bio-one) with some alterations [30]. In brief, highly metastatic 518A2 melanoma cells were starved in serum-free DMEM for 24 h and harvested directly before seeding them into Matrigel™-coated (50 μL 1:1-dilution of Matrigel™ basement membrane matrix in serum-free DMEM, 30 min at 37 °C, 5 % CO_2, 95 % humidity; BD Biosiences) cell culture inserts (2×10^5 cells in 200 μL serum-free DMEM/insert) that were placed in the receiver wells filled with 600 μL DMEM containing 10 % FBS. Cells were exposed to DMSO (vehicle) or imidazole **6** at a final concentration of 10 or 50 nM for 48 h. The medium was removed from each well of the 24-well plate (lower compartment) and replaced with 500 μL 1× cell dissociation buffer (0.5 mM EDTA, 0.1 % sodium citrate in PBS, pH 7.4) containing 1 μM calcein-AM (calcein acetoxymethyl ester; non-fluorescent, cell-permeable dye). The plates with the inserts were incubated for 30 min at 37 °C for both sufficient detachment of the cells from the membrane underside or the surface of the bottom well and conversion of intracellular calcein-AM into the membrane-impermeable fluorescent calcein. The ThinCerts™ were then discarded and the cell suspension containing only invasive cells was transferred to the wells of a black 96-well plate. Migratory cells were quantified with a microplate reader (Tecan) by measuring the

calcein fluorescence (excitation/emission wavelength: 485 nm/520 nm) that was calculated as percentage of that of DMSO-treated control cells set to 100 %.

Trans-endothelium migration assay

Hanging cell culture inserts were used to build upper and lower compartments separated by an artificial endothelium which was constituted by a basement membrane matrix and a confluent endothelial monolayer [31–33]. Briefly, Ea.hy926 endothelial cells (1×10^5 cells in 50 μL DMEM) were seeded onto the underside of an insert membrane (24-well plate inserts, translucent PET membrane, 3.0 μm pore size, greiner bio-one) and allowed to adhere for 24 h after placing the inserts upside down into humidified wells of a 6-well plate. The inner membrane of the inserts was sealed with a thin Matrigel™-layer (20 μL 1:1-dilution in serum-free DMEM, gelled for 30 min at 37 °C, 5 % CO_2, 95 % humidity; BD Biosiences) and covered with 200 μL serum-free DMEM. The inserts were placed in the wells of a 24-well plate with 600 μL DMEM containing 10 % FBS and incubated for additional 24 h to get a confluent Ea.hy926 monolayer [34]. 518A2 cells confluently grown in cell culture dishes were starved in serum-free DMEM for 24 h prior to labelling with the carbocyanine dye DiI according to the manufacturer's instructions (15 min, 37 °C, 5 μL Vybrant™ DiI Cell-Labeling Solution per 1×10^6 cells/mL serum-free medium, Molecular Probes®, life technologies). Then the medium in the inserts was discarded and 200 μL of the DiI-stained 518A2 cell suspension in serum-free DMEM (10,000 cells/insert) were pipetted to each insert. The cells were allowed to adhere overnight and incubated with non-toxic concentrations of Et-brimamin **6** (10 or 50 nM). After 48 h the medium from the inserts and the receiver wells was removed and cells on the upper side of the insert were scraped off with a cotton swab [34]. For qualitative analyses cells on the membrane underside were fixed (4 % formaldehyde in PBS, 30 min, rt), washed with PBS and mounted in Mowiol 4-88-based mounting medium with 1 μg/mL DAPI for fluorescence microscopy. For quantification of invasive cells 500 μL 1× cell dissociation buffer (0.5 mM EDTA, 0.1 % sodium citrate in PBS, pH 7.4) containing 1 μM calcein-AM were added to the wells and the plates were incubated for 30 min at 37 °C for cell detachment and calcein-AM conversion. The cell suspension containing calcein-stained endothelial cells and red-fluorescent invasive tumour cells was transferred to the wells of a black 96-well plate and analysed for their calcein (excitation/emission wavelength: 485 nm/520 nm) and DiI (excitation/emission wavelength: 550 nm/570 nm) fluorescence with a microplate reader (Tecan). The green or red fluorescence intensity of DMSO-treated control cells was set to 100 %. The ratio of red to green fluorescence intensities was taken as a measure for the percentage of trans-endothelium-migrated 518A2 cells with respect to DMSO controls and the total number of viable cells.

Results and discussion

Table 1 summarises the IC_{50} values of reference compounds and the new CA-4 analogous imidazoles in MTT cytotoxicity assays. All new compounds were first tested against the CA-4-sensitive 518A2 melanoma and the CA-4-resistant HT-29 colon carcinoma cell lines. Despite its shortcomings when applied in vivo CA-4 exhibits a great in vitro cytotoxicity with nanomolar IC_{50} values against many cancer cell lines. However, it is far less efficacious against HT-29 cells which discharge it quickly by means of their ABC (ATP-binding cassette) transporters [21]. The imidazole analogue **1** was previously shown to be efficacious against HT-29 cells, and even more so the closely related analogues **3** ('brimamin', *N*-methyl-4-(3-bromo-4,5-dimethoxyphenyl)-5-(3-amino-4-methoxyphenyl)-imidazole) and **9** that bear a *meta*-halo substituted A-ring and a *meta*-amino-*para*-methoxyphenyl B-ring [17, 18].

We now found that keeping the *meta*-bromo or -chloro substituent at the A-ring and the *meta*-amino substituent at the B-ring while replacing the *para*-methoxy group on the B-ring by an ethoxy residue led to a further increase of the cytotoxicity against both the CA-4 sensitive and resistant cell lines. For instance, the B-*meta*-amino derivatives **6** and **11** were twice as efficacious as **3** or **9**, respectively. The B-*meta*-fluoro (**7**, **12**) or B-*meta*-chloro (**8**) derivatives were even nearly ten times more efficacious than **4**, **10**, or **5**, respectively. Most active were the first generation *para*-methoxy derivative 'brimamin' (**3**), its new ethoxy congener **6** ('Et-brimamin'), and 'Et-brimfluor' **7**, the *meta*-fluoro analogue of **6**. They all displayed two-digit nanomolar IC_{50} (72 h) values against cells of 518A2 melanoma, HT-29 and HCT-116 colon carcinoma, and multidrug-resistant MCF-7/Topo breast carcinoma. CA-4 and the derivatives **3**, **6**, and **7** also inhibited the growth of Ea.hy926 hybrid endothelial cells and primary human umbilical vein endothelial cells (HUVEC) in MTT assays with IC_{50} in the lower nanomolar range. However, the compounds showed a distinct selectivity for cancer and endothelial cell lines over nonmalignant fibroblasts (CHF) which were hardly affected even at concentrations of 10 μM.

CA-4 analogous imidazoles induce mitotic cell cycle arrest

518A2 melanoma and HT-29 colon carcinoma cells were treated for 24 h with equitoxic concentrations of CA-4 or the imidazoles **3** or **6** and subjected to flow cytometric cell cycle analyses (Fig. 2). In the case of 518A2 cells a decrease of cells with G1 DNA content was found together with a slightly increased G2-M population and a significantly higher

Table 1 In vitro cytotoxicity of CA-4 and imidazoles **1**–**12** against 518A2 melanoma, HT-29 and HCT-116 colon, MCF-7/Topo breast carcinoma cells, the endothelial hybrid cell line Ea.hy926, HUVEC, and nonmalignant chicken heart fibroblasts (CHF)

	Cell lines						
	518A2	HT-29	HCT-116	MCF-7/Topo	Ea.hy926	HUVEC	CHF
CA-4	1.8±0.1	>5000	2.6±0.2	154±33	11±2	1.2±0.1	>5000
1	>100,000 [a]	64±14 [a]	n.d.	>10,000 [a]	n.d. [b]	n.d.	n.d.
2	61±1	>1000	215±17	n.d.	n.d.	n.d.	n.d.
3	29±2	15±1	27±2	100±9	28±4	23±7	>10,000
4	184±5	305±59	249±29	236±25	n.d.	n.d.	n.d.
5	2429±46	>5000	n.d.	n.d.	n.d.	n.d.	n.d.
6	14±2	6.9±1.2	5.1±0.4	72±6	15±2	14±4	>10,000
7	27±5	38±1	177±8	97±12	140±4	n.d.	>10,000
8	249±14	588±11	n.d.	n.d.	n.d.	n.d.	n.d.
9	48±3	40±1	n.d.	n.d.	n.d.	n.d.	n.d.
10	400±100[a]	530±30[a]	n.d.	n.d.	n.d.	n.d.	n.d.
11	22±2	38±4	n.d.	n.d.	n.d.	n.d.	>50,000
12	28±1	50±1	189±8	n.d.	n.d.	n.d.	>10,000

[a] Values from an earlier publication used for reference compounds [18]

[b] Not determined

IC_{50} [nM] values after 72 h exposure as the mean of three independent MTT assays±S.D

percentage of sub-diploid, apoptotic cells. The magnitude of these cell cycle alterations correlated well with the IC_{50} values found for CA-4, **3** and **6** (cf. electronic supplementary material, Tables S1, S2). The sensitivity of 518A2 cells to CA-4 and the imidazoles **3** and **6** might be due to their high proliferation rate. Treatment of CA-4-resistant HT-29 cells with 100 nM **3** or **6** led to a significant accumulation of cells in the G2-M phase which is typical of antimitotic compounds. The number of apoptotic events was only slightly increased, probably since 24 h are too short an incubation period for these cells to enter into apoptosis as a consequence of prolonged mitotic arrest [9, 35].

We substantiated these results by fluorescence microscopy of DAPI-stained nuclei of cancer cells treated with CA-4, **3** or **6** in order to differentiate between cells in G2 phase and mitotic cells based on the chromatin organisation. After 6 h incubation with appropriate concentrations the number of mitotic cells increased markedly (Table 2). The mitotic index, which was about 9 % for DMSO-treated control cells of either cell line, was significantly shifted to 40 or 32 %, respectively, of cells with condensed DNA upon stimulation with CA-4 and to more than 40 % upon exposure to brimamin (**3**) or Et-brimamin (**6**). Due to their CA-4 resistance a higher dose of 5 μM CA-4 was required to achieve accumulation of mitotic cells to an extent comparable to that caused by 100 nM of **6** (Fig. 3).

Imidazoles **3** and **6** disrupt microtubules and induce cytoskeletal reorganisation

Tubulin-binding agents interfere with the microtubule dynamics eventually blocking mitotic progression and cell division. Thus, we investigated the effects of the new *N*-methyl-4,5-diarylimidazoles on microtubule organisation and the cytoskeletal response in cancer and endothelial cells. First, we compared brimamin (**3**), Et-brimamin (**6**), and Et-brimfluor (**7**) for their efficiency in suppressing tubulin polymerisation in vitro. In 518A2 cells treated for 3 h with increasing concentrations of **3**, **6** or **7** initially intact microtubules were destructed in a concentration-dependent manner (Fig. 4). Exposure to Et-brimamin (**6**), the compound with the lowest IC_{50} (72 h) value at this cell line, induced complete disruption even at a concentration of 250 nM. In contrast, 250 nM of brimamin (**3**) or Et-brimfluor (**7**) eroded the highly organised microtubular network but left some coherent clusters of intact microtubules. Apparently, the cytotoxicity of the tested imidazoles correlates well with their ability to disrupt microtubules. This was further corroborated by quantifying the fraction of intact microtubules in treated 518A2 cells (Fig. 5).

Disruption of microtubular dynamics results in higher cellular levels of free tubulin heterodimers that are part of the detergent-soluble supernatant of cell lysates and that can be separated from intact tubulin polymers by centrifugation. As shown by Western blot analyses of the insoluble pellet fraction, microtubule disruption is induced by Et-brimamin (**6**) at lower concentrations than those required of brimamin (**3**) for the same effect. This might be due to a higher affinity of **6** for tubulin. In line with this is the greater inhibitory effect of **6** on the polymerisation of purified tubulin in a cell-free assay when compared with the effects by the less cytotoxic analogues brimfluor (**4**) or **1** (cf. electronic supplementary material, Table S4). Thus, the tubulin binding capacity of the imidazoles correlates well with their cytotoxicity against cancer cells.

Next, we investigated the cellular actin stress fibre formation as a typical response to tubulin-binding agents. Since changes in the cellular contractility upon actin stress fibre development play an important role for the antivascular

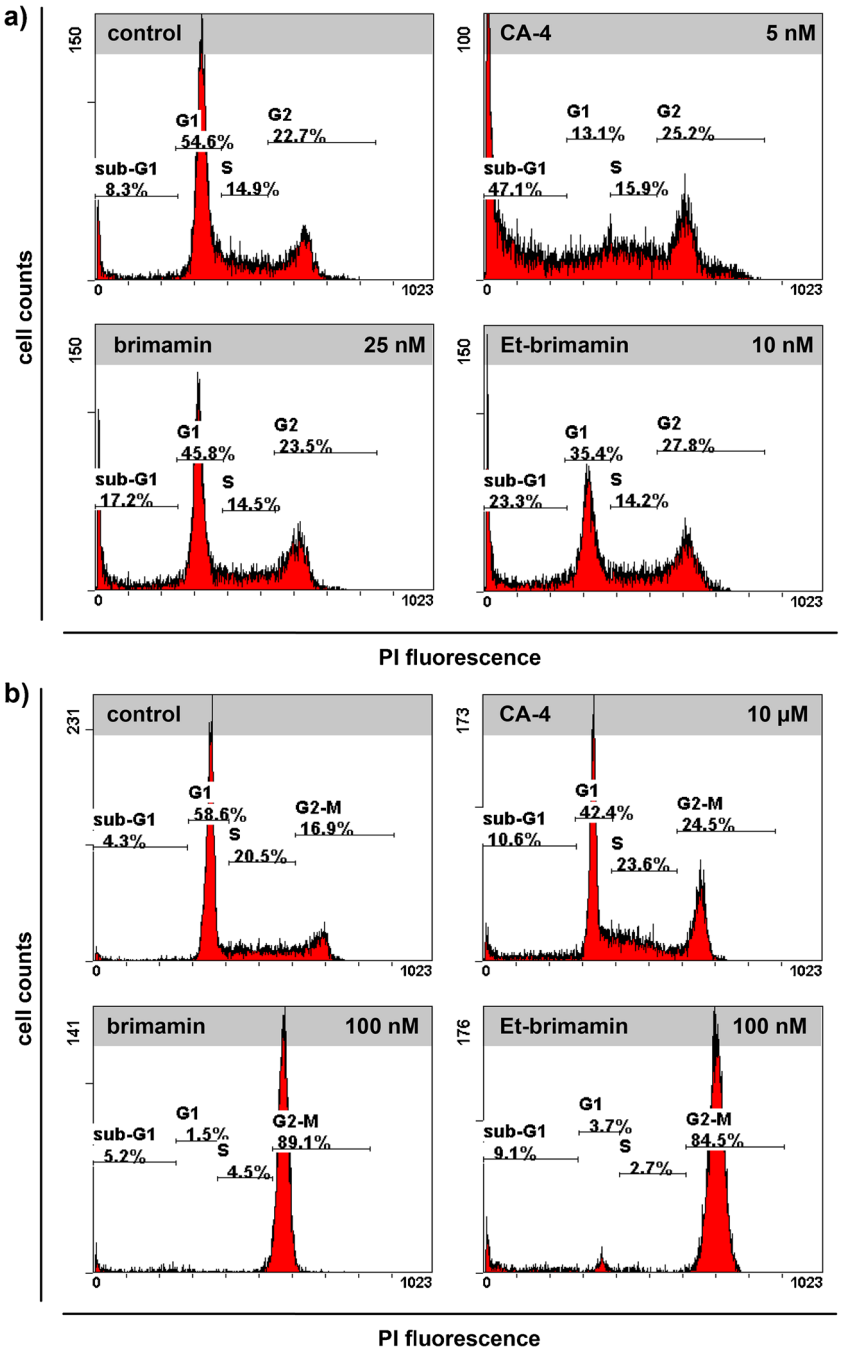

Fig. 2 Effect of CA-4, brimamin **3**, and Et-brimamin **6** on the cancer cell cycle. Effect on the cell cycle of (**a**) CA-4-sensitive 518A2 melanoma and (**b**) CA-4-resistant HT-29 colon carcinoma cells after 24 h exposure. Typical cell cycle profiles and percentage of treated cells in G1, S and G2-M phase as well as sub-G1 events (apoptotic cells) as obtained by flow cytometry after DNA staining with propidium iodide (PI)

Table 2 Percentage of mitotic cells (%) in cultures of 518A2 melanoma or HT-29 colon carcinoma cells treated with CA-4 (518A2: 5 nM, HT-29: 5 µM) or with imidazoles **3** or **6** (100 nM) for 6 h

	Control	CA-4	Brimamin 3	Et-brimamin 6
518A2	9.4±0.6	39.7±2.4	46.4±3.6	52.2±6.8
HT-29	8.9±1.7	31.7±3.4	41.2±3.8	39.2±3.2

Data obtained from counting DAPI-stained nuclei of at least 800 cells and represented as mean±SD, control: DMSO

activity of CA-4 we used primary endothelial cells (HUVEC) for these experiments. In response to exposure to CA-4 or the most active imidazole **6** HUVEC displayed a dense network of actin stress fibres when compared to DMSO-treated control cells (Fig. 6).

Stress fibre formation was associated with an increase in focal adhesions as visualised by immunofluorescent staining of focal adhesion-associated paxillin. Both processes are mediated by Rho which gets activated upon perturbation of the tubulin cytoskeleton. Eventually, they lead to an increase in cell-matrix contacts and in cell contractility [36, 37]. Given

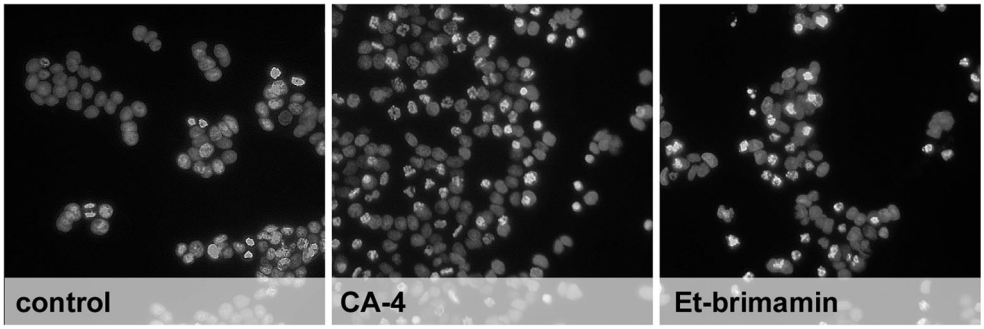

Fig. 3 Accumulation of mitotic HT-29 colon carcinoma cells. Accumulation of mitotic HT-29 colon carcinoma cells after exposure to CA-4 (5 μM) or Et-brimamin **6** (100 nM) for 6 h. Nuclei stained with DAPI (200-fold magnification)

that a balanced dynamics and assembly of microfilaments and focal adhesions is required for endothelial cell-matrix interactions and the endothelium stability [37] it is understandable that CA-4 and Et-brimamin (**6**) are likely to show some antimigratory and antivascular activity by inducing a defective focal adhesion turnover.

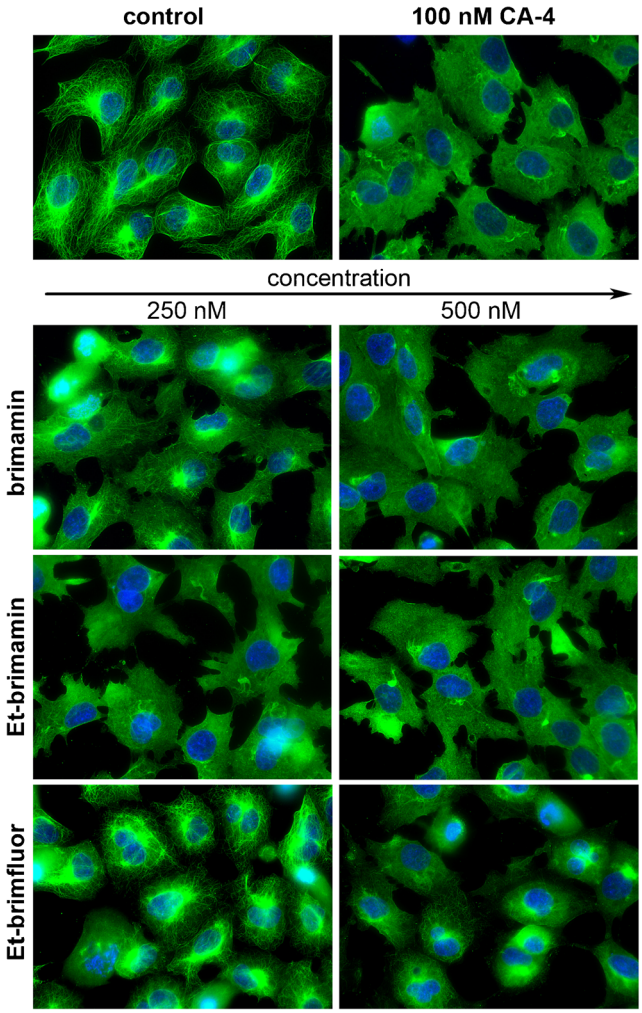

Fig. 4 Effects of CA-4 and of brimamin (**3**), Et-brimamin (**6**) and Et-brimfluor (**7**) on the microtubule organisation in 518A2 melanoma cells. Effects after 3 h incubation. Immunofluorescent labelling of alpha-tubulin (green), nuclei (blue) counterstained with DAPI (400-fold magnification)

CA-4, brimamin (**3**), and Et-brimamin (**6**) are antivascular in vitro and in vivo

The antivascular potential of the imidazoles **3** and **6** was first tested in vitro by means of the so-called tube formation assay. Endothelial cells such as HUVEC and the more often used hybrid Ea.hy926 cells differentiate into tubular, vessel-like networks upon stimulation by growth factors contained in a thin Matrigel layer that serves as a cell adhesion surface [25, 26]. We exposed preformed Ea.hy926 cell networks for 12 h to non-toxic concentrations of CA-4, brimamin (**3**) or Et-brimamin (**6**). Figure 7 shows the resulting disruption of established tubes and branches caused by the retraction of individual cells which is a good indication of a potential antivascular effect by the test compounds in vivo.

Endothelial cell migration and differentiation are essential steps in blood vessel maturation which may get stuck, though, in case of severe cytoskeletal alterations [3, 5, 37]. Since we can exclude any significant contribution by the cytotoxic component of the test compounds **3** and **6** after so short a time (viable cells after 12 h exposure to brimamin **3**: 94.9 %±3.9 % and to Et-brimamin **6**: 83.7 %±2.4 % with respect to DMSO-treated controls set to 100 %) we asume that the destruction of tubular endothelial cell networks is the result of early drug-induced cytoskeletal reorganisations leading to a breakdown of cell-cell adhesion and a loss of the stretched morphology of individual cells.

The vascular-disrupting activity of imidazoles **3** and **6** was also demonstrated in vivo by their impact on the blood vessel system of fertilised chicken eggs (Fig. 8a). After topical application of non-lethal doses onto the vascularised chorioallantoic membrane (CAM) existing blood vessels became leaky and small branches were completely distroyed with hemorrhages appearing. Though CA-4 was the most effective compound in these CAM assays doses beyond 2.5 nmol of it frequently killed the chicken embryos. In contrast, doses of 5 nmol brimamin (**3**) or of 2.5 nmol Et-brimamin (**6**) were tolerated well while showing comparable vascular-disrupting effects.

We also investigated the vascular-disrupting activity of **6** in highly vascularised xenografts of the 1411HP germ

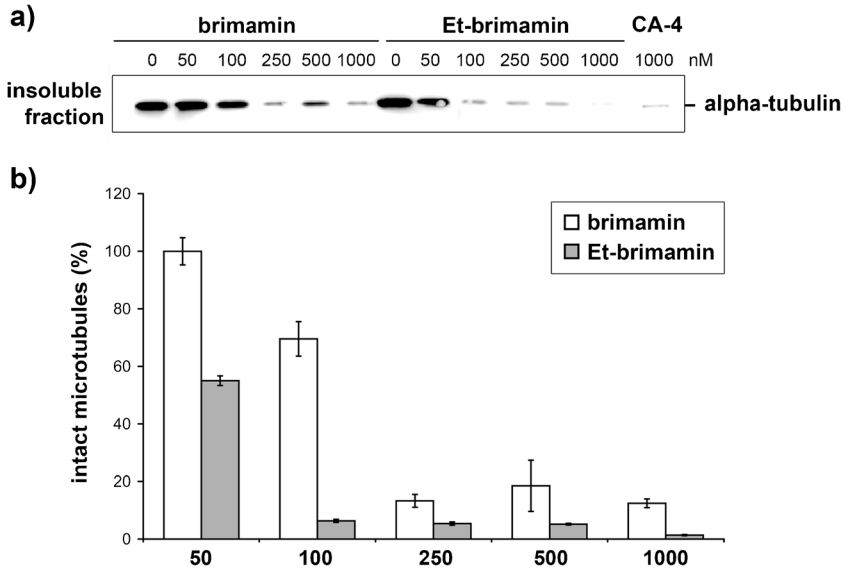

Fig. 5 Brimamin (**3**) and Et-brimamin (**6**) decrease the levels of tubulin polymers in 518A2 cells. **a**) Detergent-insoluble fractions of lysates from 518A2 melanoma cells, treated for 6 h with various concentrations of CA-4, **3** or **6**, were subjected to SDS-PAGE and the content of tubulin was visualised by immunoblotting for alpha-tubulin (55 kDa). **b**) The concentration-dependent (50–1000 nM) levels of tubulin polymers in insoluble cell lysate fractions (intact microtubules) quantified by densitometric analyses of Western blots obtained from two independent experiments, means±S.D

cell tumour cell line which were previously used as an established animal model for the test of VDA [18]. A single treatment of the xenograft bearing mice with 30 mg/kg of **6** induced a distinct tumour discoloration due to intratumoural haemorrhage (Fig. 8b). Histological examination of the treated tumour revealed features typically observed after treatment with CA-4P or other vascular-disrupting agents [5, 13] such as extensive central necrosis and a remaining thin rim of surviving tumour cells (Fig. 8c). Signs of toxicity such as a significant loss of weight were only observed in mice treated with single doses exceeding 60 mg/kg body weight.

To prove the efficacy of the new imidazoles also in CA-4 resistant tumours we undertook preliminary xenograft studies with HT-29 tumours which are far less vascularised and more slowly growing than 1411HP tumours. Here, we observed a significant reduction of the tumour growth in the treated mice (cf. electronic supplementary material, Figure S1) which nicely mirrors the capability of Et-brimamin (**6**) to overcome the CA-4 resistance of HT-29 cells in vitro (cf. Table 1). Although

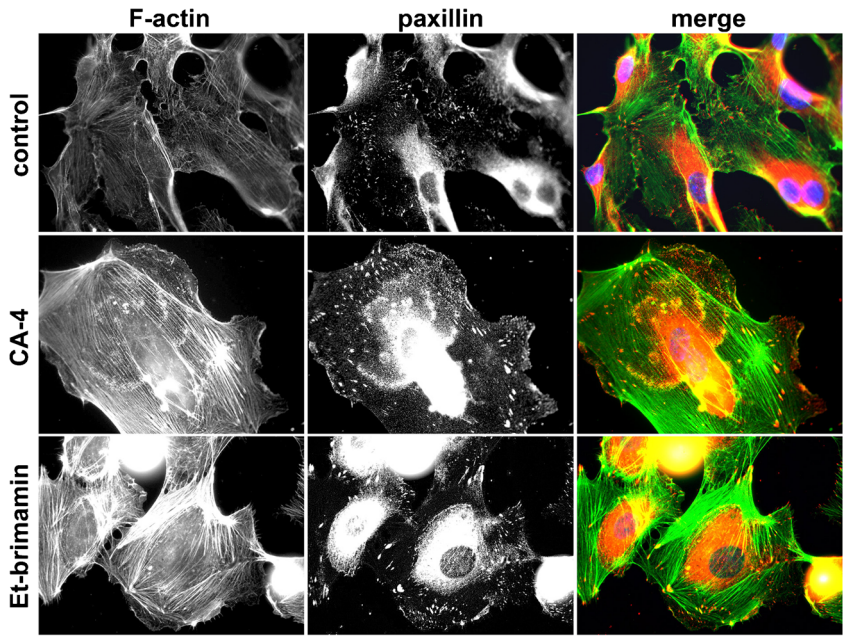

Fig. 6 Effect of CA-4 and Et-brimamin (**6**) on the cytoskeletal organisation of primary endothelial cells (HUVEC). Effect of CA-4 (10 nM, 24 h) and Et-brimamin (**6**) (50 nM, 24 h) on the cytoskeletal organisation of human umbilical vein endothelial cells. Fluorescence labelling of filamentous actin (F-actin, *green*) and paxillin-associated focal adhesions (*red*). Nuclei (*blue*, merge) counterstained with DAPI (630-fold magnification)

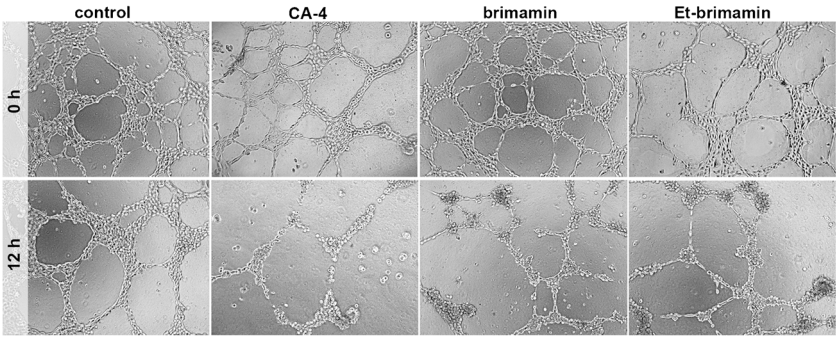

Fig. 7 Tube formation by Ea.hy926 endothelial cells grown on Matrigel. Cells were treated for 12 h with 50 nM CA-4, brimamin **3** or Et-brimamin **6** (100-fold magnification)

this has to be confirmed in a larger trial these findings recommend **6** as a promising drug candidate for the treatment of CA-4-resistant tumours. It also underlines that a strong direct tumour cell cytotoxicity is an important component of the overall activity of **6** against solid tumours, and very likely of other related imidazoles as well.

Et-brimamin (**6**) shows antimetastatic activity in in vitro metastasis models

Neo-vascularisation/angiogenesis is also the initial step in the cascade of processes eventually leading to the metastasis of tumours [28, 31, 38, 39]. Since the subcellular organisation and the dynamic turnover of microtubules, microfilaments, and focal adhesion are essential to angiogenesis- and metastasis-related cell migration, disturbing the balance of these processes might not only affect blood vessel integrity but also the migratory behaviour of prometastatic tumour cells. We assessed the most active imidazole **6** for such effects employing an in vitro model based on a modified Boyden two-chamber system where cells migrate to a lower compartment that is separated by a porous membrane and a Matrigel layer as a surrogate of the natural extracellular matrix (ECM) [29, 30, 40]. This assay provides a realistic three-dimensional model for tumour cell invasion that takes into account both the degradation of a basement membrane matrix and the active

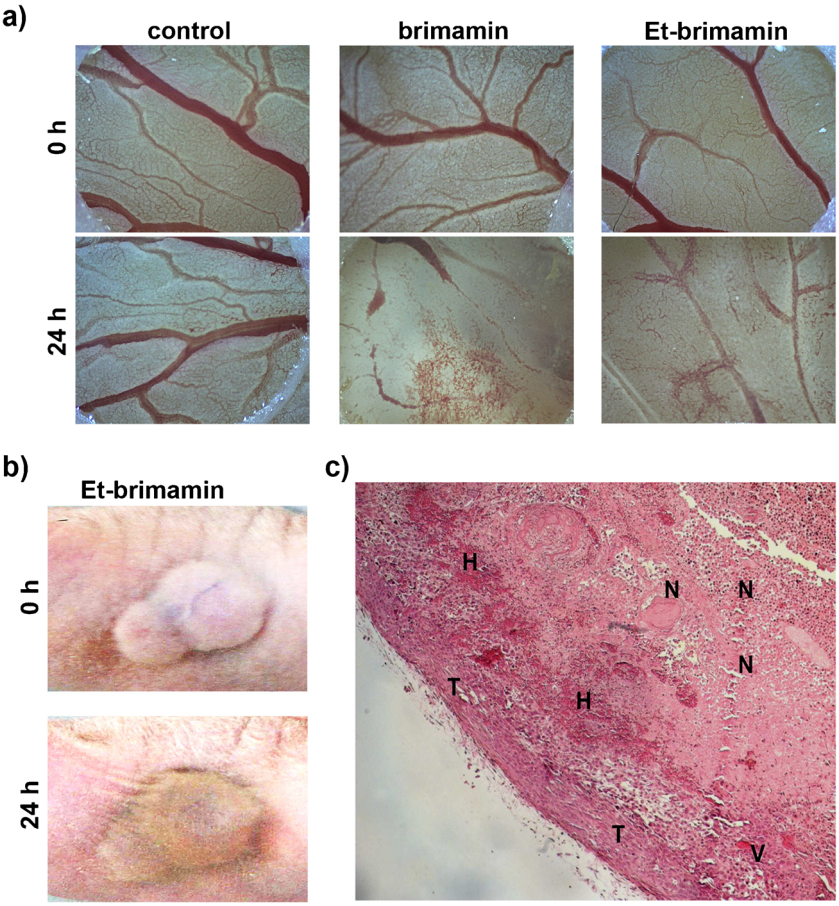

Fig. 8 Vascular-disrupting effects of brimamin (**3**) and Et-brimamin (**6**) in vivo. **a**) Effects by **3** (5 nmol) and **6** (2.5 nmol) on blood vessels in the chorioallantoic membrane (CAM) of fertilised chicken eggs (60-fold magnification). **b**) I.p. administration of **6** (30 mg/kg body weight) to a mouse bearing a 1411HP germ cell tumour xenograft leads to tumour discoloration due to haemorrhages. **c**) Lateral section of the tumour shown in **b**) (*bottom*, *left*) after HE staining featuring a large necrotic core area (N) and haemorrhages (H) surrounded by a cortical layer of vital tumour cells (T) which encompasses residual intact blood vessels (V)

movement of cells through this ECM (Fig. 9, top left) [29, 30, 40]. Directional movement towards the lower compartment was stimulated by providing FBS as a chemoattractant to tumour cells that had been starved overnight. In addition, we also employed a transwell migration assay that mimics the situation of tumour cell intravasation during metastasis by imposing an additional barrier between two compartments in the form of an endothelial cell monolayer [31–33]. This assay emulates the crucial part of the metastatic process when tumour cells enter the vasculature or penetrate the endothelium [31–33]. Once more, hanging cell culture inserts were employed for building an upper and lower compartment separated by an artificial endothelium which was constituted by a basement membrane matrix and a dense, confluent endothelial monolayer (Fig. 9, top right). Highly invasive 518A2 melanoma cells that had migrated through the ECM layer and successfully crossed the endothelium could be discriminated from endothelial cells by a preceding staining of all 518A2 cells with the non-toxic permanent dye DiI [41, 42]. All cells found in the lower compartment or at the underside of the insert membrane were detached and stained with calcein-AM. The number of invasive 518A2 cells was ascertained by measuring the calcein fluorescence intensity (transwell migration, Table 3) or the ratio of red fluorescent, DiI pre-stained 518A2 cells (only invasive 518A2 cells) to all green (calcein) fluorescent cells (endothelial and invasive 518A2 cells; trans-endothelium migration, Table 3; cf. Electronic supplementary material for original fluorescence ratios, Table S6).

Table 3 Migration of 518A2 melanoma cells through Matrigel-coated inserts (transwell migration) or a confluent endothelial cell monolayer grown on inserts (trans-endothelium migration) when exposed to vehicle or Et-brimamin **6** for 48 h

Invasive cells (%)	Control	10 nM Et-brimamin	50 nM Et-brimamin
Transwell migration	100±0.7	53.4±4.6	49.6±2.4
Trans-endothelium migration	100±2.9	73.0±2.5	69.5±4.1

Percentage of invasive cells (%) derived from intracellular calcein fluorescence relative to DMSO-treated controls. Data represent mean±SD from two independent experiments

The concentrations of Et-brimamin (**6**) used in both invasion assays (10, 50 nM) with highly invasive 518A2 melanoma cells [43, 44] were shown to be virtually non-toxic by TUNEL [TdT (terminal desoxynucleotide transferase)-mediated dUTP nick end labelling]-detection of DNA fragmentation (apoptotic cells) after 48 h (cf. electronic Supplementary material, Fig. S2, Table S5 and description of the method). Imidazole **6** suppressed the chemoattractant-stimulated migration through Matrigel-coated membranes to about 50 %

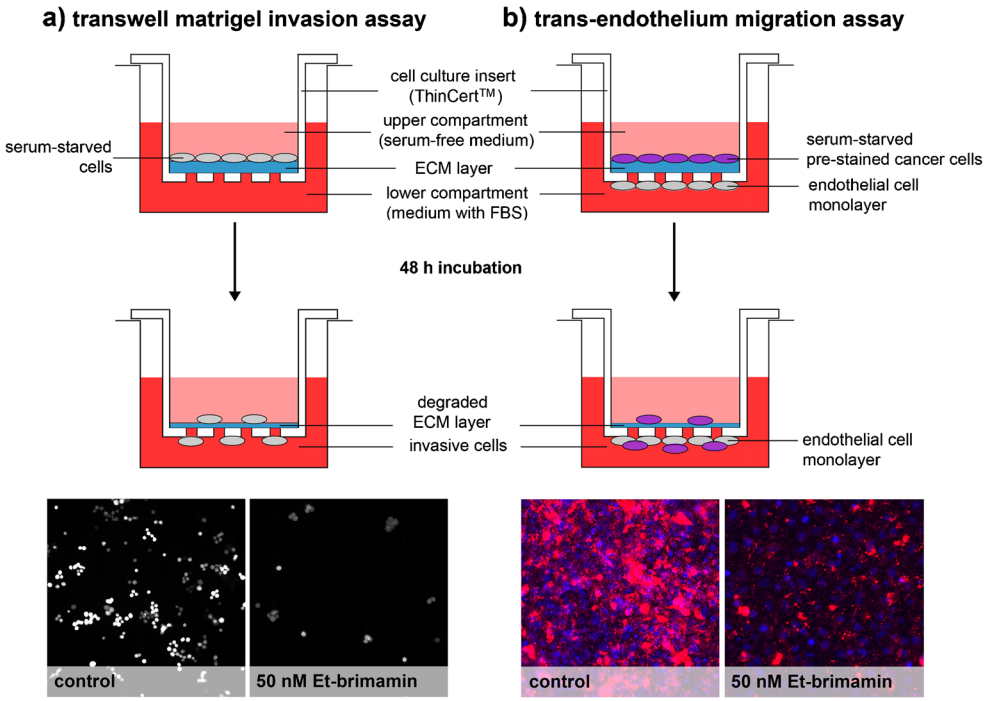

Fig. 9 Antimetastatic activity of Et-brimamin n on highly invasive 518A2 melanoma cells in transwell migration assays. *Upper panel*: schematic representation of two three-dimensional in vitro assays for the quantification of the metastatic potential of 518A2 melanoma cells, based on the ThinCert™product sheet by greiner bio-one. *Lower panel*: *left*: fluorescence micrographs of 518A2 cells on the insert membrane after calcein staining (100-fold magnification) in a transwell matrigel invasion assay; *right*: fluorescence micrographs of the coating on the underside of the insert membrane with 518A2 cells highlighted by the red DiI fluorescence (nuclei counterstained with DAPI, *blue*; 400-fold magnification) in a trans-endothelium migration assay

(Table 3, Fig. 9, bottom left). Migration of 518A2 cells through both the basement membrane matrix and a tight endothelial cell monolayer was distinctly impaired by 10 nM Et-brimamin (**6**), a concentration that hardly affected the total number of viable cells (cf. electronic supplementary material, Table S5). Application of 50 nM **6** inhibited the cell growth as detected by the calcein fluorescence of cells within the lower compartments to 70 % of the control with concomitant halving of cell invasion as assessed from their red DiI membrane fluorescence. In summary, the administration of non- or slightly toxic concentrations of **6** resulted in a reduction of transendothelial invasion/intravasation to ca. Seventy percent (Table 3, Fig. 9, bottom right).

From the reduced numbers of invasive cells we conclude that exposure to Et-brimamin (**6**) induced an extensive cytoskeletal rearrangement which is responsible for the impairment of directional 3D-migration and of squeezing through constrictions such as endothelial cell-cell interfaces or the micropores of the ThinCert™ inserts.

Conclusions

When compared to the first generation of *N*-methyl-4-aryl-5-(4-methoxyphenyl)imidazoles, the analogues bearing a *para*-ethoxy residue at the B-ring generally exhibited stronger effects on the microtubular and actin cytoskeletons of cancer and endothelial cells and on their viability and propensity to migrate or form blood vessel-like tubular structures. In contrast, a replacement of the *meta*-amino group on the B-ring by a halide had a detrimental effect in both series of imidazoles, most pronounced for the couples **3**/**4** and **6**/**7**. Et-brimamin (**6**), the B-*para*-ethoxy congener of the best performing first generation imidazole, brimamin (**3**) [18], turned out to be the best compound of the current series regarding its in vitro inhibition of cancer and endothelial cell growth and its destructive impact on the microtubules. Like the lead CA-4 both analogues **3** and **6** displayed a pronounced vascular-disrupting activity in all its facets in vitro and in vivo. This originates from initial damages to the tubulin cytoskeleton which in turn lead to an adaptation of other cellular processes such as the formation of contractile actin-myosin stress fibres and of cell-matrix focal adhesions eventually resulting in the observed loss of the endothelium integrity [3, 5]. When compared with CA-4 the imidazoles **3** and **6** were far less toxic against the nonmalignant chicken heart fibroblasts in our panel and also against the chicken embryos in the CAM assay. Excellent antitumour activity in combination with merely marginal in vivo side effects in xenograft mouse models had already been reported for brimamin **3** [18]. Hence we are confident that cardiotoxicity as a typical side effect of other clinically used inhibitors of microtubule assembly [45] will play a minor role. The 3D-migration experiments of the current study proved that there is a link also between the cytoskeletal alterations caused by CA-4 and its imidazole analogues and their antimetastatic properties. Although there had been a good deal of evidence in literature for such a link [28, 31, 39, 47–50], the known inhibition of metastatic progression in vivo by CA-4 had been ascribed mainly to its inhibition of AKT function [46]. A tentative proposal for the mechanism of action of CA-4 as well as Et-brimamin (**6**) may be based on the observation that they enhanced the maturation of stable focal adhesions in primary endothelial cells (HUVEC). This effect should prevent the formation of the typical leading edges of migrating cells. So, hindered migration would be the consequence of the loss of cellular polarity which itself originates from the enormous cytoskeleton aberrations as demonstrated in our 3D in vitro metastasis models. Both of these models involve an artificial tumour microenvironment that cells need to get past by different motility or low adhesion mechanisms that cannot be detected by two-dimensional assays [28, 47, 49, 51, 52].

As to potential clinical applications of CA-4 derived imidazoles such as **6** it should be noted that the established strategy of starving solid tumours by blocking blood vessel formation via inhibition of VEGFR (vascular endothelial growth factor receptors) often leads to enhanced aggressiveness and resistance [52–54]. The combination of VEGFR inhibitors with antivascular and antimetastatic CA-4 derivatives, both at low doses, could reduce tumour angiogenesis and additionally prevent metastasis through cytoskeletal reorganisation. Further in vivo studies with metastatic cancers, including such obtained from actual patients under therapy, are currently underway.

Acknowledgments We are indebted to Dr. Florenz Sasse (Helmholtz Centre for Infection Research, Braunschweig, Germany) for assisting with fluorescence microscopy and to Franziska Reipsch (Department of Internal Medicine IV, Halle) for technical assistance.

Conflict of interest The authors declare that there are no conflicts of interest.

References

1. Pettit G, Singh S, Hamel E et al (1989) Isolation and structure of the strong cell growth and tubulin inhibitor combretastatin A-4. Experientia 45:209–211
2. Tron GC, Pirali T, Sorba G et al (2006) Medicinal chemistry of combretastatin A4: present and future directions. J Med Chem 49: 3033–3044. doi:10.1021/jm0512903
3. Kanthou C, Tozer GM (2007) Tumour targeting by microtubule-depolymerising vascular disrupting agents. Expert Opin Ther Targets 11:1443–1457. doi:10.1517/14728222.11.11.1443
4. Tozer GM, Kanthou C, Baguley BC (2005) Disrupting tumour blood vessels. Nat Rev Cancer 5:423–435. doi:10.1038/nrc1628
5. Kanthou C, Tozer GM (2009) Microtubule depolymerizing vascular disrupting agents: novel therapeutic agents for oncology and other

pathologies: microtubule depolymerizing vascular disrupting agents. Int J Exp Pathol 90:284–294. doi:10.1111/j.1365-2613.2009.00651.x
6. Nguyen TL, McGrath C, Hermone AR et al (2005) A common pharmacophore for a diverse set of colchicine site inhibitors using a structure-based approach. J Med Chem 48:6107–6116. doi:10.1021/jm050502t
7. Yamada HY, Gorbsky GJ (2006) Spindle checkpoint function and cellular sensitivity to antimitotic drugs. Mol Cancer Ther 5:2963–2969. doi:10.1158/1535-7163.MCT-06-0319
8. Bhalla KN (2003) Microtubule-targeted anticancer agents and apoptosis. Oncogene 22:9075–9086. doi:10.1038/sj.onc.1207233
9. Kanthou C, Greco O, Stratford A et al (2004) The tubulin-binding agent combretastatin A-4-phosphate arrests endothelial cells in mitosis and induces mitotic cell death. Am J Pathol 165:1401–1411
10. Kanthou C (2002) The tumor vascular targeting agent combretastatin A-4-phosphate induces reorganization of the actin cytoskeleton and early membrane blebbing in human endothelial cells. Blood 99:2060–2069. doi:10.1182/blood.V99.6.2060
11. Quan H, Xu Y, Lou L (2007) p38 MAPK, but not ERK1/2, is critically involved in the cytotoxicity of the novel vascular disrupting agent combretastatin A4. Int J Cancer 122:1730–1737. doi:10.1002/ijc.23262
12. Fan M, Du L, Stone A et al (2000) Modulation of mitogen-activated protein kinases and phosphorylation of Bcl-2 by vinblastine represent persistent forms of normal fluctuations at G2-M. Cancer Res 60:6403–6407
13. Lunt JS, Akerman S, Hill SA et al (2011) Vascular effects dominate solid tumor response to treatment with combretastatin A-4-phosphate. Int J Cancer 129:1979–1989. doi:10.1002/ijc.25848
14. Delmonte A, Sessa C (2009) AVE8062: a new combretastatin derivative vascular disrupting agent. Expert Opin Investig Drugs 18:1541–1548. doi:10.1517/13543780903213697
15. Del Conte G, Bahleda R, Morena V et al (2012) A phase I study of ombrabulin (O) combined with bevacizumab (B) in patients with advanced solid tumors. J Clin Oncol 30:(suppl); abstr 3080
16. Salmon HW, Siemann DW (2006) Effect of the second-generation vascular disrupting agent OXi4503 on tumor vascularity. Clin Cancer Res Off J Am Assoc Cancer Res 12:4090–4094. doi:10.1158/1078-0432.CCR-06-0163
17. Wang L, Woods KW, Li Q et al (2002) Potent, orally active heterocycle-based combretastatin A-4 analogues: synthesis, structure-activity relationship, pharmacokinetics, and in vivo antitumor activity evaluation. J Med Chem 45:1697–1711. doi:10.1021/jm010523x
18. Schobert R, Biersack B, Dietrich A et al (2010) 4-(3-Halo/amino-4,5-dimethoxyphenyl)-5-aryloxazoles and -*N*-methylimidazoles that are cytotoxic against combretastatin A resistant tumor cells and vascular disrupting in a cisplatin resistant germ cell tumor model. J Med Chem 53:6595–6602. doi:10.1021/jm100345r
19. Biersack B, Muthukumar Y, Schobert R, Sasse F (2011) Cytotoxic and antivascular 1-methyl-4-(3-fluoro-4-methoxyphenyl)-5-(halophenyl)-imidazoles. Bioorg Med Chem Lett 21:6270–6273. doi:10.1016/j.bmcl.2011.09.005
20. Bonezzi K, Taraboletti G, Borsotti P et al (2009) Vascular disrupting activity of tubulin-binding 1,5-diaryl-1H-imidazoles. J Med Chem 52:7906–7910. doi:10.1021/jm900968s
21. Schobert R, Effenberger-Neidnicht K, Biersack B (2011) Stable combretastatin A-4 analogues with sub-nanomolar efficacy against chemoresistant HT-29 cells. Int J Clin Pharmacol Ther 49:71–72
22. Biersack B, Effenberger K, Schobert R, Ocker M (2010) Oxazole-bridged combretastatin A4 analogues with improved anticancer properties. ChemMedChem 5:420–427. doi:10.1002/cmdc.200900477
23. Chang C-H, Yu F-Y, Wu T-S et al (2011) Mycotoxin citrinin induced cell cycle G2/M arrest and numerical chromosomal aberration associated with disruption of microtubule formation in human cells. Toxicol Sci 119:84–92. doi:10.1093/toxsci/kfq309
24. Lieuvin A, Labbé J-C, Dorée M, Job D (1994) Intrinsic microtubule stability in interphase cells. J Cell Biol 124:985–996
25. Aranda E, Owen GI (2009) A semi-quantitative assay to screen for angiogenic compounds and compounds with angiogenic potential using the EA. hy926 endothelial cell line. Biol Res 42:377–389
26. Bauer J, Margolis M, Schreiner C et al (1992) In vitro model of angiogenesis using a human endothelium-derived permanent cell line: contributions of induced gene expression, G-proteins, and integrins. J Cell Physiol 153:437–449
27. Nitzsche B, Gloesenkamp C, Schrader M et al (2010) Novel compounds with antiangiogenic and antiproliferative potency for growth control of testicular germ cell tumours. Br J Cancer 103:18–28. doi:10.1038/sj.bjc.6605725
28. Friedl P, Wolf K (2003) Tumour-cell invasion and migration: diversity and escape mechanisms. Nat Rev Cancer 3:362–374. doi:10.1038/nrc1075
29. Entschladen F, Drell TL, Lang K et al (2005) Analysis methods of human cell migration. Exp Cell Res 307:418–426. doi:10.1016/j.yexcr.2005.03.029
30. Albini A, Iwamoto Y, Kleinman HK et al (1987) A rapid in vitro assay for quantitating the invasive potential of tumor cells. Cancer Res 47:3239–3245
31. Geiger TR, Peeper DS (2009) Metastasis mechanisms. Biochim Biophys Acta Rev Cancer 1796:293–308. doi:10.1016/j.bbcan.2009.07.006
32. Li YH, Zhu C (1999) A modified Boyden chamber assay for tumor cell transendothelial migration in vitro. Clin Exp Metastasis 17:423–429
33. Okada T, Okuno H, Mitsui Y (1994) A novel in vitro assay system for transendothelial tumor cell invasion: significance of E-selectin and alpha 3 integrin in the transendothelial invasion by HT1080 fibrosarcoma cells. Clin Exp Metastasis 12:305–314
34. Laferriere J (2001) Transendothelial migration of colon carcinoma cells requires expression of E-selectin by endothelial cells and activation of stress-activated protein kinase-2 (SAPK2/p38) in the tumor cells. J Biol Chem 276:33762–33772. doi:10.1074/jbc.M008564200
35. Orth JD, Loewer A, Lahav G, Mitchison TJ (2012) Prolonged mitotic arrest triggers partial activation of apoptosis, resulting in DNA damage and p53 induction. Mol Biol Cell 23:567–576
36. Chrzanowska-Wodnicka M, Burridge K (1996) Rho-stimulated contractility drives the formation of stress fibers and focal adhesions. J Cell Biol 133:1403–1415
37. Schwartz EL (2009) Antivascular actions of microtubule-binding drugs. Clin Cancer Res 15:2594–2601. doi:10.1158/1078-0432.CCR-08-2710
38. Carmeliet P (2005) Angiogenesis in life, disease and medicine. Nature 438:932–936. doi:10.1038/nature04478
39. Lamalice L, Le Boeuf F, Huot J (2007) Endothelial cell migration during angiogenesis. Circ Res 100:782–794. doi:10.1161/01.RES.0000259593.07661.1e
40. Boyden S (1962) The chemotactic effect of mixtures of antibody and antigen on polymorphonuclear leucocytes. J Exp Med 115:453–466
41. Kuriyama S, Yamazaki M, Mitoro A et al (1998) Analysis of intrahepatic invasion of hepatocellular carcinoma using fluorescent dye-labeled cells in mice. Anticancer Res 18:4181–4188
42. Horan PK, Melnicoff MJ, Jensen BD, Slezak SE (1990) Chapter 42 Fluorescent cell labeling for in vivo and in vitro cell tracking. Methods Cell Biol. Elsevier, 469–490
43. Hofmann UB, Houben R, Bröcker E-B, Becker JC (2005) Role of matrix metalloproteinases in melanoma cell invasion. Biochimie 87:307–314. doi:10.1016/j.biochi.2005.01.013
44. Orgaz JL, Sanz-Moreno V (2013) Emerging molecular targets in melanoma invasion and metastasis. Pigment Cell Melanoma Res 26:39–57. doi:10.1111/pcmr.12041
45. Mikaelian I, Buness A, de Vera-Mudry M-C et al (2010) Primary endothelial damage is the mechanism of cardiotoxicity of tubulin-

binding drugs. Toxicol Sci 117:144–151. doi:10.1093/toxsci/kfq189
46. Lin H-L, Chiou S-H, Wu C-W et al (2007) Combretastatin A4-induced differential cytotoxicity and reduced metastatic ability by inhibition of AKT function in human gastric cancer cells. J Pharmacol Exp Ther 323:365–373. doi:10.1124/jpet.107.124966
47. Werr J, Xie X, I-Iedqvist P et al (1998) B-integrins are critically involved in neutrophil locomotion in extravascular tissue in vivo. J Exp Med 18712091–2096
48. Huttenlocher A, Horwitz AR (2011) Integrins in cell migration. Cold Spring Harb Perspect Biol 3:a005074–a005074. doi:10.1101/cshperspect.a005074
49. Zamir E, Geiger B (2001) Molecular complexity and dynamics of cell-matrix adhesions. J Cell Sci 114:3583–3590
50. Van Nieuw Amerongen GP, van Hinsbergh VWM (2001) Cytoskeletal effects of Rho-like small guanine nucleotide-binding proteins in the vascular system. Arterioscler Thromb Vasc Biol 21:300–311. doi:10.1161/01.ATV.21.3.300
51. Haston WS, Shields JM, Wilkinson PC (1982) Lymphocyte locomotion and attachment on two-dimensional surfaces and in three-dimensional matrices. J Cell Biol 92:747–752
52. Weis SM, Cheresh DA (2011) Tumor angiogenesis: molecular pathways and therapeutic targets. Nat Med 17:1359–1370. doi:10.1038/nm.2537
53. Pàez-Ribes M, Allen E, Hudock J et al (2009) Antiangiogenic therapy elicits malignant progression of tumors to increased local invasion and distant metastasis. Cancer Cell 15:220–231. doi:10.1016/j.ccr.2009.01.027
54. Ebos JML, Lee CR, Cruz-Munoz W et al (2009) Accelerated metastasis after short-term treatment with a potent inhibitor of tumor angiogenesis. Cancer Cell 15:232–239. doi:10.1016/j.ccr.2009.01.021

- ELECTRONIC SUPPLEMENTARY MATERIAL -

Combretastatin A-4 derived imidazoles show cytotoxic, antivascular, and antimetastatic effects based on cytoskeletal reorganisation

- Investigational New Drugs -

Katharina Mahal, Bernhard Biersack, Henrike Caysa, Rainer Schobert, Thomas Mueller

Affiliations and addresses of authors:

Katharina Mahal, Bernhard Biersack, Rainer Schobert
Organic Chemistry Laboratory, University Bayreuth, Universitaetsstrasse 30, 95440 Bayreuth, Germany

Henrike Caysa, Thomas Mueller
Department of Internal Medicine IV, Oncology/Hematology, Martin-Luther-University Halle-Wittenberg, 06120 Halle-Saale, Germany

Corresponding author:
Prof. Dr. Rainer Schobert, Organic Chemistry Laboratory, University Bayreuth, Universitaetsstrasse 30, 95440 Bayreuth, Germany. Phone: +49(0)921 552670. Fax: +49(0)921 552671. E-mail: rainer.schobert@uni-bayreuth.de

Table of Contents

Materials and Methods

General remarks and instruments used

Column chromatography: silica gel 60 (230-400 mesh). Melting points (uncorrected), Electrothermal 9100; IR spectra, Perkin-Elmer Spectrum One FT-IR spectrophotometer with ATR sampling unit; NMR spectra, Bruker Avance 300 spectrometer; chemical shifts are given in parts per million (*δ*) downfield from tetramethylsilane as internal standard; Mass spectra, Thermo Finnigan MAT 8500 (EI); Microanalyses, Perkin-Elmer 2400 CHN elemental analyzer. All tested compounds are > 98% pure by elemental analysis. All starting compounds were purchased from the usual retailers and used without further purification.

Chemistry

Compounds **1**-**4** and **9**-**10** were prepared according to literature procedures [S1–S3]. The new compounds **5**-**8**, **11**, and **12** were obtained analogously.

*1-Methyl-4-(3'-bromo-4',5'-dimethoxyphenyl)-5-(3''-chloro-4''-methoxyphenyl)-imidazole x HCl (**5**)*

A mixture of 3-chloro-4-methoxybenzaldehyde (72 mg, 0.42 mmol) and 33% $MeNH_2$/ethanol (260 µL, 2.10 mmol) in ethanol (15 mL) was treated with AcOH (150 µL, 2.63 mmol) and refluxed for 2 h. After cooling down to room temperature, (3-bromo-4,5-dimethoxyphenyl)-(*p*-toluenesulfonyl)-methylisocyanide (172 mg, 0.42 mmol) and K_2CO_3 (500 mg, 3.62 mmol) were added and the reaction mixture was refluxed for 5 h. The solvent was evaporated, the residue diluted with ethyl acetate, washed with water and brine, dried over Na_2SO_4, filtered and concentrated in vacuum. The residue was purified by column chromatography (silica gel 60, ethyl acetate/methanol 9:1) giving the product as a colourless oil, which was converted into its hydrochloride salt by treatment with 3 M HCl / dioxane (1 mL) in DCM (5 mL) giving a colourless solid after evaporation of the solvent and recrystallisation from DCM/*n*-hexane. Yield: 150 mg (0.32 mmol, 76%); colourless solid of mp 137-138 °C; ν_{max} (ATR)/cm^{-1}: 3401, 3162, 2944, 2841, 2734, 2630, 1632, 1605, 1548, 1516, 1494, 1464, 1422, 1317, 1292, 1264, 1230, 1167, 1117, 1065, 1043, 1022, 995, 901, 875, 846, 824, 806, 753, 735, 705, 685; ^{1}H NMR (300 MHz, acetone-d$_6$): δ 3.76 (3 H, s), 3.85 (6 H, s), 4.03 (3 H, s); 7.16 (1 H, s), 7.3-7.4 (1 H, m), 7.5-7.8 (3 H, m), 9.31 (1 H, s); ^{13}C NMR (75.5 MHz, acetone-d$_6$): δ 34.8, 57.0, 57.2, 60.7, 113.0, 114.3, 118.0, 120.0, 123.6, 124.0, 125.1, 129.6, 129.9, 132.5, 133.5, 136.2, 147.6, 154.8, 157.9; *m/z* (%) 438 (100) [M$^+$], 436 (73) [M$^+$], 423 (52), 421 (42).

1-Methyl-4-(3'-bromo-4',5'-dimethoxyphenyl)-5-(4''-ethoxy-3''-nitrophenyl)-imidazole

A mixture of 4-ethoxy-3-nitrobenzaldehyde (82 mg, 0.42 mmol) and 33% $MeNH_2$/ethanol (260 µL, 2.10 mmol) in ethanol (15 mL) was treated with AcOH (150 µL, 2.63 mmol) and refluxed for 2 h. After cooling down to room temperature, (3-bromo-4,5-dimethoxyphenyl)-(p-toluenesulfonyl)-methylisocyanide (172 mg, 0.42 mmol) and K_2CO_3 (500 mg, 3.62 mmol) were added and the reaction mixture was refluxed for 5 h. The solvent was evaporated, the residue diluted with ethyl acetate, washed with water and brine, dried over Na_2SO_4, filtered and concentrated in vacuum. The residue was purified by column chromatography (silica gel 60, ethyl acetate/methanol 9:1) giving the product as orange oil. Yield: 170 mg (0.37 mmol, 88%); ν_{max} (ATR)/cm^{-1}: 2983, 2936, 1622, 1599, 1547, 1527, 1505, 1472, 1353, 1247, 1110, 1039, 997, 865, 808, 759, 739, 655, 634; ^{1}H NMR (300 MHz, $CDCl_3$): δ 1.41 (3 H, t, ^3J 7.0 Hz), 3.42 (3 H, s), 3.60 (3 H, s), 3.72 (3 H, s), 4.16 (2 H, q, ^3J 7.0 Hz), 6.92 (1 H, d, ^4J 2.0 Hz), 7.0-7.1 (2 H, m), 7.40 (1 H, dd, ^3J 8.7 Hz, ^4J 2.3 Hz), 7.47 (1 H, s), 7.73 (1 H, d, ^4J 2.3 Hz); ^{13}C NMR (75.5 MHz, $CDCl_3$): δ 14.2, 32.1, 55.6, 60.3, 65.5, 109.8, 115.0, 117.2, 121.8, 122.3, 126.1, 127.1, 131.2, 136.2, 137.2, 137.7, 139.9, 144.8, 152.1, 153.1; *m/z* (%) 463 (99) [M$^+$], 461 (100) [M$^+$], 447 (46), 445 (45).

1-Methyl-5-(3''-amino-4''-ethoxyphenyl)-4-(3'-bromo-4',5'-dimethoxyphenyl)-imidazole

Et-Brimamin x 2HCl (6)

1-Methyl-4-(3'-bromo-4',5'-dimethoxyphenyl)-5-(4''-ethoxy-3''-nitrophenyl)-imidazole (170 mg, 0.37 mmol) was dissolved in THF (7.5 mL). Zn powder (120 mg, 1.83 mmol) was added followed by a mixture of conc. HCl (264 µL) in THF (1 mL). After stirring for 15 min at room temperature the reaction mixture was poured onto water and basified with aqueous $NaHCO_3$ to ca. pH 8. The water phase was extracted with ethyl acetate and the organic phase was dried over Na_2SO_4, filtered and the filtrate was concentrated in vacuum. The residue was purified by column chromatography (silica gel 60, 10% methanol/ethyl acetate, R_f = 0.64) giving the aniline intermediate. This compound was dissolved in DCM (5 mL) and treated with 3M HCl/dioxane (1 mL). After stirring for 15 min the solvent was removed and the residue was recrystallized from a DCM/*n*-hexane mixture. Yield: 121 mg (0.22 mmol, 65%); colorless solid of m.p. >160°C (dec.); ν_{max} (ATR)/cm^{-1}: 3369, 2936, 2829, 2540, 1632, 1547, 1492, 1411, 1395, 1303, 1270, 1235, 1141, 1114, 1038, 993, 862, 818, 720; ^{1}H NMR (300 MHz, DMSO-d_6): δ 1.40 (3 H, t, ^3J 6.9 Hz), 3.63 (3 H, s), 3.70 (3 H, s), 3.72 (3 H, s), 4.19 (2 H, q, ^3J 6.9 Hz), 7.1-7.3 (4 H, m), 7.45 (1 H, s), 9.41 (1 H, s); ^{13}C NMR (75.5

MHz, DMSO-d_6): δ 14.4, 34.0, 56.2, 60.2, 64.6, 111.4, 113.7, 117.0, 117.5, 122.4, 124.2, 127.6, 129.3, 135.8, 146.0, 151.7, 153.3; *m/z* (%) 433 (100) [M^+], 431 (100) [M^+], 416 (31), 404 (16), 402 (15), 36 (69).

1-Methyl-4-(3'-bromo-4',5'-dimethoxyphenyl)-5-(3''-fluoro-4''-ethoxyphenyl)-imidazole ***Et-Brimfluor x HCl (7)***

A mixture of 3-fluoro-4-ethoxybenzaldehyde (71 mg, 0.42 mmol) and 33% $MeNH_2$/ethanol (260 µL, 2.10 mmol) in ethanol (15 mL) was treated with AcOH (150 µL, 2.63 mmol) and refluxed for 2 h. After cooling down to room temperature, (3-bromo-4,5-dimethoxyphenyl)-(p-toluenesulfonyl)-methylisocyanide (172 mg, 0.42 mmol) and K_2CO_3 (500 mg, 3.62 mmol) were added and the reaction mixture was refluxed for 5 h. The solvent was evaporated, the residue diluted with ethyl acetate, washed with water and brine, dried over Na_2SO_4, filtered and concentrated in vacuum. The residue was purified by column chromatography (silica gel 60, ethyl acetate/methanol 9:1). The resulting colorless oil was dissolved in DCM (5 mL) and treated with 3M HCl/dioxane. The reaction mixture was stirred at room temperature for 10 min, and the solvent was evaporated. The residue was recrystallised from DCM/*n*-hexane. Yield: 160 mg (0.34 mmol, 81%); colorless solid of mp 90 °C; v_{max} (ATR)/cm^{-1}: 3391, 3111, 2976, 2939, 2884, 2833, 2620, 1626, 1547, 1523, 1494, 1474, 1421, 1397, 1304, 1270, 1233, 1115, 1039, 995, 927, 885, 851, 809, 778, 756; ^{1}H NMR (300 MHz, DMSO-d_6): δ 1.37 (3 H, t, ^3J 6.9 Hz), 3.71 (3 H, s), 3.73 (3 H, s), 4.19 (2 H, q, ^3J 6.9 Hz), 7.14 (1 H, d, ^4J 2.0 Hz), 7.26 (1 H, d, ^4J 2.0 Hz), 7.2-7.3 (2 H, m), 7.37 (1 H, t, ^3J 17.1 Hz), 7.51 (1 H, dd, ^3J 11.9 Hz, ^4J 1.9 Hz), 9.37 (1 H, s); ^{13}C NMR (75.5 MHz, DMSO-d_6): δ 14.4, 33.9, 56.1, 60.2, 64.6, 111.5, 115.5, 116.9, 118.6, 122.5, 124.3, 128.2, 128.9, 135.7, 146.1, 148.2, 153.3; *m/z* (%) 436 (100) [M^+], 434 (100) [M^+], 421 (96), 419 (95), 340 (12), 36 (15).

1-Methyl-4-(3'-bromo-4',5'-dimethoxyphenyl)-5-(3''-chloro-4''-ethoxyphenyl)-imidazole x HCl ***8***

A mixture of 3-chloro-4-ethoxybenzaldehyde (78 mg, 0.42 mmol) and 33% $MeNH_2$/ethanol (260 µL, 2.10 mmol) in ethanol (15 mL) was treated with AcOH (150 µL, 2.63 mmol) and refluxed for 2 h. After cooling down to room temperature, (3-bromo-4,5-dimethoxyphenyl)-(*p*-toluenesulfonyl)-methylisocyanide (172 mg, 0.42 mmol) and K_2CO_3 (500 mg, 3.62 mmol) were added and the reaction mixture was refluxed for 5 h. The solvent was evaporated, the residue diluted with ethyl acetate, washed with water and brine, dried over Na_2SO_4, filtered and concentrated in

vacuum. The residue was purified by column chromatography (silica gel 60, ethyl acetate/methanol 9:1) giving the product as a colourless oil, which was converted into its hydrochloride salt by treatment with 3 M HCl / dioxane (1 mL) in DCM (5 mL) giving a colourless solid after evaporation of the solvent and recrystallisation from DCM/*n*-hexane. Yield: 130 mg (0.27 mmol, 64%); colourless solid of mp 150-151 °C; ν_{max} (ATR)/cm^{-1}: 3405, 2988, 2940, 2841, 2733, 1623, 1605, 1548, 1514, 1493, 1473, 1421, 1394, 1318, 1260, 1230, 1171, 1116, 1087, 1062, 1042, 995, 903, 875, 845, 816, 753, 735, 717, 685; ^{1}H NMR (300 MHz, acetone-d$_6$): δ 1.49 (3 H, t, ^{3}J 7.0 Hz), 3.78 (3 H, s), 3.86 (3 H, s), 3.92 (3 H, s), 4.29 (2 H, q, ^{3}J 7.0 Hz), 7.18 (1 H, s), 7.3-7.4 (1 H, m), 7.5-7.8 (3 H, m), 9.44 (1 H, s); ^{13}C NMR (75.5 MHz, acetone-d$_6$): δ 14.9, 34.8, 57.2, 60.7, 65.9, 112.9, 115.1, 118.0, 120.0, 123.5, 124.1, 125.1, 129.4, 129.9, 132.5, 133.5, 136.3, 147.5, 154.8, 157.2; *m/z* (%) 452 (100) [M^{+}], 450 (75) [M^{+}], 437 (51), 435 (39).

1-Methyl-4-(3'-chloro-4',5'-dimethoxyphenyl)-5-(4''-ethoxy-3''-nitrophenyl)-imidazole

A mixture of 4-ethoxy-3-nitrobenzaldehyde (82 mg, 0.42 mmol) and 33% $MeNH_2$/ethanol (260 µL, 2.10 mmol) in ethanol (15 mL) was treated with AcOH (150 µL, 2.63 mmol) and refluxed for 2 h. After cooling down to room temperature, (3-chloro-4,5-dimethoxyphenyl)-(*p*-toluenesulfonyl)-methylisocyanide (153 mg, 0.42 mmol) and K_2CO_3 (500 mg, 3.62 mmol) were added and the reaction mixture was refluxed for 5 h. The solvent was evaporated, the residue diluted with ethyl acetate, washed with water and brine, dried over Na_2SO_4, filtered and concentrated in vacuum. The residue was purified by column chromatography (silica gel 60, ethyl acetate/methanol 9:1) giving the product as orange oil. Yield: 170 mg (0.34 mmol, 81%); ν_{max} (ATR)/cm^{-1}: 2938, 1622, 1600, 1553, 1527, 1506, 1484, 1353, 1286, 1263, 1110, 1045, 998, 870, 829, 817, 762, 739, 656, 635; ^{1}H NMR (300 MHz, $CDCl_3$): δ 1.43 (3 H, t, ^{3}J 7.0 Hz), 3.44 (3 H, s), 3.63 (3 H, s), 3.75 (3 H, s), 4.18 (2 H, q, ^{3}J 7.0 Hz), 6.9-7.0 (2 H, m), 7.12 (1 H, d, ^{3}J 8.7 Hz), 7.41 (1 H, dd, ^{3}J 8.7 Hz, ^{4}J 2.2 Hz), 7.49 (1 H, s), 7.75 (1 H, d, ^{4}J 2.2 Hz); ^{13}C NMR (75.5 MHz, $CDCl_3$): δ 14.3, 32.1, 55.7, 60.5, 65.5, 109.1, 115.0, 119.6, 121.9, 126.1, 127.2, 127.9, 130.6, 136.2, 137.4, 137.8, 139.9, 143.9, 152.2, 153.3; *m/z* (%) 419 (36) [M^{+}], 417 (100) [M^{+}], 402 (53).

1-Methyl-5-(3''-amino-4''-ethoxyphenyl)-4-(3'-chloro-4',5'-dimethoxyphenyl)-imidazole

Et-Climamin x 2HCl (11)

1-Methyl-4-(3'-chloro-4',5'-dimethoxyphenyl)-5-(4''-ethoxy-3''-nitrophenyl)-imidazole (140 mg, 0.34 mmol) was dissolved in THF (7.5 mL). Zn powder (110 mg, 1.68 mmol) was added followed by a mixture of conc. HCl (243 µL) in THF (1 mL). After stirring for 15 min at room temperature the reaction mixture was poured onto water and basified with aqueous $NaHCO_3$ to ca. pH 8. The water phase was extracted with ethyl acetate and the organic phase was dried over Na_2SO_4, filtered and the filtrate was concentrated in vacuum. The residue was purified by column chromatography (silica gel 60, 10% methanol/ethyl acetate, R_f = 0.63) giving the aniline intermediate. This compound was dissolved in DCM (5 mL) and treated with 3M HCl/dioxane (1 mL). After stirring for 15 min the solvent was removed and the residue was recrystallized from a DCM/*n*-hexane mixture. Yield: 97 mg (0.21 mmol, 62%); colorless solid of m.p. >150°C (dec.); ν_{max} (ATR)/cm^{-1}: 3392, 2976, 2833, 2538, 1631, 1550, 1514, 1495, 1466, 1396, 1302, 1268, 1237, 1142, 1115, 1044, 996, 850, 816, 762, 722; ^{1}H NMR (300 MHz, DMSO-d_6): δ 1.40 (3 H, t, ^3J 6.9 Hz), 3.63 (3 H, s), 3.70 (3 H, s), 3.75 (3 H, s), 4.21 (2 H, q, ^3J 6.9 Hz), 7.07 (1 H, d, ^4J 2.1 Hz), 7.19 (1 H, d, ^4J 2.1 Hz), 7.3-7.4 (2 H, m), 7.45 (1 H, s), 9.41 (1 H, s); ^{13}C NMR (75.5 MHz, DMSO-d_6): δ 14.4, 34.0, 56.2, 60.4, 64.6, 110.8, 113.7, 117.5, 119.6, 123.5, 127.3, 127.7, 129.3, 135.8, 145.0, 151.7, 153.5; *m/z* (%) 388 (35) [M$^+$], 386 (100) [M$^+$], 371 (36), 36 (98).

1-Methyl-4-(3'-chloro-4',5'-dimethoxyphenyl)-5-(3''-fluoro-4''-ethoxyphenyl)-imidazole

Et-Climfluor x HCl (12)

A mixture of 3-fluoro-4-ethoxybenzaldehyde (124 mg, 0.74 mmol) and 33% $MeNH_2$/ethanol (460 µL, 3.76 mmol) in ethanol (15 mL) was treated with AcOH (260 µL, 4.63 mmol) and refluxed for 2 h. After cooling down to room temperature, (3-chloro-4,5-dimethoxyphenyl)-(*p*-toluenesulfonyl)-methylisocyanide (270 mg, 0.74 mmol) and K_2CO_3 (500 mg, 3.62 mmol) were added and the reaction mixture was refluxed for 5 h. The solvent was evaporated, the residue diluted with ethyl acetate, washed with water, dried over Na_2SO_4, filtered and concentrated in vacuum. The residue was purified by column chromatography (silica gel 60, ethyl acetate/methanol 95:5) giving the imidazole as a colorless oil. This oil was dissolved in DCM (5 mL) and treated with 3 M HCl in dioxane (1 mL). After stirring for 5 min the solvent was evaporated and the residue preciptitated from DCM/*n*-hexane. Yield: 210 mg (0.49 mmol, 66%), colorless gum; ν_{max} (ATR)/cm^{-1}: 3391, 3166, 2946, 2841, 2727, 1627, 1554, 1523, 1499, 1477, 1423, 1395, 1302, 1269, 1230, 1193, 1136, 1117, 1050, 998, 888, 844, 814, 778, 753; ^{1}H NMR (300 MHz, acetone-d_6): δ 1.44 (3 H, t, ^3J 7.0

Hz), 3.75 (3 H, s), 3.77 (3 H, s), 3.88 (3 H, s), 4.25 (2 H, q, ^3J 7.0 Hz), 7.01 (1 H, d, ^4J 2.1 Hz), 7.35 (1 H, t, $^3J_{HF}$ 18.0 Hz), 7.56 (1 H, dd, ^3J 11.7 Hz, ^4J 1.9 Hz), 9.71 (1 H, s); ^{13}C NMR (75.5 MHz, acetone-d_6): δ 15.0, 34.9, 57.1, 60.8, 65.7, 111.8, 113.8, 116.3, 119.2, 119.3, 119.6, 119.9, 120.6, 122.4, 124.4, 124.5, 128.6, 129.2, 130.1, 134.6, 136.6, 146.4, 149.8, 149.9, 151.7, 154.8, 155.0; *m/z* (%) 392 (37) [M^+], 390 (100) [M^+], 377 (21), 375 (65).

Biological studies

Cell proliferation assay (MTT assay) [S4]. The tetrazolium salt MTT (3-(4,5-dimethylthiazol-2-yl)-2,5-diphenyl-tetrazolium bromide, Carl Roth) was used to identify viable cells by reduction of MTT to a violet formazan. 518A2 melanoma, HT-29 colon adenocarcinoma, HCT-1116 colon carcinoma, MCF-7/Topo mammacarcinoma (5x10^3 cells/well), Ea.hy926 endothelial cells and non-malignant chicken fibroblasts (CHF, 1x10^4 cells/well) were seeded on 96-well cell culture plates and cultured for 24 h (37 °C, 5% CO2, 95% humidity). Incubation of cells following treatment with the test compounds **2**-**12** (dilution series ranging from 100 µM to 5 pM in PBS) was continued for 72 h. Solvent controls (DMSO) were treated identically. A 5 mg/mL stock solution of MTT in PBS was added to a final MTT concentration of 0.05%. After 2 h incubation, the microplates were centrifuged at 300 g, 4 °C for 5 min and the supernatant medium was discarded. For cell lysis and dissolving of the precipitated formazan crystals, 30 µl of a SDS-DMSO solution (10% SDS (w/v), 0.6% acetic acid in DMSO) were added to each well. The absorbance at wavelengths 570 and 630 nm (background) was measured using an automatic microplate reader (Tecan). All experiments were carried out at least in triplicates, the percentage of viable cells quoted was calculated as the mean ± S.D. with respect to the controls set to 100%.

Tubulin polymerisation assay*.* Analysis of tubulin polymerisation was performed using the tubulin polymerization assay kit (Cytoskeleton) according to manufacturer's instructions. The assay is fluorescence-based, and tubulin polymerisation was followed by measuring RFU (relative fluorescence units) on the SpectraFluorPlus (Tecan, Switzerland) using the following filters: excitation 360 nm, emission 465 nm. For comparison of the inhibitory effects of compounds maximal gradients based on kinetic curves were calculated by Magellan version 3.11 (Tecan, Switzerland).

Animal studies

The antitumour activity of **6** was analysed in nude mice bearing xenograft tumours of CA-4 resistant HT-29 cells. Each of six mice was administered a 150 µL PBS suspension of 5 million HT-29 cells into the left flank to generate subcutaneous xenograft tumours. After establishment of tumours the mice were divided in two groups each containing a larger and two smaller tumours resulting in similar mean tumour volumes at start of treatment (treatment group: 245/87/66 mm^3; control group: 245/81/66 mm^3). Different treatment schedules were tested: single i.p. application of 20 mg/kg/body weight of **6** on day 1; dual i.p applications of 20 mg/kg on days 7/8; p.o. application of 40 mg/kg on day 23; single i.p. application of 30 mg/kg on day 28. Control group received normal saline. Tumour volumes were calculated by caliper measurement using the formula $a^2 \times b \times 0.5$ with *a* being the short and *b* the long dimension. Trail was followed until the first tumour in the control group reached the maximal tolerated tumour volume. All animal studies were approved by the Laboratory Animal Care Committee of Sachsen-Anhalt, Germany.

TUNEL-based detection of apoptotic cells. DNA fragmentation in apoptotic cells was additionally measured using the TUNEL technique (Terminal desoxyribonucleotide Transferase-mediated dUTP Nick End Labelling). Labelling of 3'OH ends was performed with the commercially available FragEL™ DNA Fragmentation Detection Kit (QIA39, Calbiochem) and according to manufacturer's instructions. Briefly, cells grown in 25 cm^2-cell culture flasks ($5x10^5$ cells/well) and treated with vehicle (DMSO) or the best imidazole **6** (50 and 100 nM) for 48 h. Cells were then trypsinated, pelleted by centrifugation (300 g, 4 °C, 5 min) and fixed in 4% formaldehyde in PBS at room temperature for 10 min followed by washing of the cell pellets (300 g, 4 °C, 5 min) in 1 mL PBS and two times in 1 mL 1X TBS (Tris-buffered saline, 50 mM Tris-HCl, 150 mM NaCl, pH 7.4). After proteinase K digestion (20 µg/mL per specimen, 5 min, rt) and cell permeabilisation, about $1x10^6$ cells were resuspended in TdT-labelling reaction mixture containing TdT enzyme and fluorescein-coupled dUTPs and incubated at 37 °C for 1 h in the dark. Labelled cells were washed twice with 1 mL TBS before analysis of the green fluorescence intensity on a Beckman Coulter Cytomics FC500 flow cytometer. Data analyses were done with the CXP software (Beckman Coulter), gates defining the percentage of viable and apoptotic cells were applied with respect to DMSO-treated control.

Results

Cell cycle analyses

Table S1 Alteration in the cell cycle distribution of 518A2 melanoma cells after treatment with CA-4 and its imidazole derivatives brimamin **3** and Et-brimamin **6** at the indicated concentrations (nM) for 24 h. Percentage of cells in G1, S or G2-M phase of cell cycle progression or apoptotic cells (sub-G1). Data obtained from flow cytometric cell cycle analyses after propidium iodide staining of the cellular DNA content. c: control (DMSO)

	c	CA-4			brimamin 3			Et-brimamin 6		
conc. (nM)		**25**	**10**	**5**	**100**	**50**	**25**	**50**	**25**	**10**
sub-G1	8.3	54.8	51.2	47.1	48.4	38.1	17.2	48.8	46.7	23.3
G1	54.6	12.7	12.6	13.1	9.6	29.7	45.8	11.5	22.2	35.4
S	14.9	15.4	16.7	15.9	16.7	16.0	14.5	15.4	14.2	14.2
G2-M	22.7	17.1	19.5	25.2	25.3	16.2	23.5	24.3	16.9	27.8

Table S2 Alteration in the cell cycle distribution (%) of HT-29 colon carcinoma cells after treatment with CA-4 and its imidazole derivatives brimamin **3** and Et-brimamin **6** at the indicated concentrations (nM) for 24 h. Percentage of cells in G1, S or G2-M phase of cell cycle progression or apoptotic cells (sub-G1). Data obtained from cell cycle analyses by flow cytometry after propidium iodide staining of the cellular DNA content. c: control (DMSO)

	c	CA-4		brimamin 3		Et-brimamin 6	
conc. (nM)		**10000**	**5000**	**100**	**50**	**100**	**50**
sub-G1	4.3	10.6	10.2	5.2	12.3	9.1	14.8
G1	58.0	42.4	41.0	1.5	15.2	3.7	22.4
S	20.5	23.6	27.6	4.5	6.7	2.7	12.4
G2-M	16.9	24.5	21.2	89.1	65.9	84.5	50.9

Determination of the tubulin affinity in cell-based and cell-free assays

Table S3 Densitometry analysis of the alpha-tubulin content in detergent-insoluble cell lysate fractions (intact microtubules) visualised by Western blotting (shown in Fig. 3). Respective cell lysates were obtained from 518A2 melanoma cells exposed to various concentrations of CA-4, brimamin **3** or Et-brimamin **6** for 3 h

(nM)	brimamin 3	Et-brimamin 6	CA-4
0	100.0 ± 7.2	100.0 ± 1.3	*n.d.*
50	100.0 ± 4.7	55.0 ± 1.7	*n.d.*
100	69.5 ± 6.0	6.3 ± 0.5	*n.d.*
250	13.3 ± 2.2	5.4 ± 0.6	*n.d.*
500	18.5 ± 8.9	5.2 ± 0.3	*n.d.*
1000	12.4 ± 1.5	1.4 ± 0.2	2.1 ± 0.2

Table S4 Inhibition of tubulin polymerisation (%) by 3 µM of the imidazoles (**1**,**3**-**4**,**6**,**9**,**11**) as measured by using a fluorescence-based tubulin polymerisation kit (Cytoskeleton). Values obtained from maximal gradients of the kinetic curves as % of vehicle treated controls are representative for 3 independent measurements ± SD

compound	1	3	4	6	9	11
inhibition of tubulin polymerisation (%)	62.7 ± 4.5	89.2 ± 1.4	57.8 ± 4.8	93.6 ± 0.3	86.8 ± 2.5	91.1 ± 3.8

Preliminary animal studies

A treatment of highly vascularised 1411HP xenograft tumours with compounds **3**, **6** in some cases induced dramatic tumour regressions. This high antitumour activity [S2] can mainly be ascribed to the vascular disrupting activity. In addition, compound **6** showed high *in vitro* cytotoxic activity in resistant cell lines and even completely overcame CA-4 resistance of HT-29 cells. To evaluate the contribution of the tumour cell cytotoxicity component, compound **6** was tested for *in vivo* antitumour activity in a small panel of mice bearing HT-29 xenograft tumours, which are much less vascularised and more slowly growing than 1411HP tumours. Various treatment schedules were tested. As shown in Figure S1 treatment with **6** resulted in tumour grow inhibition relative to controls. Although this has to be confirmed in a larger study it suggests that **6** has the potential to control CA-4-resistant tumours and exerts antitumour activity in part by direct tumour cell cytotoxicity.

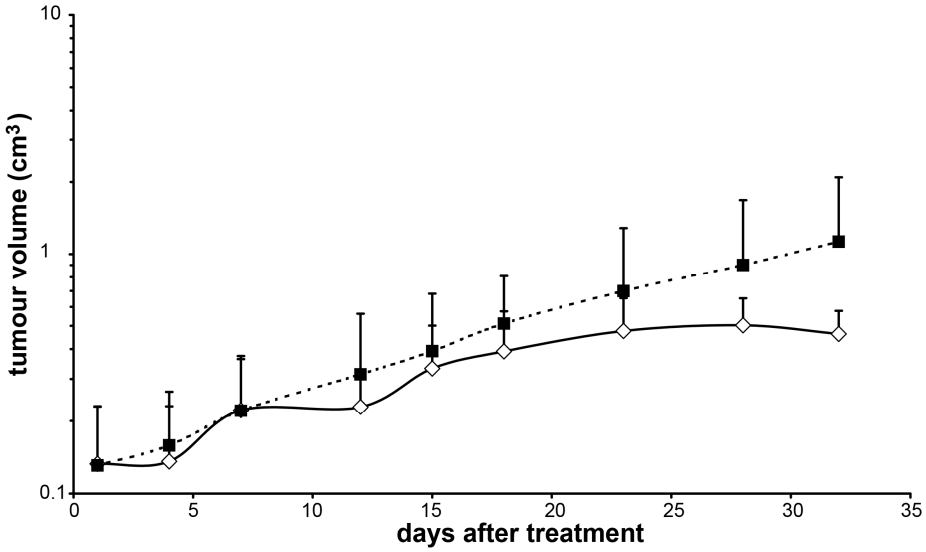

Fig. S1 Antitumour activity of **6** in CA-4-resistant HT-29 xenograft tumours. Shown are the mean tumour volumes of each group (n=3) ± standard deviation (treated: lozenges; control: black squares). Mice were treated as follows: single i.p. application of 20mg/kg body weight on day 1; dual i.p applications of 20 mg/kg on days 7/8; p.o. application of 40 mg/kg on day 23; single i.p. application of 30 mg/kg on day 28. Control group received normal saline. Tumour growth was followed until the first tumour in the control group reached the maximal tolerated tumour volume

Determination of apoptosis by flow cytometric TUNEL assays

Table S5 Flow cytometric analyses of apoptosis (%) in 518A2 melanoma cells visualised by the TUNEL technique. Cells were treated with various concentrations of Et-brimamin **6** for 48 h and stained by using transferase-mediated fluorescein-dUTP nick end labeling of 3'-OH ends of fragmented DNA

DNA fragmentation	control	50 nM Et-brimamin 6	100 nM Et-brimamin 6
vital cells (%)	95.9	76.0	60.0
apoptotic cells (%)	4.3	24.5	40.2

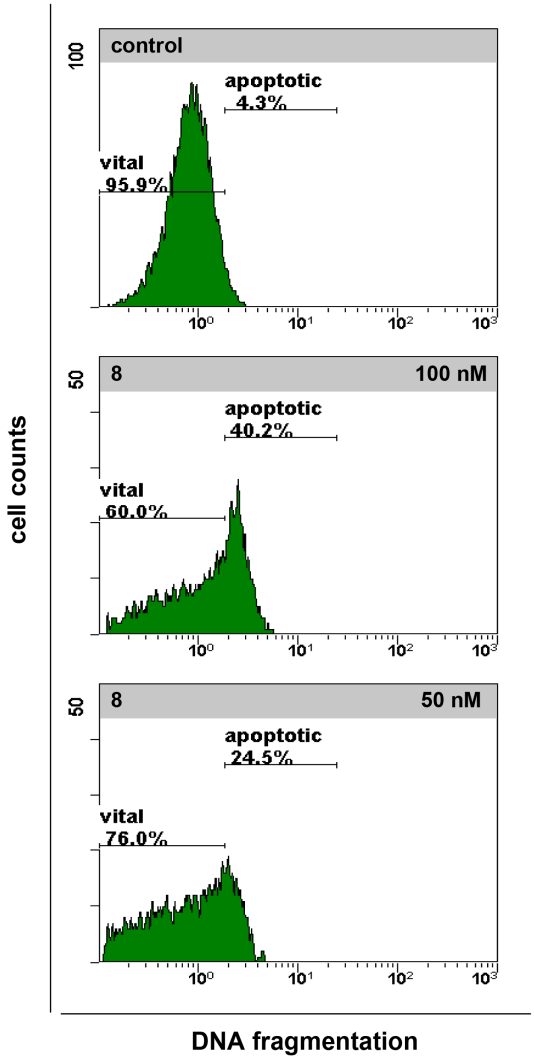

Fig. S2 Flow cytometric analyses of apoptosis (%) in 518A2 melanoma cells visualised by the TUNEL technique. Cells were treated with various concentrations of Et-brimamin **6** for 48 h and stained by using transferase-mediated fluorescein-dUTP nick end labeling of 3'-OH ends of fragmented DNA

Quantification of invasive cells in antimetastatic assays

Table S6 518A2 melanoma cells migrated through a confluent endothelial cell monolayer grown on the underside of cell culture inserts (trans-endothelium migration assay) when exposed to vehicle or Et-brimamin **6** for 48 h. Percentage of invasive cells (%) derived from measuring of the CM-DiI fluorescence of pre-stained 518A2 cells (invasive cells) or the total cell number derived from measuring of the intracellular calcein fluorescence as well as the overall invasion (invasive /total cells). Data presented as mean ± SD obtained from two independent experiments

stained cells (%)	control	10 nM Et-brimamin 6	50 nM Et-brimamin 6
invasive cells	100 ± 5.9	65.5 ± 4.9	48.8 ± 5.0
total cell number	100 ± 8.0	89.9 ± 2.8	70.2 ± 8.4
invasive/total cells	100 ± 2.9	73.0 ± 2.5	69.5 ± 4.1

References

S1 Wang L, Woods KW, Li Q, et al. (2002) Potent, Orally Active Heterocycle-Based Combretastatin A-4 Analogues: Synthesis, Structure−Activity Relationship, Pharmacokinetics, and In Vivo Antitumour Activity Evaluation. J Med Chem 45:1697–1711. doi: 10.1021/jm010523x

S2 Schobert R, Biersack B, Dietrich A, et al. (2010) 4-(3-Halo/amino-4,5-dimethoxyphenyl)-5-aryloxazoles and - *N* -methylimidazoles That Are Cytotoxic against Combretastatin A Resistant Tumour Cells and Vascular Disrupting in a Cisplatin Resistant Germ Cell Tumour Model. J Med Chem 53:6595–6602. doi: 10.1021/jm100345r

S3 Biersack B, Muthukumar Y, Schobert R, Sasse F (2011) Cytotoxic and antivascular 1-methyl-4-(3-fluoro-4-methoxyphenyl)-5-(halophenyl)-imidazoles. Bioorg Med Chem Lett 21:6270–6273. doi: 10.1016/j.bmcl.2011.09.005

S4 Berridge MV, Tan AS, McCoy KD, Wang R (1996) The biochemical and cellular basis of cell proliferation assays that use tetrazolium salts. Biochemica 4:15–19.

MANUSKRIPT IV

Contribution of JNK signaling and NF-kappaB activity to the anticancer effects of the vascular-disrupting agent Brimamin.

Katharina Mahal,[a] Aaamir Ahmad,[b] Marcus Resch,[c] Ralf Ficner,[c] Fazlul H. Sarkar,[b] Rainer Schobert,[a] Bernhard Biersack,*[a]

[a] *Organic Chemistry Laboratory, University of Bayreuth, Universitätsstraße 30, 95440 Bayreuth (Germany)*

[b] *Wayne State University School of Medicine and Karmanos Cancer Institute, Detroit, Michigan (USA)*

[c] *Department of Molecular Structural Biology, Georg August University Göttingen, Justus-von-Liebig-Weg 11, 37077 Göttingen (Germany)*

* email: bernhard.biersack@uni-bayreuth.de

to be submitted

Contribution of JNK signaling and NF-κB activity to the anticancer effects of the vascular-disrupting agent brimamin

Katharina Mahal, Aamir Ahmad, Marcus Resch, Ralf Ficner, Fazlul H. Sarkar, Rainer Schobert, Bernhard Biersack

Affiliations and addresses of authors:

Katharina Mahal, Bernhard Biersack, Rainer Schobert
Organic Chemistry Laboratory, University Bayreuth, Universitaetsstrasse 30, 95440 Bayreuth, Germany

A. Ahmad, F. H. Sarkar
Karmanos Cancer Institute, Department of Pathology, Wayne State University School of Medicine, 4100 John R. Street, Detroit 48201, Michigan (USA)

M. Resch, R. Ficner
Department of Molecular Structural Biology, Georg-August-University Göttingen, Justus-von-Liebig-Weg 11, 37077 Göttingen (Germany)

Corresponding author:
Bernhard Biersack, Organic Chemistry Laboratory, University Bayreuth, Universitaetsstrasse 30, 95440 Bayreuth, Germany. Phone: +49(0)921 552673. Fax: +49(0)921 552671. E-mail: bernhard.biersack@yahoo.com

Abstract

The 4,5-diarylimidazole brimamin inhibits the polymerization of tubulin and causes a reorganization of F-actin in Ea.hy926 endothelial cells. It displays a vascular-disrupting effect which is dependent on functional Rho kinase and JNK. Inhibition of JNK attenuates the effect of brimamin and inhibits the induction of apoptosis. Docking studies identified specific interactions between brimamin and amino acid residues in the colchicine binding pocket of bovine tubulin. In addition, brimamin showed a distinct growth inhibitory and apoptosis inducing effect at low nanomolar concentrations in cells of NF-κB-dependent human BxPC-3 pancreas carcinoma and triple-negative MDA-MB-231 breast carcinoma. These effects originate from a suppression of NF-κB activation in a dose-dependent manner. Brimamin also reduced the growth rate of MDA-MB-231 tumor xenografts in nude mice. Residual tumor cells of so-treated xenografts expressed markedly less p65 subunit protein of NF-κB than untreated control cells.

Keywords: Combretastatin A-4; Brimamin; JNK; NF-kappaB; Vascular-disrupting agents;

Introduction

The vascular-disrupting agent (VDA) combretastatin A-4 (CA-4, Figure 1) was first isolated from the bark of the South African Cape Bushwillow (*Combretum caffrum*) [1]. Fosbretabulin (CA-4P), its water-soluble phosphate prodrug selectively destroyed tumoral vasculature in clinical trials [2]. A major drawback of CA-4 is its insufficient in vivo cytotoxicity which necessitates combination regimens with other drugs. In a phase 1b trial combinations of fosbretabulin with cytotoxic agents such as carboplatin or paclitaxel were well tolerated and efficacious in heavily pretreated patients with advanced cancer [3]. Treatment with CA-4 alone often left residual conglomerates of peripheral cancer cells which quickly revascularized and thus led to a relapse of the disease [4]. The related natural catechol combretastatin A-1 and its bisphosphate (OXi4503) are also potent VDA [5] with which even complete tumor regressions could be achieved. They are more cytotoxic than CA-4 owing to the possibility of catechol redox-cycling and generation of toxic reactive oxygen species and alkylating quinoid intermediates [5,6]. Chemically stable derivatives of CA-4, which tends to isomerize to a biologically inactive *E*-alkene [7–9], were obtained by incorporation of the *Z*-alkene in heterocycles such as imidazoles, oxazoles, isoxazolines, pyridines or triazoles [4]. For instance, Wang et al. disclosed an *N*-methylimidazole-bridged derivative which retained the tubulin affinity of the parent combretastatins while showing improved water solubility and pharmacokinetics [9]. However, it is inferior to CA-4 with respect to cytotoxicity. We recently reported the preparation of brimamin (Scheme 1), an imidazole derivative bearing a 3-bromo-4,5-dimethoxyphenyl A-ring. It inhibited the growth of various tumor cell lines including combretastatin-resistant HT-29 colon cancer at distinctly lower IC_{50} concentrations than Wang's 3,4,5-trimethoxyphenyl analog [10]. Brimamin gave rise to extensive regressions in experiments with mice bearing xenografts of the highly vascularized cisplatin-resistant 1411HP testicular germ cell tumors while being well tolerated by the animals even at high doses [10]. However, the mechanism of action of brimamin was largely unknown, so far.

What was known is that the blebbing of endothelial cells induced by CA-4P depends on Rho signaling which leads to a reorganization of the actin cytoskeleton [11]. The survival of drug resistant breast and pancreas cancer cells, frequently observed after treatment with combretastatins, is often promoted by activated NF-κB, a crucial nuclear factor involved in inflammation and immunomodulation processes [12–14]. There is a connection between Rho signaling and NF-κB [15–17], and also evidence that microtubules are required for the translocation of NF-κB into the nucleus [18]. On the other hand, tubulin polymerization inhibitors such as vinblastine can activate NF-κB in epithelial cells [19]. Gemcitabine,

clinically applied against pancreas cancer, induced activation of NF-κB in BxPC-3 pancreas cancer cells, which might be a reason for the poor response of some patients [14]. The present study sheds some light on the mode of action of brimamin as opposed to that of the lead CA-4. We report on its interaction with tubulin, its dependency on various protein kinases (including Rho kinase, PI3K, ERK1/2, p38, and JNK), its influence on endothelial cells, and its efficacy against NF-κB-dependent human pancreatic and triple-negative breast carcinoma *in vitro* and *in vivo*.

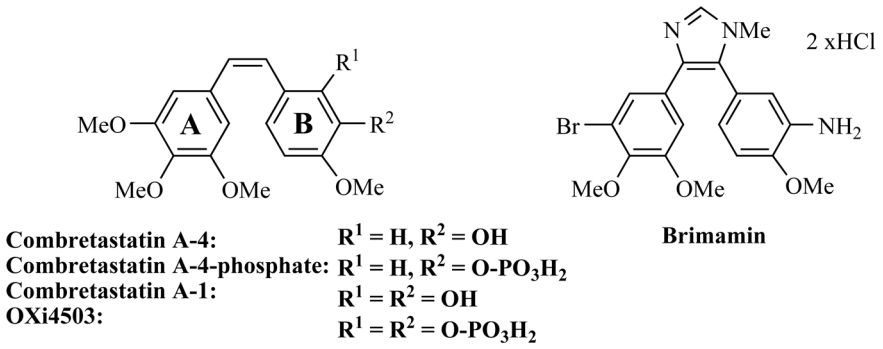

Fig. 1 Structures of the vascular-disrupting combretastatins A-4 (CA-4) and A-1 (CA-1), their phosphate pro-drugs CA-4P and OXi4503, and of brimamin

Materials and Methods

Compounds and reagents

Brimamin (*N*-methyl-4-(3-bromo-4,5-dimethoxyphenyl)-5-(3-amino-4-methoxy-phenyl)-imidazole) was prepared according to literature [10]. The kinase inhibitors HA-1077 (1-(5-isoquinolinesulfonyl)homopiperazine dihydrochloride salt), LY294002 (2-(4-morpholino)-8-phenyl-4*H*-1-benzopyran-4-one), PD98059 (2-amino-3-methoxyflavone), SB202190 (4-(4-fluorophenyl)-2-(4-hydroxyphenyl)-5-(4-pyridyl)-1*H*-imidazole), and SP600125 (anthra(1,9-*cd*)pyrazol-6(2*H*)-one) were purchased from LC Laboratories (Woburn, MA) and used without further purification. Combretastatin A-4 was obtained from Sigma-Aldrich.

Docking Calculations

Coordinate files of the ligand structures were generated using the GlycoBioChem PRODRG2 Server (http://davapc1.bioch.dundee.ac.uk/prodrg/submit.html) [20]. Molecular docking calculations were carried out with the Autodock Vina software [21]. Gasteiger partial charges [22] were calculated on ligand atoms using Autodock Tools. The X-ray structure of the tubulin-colchicine complex (PDB accession code: 1SA0) was downloaded from the Protein Data Bank (http://www.rcsb.org) and later used for docking. As for the ligand, polar hydrogen atoms were added to the protein and Gasteiger partial charges were calculated using Autodock Tools. Water molecules, heteroatoms and ligands were removed from the structure prior to docking calculations. Simulation boxes were centered on the originally crystallized ligand colchicine. Residues Lys254, Lys352, Asn101, Val318 and Ile378 were treated as flexible residues. A 18×22×20 Å simulation box was used in the docking calculations, applying an exhaustiveness option of 20 (average accuracy). For comparison reasons, the docking was also performed for colchicine. Since the standard error of Autodock Vina is 2.85 kcal mol^{-1} [21] binding affinities cannot be predicted quantitatively. This problem is not limited to Vina software [23]. Figures were prepared with the program PYMOL [24].

Cell lines and culture conditions

BxPC-3 cells and MDA-MB-231 cells were purchased from the American Type Culture Collection (Manassas, VA) and maintained in DMEM (Dulbecco's Modified Eagle Medium; Life technologies, Carlsbad, CA) supplemented with 10% FBS, 100 U/mL of penicillin and 100 µg/mL of streptomycin in a 5% CO_2 atmosphere at 37 °C. The endothelial hybrid cell line Ea.hy926 (ATCC no. CRL-2922), derived from HUVEC (human umbilical vein endothelial cells), was a gift from the Institute of Physiology, Charité Berlin, Germany. It was cultured in DMEM containing 10% FBS, 100 U/mL penicillin G, 100 µg/mL streptomycin, 0.25 µg/mL amphothericin B and 200 µg/mL gentamycine (all from Life Technologies).

Fluorescent staining of microtubules and microfilaments [25]

Ea.hy926 endothelial cells (100,000 cells/well) were grown on glass coverslips in 24-well plates for 24 h. HA-1077 (10 µM) or SP600125 (20 µM) was added 2 h before incubation with 100 nM brimamin for additional 12 h. Cells were then fixed in 4% formaldehyde in PBS (20 min, rt) and permeabilized (1% BSA, 0.1% Triton X-100 in PBS, 30 min, rt). For microtubule staining coverslips were incubated with a primary antibody against alpha-tubulin (anti-alpha-tubulin, mouse mAb, Invitrogen; 5 µg/mL, 1 h at 37 °C in humidified atmosphere)

followed by incubation with the secondary antibody conjugated to DyLight 550 dye (goat anti-mouse IgG-DyLight 550 conjugate, Pierce/Thermo Scientific; 2.5 µg/mL) for 1 h at rt in the dark. For visualization of filamentous actin (F-actin) fixed and permeabilized cells were incubated with AlexaFluor 488-conjugated phalloidin (Cell Signaling Technologies; 1 h at 37 °C in humidified atmosphere). All coverslips were mounted in Mowiol 4-88-based mounting medium containing 2.5% (w/v) DABCO and 1 µg/mL DAPI (4',6-diamidino-2-phenylindole; all from Carl Roth) for counterstaining the nuclei. Fluorescence microscopic analysis was performed using an Axio Imager.A1 fluorescence microscope (40-fold magnification, ZEISS).

Tube formation assay with Ea.hy926 endothelial cells [26]

Glass coverslips (12 mm diameter) were coated with 10 µL of pure Matrigel™ basement membrane matrix (BD Biosciences; gelation for 30 min in a humidified atmosphere at 37 °C) and placed into 24-well plates. Ea.hy926 endothelial cells were then seeded (100,000 cells/well in serum-free DMEM) on the resulting thin Matrigel layers where they usually start to differentiate into blood-vessel precursor-like networks through growth factor stimulation within the next 12 h. Rho kinase inhibitor HA-1077 (10 µM), PI3K inhibitor LY294002 (10 µM) or MAPK inhibitors SP600125 (JNK inhibitor, 20 µM) or PD98059 (ERK1/2 inhibitor, 10 µM) were added for 2 h followed by replacing the cell culture medium with fresh DMEM containing final concentrations of 50 nM CA-4 or 100 nM brimamin. The endothelial cells were then incubated for additional 24 h at 37 °C and the effect of the compounds on the tube formation process was documented by microscopy (100-fold magnification, Axiovert 135, ZEISS).

Determination of tumor and endothelial cell growth (MTT assay)

BxPC-3 cells (3,000 cells/well) and MDA-MB-231 cells (3,000 cells/well) were seeded and cultured in 96-well microplates. After overnight incubation the medium was removed and replaced with a fresh medium containing DMSO (vehicle control) or different concentrations of brimamin diluted from a 10 mM stock. After 72 h of incubation, 25 µL of 3-(4,5-dimethylthiazol-2-yl)-2,5-diphenyltetrazolium bromide (MTT) solution (0.5 mg/mL in PBS) were added to each well to a final concentration of 0.05 mg/mL and incubated for a further 2 h at 37 °C. The supernatant was aspirated and the formazan, formed by metabolically viable cells, was dissolved by adding isopropanol (100 µl). The plates were agitated on a gyratory

shaker for 30 min and the absorbance was measured at 595 nm on an Ultra Multifunctional Microplate Reader (TECAN, Durham, NC). Each experiment had eight replicate wells and the amount of DMSO in the reaction mixture never exceeded 1%. The Ea.hy926 endothelial cells were cultured and treated identically with minor alterations. Briefly, Ea.h926 cells (10,000 cells/well) were cultured in 96-well microplates for 24 h and pre-treated with non-toxic concentrations of commercially available kinase inhibitors for 2 h (10 µM of Rho-associated kinase (Rho kinase) inhibitor HA-1077 [11]; 10 µM of phosphatidylinositol 3-kinase (PI3K) inhibitor LY294002; 5 µM of extracellular-signal regulated kinase (ERK) inhibitor PD98059 [11]; 10 µM of p38 mitogen-activated protein kinase (p38-MAPK) inhibitor SB202190 [11]; 20 µM of c-Jun-N-terminal-kinase (JNK) inhibitor SP600125 [27]. Cells were then treated with combretastatin A-4 (CA-4, 10 nM) or brimamin (50 or 100 nM) for additional 48 h before adding MTT solution to each well to reach a final concentration of 0.05 mg/mL. After 2 h incubation, cell lysis and dissolution of the formazan was achieved by adding 30 µL of an SDS-DMSO solution (10% SDS, 0.6% acetic acid in DMSO) and the formazan absorbance was measured at 570 nm and 630 nm (background) with a microplate reader (TECAN). Cell viability was calculated from the resulting absorbance values with respect to DMSO controls set to 100%.

Flow cytometric analysis of apoptosis

For the quantification of early apoptosis Ea.hy926 cells grown on 6-well plates (200,000 cells/well) were treated with DMSO (control), brimamin alone (50 nM, 24 h) or combinations of brimamin (50 nM) and various kinase inhibitors (10 µM HA-1077, 10 µM LY294002, 5 µM PD98059, 10 µM SB202190, 20 µMSP600125; 2 h pre-treatment each) and prepared for flow cytometric cell cycle analyses after propidium iodide (PI) staining of the cellular DNA content [28]. Briefly, cells were harvested by trypsination, fixed (70% EtOH, 1 h, 4 °C) and washed in PBS followed by incubation with propidium iodide (PI; Carl Roth) staining solution (50 µg/mL PI, 0.1% sodium citrate, 50 µg/mL RNase A in PBS) for 30 min at 37 °C. The fluorescence intensity of 10,000 single cells (570 nm emission wavelength, excitation by a 488 nm laser source) was recorded by a Beckman Coulter Cytomics FC500 flow cytometer and analyzed by CXP software (Beckman Coulter). The percentage of apoptotic cells was determined by measuring the fraction of nuclei with a sub-diploid (sub-G1) DNA content. Sub-G1 events of DMSO treated controls and controls with kinase inhibitor treatment (< 15%), respectively, were subtracted from that observed for

brimamin treated cells.

Western blot analysis of NF-κB

For the detection of cellular NF-κB levels in endothelial cells, Ea.hy926 cells grown in 24-well plates (50,000 cells/well) were treated with CA-4 (10 nM, 50 nM) or brimamin (50 nM, 100 nM) for 1 h or 24 h and harvested by trypsination. Cell lysates and nuclear protein fractions were prepared as previously described [13,29]. In brief, cells were lysed in cell lysis buffer (20 mM Tris-HCl, 1 mM $MgCl_2$, 2 mM EGTA, 0.5% Triton X-100, pH 6.8) supplemented with protease inhibitor solution (protease inhibitor cocktail III, Calbiochem) for 10 min on ice followed by centrifugation (800 g, 5 min, 4 °C) to obtain total cell lysates. For the preparation of cell nuclei, cell membranes were lysed in mild nuclear extraction buffer (20 mM HEPES-KOH, 10 mM KCl, 0.1 mM EDTA, 0.1 mM EGTA, 1.5 mM $MgCl_2$, 1 mM DTT, pH 7.4) supplemented with protease inhibitor solution for 20 min on ice. After addition of Triton X-100 to a final concentration of 0.1% (2 min on ice) and centrifugation (3,000 g, 2 min), pelleted nuclei were lysed in 30 µL nuclear extraction buffer with 10% glycerol and 0.1% SDS. For Western blot analyses of NF-κB levels *in vivo*, cells of xenograft tissue samples were lysed in RIPA buffer (20 mM Tris-HCl, 137 mM NaCl, 1% NP-40, 2 mM EDTA, 0.5% sodium deoxycholate and 0.1% SDS) containing complete mini EDTA-free protease inhibitor cocktail (Roche, Indianapolis, IN). The total protein concentration of each sample was measured by a BCA Protein Assay (Pierce, Rockford, IL). 10 µg of total protein were separated with 12% SDS-polyacrylamide gel electrophoresis (SDS-PAGE) and transferred to nitrocellulose or PVDF membranes. Primary antibodies (anti-p65 monoclonal antibody, rabbit, Cell Signaling Technology; anti-beta-actin monoclonal antibody, mouse, Sigma Aldrich as a loading control) were added in appropriate concentrations followed by incubation with HRP-conjugated secondary antibodies. Bands were then visualized and documented by chemiluminescence.

Histone/DNA ELISA for the detection of apoptosis

The Cell Death Detection Kit (Roche, Palo Alto, CA) was used to detect apoptosis in BxPC-3 and MDA-MB-231 cells according to manufacturer's instructions [13]. Briefly, cells were treated with test compounds for 72 h. After harvesting cells by trypsination, cell lysates were prepared and separated into pellet and supernatant fractions by centrifugation (20,000 g, 10 min, rt). The supernatants represent the cytoplasmic fraction containing histone-associated

DNA fragments (nucleosomes) that were detected by a subsequent ELISA procedure. Absorbance of the amount of peroxidase-converted ABTS (2,2'-azino-bis(3-ethylbenzthiazoline-6-sulphonic acid)) reaction product was determined with an Ultra Multifunctional Microplate Reader (TECAN) at 405 nm.

Electrophoretic mobility shift assay for detection of NF-κB activation

To evaluate the effect of brimamin on the DNA-binding ability of nuclear NF-κB in BxPC-3 and MDA-MB-231 cells, they were treated either with vehicle or brimamin (10-400 nM) for 72 h. Nuclear cell lysates were prepared (see 2.8) and the electrophoretic mobility shift assay (EMSA) was performed by incubation of 8 µg nuclear protein extract with IRDye-700-labeled oligonucleotides containing the NF-κB binding sequence (LI-COR, Lincoln, NE) and 2 µg of poly desoxyinosinic-desoxycytidylic acid (poly dI-dC, background reduction) oligos as described earlier [13,29]. DNA-protein complexes formed during incubation were separated from free oligonucleotides by 8% native polyacrylamide gel electrophoresis. The gel was scanned using the Odyssey Infrared Imaging System (LI-COR, Inc.) and detected bands were analyzed by densitometry with the ImageJ software. Equal protein loading was ensured by immunoblotting of 10 µg of nuclear protein and probing with an anti-retinoblastoma (Rb) antibody (Santa Cruz Biotechnology, Santa Cruz, CA).

***In vivo* studies**

Female homozygous ICR SCID mice, aged 4 weeks, were used. The animal experimental protocol was approved by the Committee on the Ethics of Animal Experiments of Wayne State University Institutional Users of Animal Care Committee. To initiate the xenografts, 5×10^6 MDA-MB-231 cells (in serum-free medium) were injected s.c. bilaterally in the flank areas of SCID mice. The animals were examined thrice per week until they developed palpable tumors. Then the animals were randomly divided into two groups of 6 animals each. Group I was assigned as control and received only sesame seed oil without brimamin while group II mice were administered brimamin. Once the tumors were detectable brimamin treatment was started. It was administered i.p. at a dose of 20 mg/kg, about once a week. More precisely, brimamin was administered on day 1, day 9, day 14, day 20, and day 27. On day 30 the tumors in the control group weighed almost 2 g on average and thus all animals were sacrificed. The volumes of the tumors in either group were determined with the calliper every four days according to the formula $ab^2/2$, wherein ‘a’ is the length and ‘b’ the cross-

sectional diameter [Ahmad et al., 2013]. Tumors were harvested from each animal and processed for molecular analysis.

Data analysis and statistical analysis

The experimental results presented in the figures are representative of three or more independent observations. The data are presented as the mean values ± SD. Statistical comparisons between the groups were done using one-way ANOVA. Values of $p < 0.05$ were considered to be statistically significant and individual *p*-values are reported in the figures, as appropriate. ImageJ software was used for densitometric analyses of original pictures.

Results

Docking studies of the brimamin-tubulin interaction

The anticancer and vascular-disrupting effects of brimamin are likely related to its inhibition of the polymerization of tubulin which we reported previously [10]. For a deeper insight into its molecular interaction with tubulin we performed docking studies. The crystal structure geometry of dimeric bovine tubulin (PDB accession code 1SA0, 100% sequence identity to human tubulin) with ligated colchicine and Mg^{2+}-complexed GDP and GTP was used as a starting point for docking brimamin in place of colchicine [30]. These studies performed with the Autodock Vina software predicted brimamin to bind in an orientation analogous to colchicine with the A-ring proximal to Cys241 (Fig. 2a, colchicine not shown). Although pointing towards the SH-group of Cys241, the 5-methoxy oxygen of ring A is probably too far off to establish a stable hydrogen bond. In contrast, the nitrogen atom N-1 of the imidazole ring is ideally positioned for entering into a hydrogen bond with the backbone amide

hydrogen of Ala250. The NH_2 group of the second phenyl ring B then locks the ligand by acting as a H-bridge donor over to the backbone carbonyl oxygen of Thr179 (Fig. 2a). Unlike natural combretastatin analogs [31], the side chain ε-amino group of Lys352 points away from the B-ring and cannot establish any supporting interaction. An additional H-bond was calculated as plausible between the *p*-methoxy oxygen of ring B and the backbone amido NH of Val181 (Fig. 2a). This *p*-methoxy group is also entangled in a Van-der-Waals interaction with a methyl group of the same Val181. In a similar manner the methoxy groups of the A ring are involved in attractive Van-der-Waals interactions with their neighbouring amino acid residues. Due to the conserved pattern of methoxy substituents on ring A this hydrophobic interaction network is very similar for brimamin and colchicine (docking results not shown). As a result, the calculated energy for the binding of brimamin to tubulin is ca. 79% of that for colchicine (Tab. 1).

Table 1 Calculated energies for binding of brimamin and colchicine to tubulin

Ligand	**Binding energy [kcal mol^{-1}]**[a]
Brimamin	–7.1
Colchicine	–9.0

[a] Values were calculated by Autodock Vina.

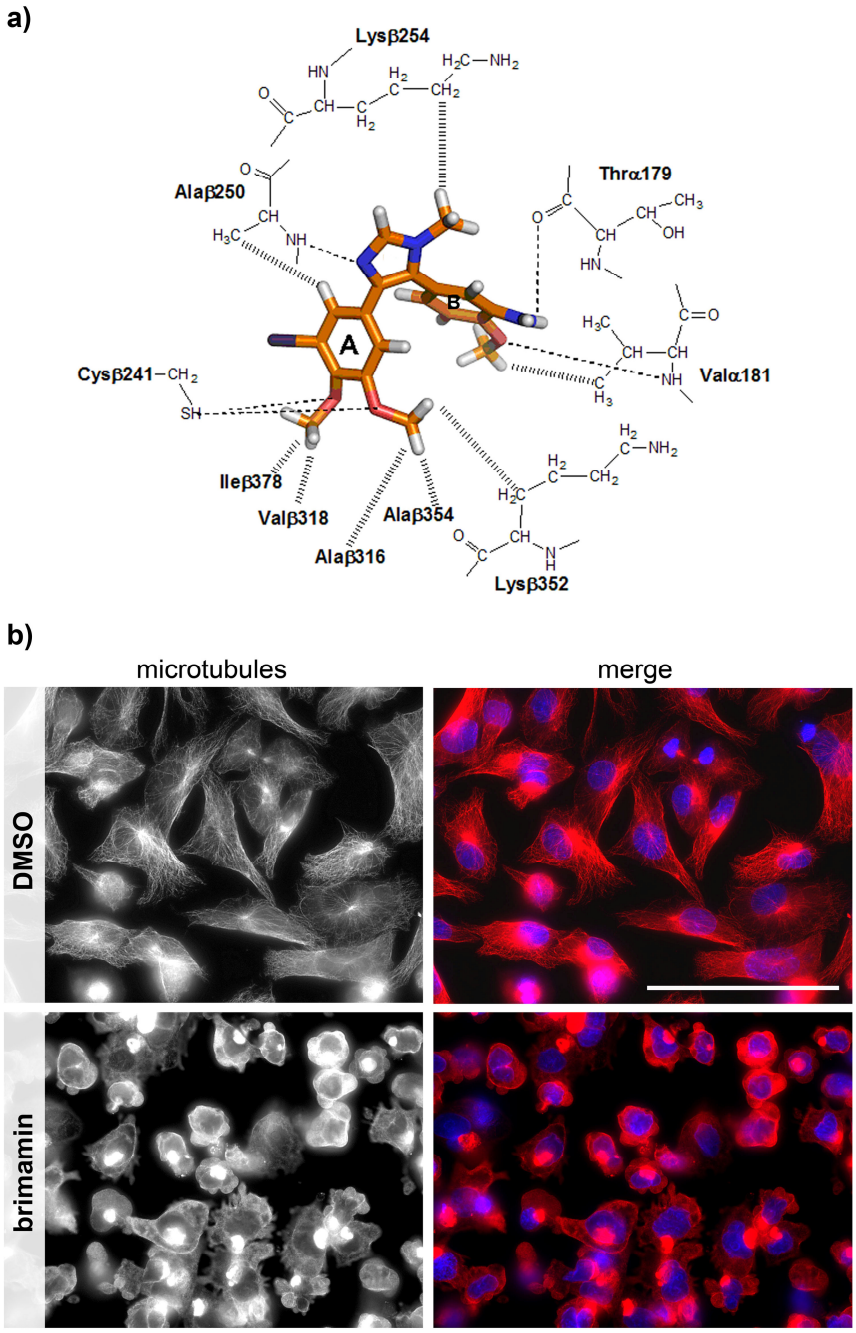

Fig. 2 Proposed binding mode of brimamin into the colchicine binding pocket within the beta-tubulin subunit (a). Schematic representations of hydrogen bonds and Van-der-Waals interactions of brimamin with bovine tubulin. Putative hydrogen bonding is indicated by dashed lines, Van-der-Waals interactions by hatched lines. Carbon is colored orange; hydrogen white; nitrogen blue; oxygen red; bromine purple. Immunostaining of microtubules in Ea.hy926 endothelial cells (b). Cells were treated with brimamin (100 nM) for 12 h. Microtubules were visualized by immunofluorescent staining of alpha-tubulin (red), nuclei were counterstained with DAPI (blue). Scale bar: 100 µm (400-fold magnification)

Effects of brimamin on the cytoskeletal organization in human endothelial cells

Next we focused on the cytoskeletal reorganization that occurs in endothelial cells upon brimamin treatment and which eventually leads to the observed disruption of tumoral vasculature. Since CA-4P is known to cause early membrane blebbing in endothelial cells [11], we also visualized the morphological changes of microtubules and actin filaments of endothelial Ea.hy926 cells treated with brimamin. Exposure to 100 nM concentrations of brimamin for 12 h led to an extensive disruption of the microtubular network followed by actin stress fiber formation (Fig. 2b, Fig. 3). This reorganization of the actin filaments in the wake of microtubule depolymerization could be prevented by pre-treating the cells with the Rho kinase inhibitor HA-1077 prior to the addition of brimamin (Fig. 3). Apparently, brimamin induces an actin cytoskeleton response through activation of RhoA and Rho kinase as has been shown for CA-4P [11,32].

The loss of microtubule and actin cytoskeleton integrity initiated by brimamin then translates into its macroscopically observable vascular-disruptive effect which can be studied at various stages of endothelial cell aggregation. In so-called tube formation assays Ea.hy926 endothelial cells were grown on matrigel and allowed to form tubular structures mimicking blood vessels. When treated with brimamin the individual cells showed an increased contractility and looser cell-cell-contacts, eventually leading to a breakup of the organized conduit system (Fig. 4).

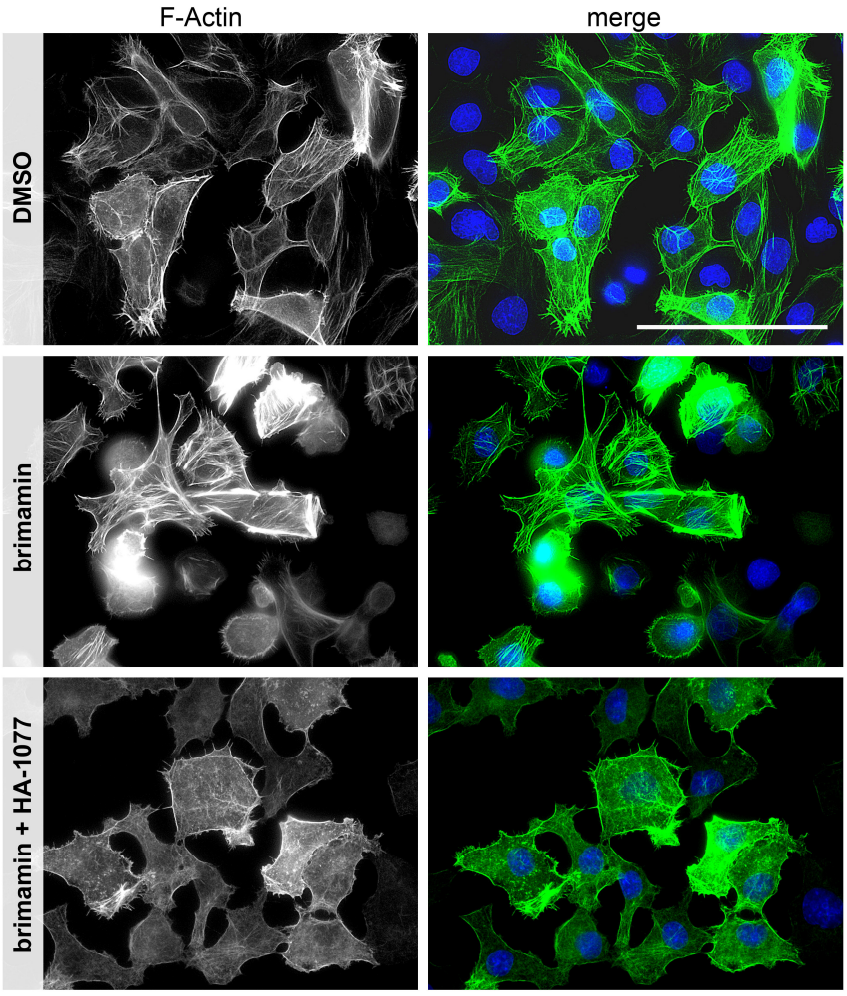

Fig. 3 Fluorescent staining of microfilaments in Ea.hy926 endothelial cells. Cells were treated either with brimamin alone (100 nM) or a combination of brimamin and Rho kinase inhibitor HA-1077 (10 µM) for 12 h. Filamentous actin (F-Actin) was visualized by staining with a fluorescent phalloidin conjugate (green), nuclei were counterstained with DAPI (blue). Scale bar: 100 µm (400-fold magnification)

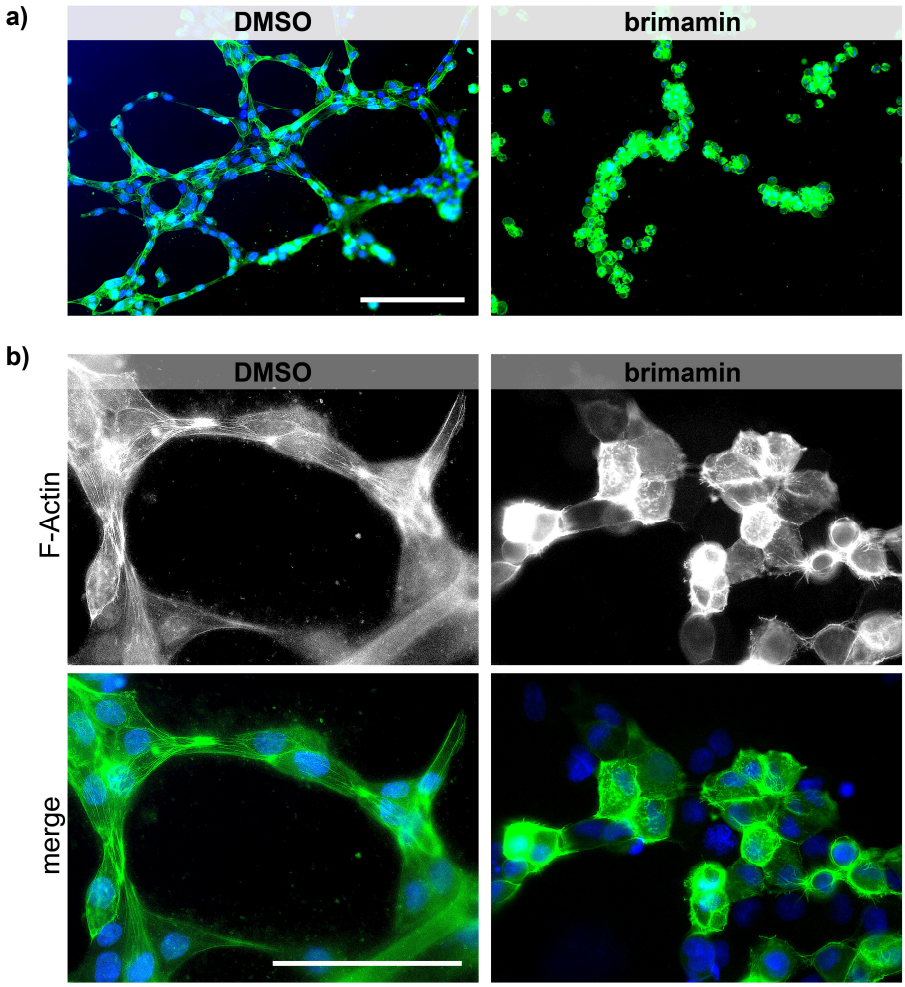

Fig. 4 Fluorescent tube formation assay with Ea.hy926 endothelial cells. Cells were grown on thin layers of matrigel basement membrane matrix (matrigel) for 12 h and then treated with vehicle (DMSO, left) or 100 nM brimamin (right) for additional 12 h followed by formaldehyde fixation and fluorescence staining of F-actin (phalloidin-AlexaFluor-488 conjugate). Nuclei were counterstained with DAPI (blue). a) Overlay of actin (green) and DNA (blue) staining in 100-fold magnification (scale bar: 200 µm). b) Fluorescent F-actin (gray) and overlay of F-actin with nuclear staining (merge) in 400-fold magnification (scale bar: 100 µm)

Contribution of protein kinase signaling to the cytotoxicity of brimamin against human endothelial cells

Certain protein kinase signaling pathways were reported to play a crucial role for the survival of endothelial cells as well as for endothelial cell differentiation into blood vessel precursors. We investigated the influence of the selective kinase inhibitors HA-1077 (Rho-associated kinase), LY294002 (PI3K), PD98059 (ERK1/2), SB202190 (p38 MAPK), and SP600125 (JNK1/2) on the cytotoxicity of brimamin against Ea.hy926 endothelial cells and on its ability

to induce apoptosis in these cells, in direct comparison with the lead CA-4.

In brief, MTT assays were performed by co-incubation of Ea.hy296 cells with non-toxic concentrations of individual kinase inhibitors and slightly toxic concentrations of either brimamin or CA-4. The addition of a phosphatidylinositol-3 kinase (PI3K) or extracellular-signal-regulated kinase (ERK) inhibitor (LY294002 or PD98059, respectively) strongly sensitized these endothelial cells for brimamin while the combination with either a Rho kinase or c-Jun-N-terminal kinase (JNK/SAPK) inhibitor (HA-1077 or SP600125, respectively) led to decreased cytotoxicity (Fig. 5a). The p38-MAPK inhibitor SB202190 did not influence the activity of brimamin. These results were counterchecked by the measurement of early apoptosis induction in endothelial cells after incubation with the respective inhibitors (Fig. 5b).

Treatment with brimamin alone (50 nM) led to a sub-diploid DNA content of about 15%. Co-incubation with the PI3K inhibitor LY294002 showed a slightly increased sub-G1 percentage, while incubation with the ERK inhibitor PD98059 strongly enhanced DNA fragmentation. This is consistent with the results obtained from the MTT assays. Since both PI3K and ERK are known to protect cells from triggering apoptosis as a consequence of the cellular stress response, inhibition of these two kinases might lead to an enhanced predisposition for microtubule disruption [33]. In contrast to the MTT results, addition of HA-1077 sensitized Ea.hy926 cells resulting in a doubling of apoptotic events. The attenuation of the growth inhibitory effect of brimamin by HA-1077, as observed in the MTT assays, might be a consequence of a retardation of the cell cycle progress by this kinase inhibitor. This explanation is supported by a slightly increased G1 phase percentage in cell cycle analyses run after 48 h (data not shown). At this early phase of brimamin treatment, Rho kinase inhibition might positively affect cell protecting signaling pathways. In the case of combination with the JNK inhibitor SP600125 we observed slightly decreased sub-G1 cell numbers consistent with the protective effect of SP600125 in the MTT assays. The activation of JNK by tubulin-binding agents such as vinblastine through prolonged G2-M arrest that eventually led to apoptosis via Bcl-2 multi-site phosphorylation had been reported previously [34]. We found that inhibition of JNK can induce microtubule stabilization to a degree that overrides the contrary effect of brimamin (data not shown). Inhibition of apoptosis induction via Bcl-2 degradation might be another effect that contributes to the reduced brimamin cytotoxicity. Nevertheless, active JNK signaling seems to be crucial for apoptosis induction after cellular sensing of cytoskeletal damages induced by brimamin.

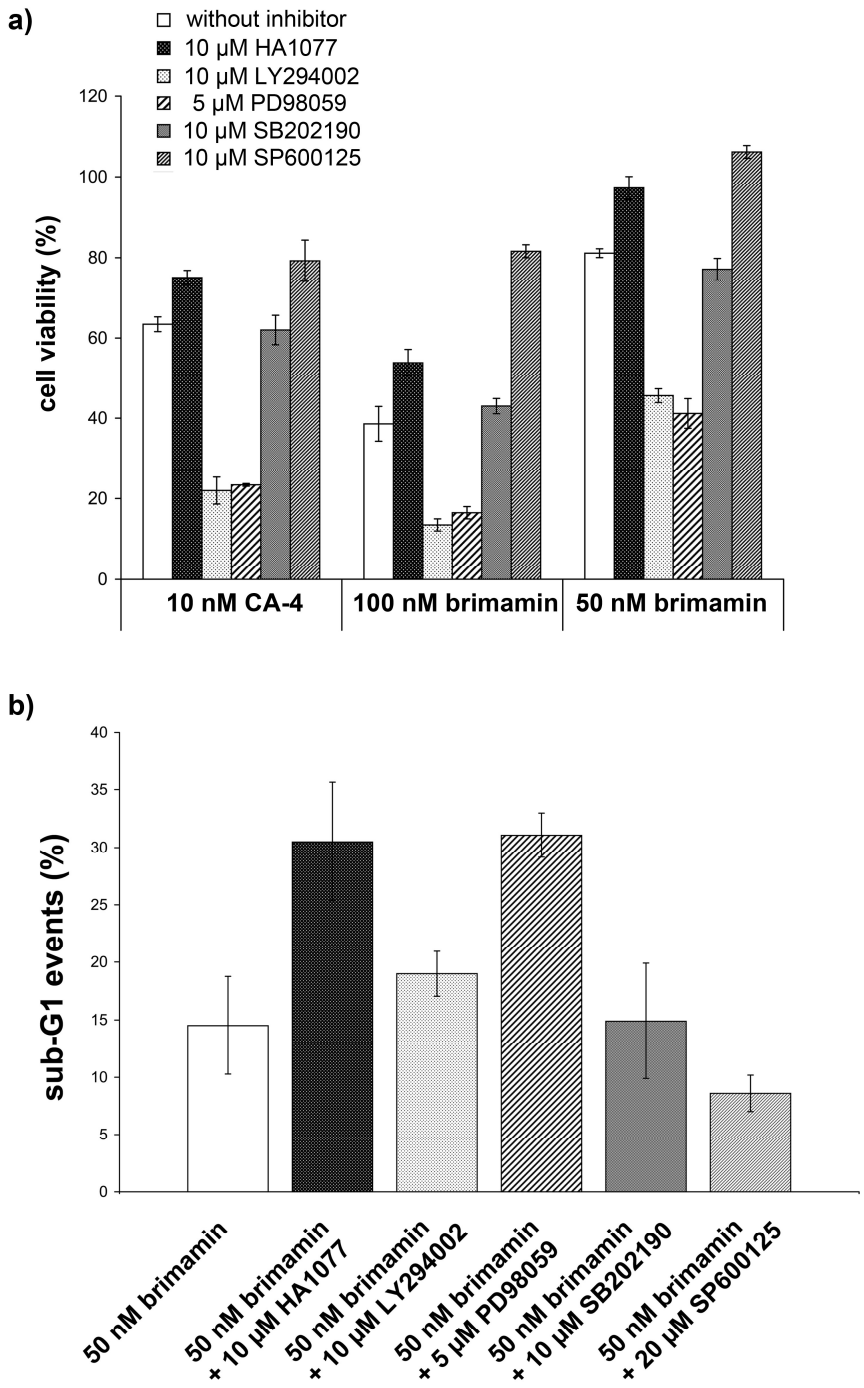

Fig. 5 Effects of known kinase inhibitors on the cell viability of Ea.hy926 endothelial cells treated with combretastatin A-4 (CA-4) or brimamin (a). Ea.hy926 cells were treated with CA-4 (10 nM) or brimamin (100 nM, 50 nM) for 48 h with or without pre-treatment with the kinase inhibitors HA-1077 (Rho-associated kinase), LY294002 (PI3K), PD98059 (ERK1/2), SB202190 (p38 MAPK) or SP600125 (JNK1/2). Cell viability (%) as obtained from three independent MTT assays, error bars represent the standard deviation. Effects of protein kinase inhibitors on the induction of apoptosis in Ea.hy926 endothelial cells by brimamin (b). Confluent Ea.hy926 cells were treated with brimamin for 24 h with or without pre-treatment with the kinase inhibitors HA-1077 (Rho-associated kinase), LY294002 (PI3K), PD98059 (ERK1/2), SB202190 (p38 MAPK) or SP600125 (JNK1/2). Induction of apoptosis was assessed from sub-G1 events (%) in flow cytometric cell cycle analyses. Results are the mean of two independent experiments in duplicate, error bars represent the standard deviation

Contribution of kinase signaling to the vascular-disruptive effects of brimamin

We applied the tube formation assay to further investigate the influence of various kinases on endothelial cell differentiation. Ea.hy926 cells when grown on thin matrigel layers form tubular networks due to growth factor stimulation and adhesion to the basement membrane matrix. Within these networks the individual cells undergo massive morphological changes (Fig. 2-4, Fig. 6). Brimamin, like the lead CA-4, induced cytoskeletal disorganization and morphological changes that impaired both maintenance and additional formation of the tubular branches. A similar picture was obtained when preformed tubular networks of Ea.hy926 cells were treated with a combination of brimamin or CA-4, respectively, and the Rho kinase inhibitor HA-1077. The latter did not help preserve the tubular network, at least not at the applied non-toxic concentrations (Fig. 6, middle row). However, Rho signaling and Rho-mediated actin stress fiber formation and the subsequent actin-myosin contractility were identified by other groups as crucial for the activity of a variety of other VDA [35]. In contrast, pre-incubation with the JNK inhibitor SP600125 led to a marked stabilization of cellular connections and a preservation of preformed tubes from disruption or increased cell contractility induced by brimamin or CA-4 (Fig. 6, bottom row).

Co-treatment with the ERK1/2 inhibitor PD98059 or the PI3K inhibitor LY294002 sensitized the Ea.hy926 cells for the vascular-disrupting effects of CA-4 or brimamin and led to a complete disintegration of any tubular aggregates. Taken together, kinase inhibitors that increase CA-4 or brimamin cytotoxicity in 2D culture also interfere with endothelial cell differentiation on membrane matrices. ERK and PI3K/Akt are known to promote pro-survival pathways and therefore might protect both proliferating and differentiating cells from apoptosis induced by microtubule damage. Rho- and JNK signaling, on the other hand, are crucial for both CA-4 and brimamin cytotoxicity and their vascular-disrupting activity. Table 2 summarizes the benefit and potential synergism of combinations of brimamin with selective kinase inhibitors.

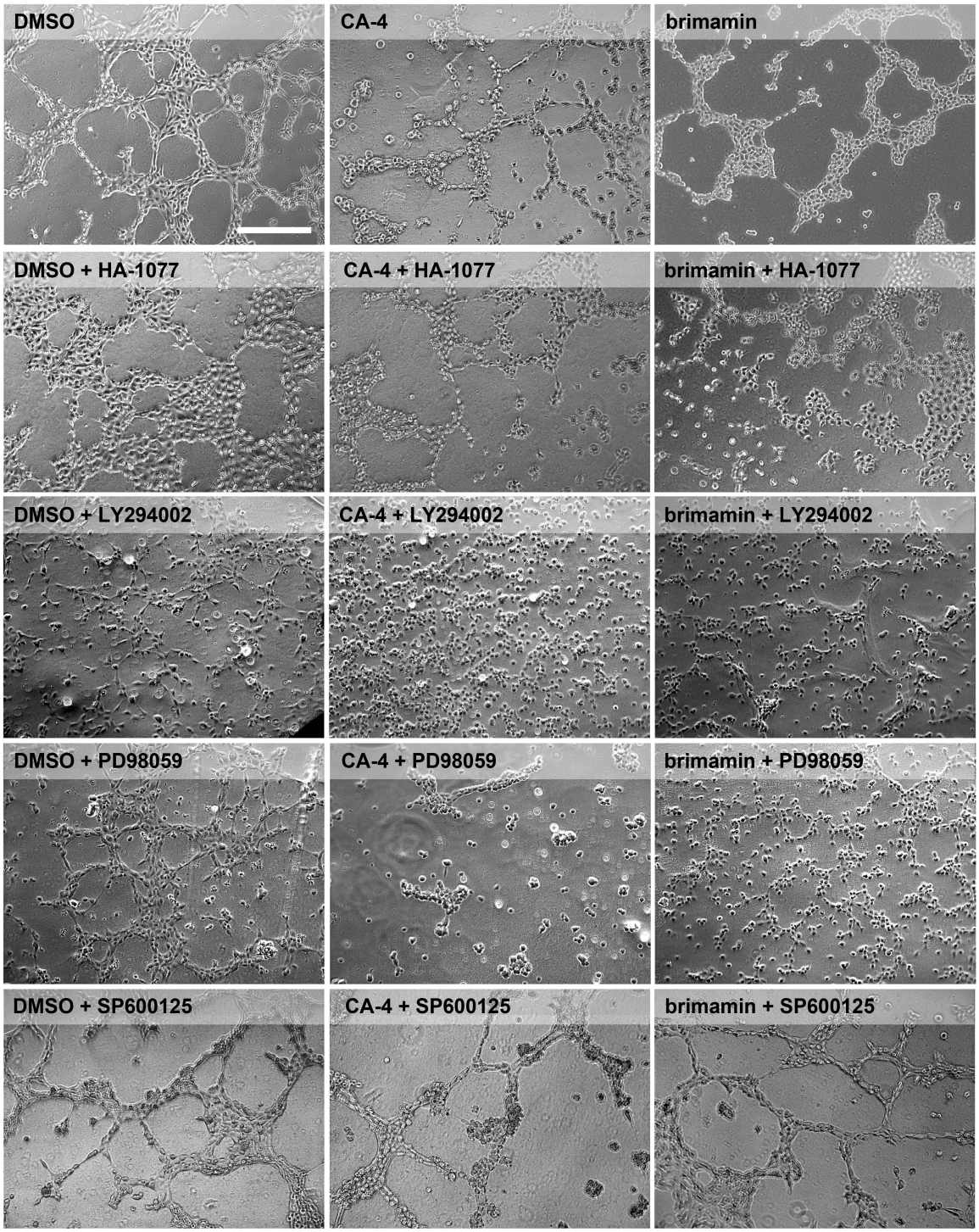

Fig. 6 Tube formation assay with Ea.hy926 endothelial cells. Cells were grown on thin layers of matrigel basement membrane matrix (matrigel) for 12 h and then treated with vehicle (DMSO), CA-4 (50 nM) or brimamin (100 nM) alone or in combination with 10 µM HA-1077, 10 µM LY294002, 5 µM PD98059 or 20 µM SP600125 for additional 12 h. Effects were monitored by light microscopy (100-fold magnification, scale bar: 200 µm)

Table 2 Contribution of kinase signalling to the cytotoxicity, apoptosis-inducing activity and vascular-disrupting activity of brimamin in endothelial cells *in vitro*. Synergistic (+) or antagonistic (-) effects when brimamin was combined with selective kinase inhibitors

		Synergistic effects by combination of kinase inhibitors with brimamin [a]		
Kinase	**VDA-relevant activity**	toxicity	apoptosis	vasc.-dis. activity
ROCK	Regulation of cell contractility via actin filament contraction, mediator of CA-4 secondary VDA effects[11,36,37]	-	+	-
PI3K	Key player in endothelial migration and reorganisation of actin cytoskeleton, induction of proliferation and survival-pathways[38–40]	+	+	+
ERK1/2	Mediator of survival pathways, protection against CA-4 induced membrane blebbing, down-regulated upon CA-4 treatment[11,33,41]	+	+	+
p38/MAPK	Contribution to CA-4 induced membrane blebbing, mediator of angiogenesis[11,42]	*n.o.*	*n.o.*	*n.d.*
JNK	Induction of apoptosis as a consequence of prolonged mitotic arrest, contribution to microtubule stability via stathmin phosphorylation[34,43,44]	-	-	-

[a] ROCK, PI3K, ERK1/2, p38/MAPK or JNK inhibition was achieved by co-treatment with the kinase inhibitors HA-1077, LY294002, PD98059, SB202190. *n.o.* not observed/no significant effects; *n.d.* not determined.

Inhibition of the nuclear translocation of NF-κB by brimamin

The dual role of NF-κB signaling in tumor progression and angiogenesis has been extensively discussed. Although the down-regulation of NF-κB in tumor cells *in vitro* and *in vivo* results in reduced gene expression of NF-κB-related, anti-apoptotic target genes and a better clinical outcome, its activation seemed to be essential for the activity of antiangiogenic agents [45,46]. NF-κB activation even has a negative effect on tumor angiogenesis and affects pro-apoptotic pathways in endothelial cells. Herein, we assessed the role of endothelial NF-κB signaling for the antivascular activity of brimamin. NF-κB activation was detected by its translocation from cytoplasmic NF-κB complexes into the nucleus where it acts as a transcription factor on various target genes. We found that short incubation (ca 1 h) with either CA-4 or brimamin led to slightly increased nuclear p65 levels in treated cells which is

in line with previous findings on HUVEC in literature [45,46] (Fig. 7a). However, after 24 h incubation the nuclear level of the NF-κB p65 subunit had dropped significantly. We suppose that this is a consequence of a progressing disruption of the microtubular cytoskeleton along which the translocation of proteins into the nuclei occurs. An effect on the total NF-κB levels and thus on its expression or degradation was not detected at any timepoint.

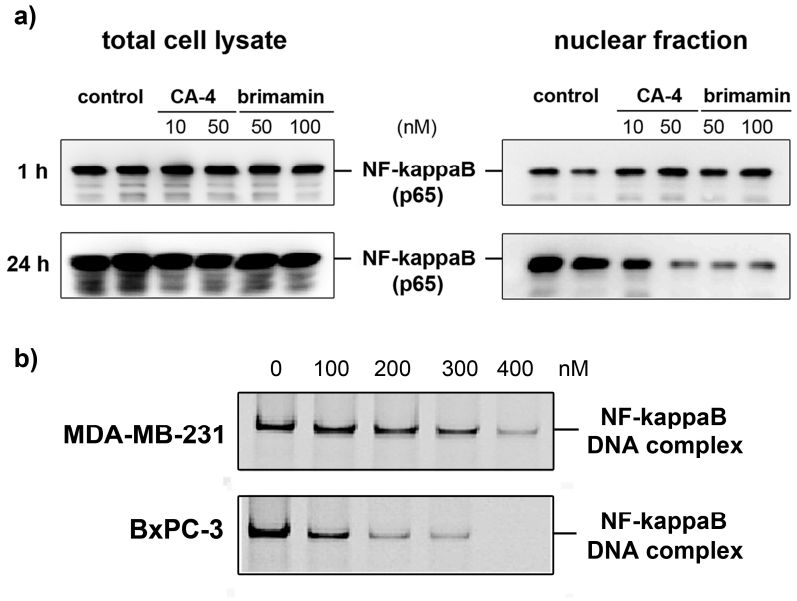

Fig. 7 Time-dependent nuclear NF-κB translocation in Ea.hy926 endothelial cells after treatment with CA-4 (10, 50 nM) or brimamin (50, 100 nM) for 1 or 24 h (a). NF-κB levels in total cell lysates or nuclear protein fractions of Ea.hy926 cells as visualized by immunoblotting for the NF-κB p65 subunit. NF-κB–DNA binding activity in nuclear protein extracts of MDA-MB-231 breast cancer or BxPC-3 pancreas carcinoma cells after treatment (72 h) with various concentrations of brimamin (b). Electrophoretic mobility shift assay (EMSA) for detection of nuclear NF-κB-DNA complexes as visualized by labeled oligonucleotide probes

Growth inhibition and apoptosis induction in pancreatic and breast cancer cells

In the light of a potential drugability of brimamin we evaluated its cytotoxicity against highly resistant cancer cell lines that depend on activated NF-κB signal transduction [38]. Brimamin was first tested by MTT assays and found highly active in BxPC-3 pancreatic cancer cells (IC_{50} = 25 ± 2 nM) and triple-negative MDA-MB-231 breast carcinoma cells (IC_{50} = 350 ± 19 nM) upon 72 h incubation. For comparison, the IC_{50} concentrations of CA-4 are 43 nM (MDA-MB-231) and 57 µM (BxPC-3) [47,48]. Next, the induction of apoptosis in BxPC-3

and MDA-MB-231 cancer cells by brimamin was evaluated by histone/DNA ELISA assays (Fig. S1, Electronic supplementary material) where it showed a strong effect at low nanomolar concentrations. Its magnitude correlated fairly well with the IC_{50} values obtained from the MTT tests.

NF-κB inactivation in pancreatic and triple-negative breast carcinoma

Brimamin significantly inhibited DNA-binding of the NF-κB transcription factor *in vitro* at nanomolar concentrations in cells of BxPC-3 pancreas carcinoma and MDA-MB-231 breast carcinoma (Fig. 7b). As a consequence, brimamin may eventually lead to a reduced activation of NF-κB-driven genes. Its impact on NF-κB was particularly strong in the BxPC-3 pancreas cancer cells which are known to respond to a treatment with the approved anticancer drug gemcitabine by an enhanced NF-κB activation [14]. Hence, a combination of brimamin with gemcitabine, which is clinically applied for pancreas cancer diseases, appears to be promising.

***In vivo* effects of brimamin on xenografts of triple-negative breast carcinoma and the NF-κB expression**

The anticancer activity of brimamin was also studied *in vivo* in an MDA-MB-231 breast cancer xenograft mouse model. When applied at doses of 20 mg/kg over a period of four weeks the compound was tolerated well and it also reduced the rate of the tumor growth significantly (Fig. 8a). Residual tumor cells of so-treated xenografts were processed further for the analysis of proteins by western blotting. This showed a down-regulation of the p65 subunit of NF-κB (Fig. 8b). These results support our *in vitro* observations described above, suggesting an effective inhibition of NF-κB signaling by brimamin which in turn is likely to be causative for the observed biological effects in the tested cancer cells.

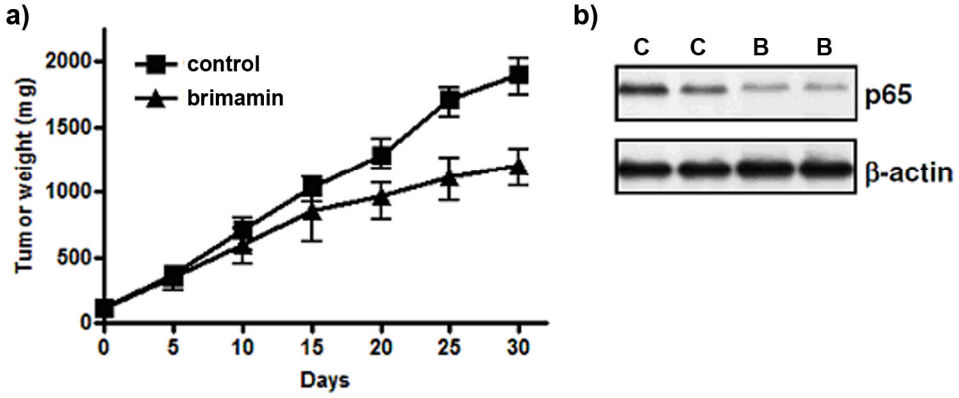

Fig. 8 Brimamin retards the growth of MDA-MB-231 tumor xenografts by inhibition of NF-κB expression. MDA-MB-231 cells were injected in SCID mice subcutaneously (bilaterally) and mice were randomized into two groups (6 mice each) – control and brimamin-treated. a) Progress of tumor weight upon application of brimamin on days 1, 9, 14, 20, and 27. b) Expression of NF-κB subunit p65 in tissue of two representative treated tumors each from control and treated mice. beta-actin: loading control, C: control, B: brimamin

Conclusions

Docking studies allowed the identification of the H-bonds and Van-der-Waals interactions by which the new VDA brimamin is anchored to amino acid residues in the colchicine-binding site of tubulin. Although these interactions differ from those of combretastatins, treatment of endothelial cells with brimamin led to microtubule disruption. The ensuing formation of actin stress fibers was shown to be dependent on Rho kinase activation. It results in early membrane blebbing as it is known for the lead CA-4 [11]. This extensive cytoskeletal reorganization is also responsible for the observed vascular-disrupting effect of brimamin. In vitro tube formation by endothelial cells was strongly impaired upon brimamin treatment as a consequence of both the cell retraction caused by dense and contractile actin stress fibers and the loss of the integrity of the microtubule cytoskeleton.

On closer inspection of the molecular mechanism we could confirm that functional JNK is involved in the cytotoxic as well as the vacular-disrupting effects of CA-4 and brimamin, in keeping with reports on the JNK dependence of other tubulin-binding agents [34,49,50]. When we added low concentrations of the JNK inhibitor SP600125 to Ea.hy926 endothelial cells in the presence of brimamin we saw a stabilization of the microtubules, or in other words, an attenuation of the vascular-disrupting effect of brimamin. We presume that the inhibitor interferes with the regulatory function of JNK in stathmin phosphorylation which is

a key event in interphase microtubule stabilization [51–53]. JNK seems to play another crucial role for the effect of tubulin binders. There is evidence that sustained JNK activation by prolonged G2-M cell cycle arrest, as initiated by drugs such as vinblastine, is associated with pro-apoptotic Bcl-2 multi-site phosphorylation that eventually results in the induction of apoptosis [34,43]. In our experiments with endothelial cells, co-treatment with SP600125 led to reduced brimamin cytotoxicity. We therefore conclude that active JNK is involved in apoptosis induction and thus is also essential for the anticancer effects of both CA-4 and brimamin. Although SP600125 re-sensitized doxorubicin-resistant cancer cells for chemotherapy [54], a therapeutic combination of this JNK inhibitor with vascular disrupting agents appears not advisable as to our results with endothelial cells.

On the other hand, there is evidence that ERK and PI3K signaling triggered by brimamin treatment might be responsible for the induction of pro-survival and anti-apoptotic pathways in endothelial cells. Combination with specific ERK and PI3K inhibitors sensitized endothelial cells to brimamin in regard to its cytotoxicity and antivascular acitivity *in vitro*. There are also clues for an involvement of the anti-apoptotic NF-κB in the mode of action of brimamin. NF-κB signaling has been implicated in tumor progression and angiogenesis. We found that in endothelial cells NF-κB is activated early upon brimamin and CA-4 treatment as shown by the nuclear translocation of its cytosolic p65 subunit. However, after longer incubation times, the nuclear level of the NF-κB p65 subunit dropped significantly. We hypothesize that this is due to the extensive cytoskeletal reorganization or microtubule disruption. It was shown before that the nuclear translocation of NF-κB in neuroblastoma cells depends on a functional cytoskeleton [18]. The effect of brimamin on the activity of NF-κB was also evaluated in pancreatic and triple-negative breast cancer. Our results confirm the connection between NF-κB down-regulation and microtubule disruption in these NF-κB expressing, clinically relevant cancer entities. Brimamin reduced the DNA affinity of NF-κB in both cancer cell lines, and it even blocked the expression of p65-RelA in cells of brimamin-treated triple-negative breast tumor xenografts in mice. Since an activation and constitutively high expression of NF-κB had previously been observed by us [13] and others [55] for many resistant cancer types, including triple-negative breast carcinoma, brimamin is a potential drug candidate for the treatment of these prognostically poor cancers.

In earlier publications by other groups, an inhibition of tubulin polymerization by vinblastine or colchicine was demonstrated to block the formation of the crucial tubulin-dynein-karyopherin α-p50 complex required for nuclear translocation of NF-κB in neuronal cells. It also led to a low nuclear NF-κB-DNA binding activity, to low nuclear concentrations of p65

RelA and p50, and to a decreased transcription of NF-κB target genes [18]. In addition, NF-κB activation upon treatment with vinblastine, colchicine or nocodazole after short incubation times has also been reported [56] and was thought to be decisive for the inhibition of tumor angiogenesis *in vivo* [45,46]. This points out the paradoxical roles of NF-κB in proliferation and apoptosis depending on the cell type. It is not surprising that there are crosslinks between NF-κB and Rho signaling pathways as observed in inflammation processes, and that the down-regulation of Rho caused an inactivation of NF-κB in various cell types including endothelial cells [15–17]. The products of the target genes of NF-κB may also inactivate JNK signaling [57]. Taken together, the negative effects of brimamin on NF-κB signaling such as reduced DNA-binding activity, lower nuclear translocation *in vitro*, and reduced p65 expression *in vivo* might indicate an improved efficacy against certain types of cancer. Considering the clinical relevance it should be mentioned that pancreatic cancer patients are routinely treated with the nucleoside gemcitabine which could possibly be combined with brimamin in a synergistic regimen since NF-κB signaling is strongly activated in gemcitabine-resistant pancreas cancer cells [38]. For example, Aggarwal et al. reported growth inhibitory effects of the natural compound curcumin on pancreas cancer cells originating from a down-regulation of NF-κB [58]. A combination of brimamin with proteasome inhibitors which block NF-κB by an alternative pathway, i.e., by inhibition of the degradation of the cellular NF-κB inhibitor IκB, would allow to further optimize the anticancer efficacy and the dosis schedule in clinical trials. A combination of these two drugs might lead to an improved outcome in patients suffering from pancreatic cancer. A Korean study from 2010 supports this assumption. It showed that the disruption of the microtubules of HeLa cells and the inactivation of their NF-κB had sensitized them for apoptosis induced by DNA damage [56]. The influence of JNK and Rho signaling on the effect of brimamin in NF-κB-dependent cancer cells remains to be elucidated in more detail. However, the great efficacy of brimamin against multidrug-resistant cancer cell lines, its good applicability [10], and its ability to inhibit tumoral pro-survival pathways make it a promising anticancer drug candidate.

***Electronic supplementary material**

The online version of this article contains supplementary material (determination of apoptosis in resistant BxPC-3 pancreas and MDA-MB-231 breast carcinoma cells; original Western blot images) which is available to authorized users.

Declaration of interests: The authors declare that there are no conflicts of interest.

References

1. G. Pettit, S. Singh, E. Hamel, C. Lin, D. Alberts, and D. Garcia-Kendall, Experientia **45**, 209 (1989).
2. C. J. Mooney, G. Nagaiah, P. Fu, J. K. Wasman, M. M. Cooney, P. S. Savvides, J. A. Bokar, A. Dowlati, D. Wang, and S. S. Agarwala, Thyroid **19**, 233 (2009).
3. G. J. Rustin, G. Shreeves, P. D. Nathan, A. Gaya, T. S. Ganesan, D. Wang, J. Boxall, L. Poupard, D. J. Chaplin, M. R. L. Stratford, J. Balkissoon, and M. Zweifel, Br. J. Cancer **102**, 1355 (2010).
4. G. C. Tron, T. Pirali, G. Sorba, F. Pagliai, S. Busacca, and A. A. Genazzani, J. Med. Chem. **49**, 3033 (2006).
5. S. E. Holwell, P. A. Cooper, M. J. Thompson, G. R. Pettit, L. W. Lippert 3rd, S. W. Martin, and M. C. Bibby, Anticancer Res. **22**, 3933 (2002).
6. L. K. Folkes, M. Christlieb, E. Madej, M. R. L. Stratford, and P. Wardman, Chem. Res. Toxicol. **20**, 1885 (2007).
7. G. R. Pettit, M. R. Rhodes, D. L. Herald, D. J. Chaplin, M. R. Stratford, E. Hamel, R. K. Pettit, J. C. Chapuis, and D. Oliva, Anticancer. Drug Des. **13**, 981 (1998).
8. G. R. Pettit, B. E. Toki, D. L. Herald, M. R. Boyd, E. Hamel, R. K. Pettit, and J. C. Chapuis, J. Med. Chem. **42**, 1459 (1999).
9. L. Wang, K. W. Woods, Q. Li, K. J. Barr, R. W. McCroskey, S. M. Hannick, L. Gherke, R. B. Credo, Y.-H. Hui, K. Marsh, R. Warner, J. Y. Lee, N. Zielinski-Mozng, D. Frost, S. H. Rosenberg, and H. L. Sham, J. Med. Chem. **45**, 1697 (2002).
10. R. Schobert, B. Biersack, A. Dietrich, K. Effenberger, S. Knauer, and T. Mueller, J. Med. Chem. **53**, 6595 (2010).
11. C. Kanthou, Blood **99**, 2060 (2002).
12. B. B. Aggarwal, S. Shishodia, S. K. Sandur, M. K. Pandey, and G. Sethi, Biochem. Pharmacol. **72**, 1605 (2006).
13. A. Ahmad, S. Banerjee, Z. Wang, D. Kong, and F. H. Sarkar, J. Cell. Biochem. **105**, 1461 (2008).
14. S. Ali, A. Ahmad, S. Banerjee, S. Padhye, K. Dominiak, J. M. Schaffert, Z. Wang, P. A. Philip, and F. H. Sarkar, Cancer Res. **70**, 3606 (2010).
15. Y. He, H. Xu, L. Liang, Z. Zhan, X. Yang, X. Yu, Y. Ye, and L. Sun, Arthritis Rheum. **58**, 3366 (2008).
16. H. Shimada and L. E. Rajagopalan, J. Biol. Chem. **285**, 12536 (2010).
17. S. Shimizu, M. Tahara, S. Ogata, K. Hashimoto, K. Morishige, K. Tasaka, and Y. Murata, Mol. Hum. Reprod. **13**, 181 (2007).
18. G. G. Mackenzie, C. L. Keen, and P. I. Oteiza, J. Neurochem. **99**, 402 (2006).
19. V. Bourgarel-Rey, S. Vallee, O. Rimet, S. Champion, D. Braguer, A. Desobry, C. Briand, and Y. Barra, Mol. Pharmacol. **59**, 1165 (2001).
20. A. W. Schüttelkopf and D. M. F. van Aalten, Acta Crystallogr. D Biol. Crystallogr. **60**, 1355 (2004).
21. O. Trott and A. J. Olson, J. Comput. Chem. NA (2009).
22. J. Gasteiger and M. Marsili, Tetrahedron **36**, 3219 (1980).
23. G. L. Warren, C. W. Andrews, A.-M. Capelli, B. Clarke, J. LaLonde, M. H. Lambert, M. Lindvall, N. Nevins, S. F. Semus, S. Senger, G. Tedesco, I. D. Wall, J. M. Woolven, C. E. Peishoff, and M. S. Head, J. Med. Chem. **49**, 5912 (2006).
24. W. DeLano, DeLano Sci. LLC San Carlos CA (2003).
25. K. Mahal, S. Schruefer, G. Steinemann, F. Rausch, R. Schobert, M. Höpfner, and B. Biersack, Cancer Chemother. Pharmacol. **in press**, (2015).
26. K. Mahal, M. Resch, R. Ficner, R. Schobert, B. Biersack, and T. Mueller, ChemMedChem **9**, 847 (2014).

27. G. M. Tozer, C. Kanthou, and B. C. Baguley, Nat. Rev. Cancer **5**, 423 (2005).
28. B. Biersack, K. Effenberger, R. Schobert, and M. Ocker, ChemMedChem **5**, 420 (2010).
29. S. Ali, Mol. Cancer Ther. **4**, 1943 (2005).
30. R. B. G. Ravelli, B. Gigant, P. A. Curmi, I. Jourdain, S. Lachkar, A. Sobel, and M. Knossow, Nature **428**, 198 (2004).
31. M. Botta, S. Forli, M. Magnani, and F. Manetti, Top. Curr. Chem. **286**, 279 (2009).
32. C. Kanthou and G. M. Tozer, Expert Opin. Ther. Targets **11**, 1443 (2007).
33. H. Quan, Y. Xu, and L. Lou, Int. J. Cancer **122**, 1730 (2007).
34. M. Fan, L. Du, A. Stone, K. Gilbert, and T. Chambers, Cancer Res. **60**, 6403 (2000).
35. C. Kanthou and G. M. Tozer, Int. J. Exp. Pathol. **90**, 284 (2009).
36. M. Chrzanowska-Wodnicka and K. Burridge, J. Cell Biol. **133**, 1403 (1996).
37. L. J. Williams, D. Mukherjee, M. Fisher, C. C. Reyes-Aldasoro, S. Akerman, C. Kanthou, and G. M. Tozer, Br. J. Pharmacol. **171**, 4902 (2014).
38. A. Arlt, A. Gehrz, S. Müerköster, J. Vorndamm, M.-L. Kruse, U. R. Fölsch, and H. Schäfer, Oncogene **22**, 3243 (2003).
39. M. Graupera, J. Guillermet-Guibert, L. C. Foukas, L.-K. Phng, R. J. Cain, A. Salpekar, W. Pearce, S. Meek, J. Millan, P. R. Cutillas, A. J. H. Smith, A. J. Ridley, C. Ruhrberg, H. Gerhardt, and B. Vanhaesebroeck, Nature **453**, 662 (2008).
40. J. Karar and A. Maity, Front. Mol. Neurosci. **4**, (2011).
41. G. C. Tron, T. Pirali, G. Sorba, F. Pagliai, S. Busacca, and A. A. Genazzani, J. Med. Chem. **49**, 3033 (2006).
42. G. Rajashekhar, M. Kamocka, A. Marin, M. A. Suckow, W. R. Wolter, S. Badve, A. R. Sanjeevaiah, K. Pumiglia, E. Rosen, and M. Clauss, J. Cell. Physiol. **226**, 800 (2011).
43. M. Kelkel, C. Cerella, F. Mack, T. Schneider, C. Jacob, M. Schumacher, M. Dicato, and M. Diederich, Carcinogenesis **33**, 2162 (2012).
44. J. D. Orth, A. Loewer, G. Lahav, and T. J. Mitchison, Mol. Biol. Cell **23**, 567 (2012).
45. S. P. Tabruyn and A. W. Griffioen, Cell Death Differ. **14**, 1393 (2007).
46. S. P. Tabruyn, S. Memet, P. Ave, C. Verhaeghe, K. H. Mayo, I. Struman, J. A. Martial, and A. W. Griffioen, Mol. Cancer Ther. **8**, 2645 (2009).
47. M. Carr, L. M. Greene, A. J. S. Knox, D. G. Lloyd, D. M. Zisterer, and M. J. Meegan, Eur. J. Med. Chem. **45**, 5752 (2010).
48. H. Wehbe, C. M. Kearney, and K. G. Pinney, Anticancer Res. **25**, 3865 (2005).
49. D. O. Moon, M. O. Kim, C. H. Kang, J. D. Lee, Y. H. Choi, and G. Y. Kim, Exp. Mol. Med. **41**, 665 (2009).
50. A. V. Singh, M. Bandi, N. Raje, P. Richardson, M. A. Palladino, D. Chauhan, and K. C. Anderson, Blood **117**, 5692 (2011).
51. L. Ciani and P. C. Salinas, BMC Cell Biol. **8**, 27 (2007).
52. D. C. H. Ng, T. T. Zhao, Y. Y. C. Yeap, K. R. Ngoei, and M. A. Bogoyevitch, J. Biol. Chem. **285**, 29001 (2010).
53. Y. Y. Yip, Y. Y. C. Yeap, M. A. Bogoyevitch, and D. C. H. Ng, Biochem. Biophys. Res. Commun. **446**, 248 (2014).
54. J.-H. Kim, T. H. Kim, H. S. Kang, J. Ro, H. S. Kim, and S. Yoon, Biochem. Biophys. Res. Commun. **387**, 450 (2009).
55. X. Wang, K. Belguise, N. Kersual, K. H. Kirsch, N. D. Mineva, F. Galtier, D. Chalbos, and G. E. Sonenshein, Nat. Cell Biol. **9**, 470 (2007).
56. H. Lee, J. Jeon, Y. S. Ryu, J. E. Jeong, S. Shin, T. Zhang, S. W. Kang, J. H. Hong, and G. M. Hur, J. Korean Med. Sci. **25**, 1574 (2010).
57. S. Papa, J. Cell Sci. **117**, 5197 (2004).
58. L. Li, B. B. Aggarwal, S. Shishodia, J. Abbruzzese, and R. Kurzrock, Cancer **101**, 2351 (2004).

Electronic Supplementary Material

Contribution of JNK signaling and NF-κB activity to the anticancer effects of the vascular-disrupting agent brimamin

Katharina Mahal, Aamir Ahmad, Marcus Resch, Ralf Ficner, Fazlul H. Sarkar, Rainer Schobert, Bernhard Biersack

Affiliations and addresses of authors:

Katharina Mahal, Bernhard Biersack, Rainer Schobert
Organic Chemistry Laboratory, University Bayreuth, Universitaetsstrasse 30, 95440 Bayreuth, Germany

A. Ahmad, F. H. Sarkar
Karmanos Cancer Institute, Department of Pathology, Wayne State University School of Medicine, 4100 John R. Street, Detroit 48201, Michigan (USA)

M. Resch, R. Ficner
Department of Molecular Structural Biology, Georg-August-University Göttingen, Justus-von-Liebig-Weg 11, 37077 Göttingen (Germany)

Corresponding author:
Bernhard Biersack, Organic Chemistry Laboratory, University Bayreuth, Universitaetsstrasse 30, 95440 Bayreuth, Germany. Phone: +49(0)921 552673. Fax: +49(0)921 552671. E-mail: bernhard.biersack@yahoo.com

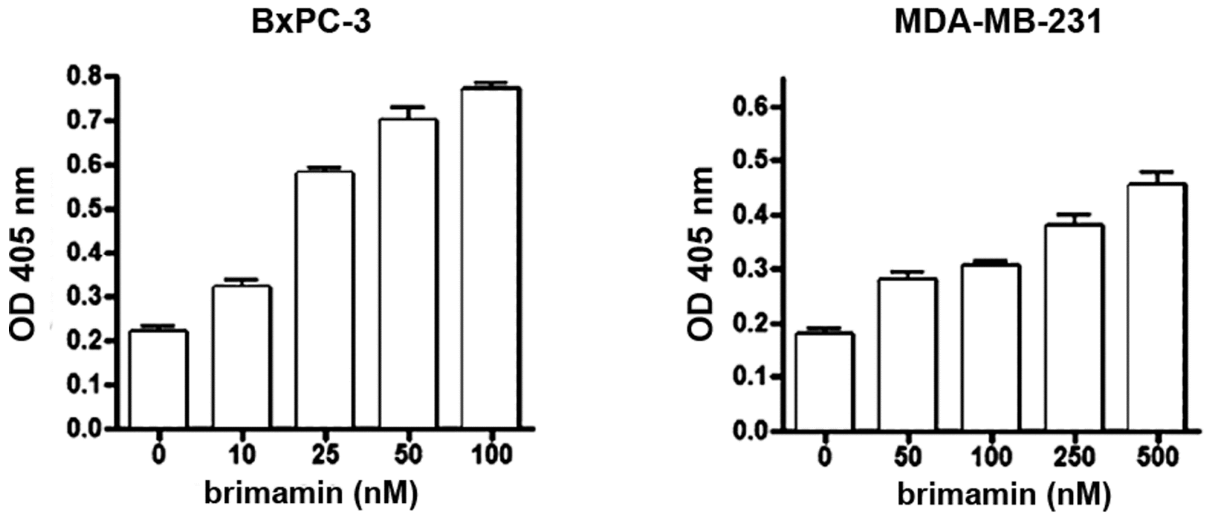

Fig. S1 Apoptosis induction by brimamin in MDA-MB-231 breast and BxPC-3 pancreas carcinoma cells after 72 h incubation time. Increasing levels of cytosolic nucleosomes upon apoptotic DNA fragmentation were detected by histone/DNA ELISA assays. OD, optical density at 405 nm wavelength

Original Western Blot images

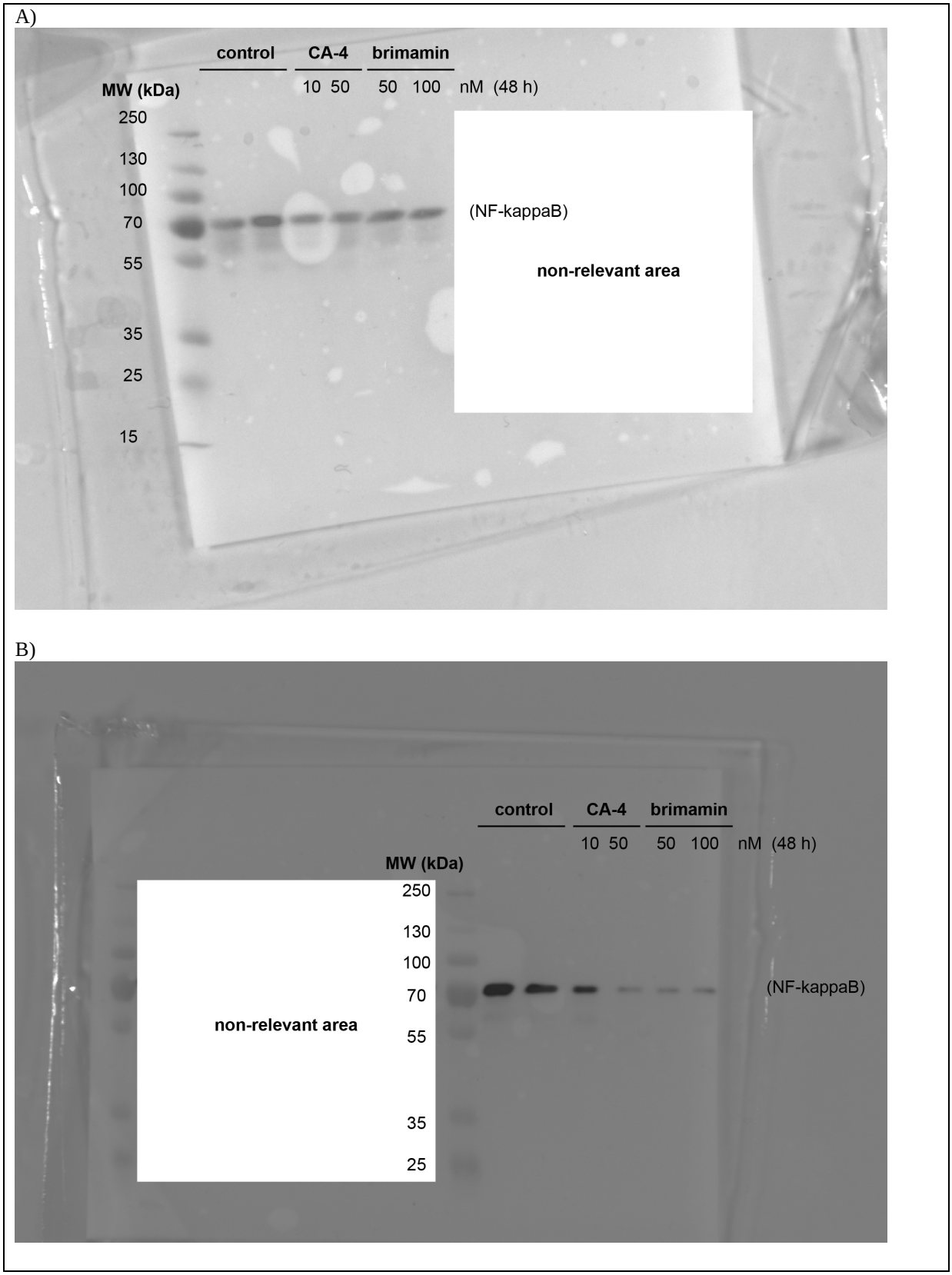

Fig. S2 Overlay of original brightfield and chemiluminescence images of Western Blots presented in Fig. 6. Analyses of total (A) and nuclear (B) NF-kappaB in Ea.hy926 cells incubated with CA-4 or brimamin at the indicated concentrations for 48 h. Molecular weight standard: PageRuler Plus Prestained Protein ladder (Cell Signaling Technology)

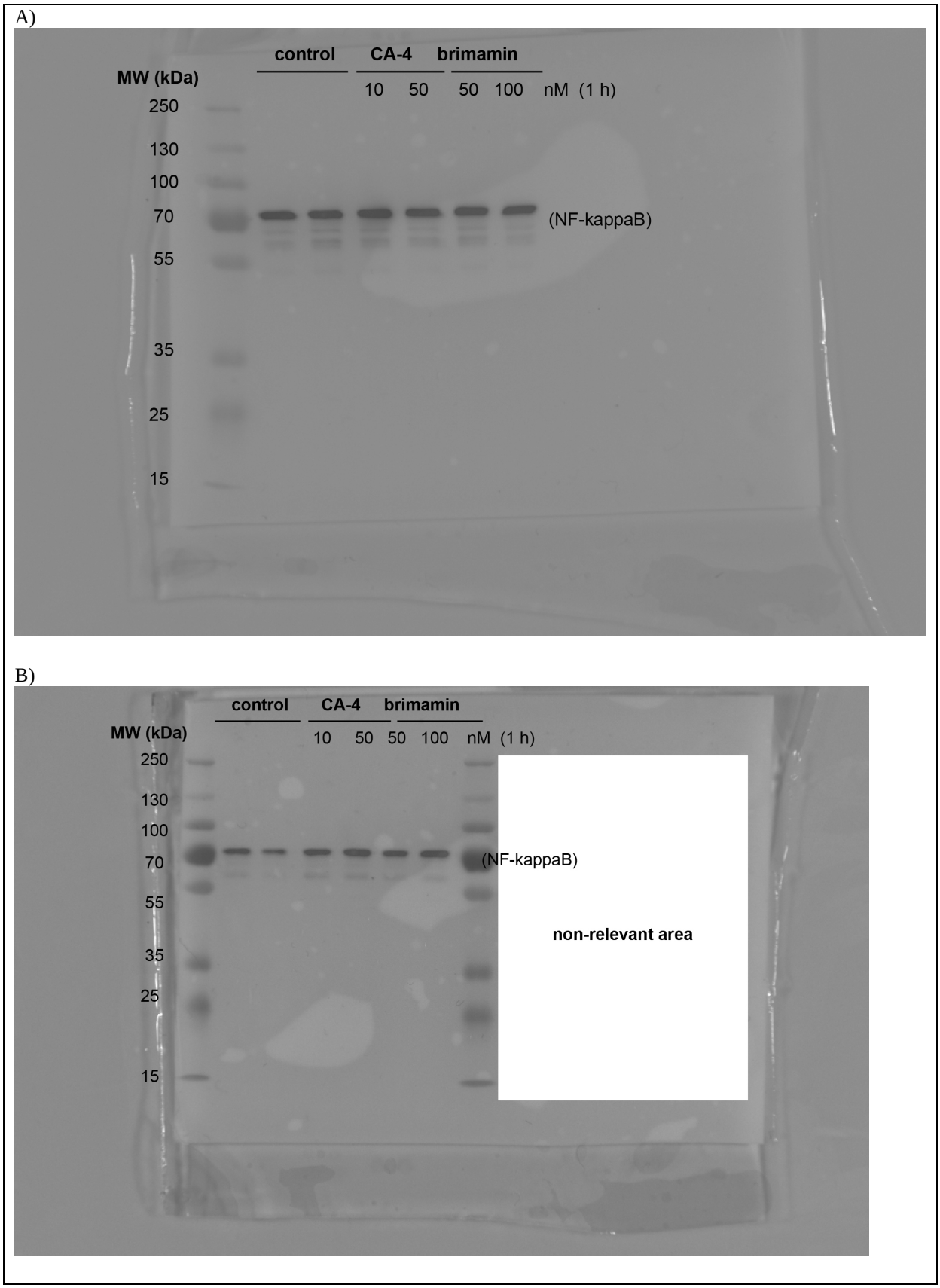

Fig. S3 Overlay of original brightfield and chemiluminescence images of Western Blots presented in Fig. 6. Analyses of total (A) and nuclear (B) NF-kappaB in Ea.hy926 cells incubated with CA-4 or brimamin at the indicated concentrations for 1 h. Molecular weight standard: PageRuler Plus Prestained Protein ladder (Cell Signaling Technology)

A)

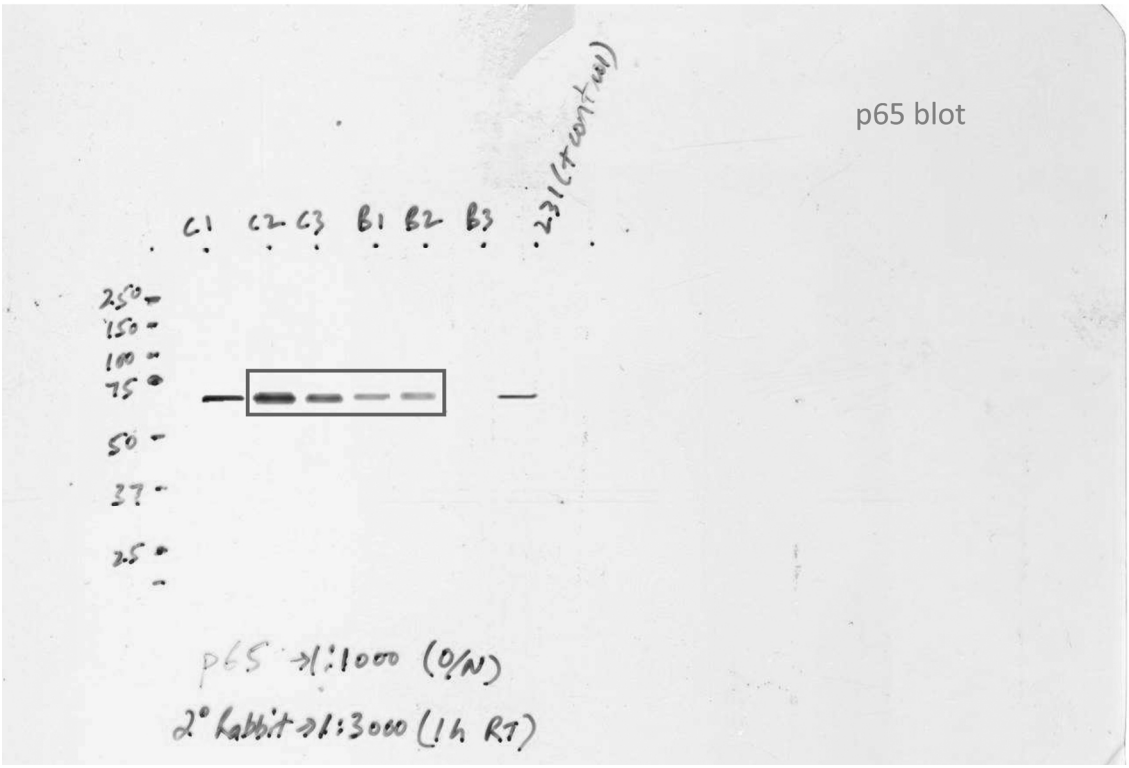

B)

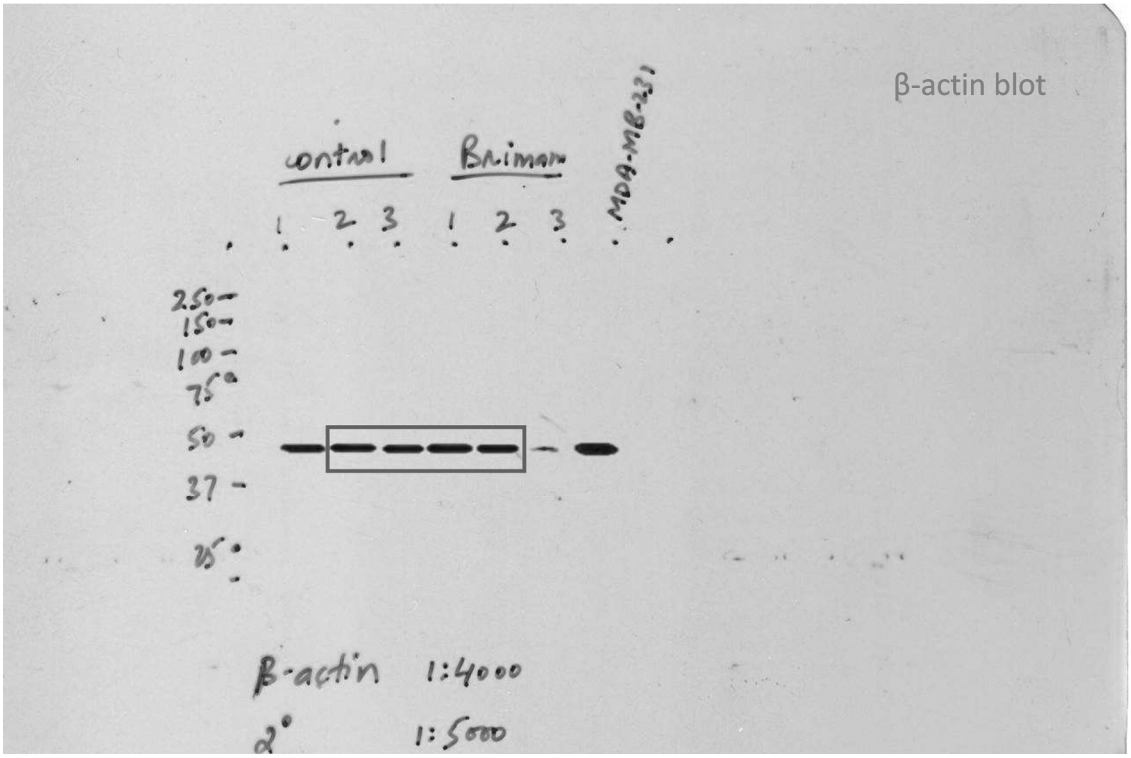

Fig. S4 Original X-ray films of Western Blots presented in Fig. 7 (relevant bands indicated by black boxes). Analyses of the p65-subunit of NF-kappB (A) in tissue lysates from MDA-MB-231 xenografts and beta-actin loading control (B). Bands of the molecular weight standard indicated on the left

Publikationen und Manuskripte zur biologischen Evaluation von Histondeacetylase-Inhibitoren:

Publikation V und Manuskript IV

PUBLIKATION V

Biological evaluation of 4,5-diarylimidazoles with hydroxamic acid appendages as novel dual mode anticancer agents.

Katharina Mahal,[a] Sebastian Schruefer,[a] Gustav Steinemann,[b] Franziska Rausch,[b] Rainer Schobert,[a] Bernhard Biersack,*[a] Michael Höpfner *[b]

[a] *Organic Chemistry Laboratory, University of Bayreuth, Universitätsstraße 30, 95440 Bayreuth (Germany)*

[b] *Institute of Physiology, Charité-Universitätsmedizin Berlin, 10117 Berlin (Germany)*

* email: bernhard.biersack@uni-bayreuth.de; michael.hoepfner@charite.de

Cancer Chemother. Pharmacol. **2015**, *75 (4)*, 691-700.

doi: 10.1007/s00280-015-2685-z

Cancer Chemother Pharmacol (2015) 75:691–700
DOI 10.1007/s00280-015-2685-z

ORIGINAL ARTICLE

Biological evaluation of 4,5-diarylimidazoles with hydroxamic acid appendages as novel dual mode anticancer agents

Katharina Mahal · Sebastian Schruefer · Gustav Steinemann · Franziska Rausch · Rainer Schobert · Bernhard Biersack · Michael Höpfner

Received: 16 December 2014 / Accepted: 16 January 2015 / Published online: 25 January 2015

Abstract
Purpose New (4-aryl-1-methylimidazol-5-yl)cinnamoyl-hydroxamic acids were prepared as potential dual mode anticancer agents combining the antivascular effect of the 4,5-diarylimidazole moiety and the histone deacetylases (HDAC) inhibition by the cinnamoyl hydroxamate.
Methods Their antiproliferative activity against a panel of primary cells and cancer cell lines was determined by MTT assays and their apoptosis induction by caspase-3 activation. Their ability to reduce the activity of HDAC was measured by enzymatic assays and Western blot analyses of cellular HDAC substrates. Additional effects on cancer cell migration were ascertained via immunofluorescence staining of cytoskeleton components and three-dimensional migration assays. The chorioallantoic membrane assay was used as an in vivo model to assess their antiangiogenic properties.
Results The 4-phenyl- and 4-(*p*-methoxyphenyl)-imidazole derivatives had a greater antiproliferative and apoptosis inducing effect in a variety of cancer cell lines when compared with the approved HDAC inhibitor SAHA, and most distinctly so in non-malignant human umbilical vein endothelial cells. Like SAHA, both compounds acted as pan-HDAC inhibitors. In 518A2 melanoma cells, they led to hyperacetylation of histones and of the cytoplasmic HDAC6 substrate alpha-tubulin. As a consequence, they inhibited the migration and invasion of these cells in transwell invasion assays. In keeping with its pronounced impact on endothelial cells, the 4-phenyl-imidazole derivative also inhibited the growth and sprouting of blood vessels in the chorioallantoic membrane of fertilized hen eggs.
Conclusions The 4-phenyl- and 4-(*p*-methoxyphenyl)-imidazole compounds combine the antivascular effects of 4,5-diarylimidazoles with HDAC inhibition by cinnamoyl hydroxamates and show additional antimetastatic activity. They are promising candidates for pleiotropic HDAC inhibitors.

Keywords Imidazole · Hydroxamate · HDAC inhibitor · Antiangiogenic agent · Antitumor agent · Antimetastatic activity

Introduction

Histone deacetylases (HDACs) are among the most promising targets for anticancer drug development [1, 2]. The classical role of HDACs is to catalyze the N-deacetylation of lysine residues of histone proteins as part of the nucleosomes and thus to regulate gene expression. However, certain members of different HDAC classes are also responsible for the post-translational modification of non-histone substrates or proteins implicated in cell growth, cell migration or differentiation [3–8]. As a consequence, their inhibition interferes with a great number of cellular processes besides altering gene expression, by affecting protein–protein interactions, signaling transduction or protein degradation [3, 4, 6, 9].

Electronic supplementary material The online version of this article (doi:10.1007/s00280-015-2685-z) contains supplementary material, which is available to authorized users.

K. Mahal · S. Schruefer · R. Schobert · B. Biersack (✉)
Organic Chemistry Laboratory, University Bayreuth, 95440 Bayreuth, Germany
e-mail: bernhard.biersack@yahoo.com

G. Steinemann · F. Rausch · M. Höpfner (✉)
Institute of Physiology, Charité-Universitätsmedizin Berlin, Virchowweg 6, 10117 Berlin, Germany
e-mail: michael.hoepfner@charite.de

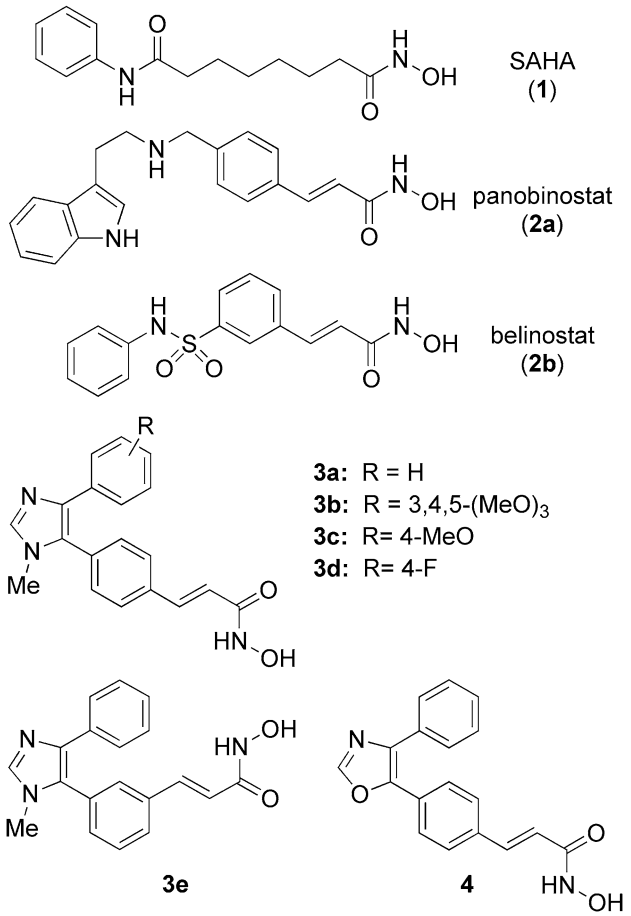

Fig. 1 Examples of established HDAC inhibitors **1** and **2** and structures of new imidazoles **3** and oxazole **4** with hydroxamic acid appendages

These changes may eventually lead to the induction of apoptosis in cancer cells treated with HDAC inhibitors (HDACi). Hydroxamic acids are prominent (pan-) HDACi and derivatives such as SAHA (suberoylanilide hydroxamic acid, vorinostat; **1**), panobinostat (**2a**) and belinostat (**2b**) were already approved for the treatment of hematological malignancies or are in advanced clinical development (Fig. 1) [10–13]. In addition, some HDACi were also shown to exhibit antiangiogenic effects in the treatment of solid tumors in combination with other anticancer drugs [14–16]. Despite promising outcomes in clinical trials, the growing problem of resistance to HDACi necessitates their continuous development [17]. Hybrid compounds with improved anticancer activity due to synergistic combination of an inhibition of HDAC and kinase inhibition or estrogen receptor modulation were recently disclosed [18–21]. In order to enhance the efficacy of HDACi and their resilience against acquired resistance, we now attached the hydroxamic acid chelator, common to many HDACi, to a second structural motif with proven anticancer activity, the 4,5-diarylimidazole or 4,5-oxazole, respectively. When aptly substituted such heterocyclic compounds retain the tubulin affinity as well as the vascular-disrupting and cytotoxic properties of the natural lead, the 1,2-diaryl-*cis*-stilbene combretastatin A-4, with the bonus of an increased chemical stability and water solubility [22, 23]. Derivatives of this compound class were also shown to be well tolerated by mice and orally applicable [22, 23]. A couple of 4,5-diarylimidazoles with hydroxamate appendages were reported by us recently to show antitumoral activity against hepatocellular carcinoma [24]. Herein, we report a greatly extended study comprising the synthesis of further (4-aryl-imidazole-5-yl)cinnamoylhydroxamic acids **3** and of an oxazole congener **4**, as well as an evaluation of their growth inhibitory effect on various chemosensitive and multidrug-resistant cancer cell lines, of their inhibition of HDAC, and their effect on blood vessel development in an in vivo model.

Materials and methods

Cell lines and culture conditions

The human melanoma cell line 518A2 (obtained from the department of Radiotherapy and Radiobiology, University Hospital Vienna, Austria), the human colon adenocarcinoma cell line HT-29 and the human colon carcinoma cell line HCT-116 (from University Hospital Erlangen, Germany), the MCF-7/Topo breast cancer, the KB-V1/Vbl cervix carcinoma cell line (both from the Institute of Pharmacy, University of Regensburg, Germany) and the HUVEC-derived endothelial hybrid cell line Ea.hy926 (Institute of Physiology, Charité Berlin, Germany) were grown in DMEM or RPMI (HT-29) medium, supplemented with 10 % fetal bovine serum (FBS), 1 % Antibiotic–Antimycotic solution (all from Gibco) and 250 µg/mL gentamycin (SERVA). The medium of the Ea.hy926 cells was additionally supplemented with an endothelial medium supplement (PAA). Experiments on primary human umbilical vein cells (HUVEC) were done at the Helmholtz Centre for Infection Research (Braunschweig, Germany). HUVEC were cultured in EGM-2 medium (Lonza). The human esophageal squamous carcinoma cell line Kyse-140 [25, 26] was grown in RPMI 1640 medium supplemented with 10 % FBS, the pancreatic carcinoid BON cells, which were established from a human pancreatic carcinoid tumor as a useful model to study the biology of neuroendocrine tumors in vitro were grown in a 1:1 mixture of DMEM and Ham's F-12 medium containing 10 % FCS (Biochrom, Berlin, Germany) and 1 % L-glutamine [27, 28]. Primary chicken heart fibroblasts (CHF) were explanted from 10-day-old chicken embryos and separated from other cell types for several weeks. Fibroblasts were finally grown in DMEM

(10 % FBS, 1 % Anti–Anti, 250 µg/mL gentamycin) and used before the twentieth passage. All cell lines were cultured and incubated at 37 °C, 5 % CO_2, 95 % humidified atmosphere. Only mycoplasma-free cell lines were used.

Stock solutions and drug application

The syntheses and characterization of all test compounds **3** and **4** can be found in the Electronic supplementary material (Chemistry). Stock solutions of these were prepared in DMSO at a concentration of 10 mM and stored at 4 °C. Suberoylanilide hydroxamic acid (SAHA, Vorinostat) was purchased from LC Laboratories and used without further purification as a 10 mM stock solution in DMSO. Stock solutions were diluted to the final concentration in media or ddH_2O before each experiment. In all experiments, the final DMSO concentration was <0.25 %.

Measurement of caspase-3 activity

The preparation of cell lysates and determination of caspase-3 activities was performed as previously described [29]. Caspase-3 activity was calculated from the cleavage of the fluorogenic substrate DEVD-AMC (Calbiochem-Novabiochem, Bad Soden, Germany). Cell lysate volumes normalized to their protein concentration were incubated with substrate solution (20 µg/mL caspase-3 substrate AC-DEVD-AMC in 20 mM HEPES, 10 % glycerol, 2 mM DTT, pH 7.5) for 1 h at 37 °C and a fluorescence increase after cleavage of the substrate was measured with a VersaFluor fluorometer (excitation 360 nm, emission 460 nm) from Bio-Rad. All experiments were done in triplicates. Caspase-3 activity was calculated as the mean ± S.D. with respect to DMSO controls set to 1.

HDAC activity fluorescence assay

The direct inhibition of HDAC by the new compounds was proved by means of a fluorescence-based HDAC activity assay. Visualization of HDAC activity was achieved by using short acetylated peptide substrates coupled to a precursor fluorophore which is released by trypsin cleavage only upon previous deacetylation. A commercially available nuclear extract from HeLa cells (HeLa nuclear extract, 2.0 mg/mL, Merck Millipore) containing a specific set of active HDACs with nuclear localization and a Fluor-de-Lys® substrate suitable for measuring broad-spectrum HDAC activity from cell extracts was used in this assay according to manufacturer's conditions. Briefly, 0.5 µg HeLa cell nuclear extract was mixed with SAHA, or **3a**, or **3c** (dilutions from 10 µM to 1 nM) and the Fluor-de-Lys substrate (25 µM Fluor-de-Lys®-Green substrate, Enzo Life Sciences) in a final volume of 50 µL of HDAC assay buffer (50 mM Tris–HCl, 137 mM NaCl, 2.7 mM KCl, 1 mM $MgCl_2$, pH 8.0) in the wells of a black 96-well plate (half-area 96-well plate, µClear®, black, medium binding, greiner bio-one). The plate was incubated at 37 °C for 60 min, and the amount of deacetylated substrate was then visualized by adding 50 µL 1× developer (0.5 mg/mL trypsin, 0.1 mM EDTA in 50 mM Tris–HCl, pH 7.4) and subsequent incubation at 37 °C for 10 min. Fluorescence intensity of the degraded HDAC substrate was measured with a microplate reader (Tecan) at an emission wavelength of 535 nm (excitation at 485 nm). Blank and solvent (DMSO) controls were treated identically. The fluorescence intensity represents the relative HDAC activity within a sample with respect to DMSO controls. IC_{50} values from dose–response curves were calculated as the mean of three independent experiments ± S.D.

Detection of histone and microtubule acetylation by immunoblotting

518A2 melanoma cells (50.000 cells/well) were grown in 24-well plates and treated with vehicle (DMSO), SAHA (5 or 10 µM) or the hydroxamic acids **3a** or **3c** (5 or 10 µM) for 3, 6, 12 or 24 h. The cells were then harvested by trypsinization, and the resulting cell pellet was lysed in 100 µL 2× protein sample buffer (20 mM DTT, 2 % (w/v) SDS, 20 % (v/v) glycerol in 125 mM Tris–HCl, pH 6.8) and boiled (95 °C, 10 min). Ten microliters of the cell lysate was subjected to SDS polyacrylamide gel electrophoresis and transferred to a PVDF membrane for subsequent Western blot analysis. Drug-induced increase in histone H2B acetylation was detected by primary antibodies for acetyl-H2B (acetyl-histone H2B (Lys5) rabbit monoclonal antibody, Cell Signaling Technology). An increase in microtubule acetylation was detected by primary antibodies for alpha-tubulin (alpha-tubulin mouse monoclonal antibody, Invitrogen) and acetylated alpha-tubulin (acetyl-alpha-tubulin rabbit monoclonal antibody, Cell Signaling Technology). The membranes corresponding to two identically loaded gels were analyzed separately for alpha-tubulin and acetylated alpha-tubulin at the respective molecular weight protein band (55 kDa). Detection of beta-actin (beta-actin mouse monoclonal antibody) was used as an additional loading control. Band intensity was recorded by chemiluminescence (secondary HRP conjugates: goat antimouse-IgG-HRP conjugate, goat antirabbit-IgG-HRP conjugate, Cell Signaling Technologies; LAS-3000 imager, Fujifilm). ImageJ and Photoshop CS5 software were used for digital image processing and presentation of relevant protein bands, and contrast and brightness settings were applied uniformly to the whole images (for original blot images, see Electronic supplementary material).

Matrigel-based transwell invasion assay

The effect of the best derivatives **3a** and **3c** on the migration of highly invasive 518A2 melanoma cells [30] was assessed with a three-dimensional model for chemoattractant-stimulated tumor cell migration. It is based on modified Boyden migration chambers and implies both degradation of matrigel (trademark name) as an extracellular matrix and active movement of the cells through this basement membrane matrix [31, 32]. Quantification of invasive cells was adapted from the manufacturer's application manual (ThinCert™ application notes, greiner bio-one) with some alterations [33]. In brief, 518A2 melanoma cells were starved in serum-free DMEM overnight and harvested before seeding them into matrigel-coated (50 µL 1:1-dilution of matrigel basement membrane matrix in serum-free DMEM, 30 min at 37 °C, 5 % CO_2, 95 % humidity; BD Biosciences) ThinCert™ cell culture inserts with porous membranes (translucent PET membrane, 8 µm pore size, greiner bio-one) at a density of 2×10^4 cells in 200 µL serum-free DMEM per insert. The inserts were then placed into a 24-well plate with 600 µL DMEM containing 10 % FBS per well. Cells were incubated with DMSO (vehicle), SAHA (**1**) or **3a** or **3c** (1 µM, 36 h). Then, cells that had migrated through the insert membrane were collected and stained by incubation with 1X cell dissociation buffer (0.5 mM EDTA, 0.1 % sodium citrate in PBS, pH 7.4) containing 1 µM calcein-AM (calcein acetoxymethyl ester; non-fluorescent, cell-permeable dye) for 15 min at 37 °C. The cell suspension containing only invasive cells was transferred to the wells of a black 96-well plate, and invasive cells were quantified with a microplate reader (Tecan) by measuring the calcein fluorescence (excitation/emission wavelengths: 485/520 nm) which was eventually calculated as percentage ± S.D. of DMSO-treated control cells set to 100 %. All experiments were carried out in triplicates (for a detailed assay procedure scheme, see Electronic supplementary material, Fig. S5).

Fluorescence labeling of microtubules and actin filaments

518A2 cells (2.5×10^4/well) were seeded on glass coverslips in 24-well plates and treated with vehicle (DMSO) or the derivatives **3a** or **3c** (5 µM, 24 h). After fixation (4 % formaldehyde in PBS, 20 min), blocking and permeabilization of the cells (1 % BSA, 0.1 % Triton X-100 in PBS, 30 min), microtubules were visualized by incubation of the coverslips with a primary antibody against alpha-tubulin (antialpha-tubulin, mouse monoclonal antibody, clone no. TU-01, 1 h at 37 °C) followed by incubation with a secondary antibody conjugated to the DyLight550 fluorescence dye (goat antimouse-IgG-DyLight550 conjugate, Thermo Scientific/Pierce, 1 h at rt in the dark). Filamentous actin (F-actin) was stained by incubation of the coverslips with 1 U AlexaFluor®-488-conjugated phalloidin (Invitrogen) for 1 h at rt. The coverslips were mounted in Mowiol 4-88-based mounting medium containing 2.5 % (w/v) DABCO and 1 µg/mL DAPI (4′,6-diamidino-2-phenyl-indole) for counterstaining the nuclei. Cytoskeletal components were documented by fluorescence microscopy (ZEISS Axio Imager.A1; 400-fold magnification).

Chorioallantoic membrane (CAM) assay with fertilized chicken eggs

White leghorn chicken eggs (SPF eggs, VALO Biomedia) were incubated (37 °C, 50–60 % humidity) until day 6 after fertilization and opened by cutting a window of 2–3 cm diameter into the pole end of the eggshell. Rings of silicon foil (8 mm diameter) were placed on the developing vessels within the CAM followed by further incubation for 24 h. A total amount of 20 nmol (40 µL of 50 µM dilutions in ddH_2O) SAHA or the endothelial cell-selective derivative **3a** were applied directly onto the CAM and alterations in the blood vessel organization in comparison to control eggs (DMSO) were documented after 0-h and 24-h post-application with a stereomicroscope (60-fold magnification, Traveller) [34].

Data analysis and statistical analysis

The experimental results presented in the figures are representative of three or more independent observations. The data are presented as the mean values ± SD. Analysis of statistical significance was done by two-sample Student's *t* tests with XLSTAT. P values < 0.05 were considered to be statistically significant. ImageJ or Photoshop CS5 software was used for digital processing of original pictures and figure preparation (for additional information on image processing, see Electronic supplementary material).

Results and discussion

Tumor cell growth inhibition and apoptosis induction

The compounds **3a–e** and **4** were tested for their antiproliferative activity against a panel of cancer and endothelial cells of different origin and with different characteristics (Table 1). To assess a compound selectivity for rapidly dividing cancer over non-malignant cells, we also included non-malignant primary chicken fibroblasts.

The derivatives **3a**, **3c**, **3d** and **3e** were active with IC_{50} values in the low micromolar range (<3 µM). On average, the anisyl derivative **3c** was the most active compound of this series in the tested cell lines which included

Table 1 Inhibitory concentrations[a] IC_{50} [μM] of SAHA (**1**) and compounds **3a-e** and **4** when applied to various cancer and endothelial cells and non-malignant fibroblasts

	SAHA (**1**)	**3a**	**3b**	**3c**	**3d**	**3e**	**4**
518A2[b]	18.7 ± 3.1	13.1 ± 0.9	>50	10.2 ± 0.3	11.1 ± 2.0	n.d.	18.6 ± 2.5
518A2[c]	1.8 ± 0.1	2.8 ± 0.6	20.8 ± 3.0	1.5 ± 0.1	2.0 ± 0.5	2.3 ± 0.1	10.2 ± 0.1
HCT-116[c]	0.9 ± 0.1	0.8 ± 0.1	7.5 ± 3.0	0.9 ± 0.1	1.0 ± 0.1	1.1 ± 0.03	5.5 ± 1.4
HT-29[b]	1.9 ± 0.3	0.5 ± 0.1	n.d.	0.4 ± 0.1	0.3 ± 0.1	n.d.	n.d.
HT-29[c]	1.8 ± 0.1	1.2 ± 0.1	7.9 ± 1.0	0.7 ± 0.1	1.5 ± 0.1	2.5 ± 0.6	8.3 ± 0.3
MCF-7/Topo[c]	13.5 ± 0.7	15.3 ± 1.3	n.d.	10.0 ± 0.9	17.4 ± 1.0	18.0 ± 1.0	8.6 ± 1.4
KB-V1/Vbl[c]	13.1 ± 0.8	5.0 ± 0.8	n.d.	8.3 ± 1.9	5.5 ± 0.4	18.2 ± 2.6	8.0 ± 0.4
Panc-1[c]	3.8 ± 1.2	1.1 ± 0.1	8.7 ± 1.0	0.9 ± 0.1	1.7 ± 0.9	2.0 ± 0.1	2.4 ± 0.2
Ea.hy926[c]	1.9 ± 0.2	0.2 ± 0.1	n.d.	0.9 ± 0.1	2.3 ± 0.3	n.d.	10.0 ± 2.6
HUVEC[c]	7.7 ± 0.1	0.6 ± 0.03	n.d.	0.8 ± 0.1	n.d.	n.d.	n.d.
CHF[c]	89.4 ± 9.8	>150 μM	n.d.	>150 μM	>150 μM	n.d.	n.d.
BON[d]	>10 μM	n.d.	n.d.	1.1 ± 0.1	2.3 ± 0.6	n.d.	n.d.
BON[e]	2.2 ± 0.5			1.3 ± 0.2	3.6 ± 0.7		
Kyse-140[d]	>10 μM	n.d.	n.d.	4.6 ± 1.1	3.5 ± 1.0	n.d.	n.d.
Kyse-140[e]	3.1 ± 0.6			1.7 ± 0.1	6.1 ± 1.5		

Human cancer cell lines: 518A2 melanoma, HCT-116 colon, HT-29 colon, MCF-7/Topo breast, KB-V1/Vbl cervix, Panc-1 pancreas, neuroendocrinic carcinoid BON (pancreas) and Kyse-140 esophageal squamous cell carcinoma. Endothelial cells: hybrid cell line Ea.hy926 and primary cells (HUVEC). Non-malignant chicken heart fibroblasts: CHF. Values represent means of at least three independent assays ± S.D

nd not determined

[a] Values derived from concentration–response curves obtained by measuring the percentage of vital cells relative to vehicle-treated controls after 24-h[b] or 72-h[c] incubation using an MTT assay, or after 24-h[d] or 48-h[e] incubation using crystal violet staining

highly invasive 518A2 melanoma and p53-wild type, ras-mutated HCT-116 colon carcinoma cells, as well as the multidrug-resistant cell lines HT-29 colon, MCF-7/Topo mammary, KB-V1/Vbl cervix, and Panc-1 pancreas carcinomas. Compound **3c** displayed a sub-micromolar IC_{50} value of 0.68 μM in the multidrug-resistant HT-29 colon cancer cells, while it was active against the drug-sensitive 518A2 melanoma cells only at an IC_{50} of 1.45 μM. The *para*-fluoro substituted congener **3d** was also among the three best performing derivatives. Interestingly, HT-29 cells responded very well upon short time incubation with **3a**, **3c** and **3d** [IC_{50} (24 h) < 1 μM], whereas only **3c** was similarly active upon 72-h incubation of these cells. In general, **3a** and **3c** displayed a higher cytotoxicity against all cell lines than SAHA which was used as a positive, clinically established control. In contrast, low activities were observed for the 3,4,5-trimethoxyphenyl derivative **3b** and for **4**, the oxazole analog of the well-performing imidazole **3a**. These results suggest that high antiproliferative activity will arise only for *N*-methylimidazoles bearing a mono-substituted 4-phenyl ring as in **3c**. Furthermore, we observed a pronounced selectivity of **3a** for both the endothelial cell line Ea.hy926 and primary endothelial cells (HUVEC) with IC_{50} (72 h) values only a tenth of those of SAHA. Interestingly, the growth of primary fibroblasts was hardly reduced by high concentrations of **3a** or the most active compound **3c**. In contrast, SAHA affected these cells at the lowest IC_{50} (72 h) value.

The inhibition of HDACs is a particularly attractive approach for the treatment of advanced neuroendocrine tumors (NET) since NET cells had responded well to established HDAC inhibitors like trichostatin A, sodium butyrate and MS-275 [35]. Epigenetic modification of esophageal squamous cell carcinomas (ESCC) likewise led to tumor-suppressive effects [36]. Hence, the compounds **3c** and **3d** were also tested on human carcinoid BON cells obtained from a rare pancreatic neuroendocrine tumor and in Kyse-140 esophageal squamous cell carcinoma cells. Compound **3c** was more efficacious than **3d** against both cancer cell lines with IC_{50} (48 h) values between 1 and 2 μM.

3c and to a lesser extent also **3d** induced apoptosis in highly migratory 518A2 melanoma as well as in BON and Kyse-140 cells apparent from an increase of the caspase-3 activity after exposure to 2.5 or 10 μM concentrations for 24 h (Fig. 2). These findings are in line with the respective results of the growth inhibition studies. The values for equimolar concentrations of SAHA were in the same range with exception of those for Kyse-140 cells where **3c** clearly was more efficient in activating caspase-3.

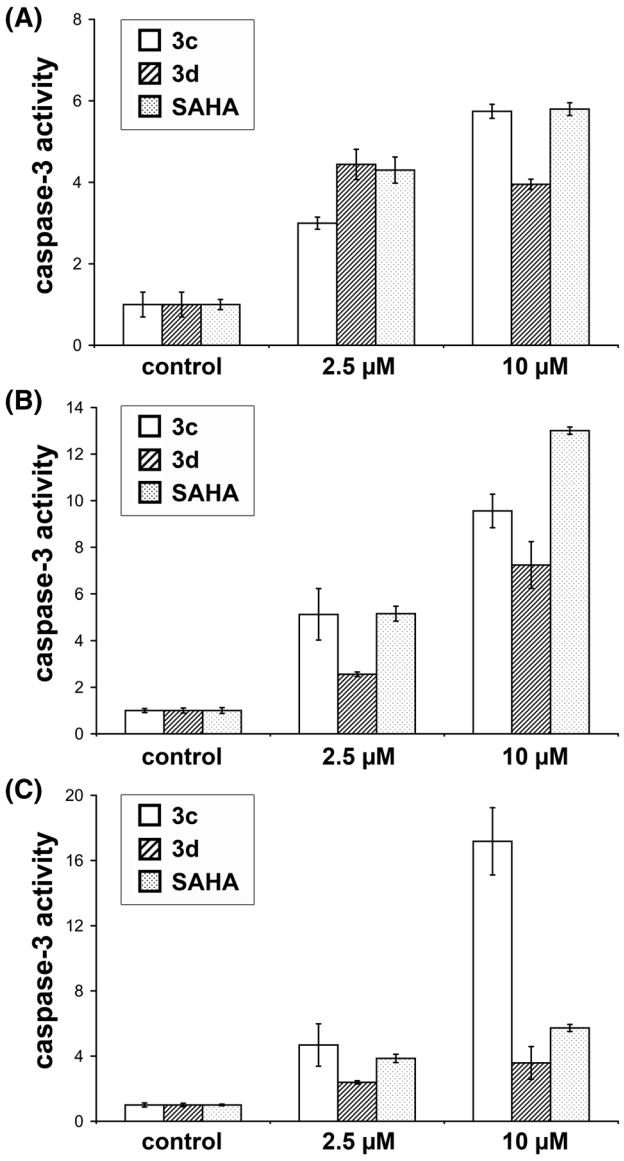

Fig. 2 Induction of caspase-3 activity. Caspase-3 activity upon 24 h exposure to SAHA (**1**) or the hydroxamic acids **3c** or **3d** in **a** 518A2 melanoma, **b** human carcinoid BON (pancreatic neuroendocrine tumor), and **c** Kyse-140 esophageal squamous cell carcinoma cells. Basal caspase-3 activity of vehicle-treated controls was set to 1. *Data* represent the mean ± S.D. of three independent experiments

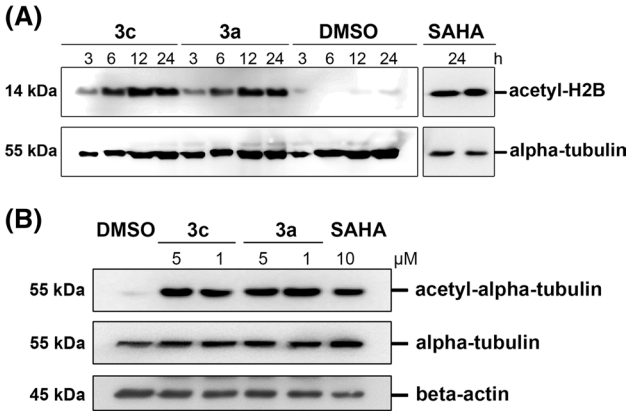

Fig. 3 Effects on histone H2B and alpha-tubulin acetylation. Increase of protein acetylation in 518A2 melanoma cells after treatment with **3a** or **3c**. **a** Time-dependent increase of histone H2B acetylation after exposure to 5 µM **3a** or **3b** for 3, 6, 12 and 24 h, or to SAHA (10 and 5 µM, 24 h) as detected by immunoblotting; alpha-tubulin: loading control. **b** Increase in microtubule (alpha-tubulin) acetylation after exposure to indicated concentrations of **3a**, **3c**, or SAHA for 24 h. Equal sample volumes were subjected to gel electrophoresis and immunoblotting for acetylated or total alpha-tubulin (55 kDa); beta-actin: loading control

Determination of HDAC inhibition via activity assays and detection of histone H2B and alpha-tubulin acetylation

To assess a direct inhibition of HDACs, we tested the compounds **3a** and **3c** on commercially available HeLa cell nuclear extract containing a specific set of active HDACs [9]. The resulting IC_{50} value calculated for **3a** (0.23 ± 0.01 µM) is similar to that of SAHA (0.23 ± 0.03 µM). Interestingly, the more cytotoxic compound **3c** inhibited HDAC activity in the extract only with a fivefold higher IC_{50} value of 1.08 ± 0.1 µM (for IC_{50} values, see Table S1 in the Electronic supplementary material).

The actual HDAC inhibition by the new compounds was additionally assessed by immunodetection of the increased portion of acetylated histone H2B which is part of the nucleosome. Exposure of 518A2 cells to 5 µM of **3a** or **3c** led to strongly increased H2B acetylation after only 3 h (Fig. 3a) and to a general increase in histone acetylation (*cf.* Electronic supplementary material, Fig. S1) when compared to DMSO-treated controls. This effect is restricted to the imidazoles with hydroxamic acid appendages and did not occur when cells were treated with the recently described, combretastatin A-4-derived imidazoles lacking hydroxamate residues (*cf.* Electronic supplementary material, Fig. S3) [23]. Furthermore, HDAC activity is not limited to the deacetylation of histones. Certain HDAC enzymes are not located in the nucleus at all. HDAC6, for instance, is occurring exclusively in the cytoplasm where it associates with microtubules. It was shown that HDAC6 removes acetyl groups from lysine residues of alpha-tubulin [37, 38]. In order to assess the HDAC specificity of the new hydroxamates **3a** and **3c,** we investigated the level of acetylated lysines of alpha-tubulin proteins in treated 518A2 melanoma cells. Both compounds led to significantly enhanced levels of acetylated tubulin (Fig. 3b). While **3a** caused levels of acetylated lysine in tubulin similarly to SAHA, **3c** was more effective in eliciting acetylated tubulin than SAHA, even at the lower concentration of 5 µM. We assume a greater inhibition of HDAC6 by compound **3c** to be responsible for this

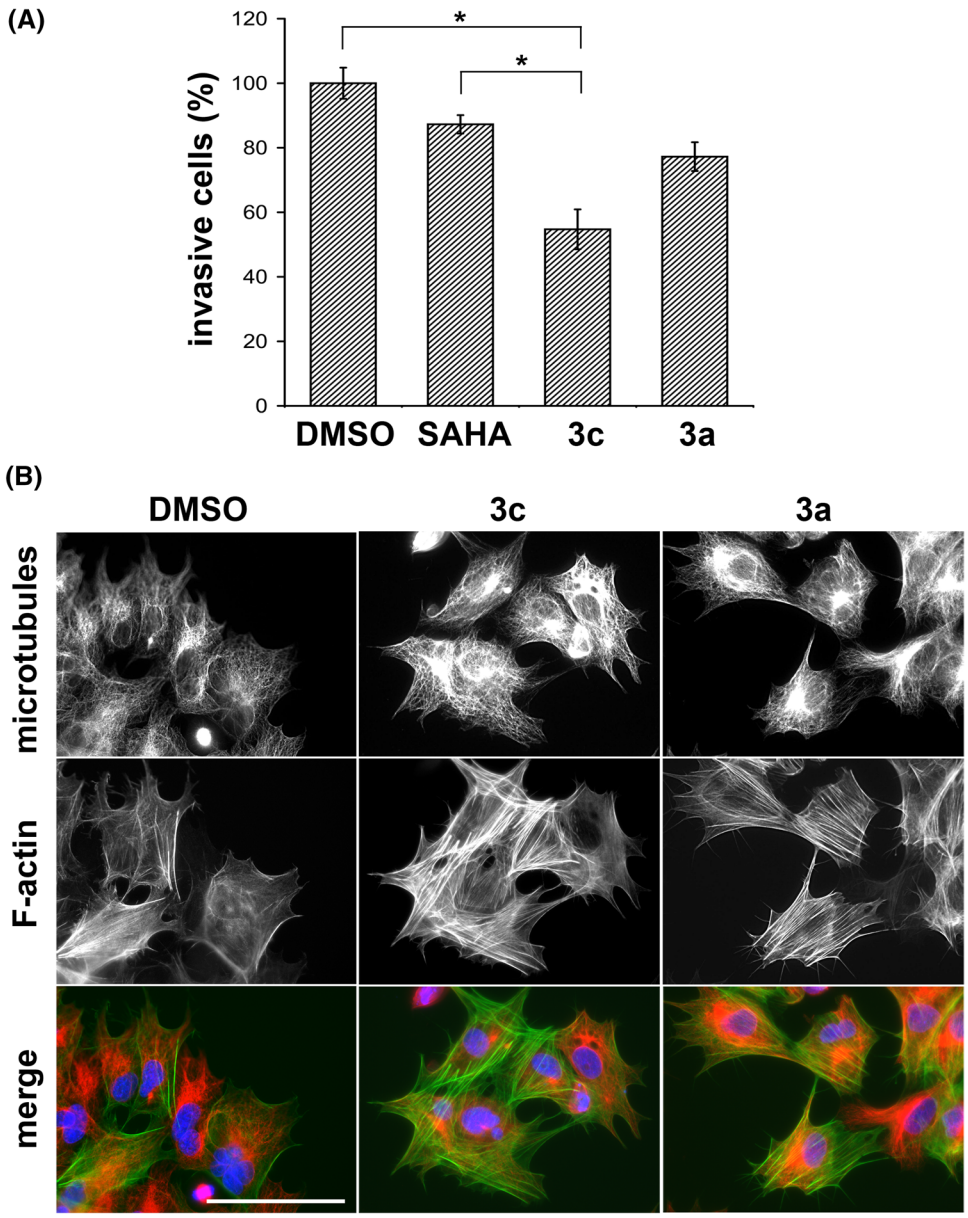

Fig. 4 Effects of **3a** or **3c** on migration and cytoskeleton of 518A2 melanoma cells. **a** Invasive 518A2 cells (%) after exposure to non-toxic concentrations of SAHA, **3c** or **3a** (1 µM, 36 h) or vehicle (DMSO). *Data* represent the mean of the calcein fluorescence of cells migrated through matrigel-coated cell culture inserts in transwell migration assays ± S.D. *Asterisks* indicate statistically significant differences ($P = 0.003$ for vehicle versus **3c**, $P = 0.006$ for SAHA versus **3c**, two-tailed Student's *t* test). **b** Fluorescence staining of microtubules (alpha-tubulin, merge: *red*) and filamentous actin (F-actin, merge: *green*) in 518A2 cells after incubation with vehicle (DMSO) or the derivatives **3a**, **3c** (5 µM, 24 h). Nuclei counterstained with DAPI (*blue*). *Scale bar* 100 µm

increase in acetylated microtubules in the 518A2 melanoma cells [37–39].

Migration and microfilament behavior of treated 518A2 melanoma cells

Like intact microtubules, a functional actin cytoskeleton is essential for directed cell migration by enabling highly dynamic structures such as membrane ruffles or lamellipodia [40]. As the actin cytoskeleton can be affected by HDAC inhibition in several ways [4, 41, 42], we investigated the effect of the derivatives **3a** and **3c** on the migration and the microfilament behavior of 518A2 melanoma cells (Fig. 4). In a three-dimensional transwell invasion assay, starved cells migrated to a lower compartment of a modified Boyden two-chamber system that is baited with fetal bovine serum as a chemoattractant and separated by a porous membrane and a matrigel layer as a surrogate for the extracellular matrix or the basement membrane of a microtumor. We found that non-toxic concentrations (1 µM, 36 h) of **3c** reduced the number of cells capable of migrating through matrigel-coated cell culture inserts to 55 % (Fig. 4a). Equimolar concentrations of SAHA reduced the directed cell invasion only to about 87 %. This pronounced antimigratory effect of compounds **3a** and **3c** might be a consequence of their interference with cytoskeletal dynamics via HDAC6 inhibition which leads to compacted microtubules and actin stress fiber formation (Fig. 4b). These structures likely lack the dynamic turnover that is essential of active migration [43].

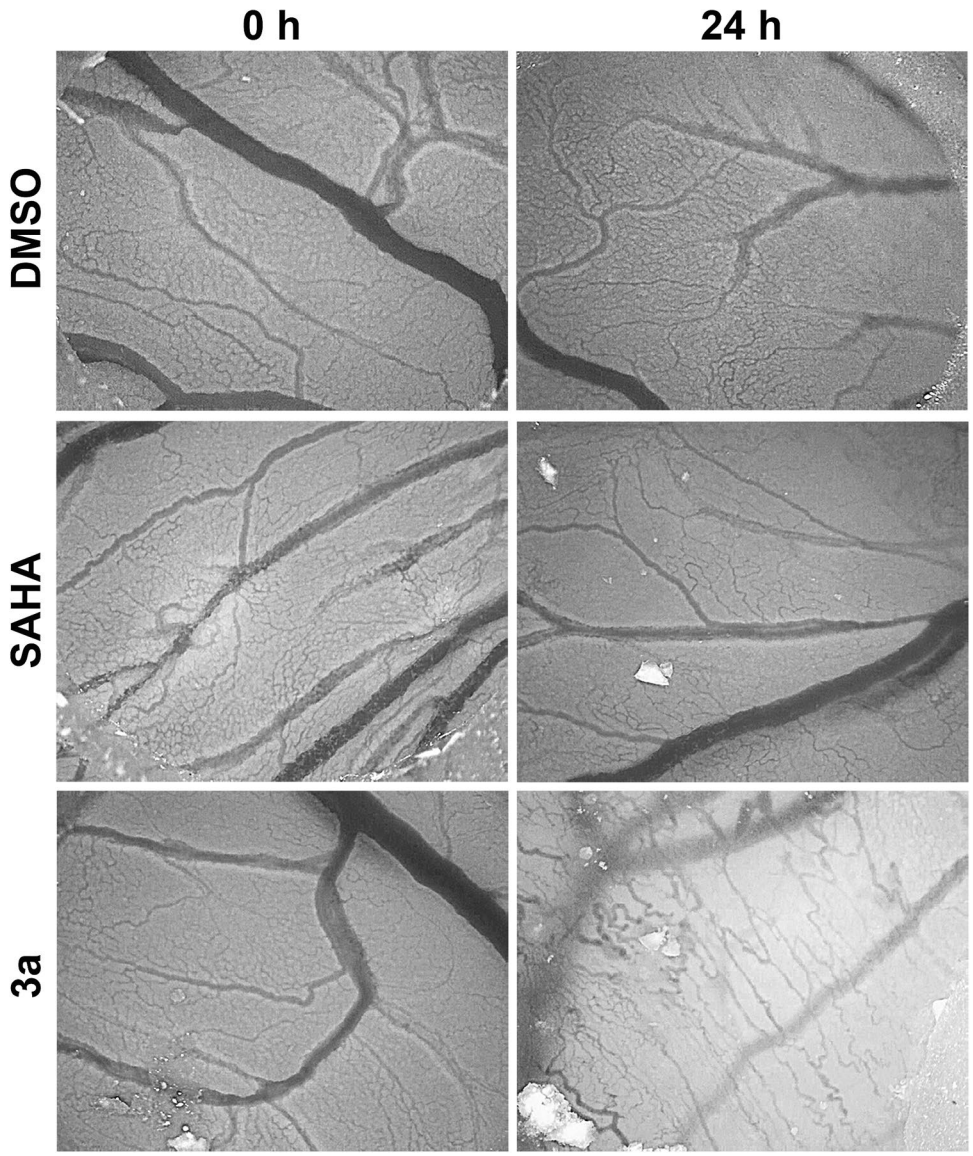

Fig. 5 Antiangiogenic effects of SAHA and **3a** (20 nmol) in a chorioallantoic membrane (CAM) assay with fertilized chicken eggs. Pictures (60-fold magnification) were taken 24 h after topical application onto the CAM of eggs at day 6 and 7 post-fertilization. *Pictures* are representative of at least three independent experiments

Antiangiogenic activity in vivo using the CAM assay

Furthermore, we tested the impact of the endothelial cell-selective derivative **3a** on blood vessel development in the chorioallantoic membrane (CAM) of fertilized chicken eggs (Fig. 5). The marginal antiangiogenic effect of SAHA was surpassed by that of **3a** which induced significant alterations of the vascular organization and reduced the sprouting of new blood vessels. A lesser effect, similar to that of SAHA, was observed for **3c** (not shown). A dose of 20 nmol of either **3a** or **3c** topically applied onto the CAM did not affect the vitality and development of the chicken embryos. Hence, both compounds **3a** and **3c** are at least as good antiangiogenic agents as SAHA or other HDACi described as such in the literature [14–16]. Mechanistically, this antiangiogenic effect of **3a** and **3c** might involve aberrant VEGF/VEGFR (vascular endothelial growth factor receptor) or the destabilization of the pro-angiogenic transcription factor HIF-1alpha [4, 44, 45] as has been discussed for SAHA. However, the exact mechanism and the contribution of conceivable signaling pathways remain to be elucidated.

Conclusions

Our initial objective to combine the antivascular effect of 4,5-diarylimidazoles with the HDAC inhibition cum downstream anticancer effects of cinnamoylhydroxamic acids was largely met. The new (4-aryl-1-methylimidazol-5-yl)cinnamoylhydroxamic acids **3a** and **3c** were more strongly antiproliferative and apoptosis inducing in various cancer and endothelial cells (Ea.hy926 and HUVEC) than the established HDAC inhibitor SAHA

(**1**), while non-malignant fibroblasts were hardly affected. The pronounced cytotoxicity of **3a** against dividing endothelial cells correlates with its strong antiangiogenic activity in the CAM model which exceeds that of SAHA by far. Like SAHA, the new conjugates are pan-HDAC inhibitors which led to an accumulation of hyperacetylated histones and alpha-tubulin in 518A2 melanoma cells, with the consequence of impaired cell migration and invasion.

In combination, the new imidazole hydroxamate conjugates are multimodal anticancer agents that should act on primary tumors of various entities, in particular well vascularized ones, and at the same time should impede the absconding of individual tumor cells and their metastatic spread. Against the background of good tolerance of the parent 4,5-diarylimidazoles in previous animal studies, we expect the new hydroxamate derivatives **3** to be suitable for in vivo xenograft studies, too. All the more so since they are well soluble in water, chemically stable, and very likely orally applicable. Finally, it should be noted that there is ample opportunity for fine-tuning mechanistic subtleties and optimizing the overall efficacy of the new antivascular HDACi of type **3** by adjusting the substituents and the three aromatic rings.

Conflict of interest None.

References

1. Nebbioso A, Carafa V, Benedetti R, Altucci L (2012) Trials with "epigenetic" drugs: an update. Mol Oncol 6:657–682. doi:10.1016/j.molonc.2012.09.004
2. New M, Olzscha H, La Thangue NB (2012) HDAC inhibitor-based therapies: can we interpret the code? Mol Oncol 6:637–656. doi:10.1016/j.molonc.2012.09.003
3. Glozak MA, Seto E (2007) Histone deacetylases and cancer. Oncogene 26:5420–5432. doi:10.1038/sj.onc.1210610
4. Aldana-Masangkay GI, Sakamoto KM (2011) The role of HDAC6 in cancer. J Biomed Biotechnol 2011:1–10. doi:10.1155/2011/875824
5. Vidali G, Boffa LC, Bradbury EM, Allfrey VG (1978) Butyrate suppression of histone deacetylation leads to accumulation of multiacetylated forms of histones H3 and H4 and increased DNase I sensitivity of the associated DNA sequences. Proc Natl Acad Sci 75:2239–2243
6. Minucci S, Pelicci PG (2006) Histone deacetylase inhibitors and the promise of epigenetic (and more) treatments for cancer. Nat Rev Cancer 6:38–51. doi:10.1038/nrc1779
7. Paris M, Porcelloni M, Binaschi M, Fattori D (2008) Histone deacetylase inhibitors: from bench to clinic. J Med Chem 51:1505–1529. doi:10.1021/jm7011408
8. Mai A, Altucci L (2009) Epi-drugs to fight cancer: from chemistry to cancer treatment, the road ahead. Int J Biochem Cell Biol 41:199–213. doi:10.1016/j.biocel.2008.08.020
9. Dokmanovic M, Clarke C, Marks PA (2007) Histone deacetylase inhibitors: overview and perspectives. Mol Cancer Res 5:981–989. doi:10.1158/1541-7786.MCR-07-0324
10. Richon VM, Emiliani S, Verdin E et al (1998) A class of hybrid polar inducers of transformed cell differentiation inhibits histone deacetylases. Proc Natl Acad Sci 95:3003–3007
11. Marks PA (2007) Discovery and development of SAHA as an anticancer agent. Oncogene 26:1351–1356. doi:10.1038/sj.onc.1210204
12. Maiso P, Carvajal-Vergara X, Ocio EM et al (2006) The histone deacetylase inhibitor LBH589 is a potent antimyeloma agent that overcomes drug resistance. Cancer Res 66:5781–5789
13. Plumb JA, Finn PW, Williams RJ et al (2003) Pharmacodynamic response and inhibition of growth of human tumor xenografts by the novel histone deacetylase inhibitor PXD101. Mol Cancer Ther 2:721–728
14. Ellis L, Hammers H, Pili R (2009) Targeting tumor angiogenesis with histone deacetylase inhibitors. Cancer Lett 280:145–153. doi:10.1016/j.canlet.2008.11.012
15. Kim H-J, Bae S-C (2011) Histone deacetylase inhibitors: molecular mechanisms of action and clinical trials as anti-cancer drugs. Am J Transl Res 3:166
16. Qian DZ (2006) Targeting tumor angiogenesis with histone deacetylase inhibitors: the hydroxamic acid derivative LBH589. Clin Cancer Res 12:634–642. doi:10.1158/1078-0432.CCR-05-1132
17. Fantin VR, Richon VM (2007) Mechanisms of resistance to histone deacetylase inhibitors and their therapeutic implications. Clin Cancer Res 13:7237–7242. doi:10.1158/1078-0432.CCR-07-2114
18. Wang J, Pursell NW, Samson MES et al (2013) Potential advantages of CUDC-101, a multitargeted HDAC, EGFR, and HER2 inhibitor, in treating drug resistance and preventing cancer cell migration and invasion. Mol Cancer Ther 12:925–936. doi:10.1158/1535-7163.MCT-12-1045
19. Mahboobi S, Dove S, Sellmer A et al (2009) Design of chimeric histone deacetylase- and tyrosine kinase-inhibitors: a series of imatinib hybrides as potent inhibitors of wild-type and mutant BCR-ABL, PDGF-Rβ, and histone deacetylases. J Med Chem 52:2265–2279. doi:10.1021/jm800988r
20. Gryder BE, Rood MK, Johnson KA et al (2013) Histone deacetylase inhibitors equipped with estrogen receptor modulation activity. J Med Chem 56:5782–5796. doi:10.1021/jm400467w
21. Guerrant W, Patil V, Canzoneri JC et al (2013) Dual-acting histone deacetylase-topoisomerase I inhibitors. Bioorg Med Chem Lett 23:3283–3287. doi:10.1016/j.bmcl.2013.03.108
22. Biersack B, Effenberger K, Schobert R, Ocker M (2010) Oxazole-bridged combretastatin a analogues with improved anticancer properties. ChemMedChem 5:420–427. doi:10.1002/cmdc.200900477
23. Schobert R, Biersack B, Dietrich A et al (2010) 4-(3-Halo/amino-4,5-dimethoxyphenyl)-5-aryloxazoles and -*N*-methylimidazoles that are cytotoxic against combretastatin a resistant tumor cells and vascular disrupting in a cisplatin resistant germ cell tumor model. J Med Chem 53:6595–6602. doi:10.1021/jm100345r
24. Di Fazio P, Lingelbach S, Schobert R, Biersack B (2014) 4,5-Diaryl imidazoles with hydroxamic acid appendages as anti-hepatoma agents. Invest New Drugs. doi:10.1007/s10637-014-0188-0
25. Shimada Y, Imamura M, Wagata T et al (1992) Characterization of 21 newly established esophageal cancer cell lines. Cancer 69:277–284
26. Sutter AP, Höpfner M, Huether A et al (2006) Targeting the epidermal growth factor receptor by erlotinib (Tarceva™) for the treatment of esophageal cancer. Int J Cancer 118:1814–1822. doi:10.1002/ijc.21512
27. Evers BM, Ishizuka J, Townsend CM, Thompson JC (1994) The human carcinoid cell line, BON: a model system for the study of carcinoid tumors. Ann N Y Acad Sci 733:393–406. doi:10.1111/j.1749-6632.1994.tb17289.x

28. Gloesenkamp CR, Nitzsche B, Ocker M et al (2011) AKT inhibition by triciribine alone or as combination therapy for growth control of gastroenteropancreatic neuroendocrine tumors. Int J Oncol 40:876–888. doi:10.3892/ijo.2011.1256
29. Gloesenkamp C, Nitzsche B, Lim AR et al (2012) Heat shock protein 90 is a promising target for effective growth inhibition of gastrointestinal neuroendocrine tumors. Int J Oncol 40:1659–1667. doi:10.3892/ijo.2012.1328
30. Hofmann UB, Houben R, Bröcker E-B, Becker JC (2005) Role of matrix metalloproteinases in melanoma cell invasion. Biochimie 87:307–314. doi:10.1016/j.biochi.2005.01.013
31. Boyden S (1962) The chemotactic effect of mixtures of antibody and antigen on polymorphonuclear leucocytes. J Exp Med 115:453–466
32. Entschladen F, Drell TL, Lang K et al (2005) Analysis methods of human cell migration. Exp Cell Res 307:418–426. doi:10.1016/j.yexcr.2005.03.029
33. Albini A, Iwamoto Y, Kleinman HK et al (1987) A rapid in vitro assay for quantitating the invasive potential of tumor cells. Cancer Res 47:3239–3245
34. Nitzsche B, Gloesenkamp C, Schrader M et al (2010) Novel compounds with antiangiogenic and antiproliferative potency for growth control of testicular germ cell tumours. Br J Cancer 103:18–28. doi:10.1038/sj.bjc.6605725
35. Baradari V, Huether A, Hopfner M et al (2006) Antiproliferative and proapoptotic effects of histone deacetylase inhibitors on gastrointestinal neuroendocrine tumor cells. Endocr Relat Cancer 13:1237–1250. doi:10.1677/erc.1.01249
36. Kim MS, Yamashita K, Baek JH et al (2006) *N*-methyl-D-aspartate receptor type 2B is epigenetically inactivated and exhibits tumor-suppressive activity in human esophageal cancer. Cancer Res 66:3409–3418
37. Zhang Y, Li N, Caron C et al (2003) HDAC-6 interacts with and deacetylates tubulin and microtubules in vivo. EMBO J 22:1168–1179
38. Hubbert C, Guardiola A, Shao R et al (2002) HDAC6 is a microtubule-associated deacetylase. Nature 417:455–458. doi:10.1038/417455a
39. Matsuyama A, Shimazu T, Sumida Y et al (2002) In vivo destabilization of dynamic microtubules by HDAC6-mediated deacetylation. EMBO J 21:6820–6831
40. Sadoul K, Wang J, Diagouraga B, Khochbin S (2011) The tale of protein lysine acetylation in the cytoplasm. J Biomed Biotechnol 2011:1–15. doi:10.1155/2011/970382
41. Kim SC, Sprung R, Chen Y et al (2006) Substrate and functional diversity of lysine acetylation revealed by a proteomics survey. Mol Cell 23:607–618. doi:10.1016/j.molcel.2006.06.026
42. Zhang X, Yuan Z, Zhang Y et al (2007) HDAC6 modulates cell motility by altering the acetylation level of cortactin. Mol Cell 27:197–213. doi:10.1016/j.molcel.2007.05.033
43. Friedl P, Wolf K (2003) Tumour-cell invasion and migration: diversity and escape mechanisms. Nat Rev Cancer 3:362–374. doi:10.1038/nrc1075
44. Deroanne CF, Bonjean C, Servotte S et al (2002) Histone deacetylases inhibitors as anti-angiogenic agents altering vascular endothelial growth factor signaling. Oncogene 21:427–436
45. Jeong J-W, Bae M-K, Ahn M-Y et al (2002) Regulation and destabilization of HIF-1α by ARD1-mediated acetylation. Cell 111:709–720

- Electronic Supplementary Material -

Biological evaluation of 4,5-diaryl imidazoles with hydroxamic acid appendages as novel dual mode anticancer agents

Cancer Chemotherapy and Pharmacology

Katharina Mahal • Sebastian Schruefer • Gustav Steinemann • Franziska Rausch • Rainer Schobert • Bernhard Biersack • Michael Höpfner

Affiliations and addresses of authors:

Katharina Mahal, Sebastian Schruefer, Rainer Schobert, Bernhard Biersack

Organic Chemistry Laboratory, University Bayreuth, 95440 Bayreuth, Germany

Gustav Steinemann, Franziska Rausch, Michael Höpfner

Institute of Physiology, Charité-Universitätsmedizin Berlin, 10117 Berlin, Germany

Corresponding authors:

Bernhard Biersack, Organic Chemistry Laboratory, University Bayreuth, 95440 Bayreuth, Germany. Phone: +49(0)921 552673. Fax: +49(0)921 552671. E-mail: bernhard.biersack@uni-bayreuth.de

Michael Höpfner, Institute of Physiology, Charité-Universitätsmedizin Berlin, Virchowweg 6, 10117 Berlin, Germany. E-mail: michael.hoepfner@charite.de

TOC

Chemistry

General

Melting points were recorded using a Gallenkamp apparatus and are uncorrected. IR: Perkin-Elmer Spectrum One FT-IR spectrophotometer equipped with an ATR sampling unit. NMR: Bruker Avance 300 spectrometer; chemical shifts are given in parts per million (δ) downfield from Me_4Si as internal standard; coupling constants (*J*) are given in Hz. MS: Varian MAT 311A (EI). ESI-MS: Waters UPLC-Q-TOF. Microanalyses indicated by the symbols of the elements were within ± 0.2% of the theoretical values for all new compounds. The starting compounds and pure solvents were purchased from the usual sources and were used without further purification. Merck silica gel 60 (230-400 mesh) was used for column chromatography.

Synthetic procedures and reaction schemes

The hydroxamates **6a-d** were prepared starting with a van-Leusen three-component reaction of TosMIC reagent **5a-d** [S1] with *t*-butyl 4-formylcinnamate and methyl amine to give the respective 1-methyl-4-phenyl-5-*p*-cinnamoate. These were treated with TFA to afford the corresponding carboxylic acids which in turn were reacted in the presence of EDCI with tetrahydropyranyloxyamine to give the O-THP protected hydroxamic acids **6a-d** (Scheme S1). The *N*-hydroxamic acids **3a-d** were obtained by deprotection of **6a-d** with HCl in dioxane [S2].

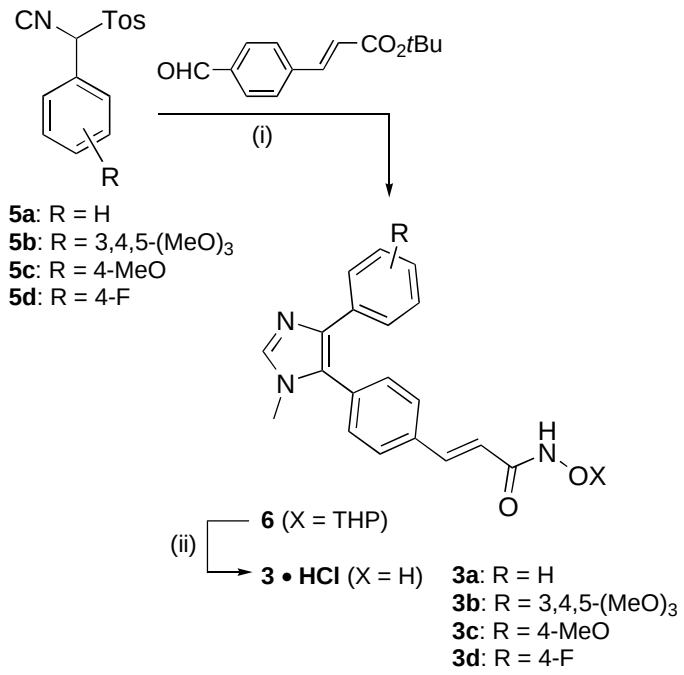

Scheme S1 Synthesis of (4-aryl-1-methylimidazol-5-yl)cinnamylhydroxamic acids 3a-d. Reagents and conditions: (i) a) $MeNH_2$, t-BuOH, reflux, 2h, then **5**, K_2CO_3, *t*-BuOH, reflux, 3h; b) TFA, CH_2Cl_2, rt, 1 h; c) THPO-NH_2, Et_3N, EDCI, DMAP, CH_2Cl_2, rt, 24 h; (ii) 4M HCl/dioxane, dioxane, rt, 1 h

The regioisomer **3e** of compound **3a** and a 4-phenyloxazole analogue **4** were also synthesized from TosMIC reagent **5a** for an activity comparison with the imidazoles **3**. Compound **3e** was prepared analogously to **3a** from *t*-butyl 3-formylcinnamate. Oxazole **7** was obtained by reaction of **5a** with *t*-butyl 4-formylcinnamate and K_2CO_3, followed by cleavage of the so formed ester and subsequent amidation of the resulting carboxylic acid with THP-protected hydroxyl amine. Hydroxamic acid **4** was finally liberated under acidic conditions (Scheme S2).

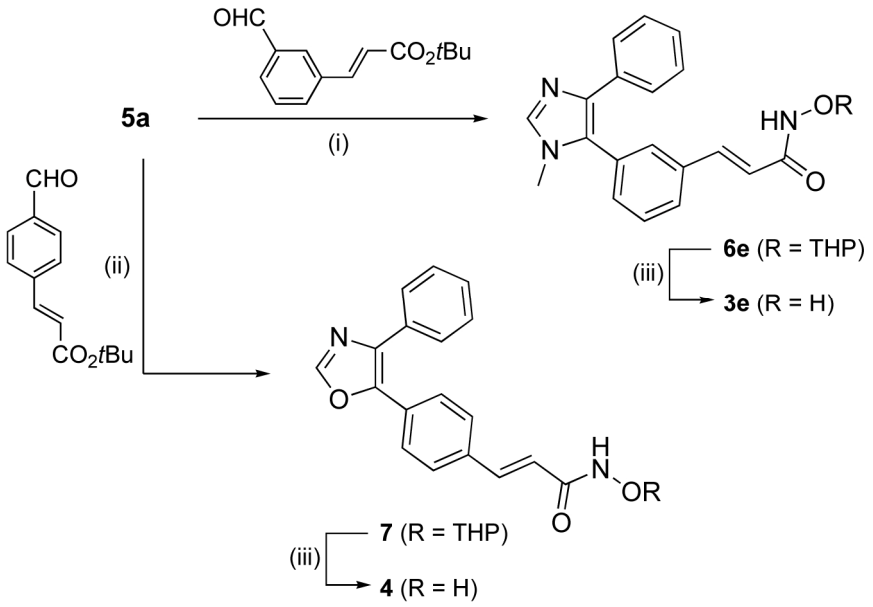

Scheme S2 Synthesis of cinnamylhydroxamic acids 3e and 4. Reagents and conditions: (i) a) $MeNH_2$, *t*-BuOH, reflux, 2h, then **5a**, K_2CO_3, *t*-BuOH, reflux, 3h; b) TFA, CH_2Cl_2, rt, 1 h; c) THPO-NH_2, Et_3N, EDCI, DMAP, CH_2Cl_2, rt, 24 h; (ii) a) K_2CO_3, *t*-BuOH, reflux, 2h; b) TFA, CH_2Cl_2, rt, 1 h; c) THPO-NH_2, Et_3N, EDCI, DMAP, CH_2Cl_2, rt, 24 h; (iii) 4M HCl/dioxane, dioxane, rt, 1 h

Characterization of new compounds 3 and 4

1-Methyl-4-phenyl-5-(4'-tetrahydropyranyloxyaminocarbonyl-ethenyl-phenyl)-imidazole (6a) (typical procedure)

A mixture of 4-formyl-*t*-butylcinnamate (97 mg, 0.42 mmol) and 33% $MeNH_2$/ethanol (260 µL, 2.10 mmol) in *t*-butanol (15 mL) was refluxed for 2 h. After cooling down to room temperature, **5a** (110 mg, 0.40 mmol) and K_2CO_3 (500 mg, 3.62 mmol) were added and the reaction mixture was refluxed for 5 h. The solvent was evaporated, the residue diluted with ethyl acetate, washed with water and brine, dried over Na_2SO_4, filtered and concentrated in vacuum. The residue was purified by column chromatography (silica gel 60, ethyl acetate/methanol 95:5) giving the *t*-butylcinnamoylimidazole intermediate as yellow oil. Yield: 90 mg (0.25 mmol, 60%); R_f = 0.76 (ethyl acetate / methanol, 9:1); IR (ATR): ν_{max} = 2982, 1706, 1634, 1601, 1512, 1481, 1456, 1443, 1367, 1321, 1285, 1249, 1206, 1143, 1123, 1069, 1041, 1014, 983, 973, 952, 915, 873, 831, 814, 778, 766, 720, 698 cm^{-1}; ^1H NMR (300

MHz, $CDCl_3$): δ = 1.53 (s, 9H), 3.50 (s, 3H), 6.40 (d, *J* = 16.0 Hz, 1H,), 7.1-7.2 (m, 3 H), 7.22 (d, *J* = 16.0 Hz, 1H), 7.32 (d, *J* = 8.2 Hz, 2H), 7.4-7.6 ppm (m, 5H); ^{13}C NMR (75.5 MHz, $CDCl_3$): δ = 28.1, 32.2, 80.6, 121.0, 126.5, 126.7, 128.1, 128.4, 130.9, 132.0, 134.5, 134.7, 137.8, 142.5, 143.5, 166.0 ppm.

The intermediate was dissolved in CH_2Cl_2 (3 mL), treated with TFA (2 mL) and stirred at room temperature for 1 h. The solvent was evaporated, the residue was dried in vacuum and used for the next step without further purification. It was dissolved in dry CH_2Cl_2 and EDCI (126 mg, 0.65 mmol), DMAP (24 mg, 0.18 mmol), triethyl amine (150 µL, 0.71 mmol) and tetrahydropyranyl hydroxylamine (91 mg, 0.78 mmol) were added. After stirring at room temperature for 24 h, the solvent was evaporated and the residue was purified by column chromatography (silica gel 60, ethyl acetate / methanol, 9:1). Yield: 70 mg (0.17 mmol, 64%), R_f = 0.41 (ethyl acetate / methanol, 9:1); IR (ATR): ν_{max} = 3099, 2937, 2873, 1672, 1633, 1601, 1512, 1484, 1387, 1338, 1318, 1258, 1201, 1184, 1129, 1111, 1106, 1047, 1020, 979, 953, 893, 871, 832, 816, 773, 718, 695 cm^{-1}; ^{1}H NMR (300 MHz, MeOD): δ = 1.6-1.9 (m, 6H), 3.56 (s, 3H), 3.6-3.7 (m, 1H), 4.0-4.1 (m, 1H), 4.9-5.0 (m, 1H), 6.52 (d, *J* = 15.9 Hz, 1H), 7.1-7.2 (m, 3H), 7.3-7.4 (m, 5H), 7.5-7.6 (m, 3H), 7.69 ppm (s, 1H); ^{13}C NMR (75.5 MHz, MeOD): δ = 17.7, 24.4, 27.3, 31.6, 61.5, 101.7, 117.5, 126.3, 126.5, 127.6, 127.8, 128.0, 130.4, 130.8, 133.2, 134.6, 137.4, 137.7, 139.9, 163.9 ppm.

1-Methyl-4-(3,4,5-trimethoxyphenyl)-5-(4'-tetrahydropyranyloxy-aminocarbonylethenylphenyl)-imidazole (6b):

A mixture of 4-formyl-*t*-butylcinnamate (97 mg, 0.42 mmol) and 33% $MeNH_2$/ethanol (260 µL, 2.10 mmol) in *t*-butanol (15 mL) was refluxed for 2 h. After cooling down to room temperature, **5b** (150 mg, 0.42 mmol) and K_2CO_3 (500 mg, 3.62 mmol) were added and the reaction mixture was refluxed for 4 h. The solvent was evaporated, the residue diluted with

ethyl acetate, washed with water and brine, dried over Na_2SO_4, filtered and concentrated in vacuum. The residue was purified by column chromatography (silica gel 60, ethyl acetate/methanol 9:1) giving 1-methyl-4-(3,4,5-trimethoxyphenyl)-5-(4-tert-butoxycarbonyl-ethenylphenyl)imidazole as yellow oil. Yield: 120 mg (0.27 mmol, 64%); R_f = 0.64 (ethyl acetate / methanol, 9:1); IR (ATR): ν_{max} 2978, 2935, 2831, 1702, 1635, 1604, 1586, 1514, 1494, 1462, 1414, 1393, 1367, 1324, 1235, 1210, 1149, 1123, 995, 911, 856, 833, 771, 729, 656, 558, 533 cm^{-1}; ^1H NMR (300 MHz, $CDCl_3$): δ 1.44 (s, 9H), 3.40 (s, 3H), 3.51 (s, 6H), 3.69 (s, 3H), 6.33 (d, J = 16.1 Hz, 1H), 6.62 (s, 2H), 7.28 (d, J = 8.2 Hz, 2H), 7.4-7.6 (m, 4H); ^{13}C NMR (75.5 MHz, $CDCl_3$): δ 27.9, 32.0, 55.4, 60.5, 80.5, 103.3, 120.9, 127.7, 128.1, 129.7, 131.0, 132.0, 134.6, 136.4, 137.4, 138.1, 142.1, 152.7, 165.8.

The *t*-butyl ester (120 mg, 0.27 mmol) was dissolved in CH_2Cl_2 (3 mL), treated with TFA (2 mL) and stirred at room temperature for 1 h. The solvent was evaporated, the residue was dried in vacuum and used for the next step without further purification. It was dissolved in dry CH_2Cl_2 and EDCI (126 mg, 0.65 mmol), DMAP (24 mg, 0.18 mmol), triethyl amine (150 µL, 0.71 mmol) and tetrahydropyranyl hydroxylamine (91 mg, 0.78 mmol) were added. After stirring at room temperature for 24 h, the solvent was evaporated and the residue was purified by column chromatography (silica gel 60, ethyl acetate / methanol, 9:1). Yield: 80 mg (0.16 mmol, 60%); R_f = 0.35 (ethyl acetate / methanol, 9:1); IR (ATR): ν_{max} 2955, 2831, 1666, 1631, 1588, 1515, 1464, 1416, 1368, 1333, 1262, 1238, 1203, 1173, 1125, 1034, 997, 946, 895, 830, 774, 727, 657 cm^{-1}; ^1H NMR (300 MHz, $CDCl_3$): δ 1.5-1.7 (m, 3H), 1.7-1.9 (m, 3H), 3.45 (s, 3H), 3.57 (s, 6H), 3.6-3.7 (m, 1H), 3.72 (s, 3H), 3.9-4.0 (m, 1H), 5.0-5.1 (m, 1H), 6.5-6.6 (m, 1H), 6.66 (s, 2H), 7.26 (d, J = 8.0 Hz, 2H), 7.4-7.5 (m, 2H), 7.56 (s, 1H, 7.66 (d, J = 15.6 Hz, 1H), 10.1-10.2 (br s, 1H); ^{13}C NMR (75.5 MHz, $CDCl_3$): δ 18.6, 24.9, 28.0, 32.2, 55.6, 60.7, 62.5, 102.5, 103.6, 118.4, 127.9, 128.3, 129.6, 131.1, 131.8, 135.1, 136.6, 137.6, 138.2, 152.9, 163.6.

1-Methyl-4-(4-methoxyphenyl)-5-(4'-tetrahydropyranyloxyamino-carbonylethenyl-phenyl)imidazole (6c):

A mixture of 4-formyl-*t*-butylcinnamate (97 mg, 0.42 mmol) and 33% $MeNH_2$/ethanol (260 µL, 2.10 mmol) in *t*-butanol (15 mL) was refluxed for 2 h. After cooling down to room temperature, **5c** (126 mg, 0.42 mmol) and K_2CO_3 (500 mg, 3.62 mmol) were added and the reaction mixture was refluxed for 4 h. The solvent was evaporated, the residue diluted with ethyl acetate, washed with water and brine, dried over Na_2SO_4, filtered and concentrated in vacuum. The residue was purified by column chromatography (silica gel 60, ethyl acetate/methanol 9:1) giving 1-methyl-4-(4-methoxyphenyl)-5-(4-tert-butoxycarbonylethenyl-phenyl)imidazole as yellow oil. Yield: 69 mg (0.21 mmol, 50%); R_f = 0.66 (ethyl acetate / methanol, 9:1); IR (ATR): ν_{max} 2975, 2928, 2833, 1702, 1634, 1611, 1519, 1494, 1457, 1392, 1367, 1323, 1292, 1245, 1209, 1147, 1103, 1032, 981, 952, 910, 872, 832, 798, 729 cm^{-1}; ^1H NMR (300 MHz, $CDCl_3$): δ 1.50 (s, 9H), 3.45 (s, 3H), 3.71 (s, 3H), 6.38 (d, *J* = 16.0 Hz, 1H), 6.71 (d, *J* = 9.0 Hz, 2H), 7.28 (d, *J* = 8.2 Hz, 2H), 7.34 (d, *J* = 9.0 Hz, 2H), 7.5-7.6 (m, 4H); ^{13}C NMR (75.5 MHz, $CDCl_3$): δ 28.2, 32.3, 55.2, 80.7, 113.7, 114.5, 121.0, 127.1, 127.2, 128.1, 128.4, 131.0, 132.2, 134.6, 137.8, 138.7, 142.6, 158.4, 166.1.

The *t*-butyl ester (69 mg, 0.21 mmol) was dissolved in CH_2Cl_2 (3 mL), treated with TFA (2 mL) and stirred at room temperature for 1 h. The solvent was evaporated, the residue was dried in vacuum and used for the next step without further purification. It was dissolved in dry CH_2Cl_2 and EDCI (98 mg, 0.51 mmol), DMAP (19 mg, 0.14 mmol), triethyl amine (117 µL, 0.55 mmol) and tetrahydropyranyl hydroxylamine (71 mg, 0.61 mmol) were added. After stirring at room temperature for 24 h, the solvent was evaporated and the residue was purified by column chromatography (silica gel 60, ethyl acetate / methanol, 9:1). Yield: 44 mg (0.11 mmol, 52%); R_f = 0.40 (ethyl acetate / methanol, 95:5); IR (ATR): ν_{max} 2941, 2861, 1663, 1627, 1519, 1496, 1464, 1442, 1341, 1293, 1246, 1203, 1174, 1129, 1113, 1031, 981, 950,

895, 872, 832, 816, 798, 729 cm^{-1}; ^{1}H NMR (300 MHz, $CDCl_3$): δ 1.5-1.6 (m, 3H), 1.8-1.9 (m, 3H), 3.46 (s, 3H), 3.5-3.6 (m, 1H), 3.68 (s, 3H), 3.9-4.0 (m, 1H), 5.0-5.1 (m, 1H), 6.5-6.6 (m, 1H), 6.70 (d, *J* = 8.9 Hz, 2H), 7.2-7.3 (m, 2H), 7.34 (d, *J* = 8.9 Hz, 2H), 7.4-7.5 (m, 1H), 7.59 (s, 1H), 7.5-7.7 (m, 1H); ^{13}C NMR (75.5 MHz, $CDCl_3$): δ 18.6, 25.0, 28.1, 32.4, 55.1, 62.5, 102.5, 113.6, 117.9, 126.6, 127.3, 128.1, 128.3, 130.9, 131.6, 134.8, 137.7, 138.3, 158.5, 163.6.

1-Methyl-4-(4-fluorophenyl)-5-(4'-tetrahydropyranyloxyamino-carbonylethenylphenyl)-imidazole (6d):

A mixture of 4-formyl-*t*-butylcinnamate (97 mg, 0.42 mmol) and 33% $MeNH_2$/ethanol (260 µL, 2.10 mmol) in *t*-butanol (15 mL) was refluxed for 2 h. After cooling down to room temperature, **5d** (121 mg, 0.42 mmol) and K_2CO_3 (500 mg, 3.62 mmol) were added and the reaction mixture was refluxed for 4 h. The solvent was evaporated, the residue diluted with ethyl acetate, washed with water and brine, dried over Na_2SO_4, filtered and concentrated in vacuum. The residue was purified by column chromatography (silica gel 60, ethyl acetate/methanol 9:1) giving 1-methyl-4-(4-fluorophenyl)-5-(4-tert-butoxycarbonylethenyl-phenyl)imidazole as yellow oil. Yield: 65 mg (0.21 mmol, 50%); R_f = 0.63 (ethyl acetate / methanol, 95:5); IR (ATR): ν_{max} 2979, 2932, 1702, 1635, 1607, 1566, 1517, 1493, 1456, 1409, 1392, 1367, 1323, 1212, 1146, 1092, 1038, 1014, 981, 952, 910, 873, 834, 813, 767, 728; ^{1}H NMR (300 MHz, $CDCl_3$): δ 1.51 (s, 9H), 3.48 (s, 3H), 6.39 (d, *J* = 16.0 Hz, 1H), 6.8-6.9 (m, 2H), 7.28 (d, *J* = 8.3 Hz, 2H), 7.3-7.4 (m, 2H), 7.5-7.6 (m, 4H); ^{13}C NMR (75.5 MHz, $CDCl_3$): δ 28.1, 32.3, 80.7, 114.9 (C-F), 115.2 (C-F), 115.6, 121.2, 127.8, 128.3 (C-F), 128.4 (C-F), 129.4, 129.5, 130.5, 130.8, 131.7, 132.5, 134.8, 137.8, 137.9, 142.4, 160.0 (C-F), 163.3 (C-F), 166.0.

The *t*-butyl ester (65 mg, 0.21 mmol) was dissolved in CH_2Cl_2 (3 mL), treated with TFA (2

mL) and stirred at room temperature for 1 h. The solvent was evaporated, the residue was dried in vacuum and used for the next step without further purification. It was dissolved in dry CH_2Cl_2 and EDCI (98 mg, 0.51 mmol), DMAP (19 mg, 0.14 mmol), triethyl amine (117 µL, 0.55 mmol) and tetrahydropyranyl hydroxylamine (71 mg, 0.61 mmol) were added. After stirring at room temperature for 24 h, the solvent was evaporated and the residue was purified by column chromatography (silica gel 60). Yield: 46 mg (0.12 mmol, 57%); R_f = 0.42 (ethyl acetate / methanol, 9:1); IR (ATR): ν_{max} 3154, 2946, 2865, 1663, 1626, 1518, 1491, 1335, 1216, 1204, 1155, 1112, 1032, 948, 892, 869, 834, 814, 728 cm^{-1}; ^1H NMR (300 MHz, $CDCl_3$): δ 1.5-1.6 (m, 3H), 1.7-1.9 (m, 3H), 3.47 (s, 3H), 3.6-3.7 (m, 1H), 3.9-4.0 (m, 1H), 5.0-5.1 (m, 1H), 6.3-6.5 (m, 1H), 6.8-6.9 (m, 2H), 7.2-7.5 (m, 6H), 7.56 (s, 1H), 7.7-7.8 (m, 1H); ^{13}C NMR (75.5 MHz, $CDCl_3$): δ 18.7, 24.8, 24.9, 27.8, 28.1, 32.3, 62.6, 102.6, 114.9 (C-F), 115.2 (C-F), 118.0, 127.9, 128.4 (C-F), 128.5 (C-F), 130.3, 130.4, 130.8, 131.5, 135.0, 137.9, 160.1 (C-F), 162.0, 163.3 (C-F).

1-Methyl-4-phenyl-5-(3'-tetrahydropyranyloxyaminocarbonylethenyl-phenyl)-imidazole (6e):

A mixture of 3-formyl-*t*-butylcinnamate (97 mg, 0.42 mmol) and 33% $MeNH_2$/ethanol (260 µL, 2.10 mmol) in *t*-butanol (15 mL) was refluxed for 2 h. After cooling down to room temperature, **5a** (110 mg, 0.40 mmol) and K_2CO_3 (500 mg, 3.62 mmol) were added and the reaction mixture was refluxed for 4 h. The solvent was evaporated, the residue diluted with ethyl acetate, washed with water and brine, dried over Na_2SO_4, filtered and concentrated in vacuum. The residue was purified by column chromatography (silica gel 60, ethyl acetate/methanol 95:5) giving the intermediate, 1-methyl-4-phenyl-5-(3-tert-butoxycarbonyl-ethenylphenyl)-imidazole as yellow oil. Yield: 98 mg (0.34 mmol, 81%); R_f = 0.53 (ethyl acetate); IR (ATR): ν_{max} 2977, 1702, 1637, 1602, 1505, 1476, 1445, 1420, 1391, 1367, 1319, 1250, 1212, 1146, 1070, 979, 910, 865, 845, 803, 774, 728, 692 cm^{-1}; ^1H NMR (300 MHz,

$CDCl_3$): δ 1.49 (s, 9H), 3.43 (s, 3H), 6.33 (d, J = 16.0 Hz, 1H), 7.1-7.3 (m, 4H), 7.4-7.5 (m, 4H), 7.5-7.6 (m, 3H); ^{13}C NMR (75.5 MHz, $CDCl_3$): δ 28.0, 32.1, 80.6, 121.1, 126.4, 126.5, 127.8, 127.9, 128.0, 129.5, 130.0, 131.3, 132.0, 134.3, 135.4, 137.5, 138.4, 142.5, 165.9.

The *t*-butyl ester (98 mg, 0.34 mmol) was dissolved in CH_2Cl_2 (3 mL), treated with TFA (2 mL) and stirred at room temperature for 1 h. The solvent was evaporated, the residue was dried in vacuum and used for the next step without further purification. It was dissolved in dry CH_2Cl_2 and EDCI (159 mg, 0.83 mmol), DMAP (31 mg, 0.23 mmol), triethyl amine (190 µL, 0.89 mmol) and tetrahydropyranyl hydroxylamine (115 mg, 0.99 mmol) were added. After stirring at room temperature for 24 h, the solvent was evaporated and the residue was purified by column chromatography (silica gel 60, ethyl acetate / methanol, 95:5). Yield: 80 mg (0.20 mmol, 59%); R_f = 0.50 (ethyl acetate / methanol, 95:5); IR (ATR) ν_{max} 3118, 2945, 2865, 1684, 1631, 1603, 1507, 1470, 1442, 1416, 1372, 1352, 1274, 1256, 1206, 1172, 1115, 1074, 1059, 1032, 997, 968, 943, 895, 861, 804, 777, 723, 690 cm^{-1}; ^{1}H NMR (300 MHz, $CDCl_3$): δ 1.5-1.7 (m, 3H), 1.7-1.9 (m, 3H), 3.47 (s, 3H), 3.5-3.6 (m, 1H), 3.9-4.0 (m, 1H), 4.9-5.0 (m, 1H), 6.3-6.4 (m, 1H), 7.1-7.6 (m, 11H); ^{13}C NMR (75.5 MHz, $CDCl_3$): δ 18.1, 24.6, 24.7, 27.6, 27.7, 32.0, 62.0, 62.4, 102.2, 117.9, 126.5, 127.8, 128.0, 129.3, 129.6, 130.5, 131.7, 133.5, 135.4, 137.4, 137.9, 140.3, 163.8.

1-Methyl-4-phenyl-5-(4'-N-hydroxyaminocarbonylethenylphenyl)-imidazole x HCl (3a), (typical procedure)

Compound **6a** (70 mg, 0.17 mmol) was dissolved in CH_2Cl_2/MeOH (5 mL, 4:1) and 4M HCl/dioxane (3 mL) was added. The reaction mixture was stirred at room temperature for 1 h. The solvent was evaporated and the residue was crystallized from ethanol / *n*-hexane. Yield: 50 mg (0.14 mmol, 82%); colorless solid of mp 189-190°C; IR (ATR): ν_{max} = 3142, 2992, 2826, 1655, 1607, 1525, 1500, 1446, 1403, 1345, 1166, 1118, 1050, 1032, 998, 957, 873, 834,

769, 723, 692 cm^{-1}; ^{1}H NMR (300 MHz, DMSO-d_6): δ = 3.68 (s, 3H), 6.63 (d, *J* = 15.9 Hz, 1H), 7.3-7.4 (m, 5H), 7.5-7.6 (m, 3H), 7.74 (d, *J* = 8.2 Hz, 2H), 9.37 (s, 1H), 10.9-11.0 ppm (br s, 1H); ^{13}C NMR (75.5 MHz, DMSO-d_6): δ = 34.1, 121.2, 126.6, 127.1, 128.3, 129.0, 129.2, 129.3, 129.6, 131.3, 136.1, 136.6, 137.0, 162.2 ppm; MS (EI, 70 eV): *m/z* 319 (15) [M^+], 304 (100), 303 (86), 291 (76), 273 (48), 247 (48), 44 (37). Anal. Calcd for $C_{19}H_{18}ClN_3O_2$: C, 64.13; H, 5.10; N, 11.81. Found: C, 64.01; H, 4.95; N, 11.95.

1-Methyl-4-(3,4,5-trimethoxyphenyl)-5-(4'-hydroxyaminocarbonyl-ethenyl-phenyl)-imidazole x HCl (3b):

6b (80 mg, 0.16 mmol) was dissolved in CH_2Cl_2/MeOH (5 mL, 4:1) and 4M HCl/dioxane (3 mL) was added. The reaction mixture was stirred at room temperature for 1 h. The solvent was evaporated and the residue was crystallized from ethanol / *n*-hexane. Yield: 65 mg (0.15 mmol, 94%); off-white solid of mp 192 °C; IR (ATR): ν_{max} 3129, 3007, 2833, 1659, 1621, 1598, 1582, 1553, 1505, 1461, 1454, 1408, 1330, 1279, 1244, 1175, 1122, 1050, 998, 830, 771, 700; ^{1}H NMR (300 MHz, DMSO-d_6): δ3.56 (s, 6H), 3.64 (s, 3H), 3.67 (s, 3H), 6.63 (d, *J* = 15.9 Hz, 1H), 6.74 (s, 2H), 7.5-7.6 (m, 3H), 7.78 (d, *J* = 8.2 Hz, 1H), 9.35 (s, 1H), 10.8-11.0 (br s, 1H); ^{13}C NMR (75.5 MHz, DMSO-d_6): δ 34.1, 55.7, 60.1, 104.6, 121.1, 122.2, 126.9, 128.3, 129.0, 129.5, 131.6, 135.7, 136.8, 137.1, 137.9, 153.0, 162.3; MS (EI) *m/z* 409 (66) [M^+], 394 (100), 379 (35), 364 (15), 50 (46). Anal. Calcd for $C_{22}H_{24}ClN_3O_5$: C, 59.26; H, 5.43; N, 9.42. Found: C, 59.10; H, 5.30; N, 9.62.

1-Methyl-4-(4-methoxyphenyl)-5-(4'-hydroxyaminocarbonylethenyl-phenyl)-imidazole x HCl (3c):

6c (44 mg, 0.11 mmol) was dissolved in CH_2Cl_2/MeOH (5 mL, 4:1) and 4M HCl/dioxane (3 mL) was added. The reaction mixture was stirred at room temperature for 1 h. The solvent

was evaporated and the residue was crystallized from ethanol / *n*-hexane. Yield: 43 mg (0.11 mmol, 100%); off-white solid of mp 189 °C; IR (ATR): ν_{max} 3113, 3048, 2962, 2837, 2622, 1651, 1601, 1514, 1453, 1405, 1342, 1297, 1261, 1185, 1121, 1049, 1028, 998, 983, 872, 825, 799, 761, 735, 710 cm^{-1}; ^{1}H NMR (300 MHz, DMSO-d_6): δ 3.56 (s, 3H), 3.75 (s, 3H), 6.60 (d, J = 15.9 Hz, 1H), 6.96 (d, J = 9.0 Hz, 2H), 7.31 (d, J = 9.0 Hz, 2H), 7.5-7.6 (m, 3H), 7.73 (d, J = 8.2 Hz, 2H), 9.32 (s, 1H), 10.9-11.0 (br s, 1H); ^{13}C NMR (75.5 MHz, DMSO-d_6): δ 34.2, 55.3, 66.4, 114.5, 119.2, 121.1, 126.7, 128.3, 128.9, 131.4, 135.7, 136.2, 160.0, 162.5; MS (EI) *m/z* 349 (5) [M^+], 334 (100), 321 (41), 303 (48), 288 (15), 277 (15), 44 (18). Anal. Calcd for $C_{20}H_{20}ClN_3O_3$: C, 62.26; H, 5.22; N, 10.89. Found: C, 62.10; H, 5.15; N, 10.99.

1-Methyl-4-(4-fluorophenyl)-5-(4'-hydroxyaminocarbonylethenyl-phenyl)-imidazole (3d):

6d (46 mg, 0.12 mmol) was dissolved in CH_2Cl_2/MeOH (5 mL, 4:1) and 4M HCl/dioxane (3 mL) was added. The reaction mixture was stirred at room temperature for 1 h. The solvent was evaporated and the residue was crystallized from ethanol / *n*-hexane. Yield: 35 mg (0.094 mmol, 78%); off-white solid of mp 170 °C; IR (ATR): ν_{max} 3115, 3043, 2995, 2836, 2626, 1654, 1606, 1546, 1512, 1482, 1404, 1371, 1345, 1240, 1168, 1122, 1051, 1032, 1012, 998, 955, 937, 831, 763, 732, 711 cm^{-1}; ^{1}H NMR (300 MHz, DMSO-d_6): δ 3.68 (s, 3H), 6.62 (d, J = 15.9 Hz, 1H), 7.2-7.3 (m, 2H), 7.4-7.6 (m, 5H), 7.74 (d, J = 8.1 Hz, 2H), 9.31 (s, 1H), 10.9-11.1 (br s, 1H); ^{13}C NMR (75.5 MHz, DMSO-d_6): δ 34.1, 115.9 (C-F), 116.2 (C-F), 121.1, 123.8, 126.6, 128.3, 129.1 (C-F), 129.3 (C-F), 129.7, 129.8, 131.3, 136.2, 136.6, 137.0, 160.6 (C-F), 162.3, 163.9 (C-F); MS (EI) *m/z* (%) 337 (15) [M^+], 322 (32), 309 (37), 293 (100), 265 (24), 45 (39). Anal. Calcd for $C_{19}H_{17}ClFN_3O_2$: C, 61.05; H, 4.58; N, 11.24. Found: C, 60.93; H, 4.50; N, 11.37.

1-Methyl-4-phenyl-5-(3'-hydroxyaminocarbonylethenyl-phenyl)-imidazole x HCl (3e):

6e (80 mg, 0.20 mmol) was dissolved in CH_2Cl_2/MeOH (5 mL, 4:1) and 4M HCl/dioxane (3 mL) was added. The reaction mixture was stirred at room temperature for 1 h. The solvent was evaporated and the residue was crystallized from ethanol / *n*-hexane. Yield: 60 mg (0.17 mmol, 85%); off-white solid of mp 228°C; IR (ATR): ν_{max} 3103, 3032, 2857, 2797, 1655, 1606, 1549, 1497, 1474, 1447, 1407, 1334, 1248, 1167, 1148, 1121, 1045, 995, 985, 971, 915, 801, 790, 768, 749, 719, 690, 667 cm^{-1}; ^{1}H NMR (300 MHz, DMSO-d_6): δ 3.68 (s, 3H), 6.55 (d, J = 15.9 Hz, 1H), 7.3-7.4 (m, 5H), 7.4-7.5 (m, 2H), 7.60 (t, J = 7.8 Hz, 1H), 7.72 (s, 1H), 7.78 (d, J = 7.8 Hz, 1H), 9.35 (s, 1H), 10.8-11.0 (br s, 1H); ^{13}C NMR (75.5 MHz, DMSO-d_6): δ 34.1, 111.5, 120.7, 126.8, 127.1, 127.3, 128.8, 129.0, 129.2, 129.7, 130.0, 131.6, 136.0, 137.1, 162.3; MS (EI) *m/z* 319 (23) [M^+], 303 (86). 275 (100), 257 (45), 232 (35), 204 (37), 189 (48). Anal. Calcd for $C_{19}H_{18}ClN_3O_2$: C, 64.13; H, 5.10; N, 11.81. Found: C, 64.00; H, 4.97; N, 11.96.

4-Phenyl-5-(4'-tetrahydropyranyloxyaminocarbonylethenyl-phenyl)-oxazole (7):

A mixture of 4-formyl-*t*-butylcinnamate (97 mg, 0.42 mmol), **5a** (110 mg, 0.40 mmol) and K_2CO_3 (500 mg, 3.62 mmol) in *t*-butanol (15 mL) was refluxed for 4 h. The solvent was evaporated, the residue diluted with ethyl acetate, washed with water and brine, dried over Na_2SO_4, filtered and concentrated in vacuum. The residue was purified by column chromatography (silica gel 60, ethyl acetate / *n*-hexane, 1:4) giving 4-phenyl-5-(4'-tert-butoxycarbonylethenylphenyl)-oxazole as yellow oil. Yield: 120 mg (0.35 mmol, 83%); R_f = 0.50 (ethyl acetate / *n*-hexane, 1:3); IR (ATR) ν_{max} 2976, 2926, 1702, 1634, 1606, 1513, 1477, 1446, 1414, 1392, 1366, 1325, 1286, 1255, 1210, 1145, 1048, 980, 954, 872, 831, 771, 716, 696 cm^{-1}; ^{1}H NMR (300 MHz, $CDCl_3$): δ 1.51 (s, 9H), 6.63 (d, J = 16.0 Hz, 1H), 7.3-7.6 (m, 10H), 7.92 (s, 1H); ^{13}C NMR (75.5 MHz, $CDCl_3$): δ 28.1, 80.5, 120.8, 126.6, 128.0, 128.1,

128.4, 128.6, 129.8, 131.9, 134.8, 135.6, 142.3, 145.0, 149.9, 166.0.

The *t*-butyl ester (120 mg, 0.35 mmol) was dissolved in CH_2Cl_2 (3 mL), treated with TFA (2 mL) and stirred at room temperature for 1 h. The solvent was evaporated, the residue was dried in vacuum and used for the next step without further purification. It was dissolved in dry CH_2Cl_2 and EDCI (126 mg, 0.65 mmol), DMAP (24 mg, 0.18 mmol), triethyl amine (150 µL, 0.71 mmol) and tetrahydropyranyl hydroxylamine (91 mg, 0.78 mmol) were added. After stirring at room temperature for 24 h, the solvent was evaporated and the residue was purified by column chromatography (silica gel 60, ethyl acetate / *n*-hexane, 1:1). Yield: 80 mg (0.21 mmol, 60%); R_f = 0.44 (ethyl acetate / *n*-hexane, 2:1); IR (ATR): ν_{max} 3205, 3124, 3007, 2951, 2870, 1671, 1651, 1614, 1519, 1352, 1342, 1221, 1201, 1183, 1129, 1112, 1092, 1044, 1031, 1019, 990, 956, 940, 889, 862, 814, 772, 696 cm^{-1}; ^1H NMR (300 MHz, $CDCl_3$): δ 1.6-1.9 (m, 6H), 3.6-3.7 (m, 1H), 3.9-4.0 (m, 1H), 4.9-5.0 (m, 1H), 6.3-6.5 (m, 1H), 7.3-7.4 (m, 3H), 7.4-7.5 (m, 2H), 7.6-7.8 (m, 5H), 7.95 (s, 1H), 8.7-8.8 (br s, 1H); ^{13}C NMR (75.5 MHz, $CDCl_3$): δ 18.7, 24.9, 28.1, 62.7, 103.0, 126.8, 128.1, 128.3, 128.5, 128.7, 130.0, 131.9, 134.8, 135.8, 145.1, 150.0, 162.4.

4-Phenyl-5-(4'-N-hydroxyaminocarbonylethenylphenyl)-oxazole (4):

Compound **7** (80 mg, 0.21 mmol) was dissolved in CH_2Cl_2 (5 mL) and 4M HCl/dioxane (3 mL) was added. The reaction mixture was stirred at room temperature for 1 h. The solvent was evaporated and the residue was crystallized from ethanol / *n*-hexane. Yield: 60 mg (0.20 mmol, 95%); colourless solid of mp 124-126 °C; IR (ATR) ν_{max} 3118, 2956, 2851, 2754, 1650, 1587, 1539, 1513, 1443, 1414, 1348, 1291, 1254, 1207, 1116, 1079, 1061, 999, 986, 872, 832, 770, 733, 696 cm^{-1}; ^1H NMR (300 MHz, DMSO-d_6): δ 6.64 (d, J = 16.0 Hz, 1H), 7.4-7.5 (m, 4H), 7.6-7.7 (m, 7H), 8.56 (s, 1H); ^{13}C NMR (75.5 MHz, $CDCl_3$): δ 120.2, 126.8, 127.7, 128.1, 128.5, 128.8, 131.8, 134.7, 135.4, 137.3, 144.5, 151.7, 162.5; MS (EI) *m/z* 306

(5), 291 (100), 274 (22), 263 (27), 245 (23), 232 (7), 217 (14), 189 (35), 165 (18), 45 (33). Anal. Calcd for $C_{18}H_{14}ClN_2O_3$: C, 70.58; H, 4.61; N, 9.15. Found: C, 70.46; H, 4.55; N, 9.22.

Biological assays

Cell proliferation assay (MTT assay) [S3]

The tetrazolium salt MTT (3-(4,5-dimethylthiazol-2-yl)-2,5-diphenyl-tetrazolium bromide, Carl Roth) was used to determine the percentage of viable cells by reduction of MTT to a violet formazan. 518A2 melanoma, HCT-1116 colon carcinoma HT-29 colon adenocarcinoma, MCF-7/Topo mammacarcinoma, KB-V1/Vbl cervix carcinoma cells ($5x10^3$ cells/well), Ea.hy926 and primary endothelial cells (HUVEC, $1x10^4$ cells/well) and non-malignant chicken heart fibroblasts (CHF, $1x10^4$ cells/well) were seeded on 96-well cell culture plates and allowed to adhere for 24 h (37 °C, 5% CO2, 95% humidity). Incubation with the test compounds **3a-e** and **4** (dilution series ranging from 100 µM to 5 pM in ddH_2O) was then continued for 24 h or 72 h. Solvent controls (DMSO) were treated identically. MTT in PBS (5 mg/mL in PBS) was added to a final MTT concentration of 0.05%. After 2 h incubation, the microplates were centrifuged (300 g, 4 °C, 5 min) and the supernatant medium was removed. Cell lysis and dissolving of the precipitated formazan crystals was performed by adding 30 µl of a SDS-DMSO solution (10% SDS (w/v), 0.6% acetic acid in DMSO) to each well. The absorbance at wavelengths 570 and 630 nm (background) was measured using an automatic microplate reader (Tecan). All experiments were carried out at least in triplicates, the percentage of viable cells quoted was calculated as the mean ± S.D. with respect to the controls set to 100%.

Determination of cell number

Drug induced changes in cell number were determined by crystal violet staining, as previously described [S4]. In brief, cells in 96-well plates were fixed with 1% glutaraldehyde and then stained with 0.1% crystal violet. Unbound dye was removed by washing the wells with ddH_2O. Bound crystal violet was solubilized with 0.2% Triton-X-100. The absorption increasing linearly with the cell number was analyzed at 570 nm using an ELISA-plate reader. All experiments were carried out at least in triplicates, the percentage of viable cells quoted was calculated as the mean ± S.D. with respect to the controls set to 100%.

Image adjustment and software used for image processing

ImageJ and Photoshop CS5 software were used for digital image processing which means uniformly applied contrast/brightness and resolution settings. Overlay images of original brightfield and chemiluminescence Western Blot images were done with Photoshop CS5. Relevant bands were cropped and presented in Figure 3 with the respective molecular weight indicated. All western blot pictures included in the article are representative for at least two independent experiments. For fluorescence microscopy figure preparation, only uncropped images representing relevant areas of the microscope slides and of at least two independent experiments were used. ImageJ and Photoshop CS5 software were used for uniformly applied contrast/brightness and resolution settings as well as for scale bar calculation.

Determination of direct HDAC inhibition

Table S1 Inhibition of histone deacetylase activity (IC_{50} [µM] [a]) by SAHA (**1**) and the imidazoles **3a** and **3c** as determined by measuring the fluorescence upon conversion of a HDAC substrate

	compound		
	SAHA (1)	**3a**	**3c**
HeLa nuclear extract	0.231 ± 0.036	0.234 ± 0.011	1.078 ± 0.05

[a] IC_{50} (µM) values from dose-response curves obtained by the amount of fluorogenic substrate (25 µM Fluor-de-Lys) with respect to DMSO controls are shown as the mean of three independent experiments ± S.D. Incubation time 60 min.

Western blot analyses of increased histone acetylation

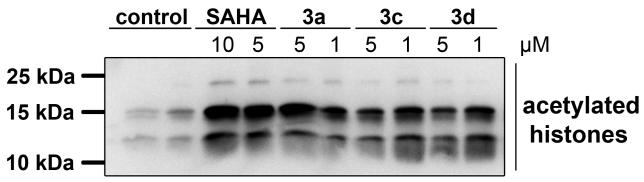

Fig. S1 Increase of histone acetylation in 518A2 melanoma cells after treatment with HDAC inhibitors. Cell lysates (10 µg total protein as determined by a standard Bradford assay; Pierce/Fisher Scientific) of 518A2 cells incubated with SAHA (5 µM, 10 µM, 24 h) or the derivatives **3a**, **3c** or **3d** (1 µM, 5 µM, 24 h) were subjected to 20% SDS-PAGE followed by visualization of unspecific histone (H2A/H2B, H3 and H4) acetylation over a molecular weight range from 25 kDa to 10 kDa using an antibody detecting acetyl-lysine residues (acetylated-lysine rabbit polyclonal antibody, Cell Signaling Technology)

Unprocessed western blot images (pertinent to Figure 3A)

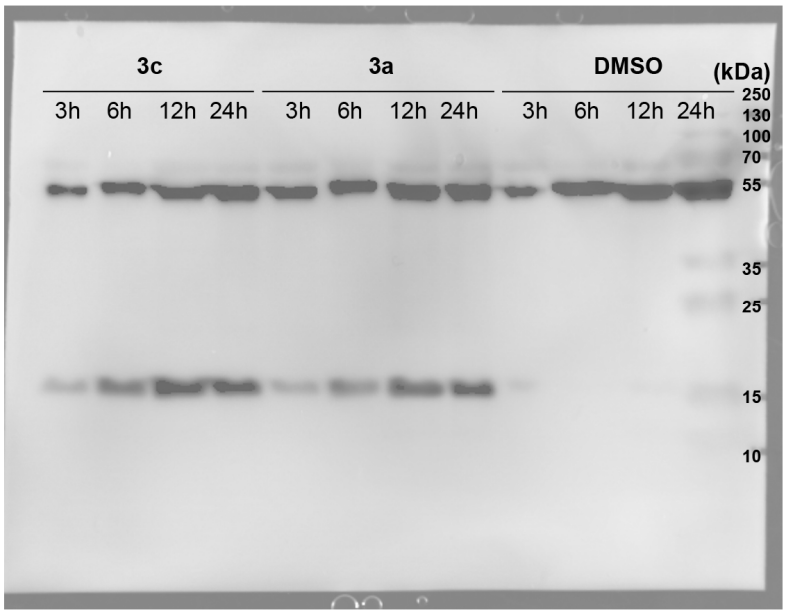

Fig. S2 Increase of protein acetylation in 518A2 melanoma cells after treatment with SAHA, **3a** or **3c.** Upper membrane: Overlay of brightfield and chemiluminescence images of the PVDF membrane after incubation with alpha-tubulin (55 kDa, loading control) and acetyl-histone H2B (ca. 14 kDa) primary antibodies. Images recorded with a LAS-3000 image reader (Fujifilm), PageRuler Plus Prestained Protein Ladder (Fermentas/Fisher Scientific) was used a molecular weight marker

Unprocessed western blot images (pertinent to Figure 3A, SAHA controls)

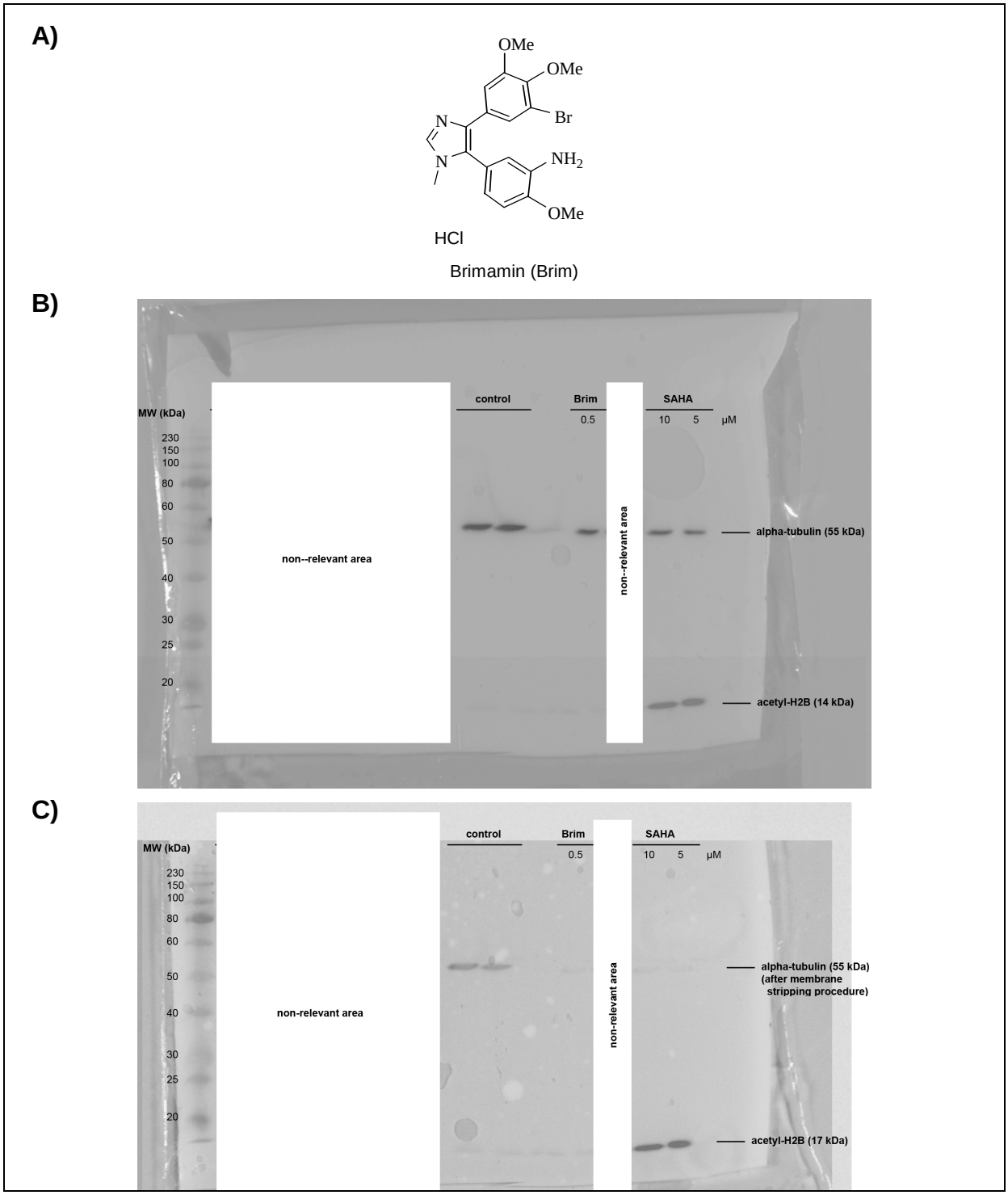

Fig. S3 Increase of histone H2B acetylation in 518A2 melanoma cells after treatment with SAHA, **3a** or **3c** or the structure-related, tubulin-binding agent Brimamin (Brim). **A)** Structure of Brimamin. **B)** Overlay of brightfield and chemiluminescence images of the PVDF membrane after incubation with alpha-tubulin (55 kDa, loading control) and acetyl-histone H2B (ca. 14 kDa) primary antibodies. **C)** Overlay of brightfield and chemiluminescence images of the PVDF membrane after treatment with the acetyl-histone H2B primary antibody alone (residual anti-alpha-tubulin removed by a stripping procedure). PageRuler Plus Prestained Protein Ladder (Fermentas/Fisher Scientific) was used a molecular weight marker

Unprocessed western blot images (pertinent to Figure 3B)

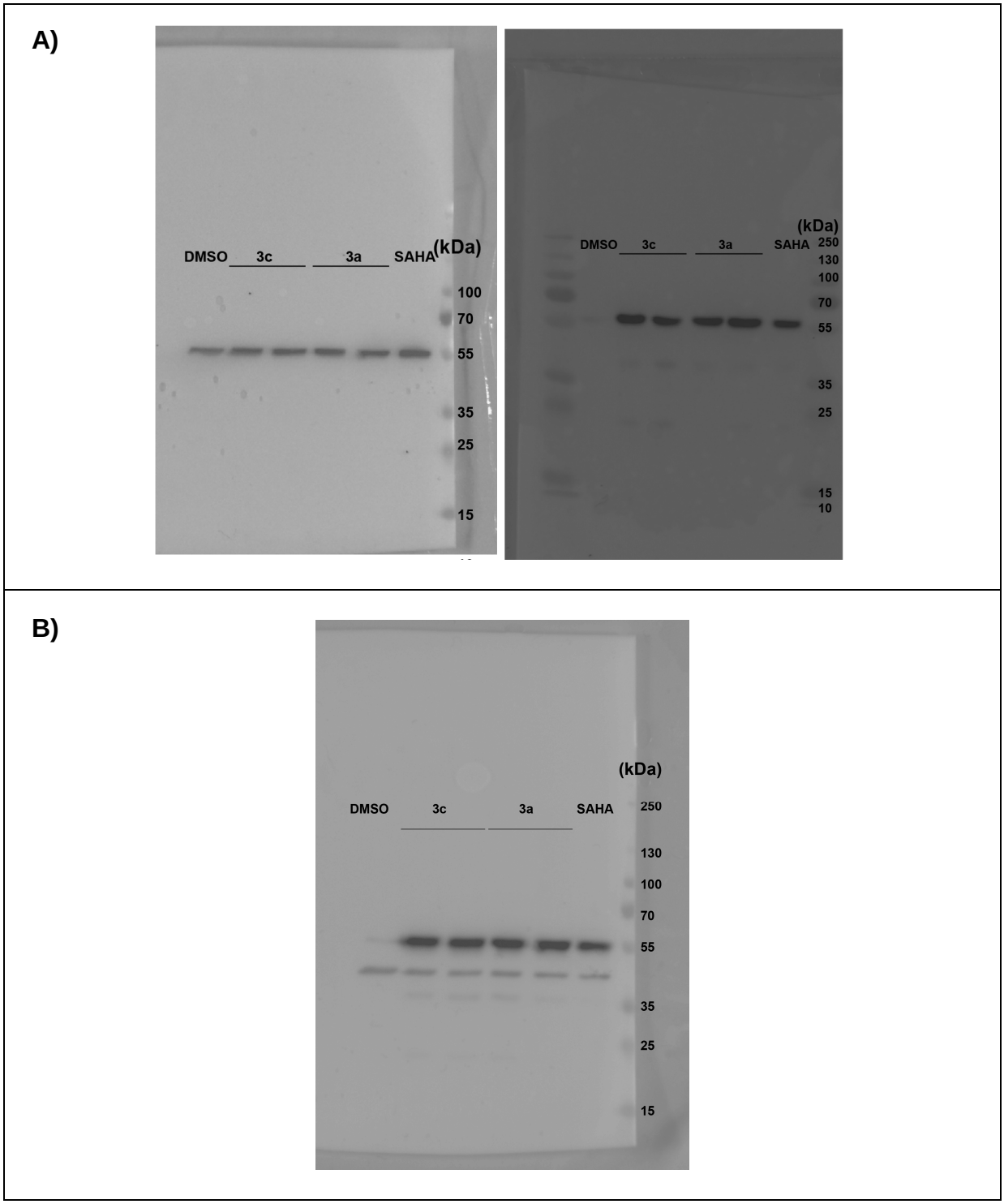

Fig. S4 Increase of tubulin acetylation in 518A2 melanoma cells after treatment with SAHA, **3a** or **3c** (Figure 3B). **A)** Upper membranes: Overlay of brightfield and chemiluminescence images of two PVDF membranes from identically loaded SDS-polyacrylamide gels after incubation with alpha-tubulin (left image) or acetyl-alpha-tubulin (right image) primary antibodies. **B)** The anti-alpha-tubulin-treated membrane (same as shown in **A)** left) was stripped and reprobed with acetyl-alpha-tubulin (55 kDa) and beta-actin (ca. 42 kDa) primary antibodies. Chemiluminescence was recorded with a LAS-3000 image reader (Fujifilm), PageRuler Plus Prestained Protein Ladder (Fermentas/Fisher Scientific) was used a molecular weight marker

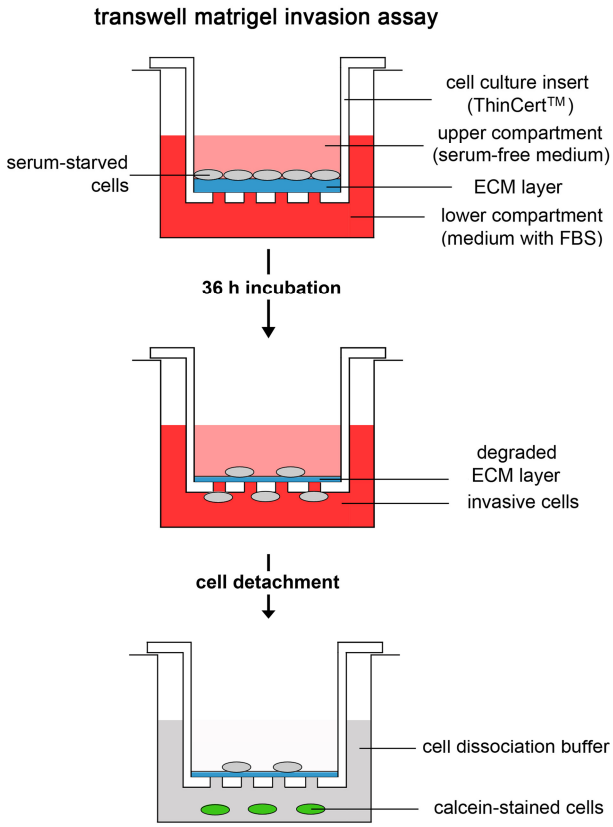

Fig. S5 Schematic representation of a three-dimensional *in vitro* assay for the quantification of the metastatic potential of highly invasive cells using ThinCert® cell culture inserts (greiner bio-one, adapted from the manufacturer's manual)

References

S1. Van Leusen AM, Boerma GJM, Helmholdt RB, et al. (1972) Tetrahedron Lett 23:2367–2368.

S2. Thaler F, Colombo A, Mai A, et al. (2010) Synthesis and Biological Evaluation of *N* -Hydroxyphenylacrylamides and *N* -Hydroxypyridin-2-ylacrylamides as Novel Histone Deacetylase Inhibitors. J Med Chem 53:822–839. doi: 10.1021/jm901502p

S3. Berridge MV, Tan AS, McCoy KD, Wang R (1996) The biochemical and cellular basis of cell proliferation assays that use tetrazolium salts. Biochemica 4:15–19.

S4. Nitzsche B, Gloesenkamp C, Schrader M, et al. (2012) Anti-tumour activity of two novel compounds in cisplatin-resistant testicular germ cell cancer. Br J Cancer 107:1853–1863. doi: 10.1038/bjc.2012.481

MANUSKRIPT VI

A new pleiotropic HDAC inhibitor targeting cancer cell signalling and cytoskeletal organisation.

Katharina Mahal,[a] Philip Kahlen,[b] Bernhard Biersack,[a] Rainer Schobert,*[a]

[a] *Organic Chemistry Laboratory, University of Bayreuth, Universitätsstraße 30, 95440 Bayreuth (Germany)*

[b] *Chair of Genetics, University of Bayreuth, Universitätsstraße 30, 95440 Bayreuth (Germany)*

* email: rainer.schobert@uni-bayreuth.de

to be submitted

4-(1-Ethyl-4-anisyl-imidazol-5-yl)-*N*-hydroxycinnamide – A new pleiotropic HDAC inhibitor targeting cancer cell signalling and cytoskeletal organisation

Katharina Mahal[a], Philip Kahlen[b], Bernhard Biersack[a], Rainer Schobert*[,a]

[a] Organic Chemistry Laboratory, University of Bayreuth, Universitätsstrasse 30, 95440 Bayreuth, Germany

Email: katharina.mahal@uni-bayreuth.de; bernhard.biersack@yahoo.com;

[b] Department of Genetics, University of Bayreuth, Universitätsstrasse 30, 95440 Bayreuth, Germany

Email: philip.kahlen@uni-bayreuth.de;

[*] Corresponding author:

Fax: +49 921 552671; Phone: +49 921 552670;

Email: rainer.schobert@uni-bayreuth.de;

Abstract

Histone deacetylases (HDAC) which play a crucial role in cancer cell proliferation have been identified as promising drug targets. However, HDAC inhibitors (HDACi) modelled on natural hydroxamic acids such as trichostatin A frequently lead to resistance or even an increased agressiveness of tumours. As a possible workaround we developed 4-(1-ethyl-4-anisyl-imidazol-5-yl)-*N*-hydroxycinnamide (etacrox), a hydroxamic acid that combines HDAC inhibition with synergistic effects of the 4,5-diarylimidazole residue. Etacrox proved highly cytotoxic against a panel of metastatic and resistant cancer cell lines while showing greater specificity for cancer over non-malignant cells when compared to the approved HDACi vorinostat. Like the latter, etacrox and the closely related imidazoles bimacroxam and animacroxam acted as pan-HDACi yet showed some specificity for certain HDAC isoforms, and for HDAC6 in particular. Akt signalling and interference with nuclear beta-catenin localisation, typical cellular responses to HDACi treatment, were elicited by etacrox at lower concentrations when compared to vorinostat. Moreover, etacrox disrupted the microtubule and focal adhesion dynamics of cancer cells and inhibited the proteolytic activity prometastatic and proangiogenic matrix metalloproteinases (MMP). As a consequence, etacrox proved strongly antimigratory and antiinvasive in three-dimensional transwell invasion assays and also antiangiogenic *in vivo* with respect to blood vessel formation in the chorioallantoic membrane (CAM) assay. These pleiotropic effects together with its good water-solubility and tolerance by mice make etacrox a promising new HDACi candidate.

Keywords: Imidazoles; hydroxamic acids; histone deacetylase inhibitors; microtubule acetylation; antimetastatic activity; transwell migration assay;

Abbreviations: HDAC, histone deacetylase; HDACi, histone deacetylase inhibitor; Etacrox, 4-(1-ethyl-4-anisyl-imidazol-5-yl)-*N*-hydroxycinnamide x HCl;

Introduction

The development of small-molecule inhibitors of human histone deacetylases (HDAC) is a promising approach to the treatment of cancer [1–6]. The enzyme family of HDAC contributes to post-translational protein modifications by catalysing the deacetylation of lysine residues in their target proteins [7,8]. These include not only DNA-associated histones but also a great number of non-histone proteins such as transcription factors and regulators, signal transduction mediators, as well as chaperone and structural proteins [9–11]. HDAC belonging to class I (HDAC1, 2, 3 and 8), class IIa (HDAC4, 5, 7, 9), and class IIb (HDAC6 and 10) [2,12] share a zinc(II) cation in the centre of their catalytic cavity, yet differ in their cellular function, (tissue) localisation and protein substrates [2,10]. For instance, HDAC1 and 2 are nuclear enzymes that catalyse the deacetylation of histones in nucleosome complexes mediating silencing of target genes [13–15]. In contrast, HDAC6 is a cytoplasmic microtubule-associated deacetylase of alpha-tubulin and a moderator of microtubule dynamics and vesicle transport along microtubules [16–20]. Other non-histone substrates are the epidermal growth factor receptor (EGFR), [20,21] the transcription factor beta-catenin, [22] STAT1/3 (signal transducers and activators of transcription), [23] and angiogenesis-relevant proteins such as the vascular endothelial growth factor receptor (VEGFR), hypoxia inducible factor-1alpha (HIF-1alpha), and cortactin, a promotor of F-actin rearrangement [24–27].

Inhibitors of zinc-dependent HDAC mimic the natural substrate acetyllysine and act by irreversibly chelating the zinc(II) centre with high-affinity ligands such as hydroxamic acids, benzamides, or carboxylates [2,5]. They are more or less specific for individual HDAC subclasses [28–30]. Figure 1 shows prominent examples. Vorinostat (a.k.a. SAHA, suberoyl anilide hydroxamic acid) is an FDA-approved pan-HDACi clinically employed against cutaneous T-cell lymphoma [10,31]. Belinostat

(PXD101) shows specificity for HDAC classes I and II and has been approved in the USA for the treatment of peripheral T-cell lymphoma [32]. Tubacin is a HDAC6 specific inhibitor currently in advanced clinical trials [17]. Regardless of their specificity most of the clinically used HDACi tend to induce resistance in tumour cells [33,34]. As a potential workaround we recently developed a new HDACi motif by covalently linking the common 2nd-generation *para*-cinnamylhydroxamate pharmacophore to 4,5-diphenylimidazoles, derived from the natural vascular-disrupting *cis*-stilbene combretastatin A-4 [35]. They showed pronounced pan-HDAC inhibition exceeding that of vorinostat, but lacked the tubulin affinity typical of the original imidazoles and of combretastatin A-4 [35–37]. Moreover, the 4,5-diaryl imidazole moiety confered an improved water-solubility and chemical stability. In the current publication, we investigate in detail the effects of three new HDACi (**1**-**3**) of this imidazole-cinnamylhydroxamic acid type on cancer cell signalling pathways, in particular those affected by vorinostat, on protein turnover, and on cytoskeletal alterations. With the current discussion [38,39] in mind of HDACi as potential inducers of an epithelial-to-mesenchymal transition (EMT), we also took a closer look at their antimetastatic potential by means of three-dimensional *in vitro* models.

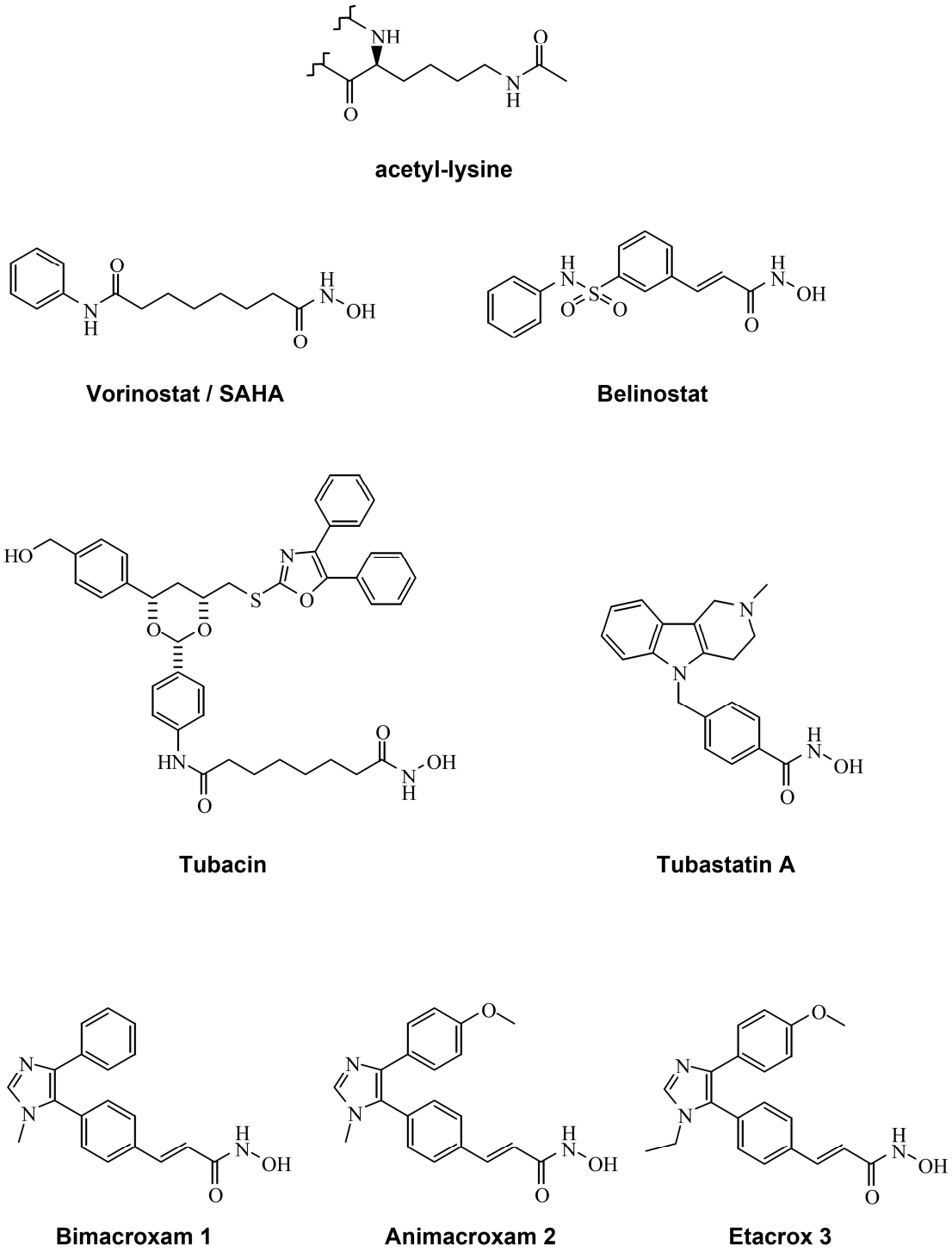

Fig. 1 – Chemical structures of HDAC substrate acetyllysine and HDAC inhibitors. *Top right and middle row:* the known non-isoform-specific HDACi vorinostat / SAHA (suberoyl anilide hydroxamic acid) and belinostat, and the HDAC6-specific inhibitors tubacin and tubastatin A. *Bottom row*: new HDACi conjugates named bimacroxam (**1**), animacroxam (**2**), and etacrox (**3**).

Materials and methods

Materials

Vorinostat and Tubastatin A were purchased from LC Laboratories and used without further purification. Stock solutions were prepared in DMSO at a final concentration of 10 mM. The primary antibodies for the detection of acetylated proteins (anti-acetyl-alpha-tubulin (Lys40) rabbit monoclonal antibody (mAb), anti-acetyl-histone H2B (Lys5) rabbit mAb; anti-acetylated lysine rabbit polyclonal antibody (pAb)) as well as the anti-Akt (pan) rabbit mAb, anti-phospho-Akt (Ser473) rabbit mAb were from Cell Signaling Technology. The anti-caspase-9 mouse mAb was purchased from Calbiochem, the anti-alpha-tubulin mouse mAb from invitrogen. Focal adhesion staining and detection of beta-catenin was done with anti-paxillin mAb or beta-catenin mAb, both from BD Transduction Laboratories. All secondary antibody-horseradish peroxidase (HRP) conjugates (anti-mouse IgG, HRP-linked antibody; anti-rabbit IgG, HRP-linked antibody) were from Cell Signaling Technology. Secondary antibodies for immunofluorescence microscopy were purchased from Pierce/Thermo Scientific (goat anti-mouse IgG (H+L), cross adsorbed secondary antibody-DyLight 550 conjugate) or invitrogen/life technologies (goat anti-mouse IgG (H+L) secondary antibody-AlexaFluor488 conjugate, goat anti-rabbit IgG secondary antibody-AlexaFluor488 conjugate). The Phalloidin-AlexaFluor594 conjugate for staining filamentous actin was from invitrogen/life.

Chemistry

The HDACi **1** and **2** were synthesised analogously to previous publications [36,38]. The synthesis of derivative **3** is depicted in Scheme 1 (*cf.* Supplementary Material for details). Compounds **1**-**3** were employed as 10 mM or 100 mM stock solutions of their hydrochloride salts in DMSO.

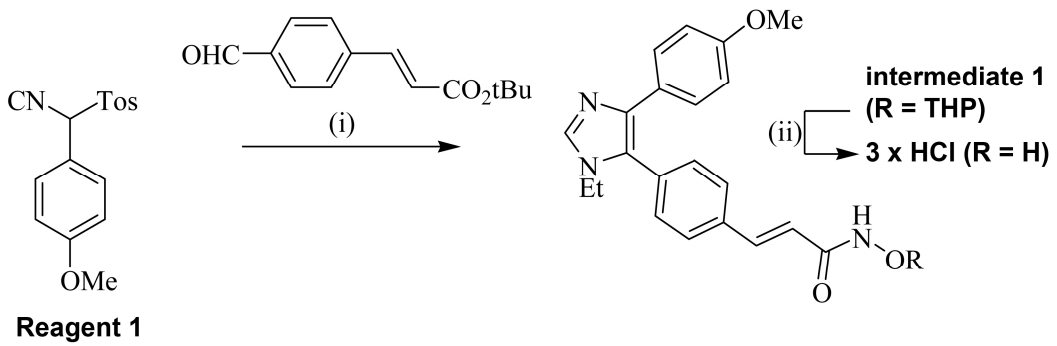

Scheme 1 – Synthesis of the new HDACi 3. Reagents and conditions: (i) a) 2M $EtNH_2$/THF, t-BuOH, reflux, 2h, then **Reagent 1**, K_2CO_3, *t*-BuOH, reflux, 3h; b) TFA, CH_2Cl_2, rt, 1 h; c) THPO-NH_2, Et_3N, EDCI, DMAP, CH_2Cl_2, rt, 24 h; (ii) 4M HCl/dioxane, dioxane, rt, 1 h (*cf.* supplementary material for synthetic details and product characterisation).

Cell lines and culture conditions

The human melanoma cell line 518A2 (Department of Radiotherapy and Radiobiology, University Hospital Vienna) [39], the human colon adenocarcinoma cell line HT-29 (DSMZ no.: ACC 299), the MCF-7/Topo breast cancer (DSMZ no.: ACC 115) and the KB-V1/Vbl cervix carcinoma cell line (DSMZ no.: ACC 149) and immortalised M-MSV-Balb/3T3 mouse fibroblasts (Moloney-murine sarcoma virus-transformed; ATCC no.: CCL-163.2; Chair of Biomaterials, University of Bayreuth, Germany) were grown in DMEM or RPMI (HT-29) medium, supplemented with 10% fetal bovine serum (FBS), 1% Antibiotic-Antimycotic solution (all from Gibco) and 250 µg/mL gentamycin (SERVA). MCF-7/Topo and KB-V1/Vbl were grown under selective conditions by adding the maximal tolerated dose of topotecan (500 nM; Topo) or vinblastine (350 nM; Vbl) 24 h after each passage to maintain the expression of multidrug-resistance-related efflux transporters. Experiments on HeLa and Hek-293 cells for protein production or cell lysate preparation (DSMZ no.: ACC 57, ACC 305) were done at the Department of Genetics, University of Bayreuth. The HUVEC-derived endothelial hybrid cell line Ea.hy926 (ATCC no.: CRL-2922; Institute of Physiology, Charité Berlin, Germany) [40–42] was grown in conditioned DMEM

with an endothelial medium supplement (PAA/GE Healthcare) added. Experiments on primary human umbilical vein cells (HUVEC) were conducted at the Helmholtz Centre for Infection Research (Braunschweig, Germany). HUVEC were cultured in EGM-2 medium (Lonza). Primary chicken heart fibroblasts (CHF) were explanted from 10 day-old chicken embryos and separated from other cell types for several weeks. The established cell line based on single fibroblasts was finally grown in DMEM (10% FBS, 1% Anti-Anti, 250 µg/mL gentamycin) and used before the 20th passage. All cell lines were cultured and incubated at 37 °C, 5% CO_2, 95% humidified atmosphere. Only mycoplasm-free cells and cell lines were used.

Isolation of HDAC active cell lysate fractions and preparation of recombinant HDAC isoforms

Cell lysate fractions from HeLa cells were obtained by a modified protocol for nuclei preparation by Dignam *et al.* [43]. Briefly, cell pellets from mass cultures were resuspended and incubated in cell extraction buffer (20 mM HEPES, 10 mM KCl, 0.1 mM EDTA, 0.1 mM EGTA, 1.5 mM $MgCl_2$, 0.5 mM DTT) containing 0.1% Triton X-100 to lyse cell membranes and leave intact nuclei. After centrifugation (3,000 g, 2 min), the supernatant containing cytosolic proteins was aspirated from the nuclei pellet and the protein concentration of the cytosolic fraction was determined by a standard Bradford assay (Pierce/Thermo Scientific; for a detailed description of cell lysate fractioning and determination of cell lysate fraction purity, *cf.* Supplementary material and Figure S4). The human HDAC1 gene was amplified from a HeLa cDNA library (HDAC1 sequence from human cDNA, Genbank accession no. NM04964; Sigma Aldrich). Hek-293 cells were transfected with the resulting plasmid construct (pCS2-GST-TEV_3-hHDAC1; for HDAC1 fusion protein purification and identification, *cf.* Supplementary material, Figure S5). Recombinant GST-HDAC1 (glutathione S-transferase) fusion protein were concentrated from Hek-293 mass culture lysates

(20 mM Tris-HCl, 100 mM NaCl, 10 mM NaF, 20 mM beta-glycerophosphate, 0.1% Triton X-100, pH 7.7) and GST affinity tag pulldown according to manufacturer's conditions (glutathione agarose beads, Pierce/Thermo Scientific). Glutathione (GSH)-beads were repeatedly washed (50 mM Tris-HCl, pH 8.0) and eluted with 50 mM Tris-HCl, 50 mM reduced GSH. Eluates were concentrated and buffer exchanged (50 mM Tris-HCl, pH 8.0) by centrifugal filter columns according to manufacturer's manual (Amicon Ultra-0.5 mL Centrifugal Filters, 10K device, Merck Millipore). The protein concentration of the final HDAC1 protein solution was determined by a standard Bradford assay (Pierce/Thermo Scientific; 0.21 mg/mL total protein).

HDAC activity assay

A fluorescence-based HDAC activity assay was used to assess the compound specificity for distinct HDAC classes. Visualisation of HDAC activity was achieved by using short acetylated peptide substrates coupled to a precursor fluorophore which was released by trypsin cleavage only upon previous deacetylation. The Fluor-de-Lys substrate used allows to measure broad-spectrum HDAC activity from extracts or recombinant protein. Herein, cell lysate fractions (HeLa nuclear and cytosolic extracts) or recombinant human HDAC1 and HDAC6 (HDAC1 (GST-tag) isolated from transfected Hek-293 mass cultures; HDAC6 (His-tag), Enzo Life Sciences) were incubated with vorinostat or the compounds **1** or **3** and the Fluor-de-Lys substrate (Fluor-de-Lys®-Green substrate, Enzo Life Sciences) according to manufacturer’s conditions. A commercially available nuclear extract from Hela cells (HeLa nuclear extract, 2.0 mg/mL, Merck Millipore) was used as a reference without further evaluation. In brief, each sample (50 µL) containing 5 µL predilution of the test compounds (dilution series ranging from 100 µM to 100 nM), 20 µL protein dilution (0.5 µg HeLa nuclear extract, 1 µg HeLa cytosolic extract, 0.4 µg HDAC1,

0.2 µg HDAC6) and 25 µL 50 µM or 100 µM Fluor-de-Lys substrate (final concentration of 25 µM for lysate fractions or 50 µM for HDAC6; all in HDAC assay buffer: 50 mM Tris-HCl, 137 mM NaCl, 2.7 mM KCl, 1 mM $MgCl_2$, pH 8.0) were incubated in the wells of a black 96-well plate (half-area 96-well plate, µClear®, black, medium binding, greiner bio-one) at 37 °C for 60 min. The amount of deacetylated substrate was then visualised by adding 50 µL 1X developer (0.5 mg/mL trypsin, 0.1 mM EDTA, 0.1 mM vorinostat in 50 mM Tris-HCl, pH 7.4) and subsequent incubation at 37 C for 10 min. Fluorescence intensity of the degraded HDAC substrate was measured with a microplate reader (Tecan) at an emission wavelength of 535 nm (excitation at 485 nm). All experiments were conducted in duplicates, blank and solvent (DMSO) controls were treated identically. The fluorescence intensity represents the relative HDAC activity within a sample with respect to DMSO controls set to 100%. IC_{50} values from dose-response curves were calculated as the mean of at least two independent experiments ± S.D.

Western blot analyses of cancer cell lysates

518A2 melanoma or HT-29 colon carcinoma cells (50,000 cells/well) were grown in 24-well plates and incubated with vehicle (DMSO) or slightly toxic concentrations of vorinostat or the hydroxamic acids **1** or **3** for the indicated times. The cells were harvested by trypsination, centrifuged at 300 g for 5 min and the resulting cell pellet was lysed in 100 µL 2X protein sample buffer (20 mM DTT, 2% (w/v) SDS, 20% (v/v) glycerol in 125 mM Tris-HCl, pH 6.8) and boiled (95 °C, 10 min). 10 µL of the cell lysate were subjected to SDS polyacrylamide gel electrophoresis (SDS-PAGE) and transferred to polyvinylidene difluoride membranes (PVDF, Carl Roth). For subsequent detection of acetylated or phosphorylated proteins membranes were blocked and incubated with appropriate primary antibody dilutions in 3% bovine serum albumin (BSA) in phosphate-buffered saline (PBS). For analysis of all other

proteins membranes were blocked and treated with antibody dilutions in 5% milk powder in PBS. Band intensity was recorded by visualisation of chemiluminescence (secondary antibody-HRP conjugates; ECL detection system, SERVA) using a LAS-3000 imager (Fujifilm). If not stated otherwise, alpha-tubulin was used as a suitable loading control as previously shown [37]. The additional visualisation of acetylated alpha-tubulin was performed on a separate membrane from an identically loaded gel. ImageJ software was used for densitometric analyses of the protein bands. Photoshop CS5 was employed for digital image processing (contrast/brightness setting) which was uniformly applied to the entire images, and for presentation of relevant proteins bands (*cf.* Supplementary material for original and uncropped membrane images, Figures S6-S10).

Separation of detergent-soluble and -insoluble microtubule fractions of cell lysates

518A2 cells cultured in 24-well plates (50,000 cells/well) were treated with DMSO (control), vorinostat or etacrox **3** (5 µM, 10 µM) for 24 h and then harvested by trypsination followed by centrifugation (400 g, 5 min, room temperature). The resulting cell pellet was resuspended in 100 µL hypotonic cell lysis buffer (20 mM Tris-HCl, 1 mM $MgCl_2$, 2 mM EGTA, 0.5% Triton X-100, pH 6.8) supplemented with protease inhibitor (protease inhibitor cocktail set III, EDTA-free, Calbiochem) and incubated for 10 min at room temperature. Centrifugation at 12,000 g for 10 min at room temperature separated detergent-insoluble, polymeric microtubules (insoluble pellet fraction) from soluble, depolymerised tubulin (supernatant) [44,45]. Both fractions were mixed with 100 µL 2X protein sample buffer, boiled at 95 °C for 10 min and subjected to SDS-PAGE and Western blot analyses.

Woundhealing assay and immunofluorescence microscopy

518A2 cells were used for fluorescence microscopy analyses of acetylated microtubules and Akt phosphorylation, M-MSV-Balb/3T3 cells were used to assess the effect of the HDACi on fibroblast migration. Cells were seeded on glass coverslips in 24-well plates (25,000 cells/well) and incubated overnight. For woundhealing assays, an artificial wound was generated by scraping through the fibroblast monolayer with a 10 µL-pipette tip. For induction of epidermal growth factor (EGF)-mediated effects, cells were starved overnight in serum-free DMEM and human EGF (200 ng/mL hEGF in 0.1% BSA/PBS; medicyte) was added 2 h after addition of the test compounds. The cells were then treated with DMSO (control), vorinostat or etacrox **3** for 6 h or 24 h. After fixation in 4% formaldehyde in PBS (20 min, room temperature) cells were blocked and permeabilised (1% BSA, 0.1% Triton X-100 in PBS, 30 min). Microtubules, microtubule acetylation, focal adhesion density as well as localisation of beta-catenin and Akt phosphorylation were visualised by incubation of the coverslips with primary antibodies (1 h, 37 °C, 95% humidity) against alpha-tubulin, acetyl-alpha-tubulin, paxillin, beta-catenin or phosphorylated-Akt (phospho-Akt) followed by incubation with secondary antibody-fluorophore conjugates (1 h at room temperature in the dark). The coverslips were mounted in Mowiol 4-88-based mounting medium containing 2.5% (w/v) DABCO and 1 µg/mL DAPI (4',6-diamidino-2-phenyl-indole, Carl Roth) for counterstaining the nuclei. Subcellular localisation was documented by fluorescence microscopy (ZEISS Axio Imager.A1; 400-fold magnification). Photoshop CS5 was used for digital image processing (brightness/contrast settings) that was uniformly applied to the whole fluorescence images and for figure preparation (color channel merging tools, resolution settings). ImageJ software was used for scale bar calculation.

Determination of matrix metalloproteinase (MMP) inhibition by FITC-gelatine degradation and gelatin zymography

To assess any direct inhibition of matrix metalloproteinases (MMPs) by the compounds we used a standard assay for monitoring gelatinolytic activity via fluorescence measurements and gelatin zymography with some alterations [46–48]. 518A2 melanoma cells which express high levels of MMP-2 and MMP-9 [49] were used for the gelatin degradation studies. For MMP preparation confluently-grown 518A2 cells in 25 cm^2-cell culture dishes were cultured in conditioned medium (serum-free DMEM, 200 KIU/mL aprotinin) for 24 h and detached cells were removed from the supernatant by centrifugation. To determine the overall MMP inhibition, 20 µL MMP-rich medium were pre-treated with 5 µL pre-dilutions of DMSO (< 1% per sample) or the test compounds (final concentrations of 10-500 µM vorinostat or Etaerox **3**) in MMP assay buffer (50 mM Tris-HCl, 0.1 mM $CaCl_2$, pH 7.4) for 30 min and then mixed with 75 µL MMP assay buffer containing 5 µg fluorescein isothiocyanate-labelled gelatin (FITC-gelatin, Sigma Aldrich; *cf.* Supplementary material for FITC-gelatin labelling) and incubated at 37 °C for 24 h. 10 µL developing buffer (1 M Tris-HCl, pH 9.0) were added to each sample and proteins were extracted by adding 400 µL 100% EtOH (p.a.) and vortexing at room temperature. Precipitated proteins were pelleted by centrifugation (12,000 g, 10 min, rt) and the supernatant containing degraded FITC-labelled fragments was analysed in a black 96-well plate in triplicates of 100 µL. FITC fluorescence was measured using a microplate reader (excitation/emission wavelength: 485(20) nm/535(20) nm). Blank and solvent controls were treated equally. Data are represented as the mean of at least two independent measurements (in triplicates) using the same lot of conditioned medium and calculated with respect to DMSO controls set to 100% FITC-gelatin degradation and to samples without MMPs (serum-free medium) set to 0 (MMP activity). For

assessing the MMP inhibition from MMP-gelatin zymography, conditioned medium was separated by SDS-polyacrylamide gels with co-polymerised gelatin and incubated with the test compounds to inhibit gelatin degradation after MMP refolding. The procedure was carried out as previously described [49]. In brief, a mixture of 2.5 µL non-reducing, denaturating 2X SDS-protein loading buffer and 2.5 µL conditioned DMEM (supernatant DMEM + 0.1% BSA + 200 KIU Aprotinin/mL from 518A2 melanoma cultures) was subjected to 10%-SDS-PAGE with co-polymerised gelatine (0.1 mg/mL). Gels were cut into pieces containing two equal loaded lanes containing electrophoretically separated MMP-2 (ca. 62/72 kDa) and MMP-9 (ca. 92 kDa), washed with Triton X-100 containing washing buffer (50 mM Tris-HCl, 2% Triton X-100, pH 7.4, 10 min) to exchange SDS by the non-ionic detergent and achieve partially refolding of the MMPs. The gel slices were separately incubated with 10 mL MMP assay buffer containing DMSO (control), vorinostat (10 µM) or etacrox **3** (10 µM, 50 µM) at 37 °C for 16 h, stained with Coomassie blue and destained until relevant bands became visible. Zymograms were documented and processed (*cf.* Supplementary material, Figure S11 for original zymogram images).

Tube formation assay with endothelial cells

The ability of permanent Ea.hy926 endothelial hybrid cells to form vascular-like networks upon growth factor stimulation was used to assess the antiangiogenic activity of imidazoles **1** and **3** *in vitro* [41,42]. Ea.hy926 cells (5×10^4/well) were seeded on thin Matrigel™ (basement membrane matrix, high concentration, with growth factors, BD Biosciences) layers pre-gelled in the wells of a black 96-well cell culture plate (10 µL of pure matrigel solution, 30 min at 37 °C) prior to adding DMSO or the compounds **1** or **3** (10 µM) and grown for 24 h. The tubular networks were documented by light microscopy (100-fold magnification, Axiovert 135, AxioCam MRc 5, ZEISS). To exclude false-positive effects due to the cytotoxicity of the

compounds rather than antiangiogenic effects, MTT was additionally added to each well (25 µL 0.5% MTT solution in PBS). After incubation for 2 h at 37 °C the plates were centrifuged (300 g, 4 °C, 5 min) and the supernatant was aspirated. The cells were lysed and the precipitated formazan was redissolved by adding 100 µL of an SDS-DMSO solution (10% SDS, 0.6% acetic acid in DMSO) to each well. The absorbance at wavelengths 570 and 630 nm (background) was measured with an automatic ELISA microplate reader (Tecan) and the percentage of viable cells was calculated with respect to the controls.

Chorioallantoic membrane (CAM) assay with fertilised chicken eggs [50]

White leghorn chicken eggs (SPF eggs, VALO Biomedia) were incubated (37 °C, 50-60% humidity) until day 5 after fertilisation and opened by cutting a window of 2-3 cm diameter into the pole end of the eggshell. Rings of silicon foil (9 mm diameter) were placed on the developing vessels within the CAM followed by further incubation for 24 h. A total amount of 20 nmol (50 µL of 200 µM dilutions in saline) vorinostat or imidazole **3** were daily (0 h and 24 h-application) applied onto the CAM. Alterations in the blood vessel organisation in comparison to control eggs (DMSO) were documented after 0 h, 24 h and 48 h post application with a stereomicroscope (60-fold magnification, Traveller).

Transwell invasion assay

The effect of etacrox **3** on the migration of cancer cells was assessed with a three-dimensional transwell model for chemoattractant-stimulated, directed tumour cell migration. It is based on modified Boyden migration chambers and implies both degradation of matrigel as an extracellular matrix and active movement of the cells through this basement membrane matrix [51,52]. Quantification of invasive cells was adapted from the manufacturer's application manual (ThinCert™ application notes,

greiner bio-one) with some alterations [53]. We compared four cell lines with distinct characteristic migration behaviour (highly-invasive 518A2 melanoma cells[54], HT-29 colon carcinoma and resistant MCF-7/Topo breast carcinoma cells, transformed M-MSV-Balb/3T3 mouse fibroblasts). In brief, 518A2, HT-29, MCF-7/Topo cancer cells or M-MSV-Balb/3T3 fibroblasts were starved in serum-free DMEM for 24 h and harvested before seeding them into matrigel-coated (50 µL 1:1-dilution of matrigel basement membrane matrix in serum-free DMEM, gelled for 30 min at 37 °C, 5% CO_2, 95% humidity; BD Biosiences) ThinCert™ cell culture inserts with porous membranes (translucent PET membrane, 3 µm pore size, greiner bio-one; 20,000 cells per insert in 200 µL serum-free DMEM). The inserts were placed into a 24-well plate with 600 µL DMEM containing 10% FBS per well and incubated with DMSO (control), vorinostat, or **3** for 48 h. In the case of MCF-7/Topo cells, an additional set-up was treated with 200 ng/mL hEGF (human epidermal growth factor, in 0.1% BSA/PBS; medicyte) per insert. Then, cells migrated through the insert membrane were collected and stained by incubation with 1X cell dissociation buffer (0.5 mM EDTA, 0.1% sodium citrate in PBS, pH 7.4) containing 1 µM calcein-AM (calcein acetoxymethyl ester; non-fluorescent, cell-permeable dye) for 15 min at 37 °C. The cell suspension containing only invasive cells was transferred to the wells of a black 96-well plate. Invasive cells were quantified with a microplate reader (Tecan) by measuring the calcein fluorescence (excitation/emission wavelength: 485 nm/520 nm) that was calculated as percentage ± S.D. of DMSO-treated control cells set to 100%. Since calcein conversion and influx/efflux could vary between the cell lines, 10 µL of the cell suspension were additionally counted with a hemocytometer (in triplicates) to assess the number of invasive cells within the bottom wells. All experiments were carried out at least in triplicates.

Image preparation, densitometry and statistical analyses

Original images were edited with ImageJ or Photoshop CS5 software, alterations in contrast/brightness and resolution settings were uniformly applied to the entire image. Relevant bands were cropped where applicable (*cf.* Supplementary material for original images). Western blot bands were densitometrically analysed with the ImageJ software. Where applicable, band intensities were normalised to loading controls. Resulting values are shown as the mean of at least two representative experiments ± standard deviation (S.D.). Analysis of focal adhesion density from immunofluorescence images was done with ImageJ by setting a threshold area for paxillin stained particles [55]. On the resulting pictures, single cells were selected (selection along cell borders) and the particles within cell bodies were analysed. Measurements include pixel densities which represent the focal adhesion area normalised to the whole cell area. At least ten microscopic images from representative areas on microscope slides were analysed and the values for focal adhesions were calculated as the mean ± S.D. with respect to DMSO-treated controls set to 1. Significance of the microinvasion assay data was assessed by Student's *t*-test ($P < 0.05$) using the XLSTAT add-in.

Results and Discussion

The imidazoles **1**-**3** were tested in MTT assays for their antiproliferative effect on cancer cells, endothelial cells, and fibroblasts. Table 1 summarises the respective IC_{50} values including those for vorinostat which serves as a reference pan-HDACi. As previously shown, bimacroxam **1** displayed a high toxicity against endothelial cells (Ea.hy926, HUVEC) [37] while the new etacrox **3** turned out to be most active with lowest IC_{50} (72 h) values against most of the tested cancer cell lines including the multidrug-resistant HT-29 colon, MCF-7/Topo mammary, and KB-V1/Vbl cervix carcinoma cells. Non-malignant primary fibroblasts (CHF) were hardly affected by vorinostat or the imidazoles **1**-**3** which is typical of HDACi in general.

Table 1. Inhibitory concentrations[a] IC_{50} [nM] of vorinostat and the compounds **1**-**3** when applied to various human cancer cell lines, human primary endothelial cells (HUVEC), Ea.hy926 hybrid endothelial cells, transformed mouse fibroblasts (M-MSV-Balb/3T3) and primary non-malignant chicken fibroblasts (CHF).

cell lines	compounds			
	Vorinostat	**1**	**2**	**3**
518A2	1.8 ± 0.1 [b]	2.8 ± 0.6 [b]	1.5 ± 0.1 [b]	0.95 ± 0.1
518A2 (24 h)	18.7 ± 0.1	13.1 ± 0.9	10.2 ± 0.3	6.6 ± 0.4
HT-29	1.8 ± 0.1 [b]	1.2 ± 0.1 [b]	0.68 ± 0.06 [b]	0.35 ± 0.03
HT-29 (24 h)	1.9 ± 0.3	0.5 ± 0.1	0.8 ± 0.1	1.0 ± 0.2
MCF-7/Topo	13.5 ± 0.7 [b]	15.3 ± 1.3 [b]	10.0 ± 0.9 [b]	5.6 ± 0.3
KB-V1/Vbl	13.1 ± 0.8 [b]	5.0 ± 0.8 [b]	8.3 ± 1.9 [b]	2.9 ± 0.9
Panc-1	3.8 ± 1.2 [b]	1.1 ± 0.1 [b]	0.94 ± 0.08 [b]	0.95 ± 0.06
HUVEC	7.7 ± 0.1 [b]	0.60 ± 0.03 [b]	0.83 ± 0.03 [b]	1.3 ± 0.3
Ea.hy926	1.9 ± 0.2 [b]	0.16 ± 0.03 [b]	0.90 ± 0.15 [b]	0.99 ± 0.13
M-MSV-Balb/3T3	1.42 ± 0.3	0.5 ± 0.04	1.4 ± 0.1	1.43 ± 0.2
CHF	> 89.4 ± 9.8 [b]	> 150 [b]	> 150 [b]	> 150

[a] Values are derived from dose-response curves obtained by measuring the percentage of viable cells relative to untreated controls after 24 h or 72 h exposure to the test compounds using an MTT assay; human cancer cell lines: 518A2 melanoma, HT-29 colon, MCF-7/Topo breast, KB-V1/Vbl cervix and Panc-1 pancreatic carcinomas. [b] Values from an earlier publication [37]. Values represent means of four independent experiments.

For bimacroxam **1** and animacroxam **2**, a correlation between growth inhibition and an induction of apoptosis via caspase-3 activation was already detected [37]. For etacrox **3**, we now examined the involvement of caspase-9 in its effect on 518A2 cells (Figure 2A) as well as the extent of DNA fragmentation as a consequence of apoptotic cell death in the most-sensitive HT-29 cell line via TUNEL assays (*cf.* Supplementary material, Figure S1 and Table S1). We found that growth inhibition is at least partially due to the induction of apoptosis. Cell cycle analyses with 518A2 melanoma, HT-29 colon and MCF-7/Topo breast carcinoma cells revealed a concentration- and cell line-dependent cell cycle arrest after incubation with etacrox **3** for 24 h (*cf.* Supplementary material, Figure S2). High compound concentrations led to an accumulation of 518A2 and MCF-7/Topo cells in the G2/M-phase while a significant G1-phase arrest and a concomitant reduction of cells in S-phase were observed for HT-29 cells at equitoxic concentrations (Figure S2). These cell cycle alterations were in line with the results of western blot analyses of the cellular levels of the cell cycle regulator p27/Kip1 (G1 marker) in 518A2 and HT-29 cells (*cf.* Supplementary material, Figure S3).

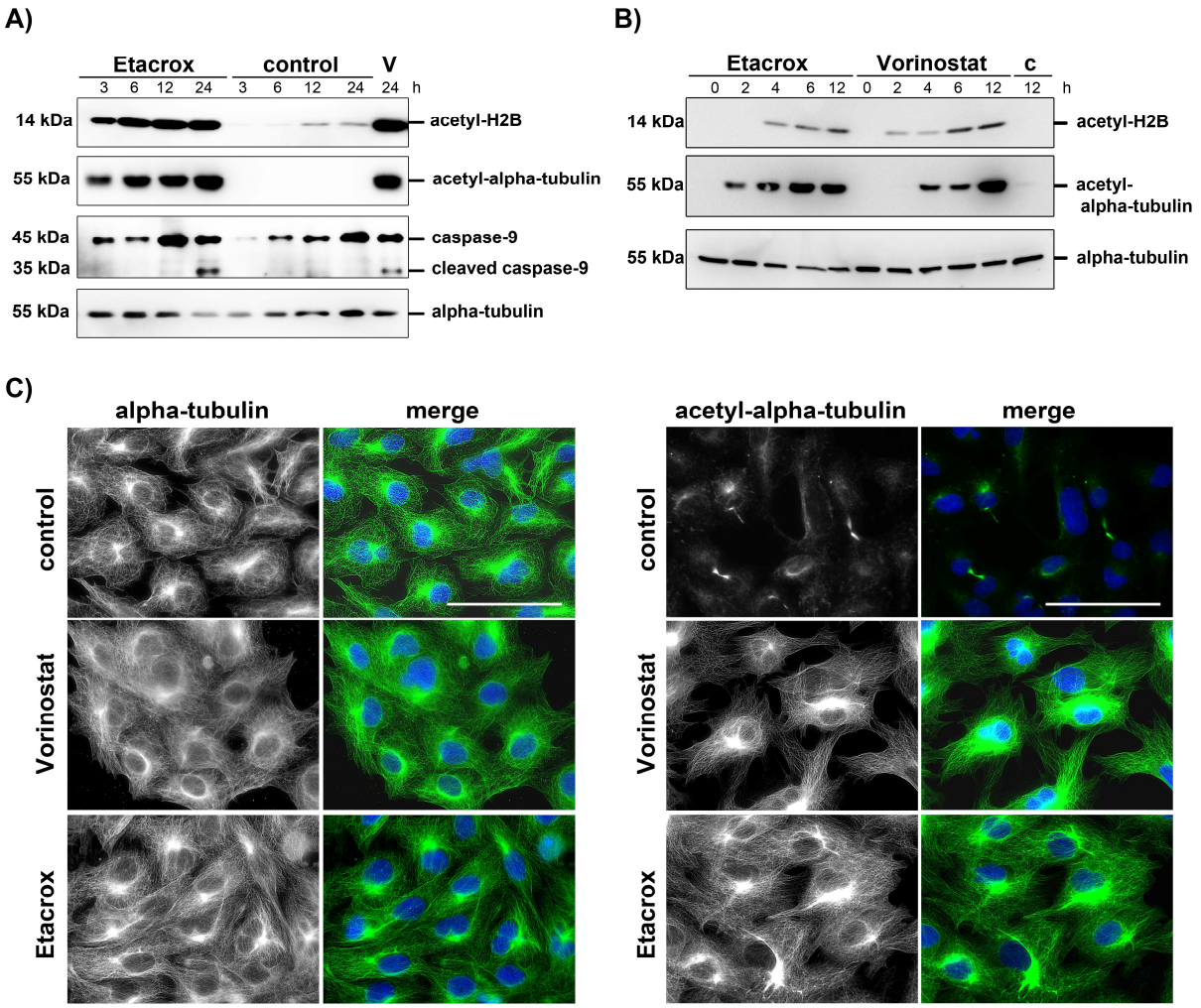

Fig. 2 – Effects of etacrox 3 and vorinostat on cancer cells. (A) Time-dependent (3-24 h) increase in histone H2B (acetyl-H2B) and microtubule acetylation (acetyl-alpha-tubulin) as well as caspase-9 cleavage: 518A2 melanoma cells were treated with DMSO (control), 2.5 µM etacrox **3** or 5 µM vorinostat (V) for the indicated times, then lysed and the levels of acetylated proteins or full-length and cleaved caspase-9 were monitored by immunoblotting with specific antibodies. (B) Time-dependent (2-12 h) increase in H2B or microtubule acetylation after treatment of HT-29 colon carcinoma cells with DMSO (c), 1 µM etacrox **3** or 2 µM vorinostat (IC_{50} (24 h) concentrations). (C) Organisation of microtubules (alpha-tubulin) and increasingly acetylated microtubules (acetyl-alpha-tubulin) in 518A2 cells treated with DMSO (control), 2.5 µM **3** or 5 µM vorinostat for 24 h as visualised by immunofluorescence microscopy. Nuclei counterstained with DAPI (merge, blue), 400-fold magnification, scale bar: 100 µm.

The fact that etacrox **3**, more clearly than its congeners **1** and **2**, outperformed the established drug vorinostat both in terms of efficacy against and selectivity for cancer cells prompted us to elucidate its molecular mode of action and the individual contributions of imidazole and hydroxamic acid moieties in full detail. These

experiments focussed on the HDACi activity of **3**, and on its antiinvasive effects in highly metastatic 518A2 melanoma, resistant HT-29, and MCF-7/Topo carcinoma cells, as well as on its antiangiogenic effects on endothelial cells.

First we proved its pan-HDACi activity by ascertaining the hyperacetylation of typical deacetylase substrates as a result of its presence. The acetylation status of histone H2B and alpha-tubulin clearly increased after incubation with etacrox **3** as to Western blot analyses of 518A2 cell lysates taken at different points in time (Figure 2A).

The strong increase in alpha-tubulin acetylation could also be visualised by immunofluorescence microscopy of acetylated microtubules in 518A2 cells (Figure 2C). It is apparently mediated by inhibition of the cytoplasmic class IIb deacetylase HDAC6 [17]. Interestingly, in HT-29 cells where etacrox **3** was most effective (IC_{50} (72 h): 0.35 µM, IC_{50} (24 h): 1.0 µM), treatment with near-IC_{50} (24 h) concentrations of vorinostat and etacrox **3** revealed a differential time-dependent increase in H2B or microtubule acetylation (Figure 2B). The acetylation level of alpha-tubulin was increased already after a short incubation (2 h) with etacrox **3** while such an effect was not detectable after vorinostat treatment. Histone acetylation apparently occurs prior to microtubule acetylation upon Vorinostat treatment. These differences might be due to diverse modes of cellular drug uptake and distribution or to different HDAC subtype affinities of vorinostat and the imidazole **3**.

To clarify this, the inhibitory effect of **1** and **3** *in vitro* on recombinant HDAC1 and HDAC6 proteins as representatives for typical class I and class II HDAC isoforms was measured by a fluorometric assay. Vorinostat displayed the lowest IC_{50} value (ca. 10 nM) for the inhibition of HDAC1 while bimacroxam **1** (ca. twofold) and etacrox **3** (ca. tenfold) were significantly less efficacious (Table 2).

Probably as a consequence of its reduced affinity for HDAC1, etacrox **3** inhibited HDAC6 much better (IC_{50}: 66 nM) than vorinostat (IC_{50}: 154 nM). Tubastatin A, a selective HDAC6 inhibitor displayed IC_{50} values in a similar range [56,57]. We also tested the HDAC inhibitory effect on HeLa nuclear and cytosolic cell lysate fractions which may contain a specific set of HDAC isoforms. Class I as well as class II HDAC were shown to shuttle between the cytoplasm and the nucleus with a typical equilibrium distribution [58]. HDAC1 and HDAC2 (class I) for instance were predominantly found in nuclei, while HDAC3 can be cytoplasm membrane-associated and HDAC8 is essentially in the cytoplasm taking part in the regulation of actin-mediated cell contractility [58–60]. In contrast, class IIb HDAC6 localises exclusively in the cytotoplasm.

Table 2. HDAC inhibition [IC_{50} (µM)][a] by vorinostat and the imidazoles **1** and **3** as determined by the conversion of HDAC substrate to fluorophores. HDAC active isolates from nuclei or cytosolic fractions of HeLa cell lysates or recombinant HDAC1 and HDAC6 were incubated with the HDAC substrate and analysed by fluorescence measurements.

HDAC isoforms	**compounds**			
	Vorinostat	**1**	**3**	**Tubastatin A**
HeLa nuclear extract [a]	0.231 ± 0.036 [b]	0.234 ± 0.011 [b]	0.504 ± 0.024	*n.d.*
HeLa cytosolic extract [a]	0.147 ± 0.023	0.132 ± 0.014	0.036± 0.014	*n.d.*
HDAC1 [a]	0.010 ± 0.003	0.028 ± 0.011	0.187 ± 0.037	> 1
HDAC6 [a]	0.154 ± 0.071	0.107 ± 0.023	0.066 ± 0.017	0.087 ± 0.038

[a] IC_{50} values derived from dose-response curves obtained by measuring the percentage of deacetylated, fluorogenic substrate (25 µM Fluor-de-Lys substrate) relative to DMSO controls. HeLa nuclear extract: 0.5 µg; HeLa cytosolic extract: 1 µg; HDAC1 0.4 µg, HDAC6: 0.2 µg. Commercially available HeLa nuclear extract was used as a reference. Incubation time 60 min. [b] Values from an earlier publication [37]; *n.d.* not determined.

HeLa nuclear and cytoplasmic extracts contain a variety of HDAC isoforms and the IC_{50} values for their inhibition by vorinostat and etacrox **3** showed a tendency similar to that observed in the tests with the recombinant enzymes (Table 2). Vorinostat was most effective in the nuclear fraction but far less so against cytosolic HDAC, when compared with etacrox **3**. We assume that the imidazoles are specific to a certain degree for HDAC6 or other cytoplasmic HDAC and thus they might also influence HDAC6-related cellular events more markedly than vorinostat.

For instance, HDAC6 acts as a tubulin deacetylase interfering with microtubule dynamics, vesicle transport along microtubules, and with the clearance of misfolded proteins by aggresome formation [19,20,61]. In 518A2 cells treated with etacrox **3** or vorinostat we found elevated levels of polymerised and of acetylated tubulin as is typical of the treatment with inhibitors of HDAC6 in general (Figure 3) [18,55]. This indicates that tubulin acetylation increases the microtubule stability and shifts the polymerisation-depolymerisation equilibrium of alpha-beta-tubulin heterodimers in favour of the polymers.

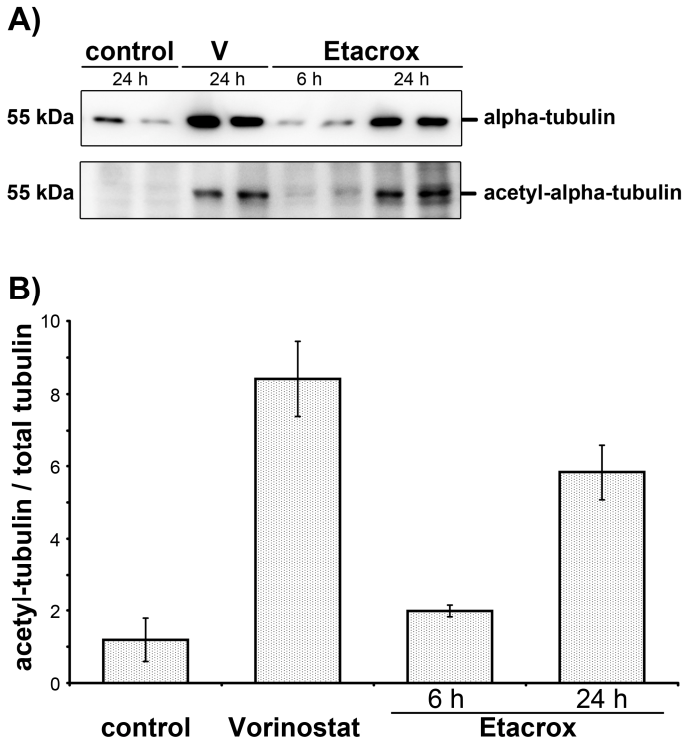

Fig. 3 – Effects of etacrox 3 and vorinostat on microtubule acetylation and stability in 518A2 melanoma cells. (A) Western blot analyses of acetylated lysine residues (acetyl-alpha-tubulin) of polymeric microtubule fractions (alpha-tubulin) in cell lysates. 518A2 cells were treated with DMSO (control), 10 µM vorinostat (V) or 5 µM etacrox **3** for 6 h or 24 h. Fractionated cell lysates containing detergent-insoluble microtubules (tubulin polymers) were subjected to immunoblotting for acetylated microtubules. (B) Graphical representation of increased microtubule acetylation with concomitant microtubule stability shown by the ratio of acetyl-tubulin to total alpha-tubulin in polymer cell lysate fractions. Values shown are obtained from densitometry analyses of representative bands from two independent experiments and are calculated with respect to DMSO-treated controls set to 1 ± S. D.

We also checked for a potential involvement of cell-matrix and cell-cell adhesion molecules in this process by visualising paxillin-associated focal adhesions and beta-catenin in 518A2 and primary endothelial cells via immunofluorescence staining (Figure 4). Both proteins were shown by other groups to be affected by HDAC6 inhibition [16,22,55]. The resulting hyperacetylation of microtubules diminishes cell-matrix adhesion dynamics and leads to a thickening of individual focal adhesion nodes [55]. For beta-catenin it was shown that HDAC6 activity may lead to its release from cadherin-catenin adherens junction complexes, followed by a translocation into

the nucleus and transcriptional activation [22]. Thus, impairing focal adhesion dynamics that are relevant for cell migration, and hindering translocation of beta-catenin to the nucleus by HDAC6 inhibition may reduce the invasive potential of cancer cells and the migratory behaviour of endothelial cells during neovessel formation. Figure shows the influence of etacrox **3** on focal adhesions in 518A2 melanoma and primary endothelial cells (HUVEC) and its reduction of nuclear beta-catenin translocation in EGF-stimulated melanoma cells. The latter is apparent from an accumulation of beta-catenin along the cell membrane.

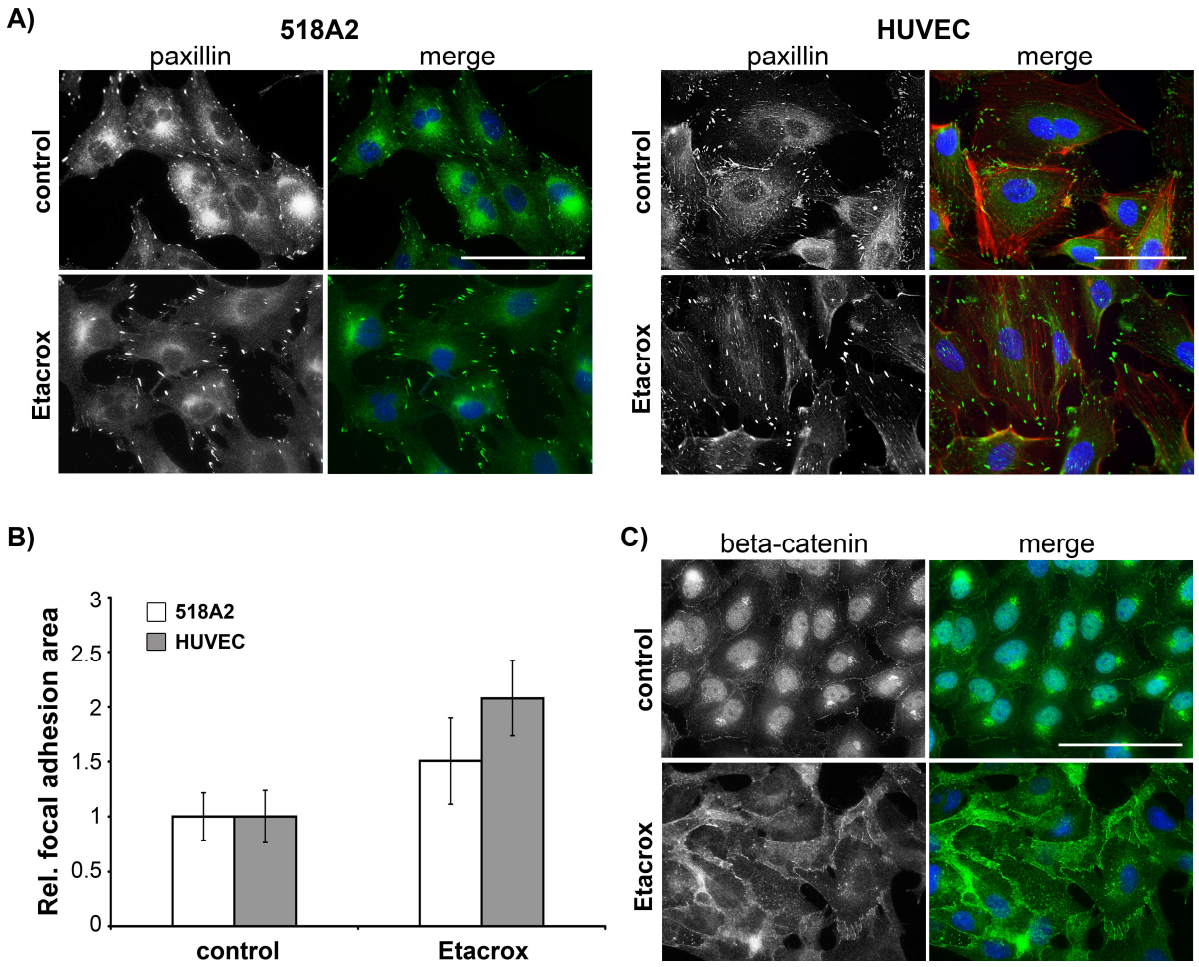

Fig. 4 – Effects of etacrox 3 on focal adhesions and beta-catenin localisation. (A) Focal adhesion density in 518A2 melanoma and primary endothelial cells (HUVEC) treated with etacrox **3** (2.5 µM, 24 h) as visualised by immunofluorescence staining of paxillin (green). HUVEC co-stained for F-actin with phalloidin (red, merge). (B) Densitometric quantification of the focal adhesion area relative to whole cell bodies in 518A2 cells (white bars) and HUVEC (grey bars) with respect to vehicle controls set to 1. (C) Beta-catenin localisation in EGF-stimulated 518A2 cells treated with etacrox **3** (5 µM, 24 h) visualised by immunofluorescence staining (green, merge). Nuclei counterstained with DAPI (blue, merge). 400-/630-fold magnification (518A2/HUVEC), scale bars: 100/50 µm.

Another effect reported of vorinostat is its interference with signal transduction by inhibition of Akt phosphorylation [62]. We now found significantly reduced levels of phosphorylated Akt also in 518A2 cells treated with equimolar concentrations of bimacroxam **1**, etacrox **3** or vorinostat (Figure 5). Obviously, bimacroxam **1** or etacrox **3** inhibited the phosphorylation of Akt more strongly and at lower

concentrations when compared with vorinostat. This might once more be a consequence of their higher specificity for cytoplasmic HDACs.

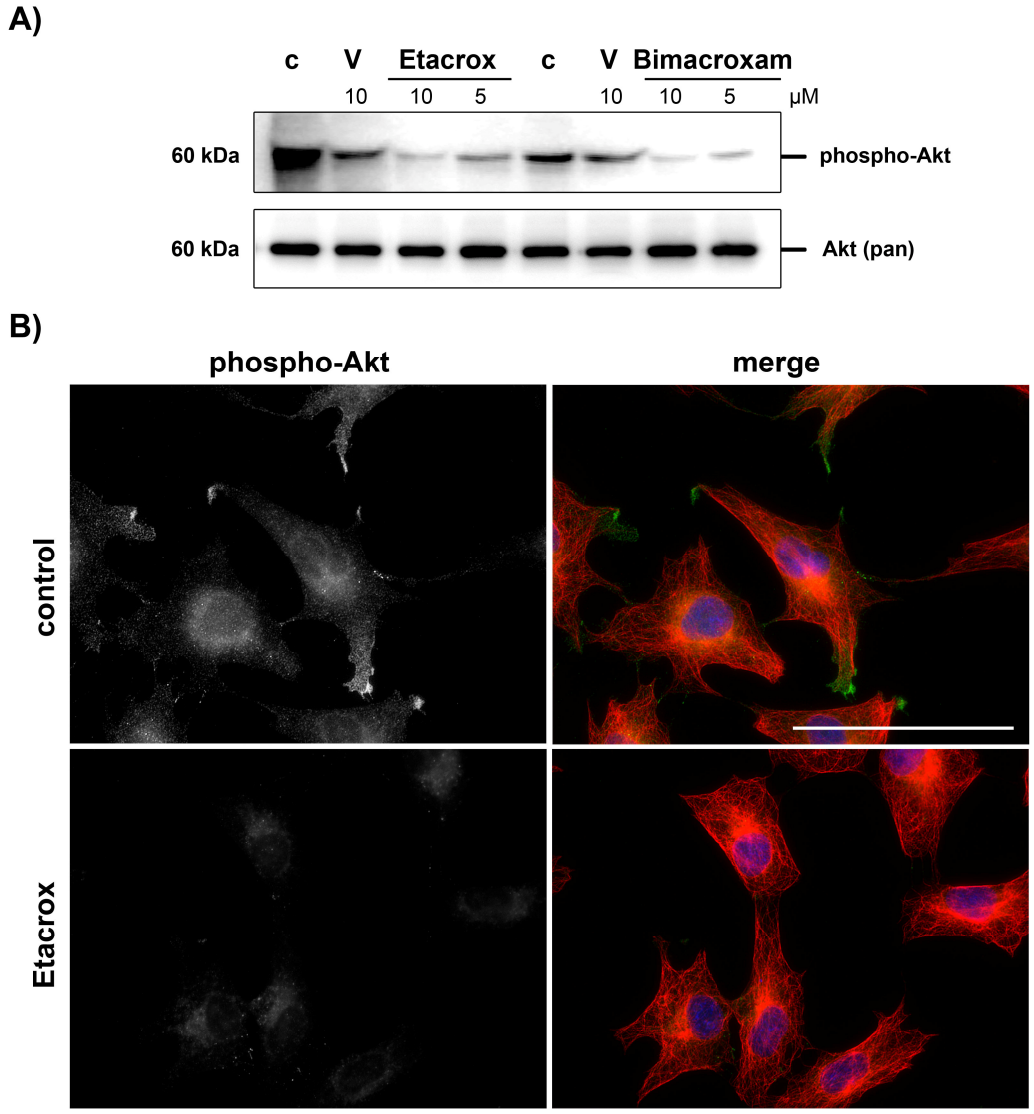

Fig. 5 – Inhibition of Akt phosphorylation in 518A2 melanoma cells by vorinostat, bimacroxam 1 and etacrox 3. Subconfluently-grown cells, pre-treated for 2 h with EGF (200 ng/mL) were incubated for 6 h with DMSO (control), 10 µM vorinostat (V), etacrox **3**, or bimacroxam **1** (10 µM, 5 µM). (A) Western blot analyses of lysed cells using specific antibodies for phosphorylated Akt (phospho-Akt) and total Akt (pan-Akt). (B) Immunofluorescent visualisation of cell bodies by microtubule staining (merge, red) and phosphorylated Akt (phospho-Akt, green), nuclei counterstained with DAPI (merge, blue), 400-fold magnification, scale bar: 100 µm.

In the first place, the new imidazole-hydroxamate conjugates **1**-**3** were devised to more effectively target pro-metastatic factors in tumour progression such as matrix

metalloproteinases (MMP) which allow invasive cancer cells to degrade and remodel the extracellular matrix (ECM) surrounding solid tumours and to invade blood vessels and colonise distant organs [54]. Like HDAC, MMP are zinc-dependent enzymes amenable to inhibition by hydroxamic acid chelators [63]. The effects of HDACi on MMP expression and secretion by human cancers have been discussed controversially in literature. In glioma cells, vorinostat showed but a modest effect on the activity and expression of gelatinases (MMP-2 and MMP-9) [64]. In other cell lines, the pan-HDACi vorinostat and trichostatin A were found to lead to reduced MMP-9 expression [65,66] or to an increase of MMP-9 mRNA levels and expression [67]. However, vorinostat was shown not to interact directly with MMPs [63]. Against this background, we performed experiments employing a fluorophore (FITC)-labelled gelatin substrate that can be degraded by MMP-2 and MMP-9 as secreted by highly-invasive 518A2 melanoma cells to leave small FITC-gelatin fragments the fluorescence intensity of which can be quantified [49]. For an assessmant of MMP-2 and MMP-9 inhibition by vorinostat and the hydroxamic acids **1**-**3** varying concentrations of these compounds were added to FITC-gelatin prior to addition of supernatant 518A2 medium for a 24 h digest reaction.

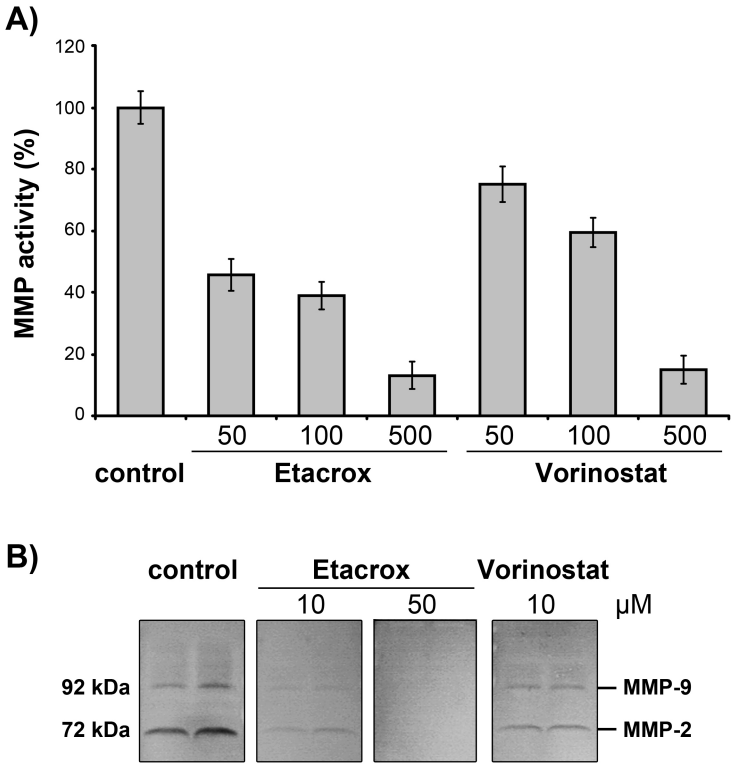

Fig. 6 – Inhibitory effects of vorinostat and etacrox 3 on matrix metalloproteinase (MMP) activity. (A) MMP-2 and MMP-9 secreted by 518A2 cells (MMP activity) and 5 µg FITC-labelled gelatin were incubated with 50-500 µM of vorinostat or tacrox **3** for 24 h. Gelatinolytic activity was measured by the fluorescence of degraded, soluble FITC-gelatin fragments and is shown as the percentage of DMSO-treated controls set to 100% and MMP-free samples set to 1; means of three independent measurements ± S.D. (B) Gelatin zymograms of supernatant medium of 518A2 cells separated by SDS-Gelatin-PAGE were incubated with the indicated concentrations of Vorinostat or Etacrox **3** for 16 h after MMP refolding. Band intensities (inverted colors) representing the in-gel-efficacy of MMP-2 (72 kDa) and MMP-9 (92 kDa) in degrading copolymerised gelatin.

As expected, high concentrations of vorinostat were necessary to cause a significant reduction of the overall MMP activity (i.e., of MMP-2 plus MMP-9) when compared to etacrox **3** (Figure 6A). This was confirmed by gelatin zymography where equal volumes of conditioned medium were subjected to SDS-PAGE with co-polymerised gelatin (Figure 6B). The resulting gels were incubated in the absence (DMSO control) or presence of the compounds prior to detection of gelatin degradation at relevant molecular weight heights as white bands on dark Coomassie-stained background.

10 µM and 50 µM of etacrox **3** were sufficient to reduce the activity of both MMP-2 and MMP-9 after 24 h incubation of the gels.

Next, we assessed the antiangiogenic activity of the imidazoles by *in vitro* tube formation assays which exploit the propensity of endothelial cells to form vessel-like networks upon stimulation with growth factors. Ea.hy926 cells were incubated with imidazoles **1** or **3** immediately after seeding them onto thin matrigel layers. Although a partial destruction of tubular segments by the imidazoles applied at a concentration of 10 µM was observed (Figure 7A) we cannot attribute this effect to any antiangiogenic activity since the cytotoxicity of **1** and **3** in parallel MTT-assays was also considerable (reduction to 40-50% of initial cells). However, a topical application of etacrox **3** onto developing blood vessels in the chorioallantoic membrane (CAM) of fertilised chicken eggs resulted in a significant suppression of further vascularisation and a degeneration of established blood vessels (Figure 7B).

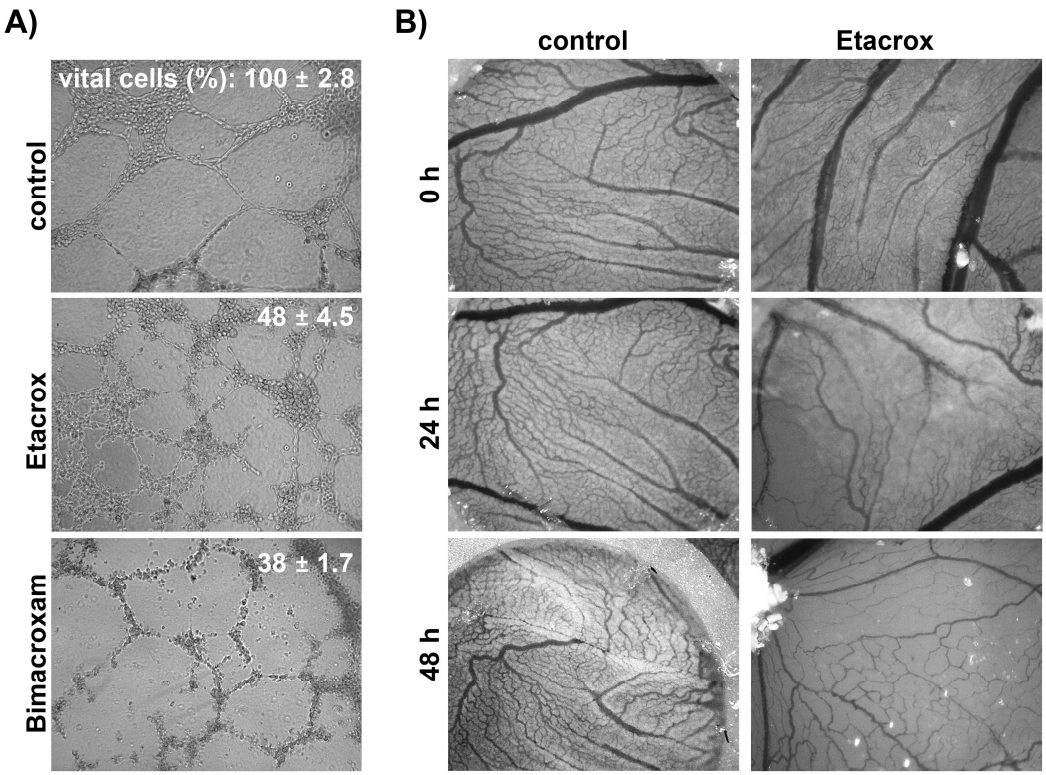

Fig. 7 – Antiangiogenic activity of bimacroxam 1 and etacrox 3 in *in vitro* and i*n vivo* models. (A) Formation of tubular, blood-vessel-like networks by Ea.hy926 endothelial cells when grown on matrigel, and interference of 10 µM of imidazoles **1** and **3** (tube formation assay; 24 h). Light micrographs, 100-fold magnification, percentage of remaining vital cells was determined by MTT reduction relative to DMSO-treated controls set to 100% (values shown are representative of three independent experiments ± S.D). (B) Effects by etacrox **3** (20 nmol/day) on developing blood vessels in the chorioallantoic membrane (CAM) of fertilised chicken eggs (60-fold magnification).

We assume that this suppression of blood vessel formation is linked not only to MMP-2 inhibition [68] and the various cytoskeletal alterations explained above, but also to drug-induced acetylations of other cellular proteins playing a role in angiogenic signalling and endothelial cell motility. The antiangiogenic effects ocassionally observed for other HDACi were accounted for in literature by reduced VEGFR signalling [24] and a destabilisation of the proangiogenic hypoxia-inducable factor HIF-1alpha [25].

In three-dimensional, chemotactic transwell migration studies we further evaluated the potential of etacrox **3** to inhibit invasion and migration of cancer cells. In these assays serum-starved cells seeded into the upper compartment of a two-chamber

setup need to pass a matrigel layer atop a microporous membrane, as a surrogate of the natural ECM, to invade the lower compartment containing high concentrations of a chemoattractant. Cancer cells aquire the ability of directed three-dimensional (3D) migration by adjusting focal adhesion and actin filament turnover as well as microtubule dynamics and the pertinent kinase signalling [51,52,69]. Cell polarity and directed migration also requires at least a partial degradation or remodelling of the surrounding ECM by regulated extracellular proteolysis [70]. Thus, *in vitro* transwell invasion assays reflect the natural environment and behaviour of invasive cancer cells [69,70]. In our experiments, 518A2 melanoma cells and transformed M-MSV-Balb/3T3 mouse fibroblasts were the best at overcoming the artificial ECM barrier while HT-29 colon carcinoma and resistant MCF-7/Topo mammary carcinoma cells proved less invasive (Figure 8A).

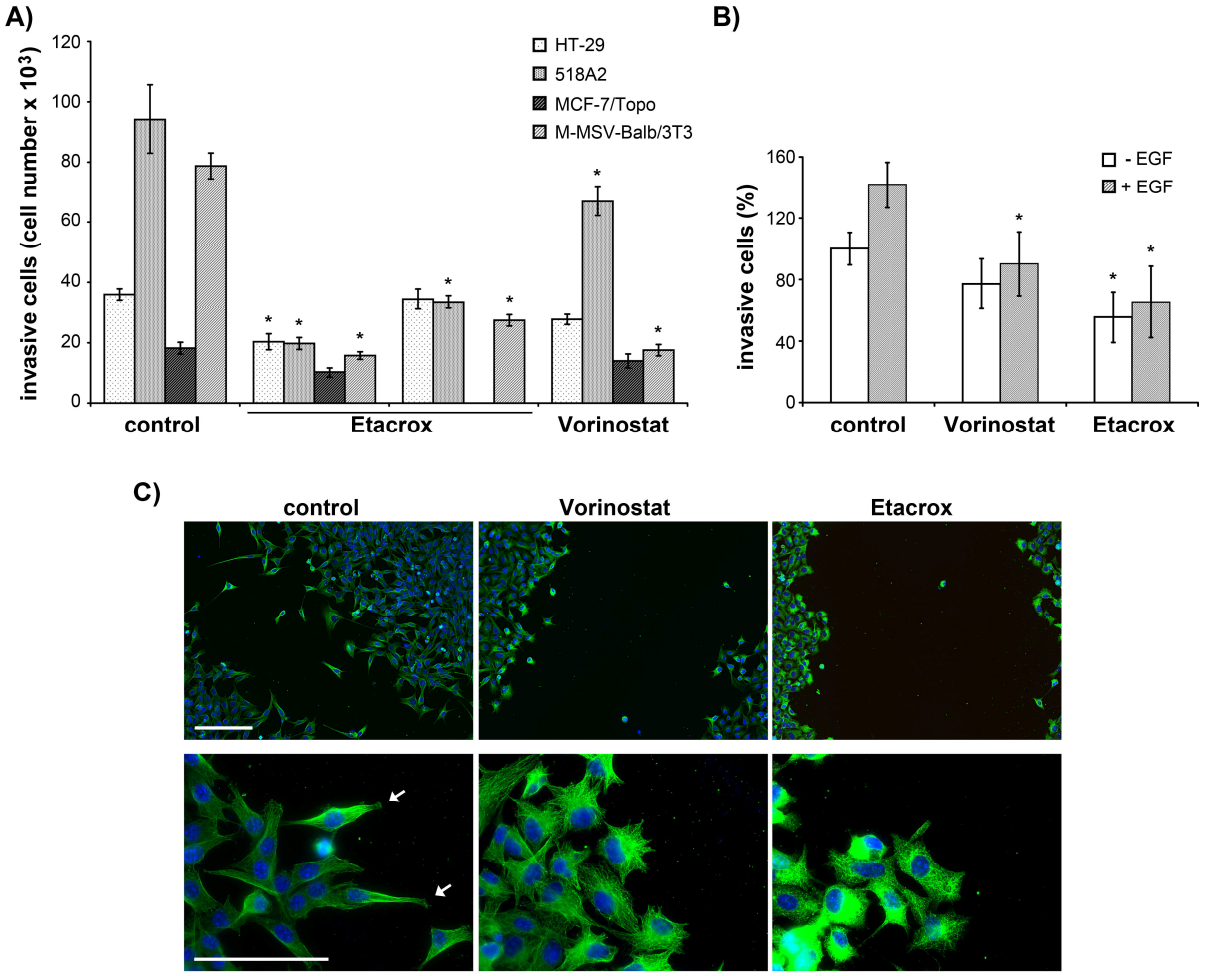

Fig. 8 – Reduced migration of invasive cell lines treated with vorinostat and etacrox in two- and three-dimensional *in vitro* models. (A) Migration of human HT-29 colon carcinoma, 518A2 melanoma, MCF-7/Topo breast cancer cells and transformed M-MSV-Balb/3T3 mouse fibroblasts through matrigel-coated cell culture inserts upon incubation with DMSO (control), vorinostat (HT-29, M-MSV-Balb/3T3: 1 µM; 518A2: 1 µM; MCF-7/Topo: 5 µM) or etacrox **3** (HT-29: 0.5/0.25 µM; 518A2, M-MSV-Balb/3T3: 1/0.5 µM; MCF-7/Topo: 5 µM) for 48 h. The number of invasive cells obtained from independent experiments was normalised to controls and shown ± S.D. (B) Migration of epidermal growth factor receptor (EGFR)-positive MCF-7/Topo cells additionally incubated with 200 ng/mL EGF, influenced by treatment with 10 µM vorinostat or 5 µM etacrox **3** for 48 h. DMSO-treated (control) cells without EGF stimulation were set to 100% ± S.D. Asterisks indicate statistically significant differences [$P \leq 0.05$ for control versus treated samples calculated by Student's *t*-test]. (C) Fibroblast 2D-migration across an artificial wound generated within an M-MSV-Balb/3T3 cell monolayer after 24 h treatment with DMSO, 5 µM vorinostat or 1 µM etacrox **3**. Fibroblast-characteristic microtubule protrusions (indicated by arrows) visualised by immunofluorescent alpha-tubulin staining (green), nuclei counterstained with DAPI (blue). Upper row: 100-fold magnification, scale bar: 200 µm; lower row: 400-fold magnification, scale bar: 100 µm.

All cell lines were treated with merely slightly toxic concentrations of vorinostat or etacrox **3** to ensure that any reduced migration originates predominantly from compound-induced signalling and cytoskeleton alterations and not from cytotoxicity. The reduction of invasive cells in etacrox-treated samples was significant and surpassed that in samples treated with equimolar concentrations of vorinostat in all tested cell lines. Although the number of cells migrating across the matrigel barrier is partly dependent on cell line-specific proliferation rates, control experiments showed that endothelial cells or non-malignant fibroblasts treated with DMSO or HDACi did not migrate through the barrier in substantial numbers within the incubation period (invasive cells < 10%, data not shown).

MCF-7/Topo breast carcinoma cells that were additionally stimulated by EGF displayed an invasiveness increased by about 40% when compared to non-stimulated cells. This stimulation could be completely precluded by pre-treatment with vorinostat or etacrox **3** (Figure 8B). This is a further indication for interference with EGFR-translocation and -signalling playing a role in the antimigratory activity of these HDACi [20,71].

The tumorigenic MSV-Balb/3T3 fibroblasts were included in the migration studies since cancer cells are believed to undergo an EMT, changing their expression profile towards mesenchymal characteristics, and behave fibroblast-like during ECM invasion and blood vessel intravasation, avoiding cell-cell adhesion [70,72]. A prerequisite for such a directed fibroblast-like migration are functional microtubules as mediators of cell polarisation [73–75]. Since microtubule stability and function was shown to be affected by vorinostat and etacrox **3**, we also investigated their influence on the migratory behaviour and the cell shape of MSV-Balb/3T3 fibroblasts in so-called ‘wound healing’ assays. In these, an artificial wound is scraped in a confluent fibroblast monolayer which is then left to overgrow and eventually close with

migrating cells (Figure 8C). Treatment of MSV-Balb/3T3 fibroblasts with vorinostat or etacrox changed their phenotype via induction of actin stress fibres [37] and focal adhesions (*cf.* Figures 2C and 4), slowed down their migratory speed, and retarded the closure of the 'wound'. In contrast, untreated control cells migrated half the distance to the opposite monolayer frontiers within 24 h. Their predominant phenotype is characterised by elongated cell bodies with microtubule protrusions.

Conclusions

The new 4-(1-ethyl-4-anisyl-imidazol-5-yl)-*N*-hydroxycinnamide (etacrox) is superior to the clinically used HDACi vorinostat in terms of the magnitude and subtype specificity of HDAC inhibition and also with respect to the broadness of its additional anticancer properties. These include antiangiogenic, antimigratory, and antiinvasive activities which are based partly on the HDACi function of the hydroxamic acid moiety. Etacrox is also superior to its close 1-methyl analogues concerning HDAC6 specificity and cancer cell toxicity. We hypothesise that *in vitro* nuclear HDAC such as HDAC1 are less affected by it than by vorinostat while class II HDAC such as HDAC6 were inhibited to a greater extent. This might be a consequence of a higher general affinity for cytoplasmic HDAC or of a compound-specific cellular uptake and subcellular distribution.

Etacrox is a pleiotropic anticancer drug candidate which addresses several crucial targets in the 'invasion–metastasis cascade' of cancer development and spread. It reduces the levels of active MMP-2 and -9 which are important for tumour vascularisation and ECM invasion. By inhibiting cancer cell signalling via Akt and beta-catenin etacrox contributes to enhanced cell-cell contacts and a reduction of cancer cell migration and invasiveness and also to an improved cytotoxicity. The combination of stress fibre and focal adhesion induction with hyperacetylation of

tubulin leads to a largely disfunctional cytoskeleton of cancer and endothelial cells, thus amplifying both the antiangiogenic and antiinvasive effects of etacrox. Tumorigenic fibroblasts, which are much akin to tumour cells having gone through the epithelial-mesenchymal transition in the course of metastasis, were likewise affected by etacrox. It is a promising new HDACi candidate, not least when considering its excellent water solubility and its tolerance by mice which showed no loss of weight or any other negative symptoms when treated twice with 150 mg/kg body weight on two consecutive days in preliminary tests.

Supplementary Information available.

Chemical synthesis and characterisation of etacrox **3**; method descriptions; additional data for TUNEL-apoptosis assays, cell cycle analyses, Western blot analyses; original images of Western blot membranes, gelatin zymograms, preliminary animal studies.

References

[1] W.K. Kelly, P.A. Marks, Drug Insight: histone deacetylase inhibitors—development of the new targeted anticancer agent suberoylanilide hydroxamic acid, Nat. Clin. Pract. Oncol. 2 (2005) 150–157. doi:10.1038/ncponc0106.

[2] W.S. Xu, R.B. Parmigiani, P.A. Marks, Histone deacetylase inhibitors: molecular mechanisms of action, Oncogene. 26 (2007) 5541–5552. doi:10.1038/sj.onc.1210620.

[3] S. Minucci, P.G. Pelicci, Histone deacetylase inhibitors and the promise of epigenetic (and more) treatments for cancer, Nat. Rev. Cancer. 6 (2006) 38–51. doi:10.1038/nrc1779.

[4] A. Mai, L. Altucci, Epi-drugs to fight cancer: From chemistry to cancer treatment, the road ahead, Int. J. Biochem. Cell Biol. 41 (2009) 199–213. doi:10.1016/j.biocel.2008.08.020.

[5] M. New, H. Olzscha, N.B. La Thangue, HDAC inhibitor-based therapies: Can we interpret the code?, Mol. Oncol. 6 (2012) 637–656. doi:10.1016/j.molonc.2012.09.003.

[6] M. Dokmanovic, C. Clarke, P.A. Marks, Histone Deacetylase Inhibitors: Overview and Perspectives, Mol. Cancer Res. 5 (2007) 981–989. doi:10.1158/1541-7786.MCR-07-0324.

[7] D.M.P. Phillips, The presence of acetyl groups in histones, Biochem. J. 87 (1963) 258.

[8] K. Sadoul, C. Boyault, M. Pabion, S. Khochbin, Regulation of protein turnover by acetyltransferases and deacetylases, Biochimie. 90 (2008) 306–312. doi:10.1016/j.biochi.2007.06.009.

[9] S.C. Kim, R. Sprung, Y. Chen, Y. Xu, H. Ball, J. Pei, et al., Substrate and Functional Diversity of Lysine Acetylation Revealed by a Proteomics Survey, Mol. Cell. 23 (2006) 607–618. doi:10.1016/j.molcel.2006.06.026.

[10] M. Ocker, Deacetylase inhibitors - focus on non-histone targets and effects, World J. Biol. Chem. 1 (2010). doi:10.4331/wjbc.v1.i5.55.

[11] S. Spange, T. Wagner, T. Heinzel, O.H. Krämer, Acetylation of non-histone proteins modulates cellular signalling at multiple levels, Int. J. Biochem. Cell Biol. 41 (2009) 185–198. doi:10.1016/j.biocel.2008.08.027.

[12] P.A. Marks, Discovery and development of SAHA as an anticancer agent, Oncogene. 26 (2007) 1351–1356. doi:10.1038/sj.onc.1210204.

[13] C.S. Mitsiades, N.S. Mitsiades, C.J. McMullan, V. Poulaki, R. Shringarpure, T. Hideshima, et al., Transcriptional signature of histone deacetylase inhibition in multiple myeloma: biological and clinical implications, Proc. Natl. Acad. Sci. U. S. A. 101 (2004) 540–545.

[14] K.B. Glaser, M.J. Staver, J.F. Waring, J. Stender, R.G. Ulrich, S.K. Davidsen, Gene expression profiling of multiple histone deacetylase (HDAC) inhibitors: defining a common gene set produced by HDAC inhibition in T24 and MDA carcinoma cell lines, Mol. Cancer Ther. 2 (2003) 151–163.

[15] M.A. Glozak, E. Seto, Histone deacetylases and cancer, Oncogene. 26 (2007) 5420–5432. doi:10.1038/sj.onc.1210610.

[16] G.I. Aldana-Masangkay, K.M. Sakamoto, The Role of HDAC6 in Cancer, J. Biomed. Biotechnol. 2011 (2011) 1–10. doi:10.1155/2011/875824.

[17] C. Hubbert, A. Guardiola, R. Shao, Y. Kawaguchi, A. Ito, A. Nixon, et al., HDAC6 is a microtubule-associated deacetylase, Nature. 417 (2002) 455–458. doi:10.1038/417455a.

[18] A. Matsuyama, T. Shimazu, Y. Sumida, A. Saito, Y. Yoshimatsu, D. Seigneurin-Berny, et al., In vivo destabilization of dynamic microtubules by HDAC6-mediated deacetylation, EMBO J. 21 (2002) 6820–6831.
[19] N.A. Reed, D. Cai, T.L. Blasius, G.T. Jih, E. Meyhofer, J. Gaertig, et al., Microtubule Acetylation Promotes Kinesin-1 Binding and Transport, Curr. Biol. 16 (2006) 2166–2172. doi:10.1016/j.cub.2006.09.014.
[20] Y. s. Gao, C.C. Hubbert, T.P. Yao, The Microtubule-associated Histone Deacetylase 6 (HDAC6) Regulates Epidermal Growth Factor Receptor (EGFR) Endocytic Trafficking and Degradation, J. Biol. Chem. 285 (2010) 11219–11226. doi:10.1074/jbc.M109.042754.
[21] H. Song, C.-W. Li, A.M. Labaff, S.-O. Lim, L.-Y. Li, S.-F. Kan, et al., Acetylation of EGF receptor contributes to tumor cell resistance to histone deacetylase inhibitors, Biochem. Biophys. Res. Commun. 404 (2011) 68–73. doi:10.1016/j.bbrc.2010.11.064.
[22] Y. Li, X. Zhang, R.D. Polakiewicz, T.-P. Yao, M.J. Comb, HDAC6 Is Required for Epidermal Growth Factor-induced -Catenin Nuclear Localization, J. Biol. Chem. 283 (2008) 12686–12690. doi:10.1074/jbc.C700185200.
[23] R. Wang, P. Cherukuri, J. Luo, Activation of Stat3 sequence-specific DNA binding and transcription by p300/CREB-binding protein-mediated acetylation, J. Biol. Chem. 280 (2005) 11528–11534. doi:10.1074/jbc.M413930200.
[24] C.F. Deroanne, C. Bonjean, S. Servotte, L. Devy, A. Colige, N. Clausse, et al., Histone deacetylases inhibitors as anti-angiogenic agents altering vascular endothelial growth factor signaling, Oncogene. 21 (2002) 427–436.
[25] J.-W. Jeong, M.-K. Bae, M.-Y. Ahn, S.-H. Kim, T.-K. Sohn, M.-H. Bae, et al., Regulation and destabilization of HIF-1α by ARD1-mediated acetylation, Cell. 111 (2002) 709–720.
[26] D. Kaluza, J. Kroll, S. Gesierich, T.-P. Yao, R.A. Boon, E. Hergenreider, et al., Class IIb HDAC6 regulates endothelial cell migration and angiogenesis by deacetylation of cortactin, EMBO J. 30 (2011) 4142–4156.
[27] X. Zhang, Z. Yuan, Y. Zhang, S. Yong, A. Salas-Burgos, J. Koomen, et al., HDAC6 Modulates Cell Motility by Altering the Acetylation Level of Cortactin, Mol. Cell. 27 (2007) 197–213. doi:10.1016/j.molcel.2007.05.033.
[28] M.S. Finnin, J.R. Donigian, A. Cohen, V.M. Richon, R.A. Rifkind, P.A. Marks, et al., Structures of a histone deacetylase homologue bound to the TSA and SAHA inhibitors, Nature. 401 (1999) 188–193. doi:10.1038/43710.
[29] F.F. Wagner, D.E. Olson, J.P. Gale, T. Kaya, M. Weïwer, N. Aidoud, et al., Potent and Selective Inhibition of Histone Deacetylase 6 (HDAC6) Does Not Require a Surface-Binding Motif, J. Med. Chem. 56 (2013) 1772–1776. doi:10.1021/jm301355j.
[30] O. Khan, N.B. La Thangue, HDAC inhibitors in cancer biology: emerging mechanisms and clinical applications, Immunol. Cell Biol. 90 (2012) 85–94. doi:10.1038/icb.2011.100.
[31] H.-J. Kim, S.-C. Bae, Histone deacetylase inhibitors: molecular mechanisms of action and clinical trials as anti-cancer drugs, Am. J. Transl. Res. 3 (2011). http://www.ncbi.nlm.nih.gov/pmc/articles/PMC3056563/ (accessed August 2, 2014).
[32] J.A. Plumb, P.W. Finn, R.J. Williams, M.J. Bandara, M.R. Romero, C.J. Watkins, et al., Pharmacodynamic response and inhibition of growth of human tumor xenografts by the novel histone deacetylase inhibitor PXD101, Mol. Cancer Ther. 2 (2003) 721–728.

[33] V.R. Fantin, V.M. Richon, Mechanisms of Resistance to Histone Deacetylase Inhibitors and Their Therapeutic Implications, Clin. Cancer Res. 13 (2007) 7237–7242. doi:10.1158/1078-0432.CCR-07-2114.
[34] V.R. Fantin, A. Loboda, C.P. Paweletz, R.C. Hendrickson, J.W. Pierce, J.A. Roth, et al., Constitutive activation of signal transducers and activators of transcription predicts vorinostat resistance in cutaneous T-cell lymphoma, Cancer Res. 68 (2008) 3785–3794. doi:10.1158/0008-5472.CAN-07-6091.
[35] R. Schobert, B. Biersack, A. Dietrich, K. Effenberger, S. Knauer, T. Mueller, 4-(3-Halo/amino-4,5-dimethoxyphenyl)-5-aryloxazoles and - *N* -methylimidazoles That Are Cytotoxic against Combretastatin A Resistant Tumor Cells and Vascular Disrupting in a Cisplatin Resistant Germ Cell Tumor Model, J. Med. Chem. 53 (2010) 6595–6602. doi:10.1021/jm100345r.
[36] P. Di Fazio, S. Lingelbach, R. Schobert, B. Biersack, 4,5-Diaryl imidazoles with hydroxamic acid appendages as anti-hepatoma agents, Invest. New Drugs. (2014). doi:10.1007/s10637-014-0188-0.
[37] K. Mahal, S. Schruefer, G. Steinemann, F. Rausch, R. Schobert, B. Biersack, et al., Biological evaluation of 4,5-diarylimidazoles with hydroxamic acid appendages as novel dual mode anticancer agents, Cancer Chemother. Pharmacol. (2015). doi:10.1007/s00280-015-2685-z.
[38] K. Mahal, S. Schruefer, G. Steinemann, F. Rausch, R. Schobert, M. Höpfner, et al., Biological evaluation of 4,5-diaryl imidazoles with hydroxamic acid appendages as novel dual mode anticancer agents, Cancer Chemother. Pharmacol. in press (2015).
[39] B. Jansen, H. Schlagbauer-Wadl, H.-G. Eichler, K. Wolff, A. van Elsas, P.I. Schrier, et al., Activated N-ras contributes to the chemoresistance of human melanoma in severe combined immunodeficiency (SCID) mice by blocking apoptosis, Cancer Res. 57 (1997) 362–365.
[40] C.J. Edgell, C.C. McDonald, J.B. Graham, Permanent cell line expressing human factor VIII-related antigen established by hybridization, Proc. Natl. Acad. Sci. 80 (1983) 3734–3737.
[41] J. Bauer, M. Margolis, C. Schreiner, C.-J. Edgell, J. Azizkhan, E. Lazarowski, et al., In vitro model of angiogenesis using a human endothelium-derived permanent cell line: Contributions of induced gene expression, G-proteins, and integrins, J. Cell. Physiol. 153 (1992) 437–449.
[42] E. Aranda, G.I. Owen, A semi-quantitative assay to screen for angiogenic compounds and compounds with angiogenic potential using the EA. hy926 endothelial cell line, Biol. Res. 42 (2009) 377–389.
[43] J.D. Dignam, R.M. Lebovitz, R.G. Roeder, Accurate transcription initiation by RNA polymerase II in a soluble extract from isolated mammalian nuclei, Nucleic Acids Res. 11 (1983) 1475–1489.
[44] C.-H. Chang, F.-Y. Yu, T.-S. Wu, L.-T. Wang, B.-H. Liu, Mycotoxin Citrinin Induced Cell Cycle G2/M Arrest and Numerical Chromosomal Aberration Associated with Disruption of Microtubule Formation in Human Cells, Toxicol. Sci. 119 (2011) 84–92. doi:10.1093/toxsci/kfq309.
[45] A. Lieuvin, J.-C. Labbé, M. Dorée, D. Job, Intrinsic microtubule stability in interphase cells, J. Cell Biol. 124 (1994) 985–996.
[46] N. Teramura, K. Tanaka, K. Iijima, O. Hayashida, K. Suzuki, S. Hattori, et al., Cloning of a Novel Collagenase Gene from the Gram-Negative Bacterium Grimontia (Vibrio) hollisae 1706B and Its Efficient Expression in Brevibacillus choshinensis, J. Bacteriol. 193 (2011) 3049–3056. doi:10.1128/JB.01528-10.

[47] L. Troeberg, H. Nagase, Zymography of metalloproteinases, Curr. Protoc. Protein Sci. (2004) 21–15.
[48] P.A. Snoek, J.W. Von den Hoff, Zymographic techniques for the analysis of matrix metalloproteinases and their inhibitors., (2005). http://repository.ubn.ru.nl/handle/2066/47379 (accessed November 20, 2014).
[49] C. Spoerlein, K. Mahal, H. Schmidt, R. Schobert, Effects of chrysin, apigenin, genistein and their homoleptic copper(II) complexes on the growth and metastatic potential of cancer cells, J. Inorg. Biochem. 127 (2013) 107–115. doi:10.1016/j.jinorgbio.2013.07.038.
[50] B. Nitzsche, C. Gloesenkamp, M. Schrader, M. Ocker, R. Preissner, M. Lein, et al., Novel compounds with antiangiogenic and antiproliferative potency for growth control of testicular germ cell tumours, Br. J. Cancer. 103 (2010) 18–28. doi:10.1038/sj.bjc.6605725.
[51] S. Boyden, The chemotactic effect of mixtures of antibody and antigen on polymorphonuclear leucocytes, J. Exp. Med. 115 (1962) 453–466.
[52] F. Entschladen, T.L. Drell, K. Lang, K. Masur, D. Palm, P. Bastian, et al., Analysis methods of human cell migration, Exp. Cell Res. 307 (2005) 418–426. doi:10.1016/j.yexcr.2005.03.029.
[53] A. Albini, Y. Iwamoto, H.K. Kleinman, G.R. Martin, S.A. Aaronson, J.M. Kozlowski, et al., A rapid in vitro assay for quantitating the invasive potential of tumor cells, Cancer Res. 47 (1987) 3239–3245.
[54] U.B. Hofmann, R. Houben, E.-B. Bröcker, J.C. Becker, Role of matrix metalloproteinases in melanoma cell invasion, Biochimie. 87 (2005) 307–314. doi:10.1016/j.biochi.2005.01.013.
[55] A.D.-A. Tran, T.P. Marmo, A.A. Salam, S. Che, E. Finkelstein, R. Kabarriti, et al., HDAC6 deacetylation of tubulin modulates dynamics of cellular adhesions, J. Cell Sci. 120 (2007) 1469–1479. doi:10.1242/jcs.03431.
[56] S. Vishwakarma, L.R. Iyer, M. Muley, P.K. Singh, A. Shastry, A. Saxena, et al., Tubastatin, a selective histone deacetylase 6 inhibitor shows anti-inflammatory and anti-rheumatic effects, Int. Immunopharmacol. 16 (2013) 72–78. doi:10.1016/j.intimp.2013.03.016.
[57] K.V. Butler, J. Kalin, C. Brochier, G. Vistoli, B. Langley, A.P. Kozikowski, Rational Design and Simple Chemistry Yield a Superior, Neuroprotective HDAC6 Inhibitor, Tubastatin A, J. Am. Chem. Soc. 132 (2010) 10842–10846. doi:10.1021/ja102758v.
[58] K. Sadoul, J. Wang, B. Diagouraga, S. Khochbin, The Tale of Protein Lysine Acetylation in the Cytoplasm, J. Biomed. Biotechnol. 2011 (2011) 1–15. doi:10.1155/2011/970382.
[59] M.S. Longworth, L.A. Laimins, Histone deacetylase 3 localizes to the plasma membrane and is a substrate of Src, Oncogene. 25 (2006) 4495–4500.
[60] D. Waltregny, Histone deacetylase HDAC8 associates with smooth muscle -actin and is essential for smooth muscle cell contractility, FASEB J. (2005). doi:10.1096/fj.04-2303fje.
[61] H. Ouyang, Y.O. Ali, M. Ravichandran, A. Dong, W. Qiu, F. MacKenzie, et al., Protein Aggregates Are Recruited to Aggresome by Histone Deacetylase 6 via Unanchored Ubiquitin C Termini, J. Biol. Chem. 287 (2012) 2317–2327. doi:10.1074/jbc.M111.273730.
[62] M.B. Wozniak, R. Villuendas, J.R. Bischoff, C.B. Aparicio, J.F. Martínez Leal, P. de La Cueva, et al., Vorinostat interferes with the signaling transduction pathway of T-cell receptor and synergizes with phosphoinositide-3 kinase

inhibitors in cutaneous T-cell lymphoma, Haematologica. 95 (2010) 613–621. doi:10.3324/haematol.2009.013870.
[63] J.A. Day, S.M. Cohen, Investigating the Selectivity of Metalloenzyme Inhibitors, J. Med. Chem. 56 (2013) 7997–8007. doi:10.1021/jm401053m.
[64] Z. An, C.B. Gluck, M.L. Choy, L.J. Kaufman, Suberoylanilide hydroxamic acid limits migration and invasion of glioma cells in two and three dimensional culture, Cancer Lett. 292 (2010) 215–227. doi:10.1016/j.canlet.2009.12.006.
[65] F. Wang, Y. Qi, X. Li, W. He, Q.-X. Fan, H. Zong, HDAC inhibitor trichostatin A suppresses esophageal squamous cell carcinoma metastasis through HADC2 reduced MMP-2/9, Clin. Invest. Med. 36 (2013) E87–E94.
[66] Q.-Y. Choo, P.C. Ho, Y. Tanaka, H.-S. Lin, Histone deacetylase inhibitors MS-275 and SAHA induced growth arrest and suppressed lipopolysaccharide-stimulated NF- B p65 nuclear accumulation in human rheumatoid arthritis synovial fibroblastic E11 cells, Rheumatology. 49 (2010) 1447–1460. doi:10.1093/rheumatology/keq108.
[67] D. Kong, A. Ahmad, B. Bao, Y. Li, S. Banerjee, F.H. Sarkar, Histone Deacetylase Inhibitors Induce Epithelial-to-Mesenchymal Transition in Prostate Cancer Cells, PLoS ONE. 7 (2012). doi:10.1371/journal.pone.0045045.
[68] J. Fang, Y. Shing, D. Wiederschain, L. Yan, C. Butterfield, G. Jackson, et al., Matrix metalloproteinase-2 is required for the switch to the angiogenic phenotype in a tumor model, Proc. Natl. Acad. Sci. 97 (2000) 3884–3889. doi:10.1073/pnas.97.8.3884.
[69] T.R. Geiger, D.S. Peeper, Metastasis mechanisms, Biochim. Biophys. Acta BBA - Rev. Cancer. 1796 (2009) 293–308. doi:10.1016/j.bbcan.2009.07.006.
[70] P. Friedl, K. Wolf, Tumour-cell invasion and migration: diversity and escape mechanisms, Nat. Rev. Cancer. 3 (2003) 362–374. doi:10.1038/nrc1075.
[71] H. Song, C.-W. Li, A.M. Labaff, S.-O. Lim, L.-Y. Li, S.-F. Kan, et al., Acetylation of EGF receptor contributes to tumor cell resistance to histone deacetylase inhibitors, Biochem. Biophys. Res. Commun. 404 (2011) 68–73. doi:10.1016/j.bbrc.2010.11.064.
[72] J.P. Thiery, Epithelial-mesenchymal transitions in tumour progression, Nat. Rev. Cancer. 2 (2002) 442–454. doi:10.1038/nrc822.
[73] S. Etienne-Manneville, Microtubules in Cell Migration, Annu. Rev. Cell Dev. Biol. 29 (2013) 471–499. doi:10.1146/annurev-cellbio-101011-155711.
[74] C. Ballestrem, B. Wehrle-Haller, B. Hinz, B.A. Imhof, Actin-dependent lamellipodia formation and microtubule-dependent tail retraction control-directed cell migration, Mol. Biol. Cell. 11 (2000) 2999–3012.
[75] C.M. Waterman-Storer, R.A. Worthylake, B.P. Liu, K. Burridge, E.D. Salmon, Microtubule growth activates Rac1 to promote lamellipodial protrusion in fibroblasts, Nat. Cell Biol. 1 (1999) 45–50. doi:10.1038/9018.

- Supplementary Material -

4-(1-Ethyl-4-anisyl-imidazol-5-yl)-*N*-hydroxycinnamide – A new pleiotropic HDAC inhibitor targeting cancer cell signalling and cytoskeletal organisation

Experimental Cell Research

Katharina Mahal[a], Philip Kahlen[b], Bernhard Biersack[a], Rainer Schobert*[,a]

[a] Organic Chemistry Laboratory, University of Bayreuth, Universitätsstrasse 30, 95440 Bayreuth, Germany

Email: katharina.mahal@uni-bayreuth.de; bernhard.biersack@yahoo.com;

[b] Department of Genetics, University of Bayreuth, Universitätsstrasse 30, 95440 Bayreuth, Germany

Email: philip.kahlen@uni-bayreuth.de;

[*] Corresponding author:

Fax: +49 921 552671; Phone: +49 921 552670;

Email: rainer.schobert@uni-bayreuth.de;

TOC

Methods and experimental procedures

General remarks and instruments used

Column chromatography: silica gel 60 (230-400 mesh). Melting points (uncorrected), Electrothermal 9100; IR spectra, Perkin-Elmer Spectrum One FT-IR spectrophotometer with ATR sampling unit; NMR spectra, Bruker Avance 300 spectrometer; chemical shifts are given in parts per million (δ) downfield from tetramethylsilane as internal standard; Mass spectra, Thermo Finnigan MAT 8500 (EI); Microanalyses, Perkin-Elmer 2400 CHN elemental analyzer. All tested compounds are > 98% pure by elemental analysis. All starting compounds were purchased from the usual retailers and used without further purification.

Cell proliferation assay (MTT assay) [1]

The tetrazolium salt MTT (3-(4,5-dimethylthiazol-2-yl)-2,5-diphenyl-tetrazolium bromide, Carl Roth) was used to identify viable cells by reduction of MTT to a violet formazan. 518A2 melanoma, HCT-1116 colon carcinoma, HT-29 colon adenocarcinoma, MCF-7/Topo mammacarcinoma, KB-V1/Vbl cervix carcinoma, M-MSV-Balb/3T3 mouse fibroblasts ($5x10^3$ cells/well), Ea.hy926 and primary endothelial cells (HUVEC) and non-malignant chicken fibroblasts (CHF, $1x10^4$ cells/well) were seeded on 96-well cell culture plates and cultured for 24 h (37 °C, 5% CO_2, 95% humidity). Incubation with the test compounds **1**-**3** (dilution series ranging from 100 µM to 5 pM in ddH_2O) was continued for 24 h or 72 h. Solvent controls (DMSO) were treated identically. A stock solution of MTT (0.5% in PBS) was added to a final MTT concentration of 0.05%. After 2 h incubation the microplates were centrifuged (300 g, 4 °C, 5 min) and the supernatant medium was discarded prior to cell lysis and dissolving of the precipitated formazan crystals in 30 µl of a SDS-DMSO solution (10% SDS (w/v), 0.6% acetic acid in DMSO) per well. The absorbance at wavelengths 570 and 630 nm (background) was measured using an

automatic microplate reader (Tecan). All experiments were carried out at least in triplicates, the percentage of viable cells quoted was calculated as the mean ± S.D. with respect to the controls set to 100%.

Cell cycle analyses

518A2 melanoma (1×10^5 cells/well), HT-29 colon or MCF-7/Topo breast carcinoma cells (2×10^5 cells/well) grown on 6-well cell culture plates were treated with DMSO (control), vorinostat or the new imidazoles **1**-**3** for 24 h. Cells were collected by trypsination, fixed (ice-cold 70% EtOH, 1 h, 4 °C), and incubated with propidium iodide (PI, Carl Roth) staining solution (50 µg/mL PI, 0.1% sodium citrate, 50 µg/mL RNase A in PBS) for 30 min at 37 °C. The fluorescence intensity of 10,000 single cells at an emission wavelength of 620 nm (excitation with a 488 nm laser source) was recorded with a Beckman Coulter Cytomics FC500 flow cytometer and analysed for the distribution of single cells (%) to G1, S and G2/M phase of the cell cycle as well as for the content of sub-G1 events (apoptotic cells) by using the CXP software (Beckman Coulter).

TUNEL-based detection of apoptotic cells

DNA fragmentation in apoptotic cells was additionally measured using the TUNEL technique (Terminal desoxyribonucleotide Transferase-mediated dUTP Nick End Labelling). Labelling of 3'OH ends was performed with the commercially available FragEL™ DNA Fragmentation Detection Kit (QIA39, Calbiochem) and according to manufacturer's instructions. Briefly, HT-29 cells grown in 25 cm^2-cell culture flasks ($5x10^5$ cells/well) and treated with vehicle (DMSO), 5 µM Vorinostat or the best imidazoles **1**-**3** (5 µM Bimacroxam **1**, 5 µM Animacroxam **2** or 2.5 µM Etacrox **3**) for 24 h. Cells were then trypsinated, pelleted by centrifugation (300 g, 4 °C, 5 min) and fixed in 4% formaldehyde in PBS at room temperature for 10 min followed by

washing of the cell pellets (300 g, 4 °C, 5 min) in 1 mL PBS and two times in 1 mL 1X TBS (Tris-buffered saline, 50 mM Tris-HCl, 150 mM NaCl, pH 7.4). After proteinase K digestion (20 µg/mL per specimen, 5 min, rt) and cell permeabilisation, about $1x10^6$ cells were resuspended in TdT-labelling reaction mixture containing TdT enzyme and fluorescein-coupled dUTPs and incubated at 37 °C for 1 h in the dark. Labelled cells were washed twice with 1 mL TBS before analysis of the green fluorescence intensity on a Beckman Coulter Cytomics FC500 flow cytometer. Data analyses were done with the CXP software (Beckman Coulter), gates defining the percentage of viable and apoptotic cells were applied with respect to DMSO-treated control.

Preparation of cell lysate fractions and determination of cell lysate fraction purity

Cell lysate fractions from HeLa cells were obtained by a modified protocol [2] for nuclei preparation by Dignam *et al.* [3]. Cell pellets from mass cultures were resuspended in cell extraction buffer (20 mM HEPES-KOH, 10 mM KCl, 0.1 mM EDTA, 0.1 mM EGTA, 1.5 mM $MgCl_2$, 0.5 mM DTT, pH 7.4) and incubated on ice for 15 min before adding an equal volume of cell extraction buffer containing 0.2% Triton X-100. After centrifugation (3,000 g, 2 min, 4 °C), the supernatant containing cytosolic proteins was aspirated (*cf.* Figure S4). Lysis of the cells and purity of extracted and intact nuclei was additionally monitored by light and fluorescence microscopy after DAPI staining. The protein concentration of the cell lysate fraction was determined by using a standard Bradford assay (Pierce/Thermo Scientific; HeLa cytosolic extract: 2.3 mg/mL). Total cell lysates were prepared in cell lysis buffer (20 mM Tris-HCl, 1 mM $MgCl_2$, 2 mM EGTA, 0.5% Triton X-100, pH 6.8) supplemented with protease inhibitor (protease inhibitor cocktail set III, EDTA-free, Calbiochem) by using a homogenizer (glass douncer) and according to standard procedures. For subsequent evaluation of cell lysate fraction purity by Western blot analyses, equal

volumes of the whole cell lysate or the cytosolic fraction were mixed with 2X Laemmli buffer and boiled at 95 °C for 10 min prior to SDS-PAGE and transfer to PVDF membranes. Alpha-tubulin and nucleoporin-153 (NUP153) antibodies (anti-alpha-tubulin mouse monoclonal antibody (mAb), invitrogen; anti-NUP153 [clone no. QE5] mouse mAb, abcam) were used as marker for the purity of the cytosolic or nuclear fraction, respectively [4,5]. The respective Western blot is shown in Figure S4.

FITC-labelling of gelatin

Gelatin for the fluorescent monitoring of gelatin degradation by matrix metalloproteinases (MMPs) was labelled with fluorescein isothiocyanate (FITC, Sigma Aldrich) according to manufacturer's manual with some alterations. In brief, 2 mg/mL gelatin (Sigma Aldrich) were dissolved in 0.1 M sodium carbonate buffer (pH 9.0) at 40 °C for 10 min under stirring. 50 µL of a 1 mg/mL FITC stock in DMSO were added dropwise into 1 mL gelatin solution while stirring at 30 °C and the labelling reaction was proceeded for 12 h at 30 °C in the dark. Then, NH_4Cl was added to a final concentration of 50 mM and the solution was stirred for a further 2 h incubation at 30 °C to prevent gelling of the gelatin. The protein solution was then dialysed against PBS (SnakeSkin dialyses tubing, 35 kDa cut-off, Pierce/Thermo Scientific) at 30 °C in the dark for 1 d. The protein concentration was determined by using a nanodrop UV/vis spectrometer (Thermo Scientific) and the solution was diluted to a final concentration of 1 mg/mL. The coupling efficiency (FITC/protein ratio) should range between 0.3 and 1.0 and was determined as 0.53.

Animal studies

The antiangiogenic activity of Etacrox **3** was studied on the established model of highly vascularised 1411HP xenograft tumours previously described [6]. This study was approved by the Laboratory Animal Care Committee of Sachsen-Anhalt,

Germany. Nude mice (Harlan and Winkelmann, Borchen, Germany) received 150 mg/kg body weight of compound **3** by intraperitoneal injection on day 1 and day 2 and effects on apical tumour blood vessels was documented after 24 h with a Canon IXUS 50.

Additional and original data

Chemistry/compound synthesis. Compounds **1**-**2** prepared according to a previous publication [7,8]. The new compound **3** was obtained analogously.

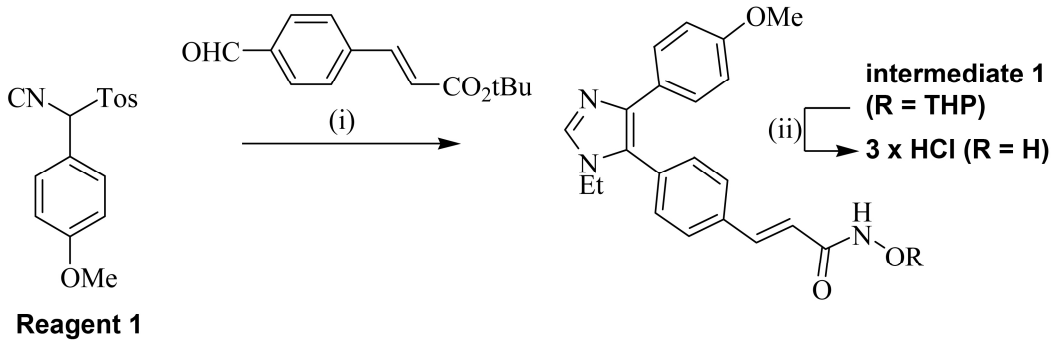

Scheme S1 – Synthesis of the imidazole-based HDAC inhibitior 3. Reagents and conditions: (i) 2M $EtNH_2$/THF, t-BuOH, reflux, 2h, then **Reagent 1**, K_2CO_3, *t*-BuOH, reflux, 3h; b) TFA, CH_2Cl_2, rt, 1 h; c) THPO-NH_2, Et_3N, EDCI, DMAP, CH_2Cl_2, rt, 24 h; (ii) 4M HCl/dioxane, dioxane, rt, 1 h.

*1-Ethyl-4-(4-methoxyphenyl)-5-(4'-tetrahydropyranyloxyaminocarbonylethenyl-phenyl)-imidazole (**intermediate 1**)*

A mixture of 4-formyl-*t*-butylcinnamoate (97 mg, 0.42 mmol) and 2M $EtNH_2$/THF (1.05 mL, 2.10 mmol) in *t*-butanol (15 mL) was refluxed for 2 h. After cooling down to room temperature, **Reagent 1** (126 mg, 0.42 mmol) and K_2CO_3 (500 mg, 3.62 mmol) were added and the reaction mixture was refluxed for 4 h. The solvent was evaporated, the residue diluted with ethyl acetate, washed with water and brine, dried over Na_2SO_4, filtered and concentrated in vacuum. The residue was purified by column chromatography (silica gel 60, ethyl acetate/methanol 9:1) giving the t-butylcinnamoylimidazole intermediate as yellow oil. Yield: 72 mg (0.18 mmol, 43%); R_f = 0.73 (ethyl acetate / methanol, 9:1); ν_{max} (ATR)/cm^{-1}: 2976, 2932, 2835, 1702, 1634, 1611, 1563, 1518, 1494, 1457, 1407, 1392, 1367, 1323, 1292, 1244, 1209, 1173, 1146, 1104, 1030, 981, 949, 871, 832, 799, 767, 730, 660; ^{1}H NMR (300 MHz,

$CDCl_3$): δ 1.23 (3 H, t, J = 7.3 Hz), 1.51 (9 H, s), 3.71 (3 H, s), 3.7-3.9 (2 H, m), 6.39 (1 H, d, J = 16.0 Hz), 6.71 (2 H, d, J = 9.0 Hz), 7.3-7.4 (4 H, m), 7.5-7.6 (4 H, m); ^{13}C NMR (75.5 MHz, $CDCl_3$): δ 16.3, 28.1, 40.1, 55.0, 80.6, 113.7, 114.4, 120.9, 126.5, 127.1, 127.5, 127.9, 128.4, 131.0, 132.0, 132.5, 134.6, 135.5, 136.2, 138.5, 142.5, 158.2, 166.0.

The intermediate (72 mg, 0.18 mmol) was dissolved in CH_2Cl_2 (3 mL), treated with TFA (2 mL) and stirred at room temperature for 1 h. The solvent was evaporated, the residue was dried in vacuum and used for the next step without further purification. It was dissolved in dry DCM and EDCI (98 mg, 0.51 mmol), DMAP (19 mg, 0.14 mmol), triethyl amine (117 µL, 0.55 mmol) and tetrahydropyranyl hydroxylamine (71 mg, 0.61 mmol) were added. After stirring at room temperature for 24 h, the solvent was evaporated and the residue was purified by column chromatography (silica gel 60, ethyl acetate / methanol, 9:1). Yield: 52 mg (0.12 mmol, 67%); R_f = 0.37 (ethyl acetate / methanol, 95:5); ν_{max} (ATR)/cm^{-1}: 3158, 2941, 2869, 1662, 1626, 1613, 1518, 1494, 1462, 1442, 1336, 1294, 1245, 1203, 1174, 1129, 1112, 1030, 981, 948, 895, 872, 831, 816, 800, 727, 661; ^1H NMR (300 MHz, $CDCl_3$): δ 1.1-1.3 (3 H, m), 1.5-1.6 (3 H, m), 1.8-1.9 (3 H, m), 3.5-3.6 (1 H, m), 3.66 (3 H, s), 3.7-3.9 (2 H, m), 4.0-4.1 (1 H, m), 5.0-5.1 (1 H, m), 6.4-6.5 (1 H, m), 6.68 (2 H, d, J = 8.9 Hz), 7.2-7.3 (2 H, m), 7.31 (2 H, d, J = 8.9 Hz), 7.4-7.5 (1 H, m), 7.62 (1 H, s), 7.7-7.8 (1 H, m); ^{13}C NMR (75.5 MHz, $CDCl_3$): δ 16.3, 18.6, 25.0, 28.1, 40.2, 55.1, 62.5, 102.5, 113.6, 126.6, 126.8, 128.0, 131.0, 132.1, 134.9, 136.2, 138.3, 158.3.

1-Ethyl-4-(4-methoxyphenyl)-5-(4'-hydroxyaminocarbonylethenyl-phenyl)-imidazole

Ethyl-Animacroxam x HCl (3)

The THP-protected hydroxamate (**intermediate 1**, 52 mg, 0.12 mmol) was dissolved in CH_2Cl_2/MeOH (5 mL, 4:1) and 4M HCl/dioxane (3 mL) was added. The reaction mixture was stirred at room temperature for 1 h. The solvent was evaporated and the

residue was crystallized from ethanol / *n*-hexane. Yield: 48 mg (0.12 mmol, 100%); off-white solid of mp 194-196°C; v_{max} (ATR)/cm^{-1}: 3126, 3000, 2970, 2833, 2765, 2626, 1653, 1603, 1571, 1540, 1510, 1462, 1427, 1412, 1349, 1299, 1258, 1181, 1113, 1085, 1053, 1027, 987, 828, 798, 766, 735, 692; ^{1}H NMR (300 MHz, DMSO-d_6): δ 1.27 (3 H, t, J = 7.3 Hz), 3.74 (3 H, s), 4.02 (2 H, q, J = 7.3 Hz), 6.65 (1 H, d, J = 15.9 Hz), 6.95 (2 H, d, J = 9.0 Hz), 7.33 (2 H, d, J = 9.0 Hz), 7.5-7.6 (3 H, m), 7.73 (2 H, d, J = 8.2 Hz), 9.41 (1 H, s), 11.0-11.1 (1 H, br s); ^{13}C NMR (75.5 MHz, DMSO-d_6): δ 14.8, 42.3, 55.3, 114.4, 119.1, 121.2, 126.9, 127.8, 128.4, 128.8, 129.7, 131.5, 134.7, 136.6, 137.0, 159.8, 162.3; *m/z* (%) 363 (7) [M^+], 347 (100), 317 (41), 280 (18), 45 (21).

Determination of apoptosis by flow cytometric TUNEL assays

Table S1 – Flow cytometric analyses of apoptosis (%) in 518A2 melanoma cells visualised by the TUNEL technique. Cells were treated with various concentrations of Vorinostat and the imidazoles **1**-**3** for 24 h and stained by using transferase-mediated fluorescein-dUTP nick end labeling of 3'-OH ends of fragmented DNA.

analysed cells (%)	control	5 µM Bimacroxam 1	5 µM Animacroxam 2	2.5 µM Etacrox 3	5 µM Vorinostat
vital	**91,5**	**48,6**	**51,0**	**65,1**	**61,6**
apoptotic	**8,5**	**51,4**	**49,0**	**34,9**	**38,4**
S.D.	1,2	1,7	1,8	2,8	1,3

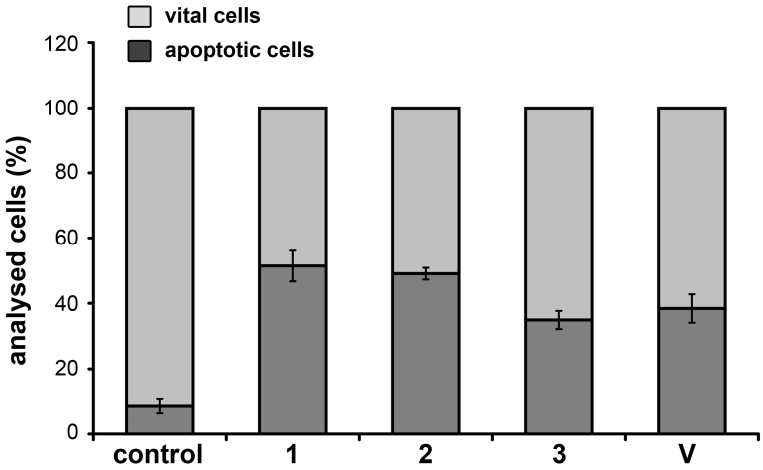

Fig. S1 – Flow cytometric analyses of apoptosis (%) in HT-29 colon carcinoma cells visualised by the TUNEL technique. Graphical representation of values represented in Table S1.

Cell cycle analyses and Western blot analyses of p27/Kip1

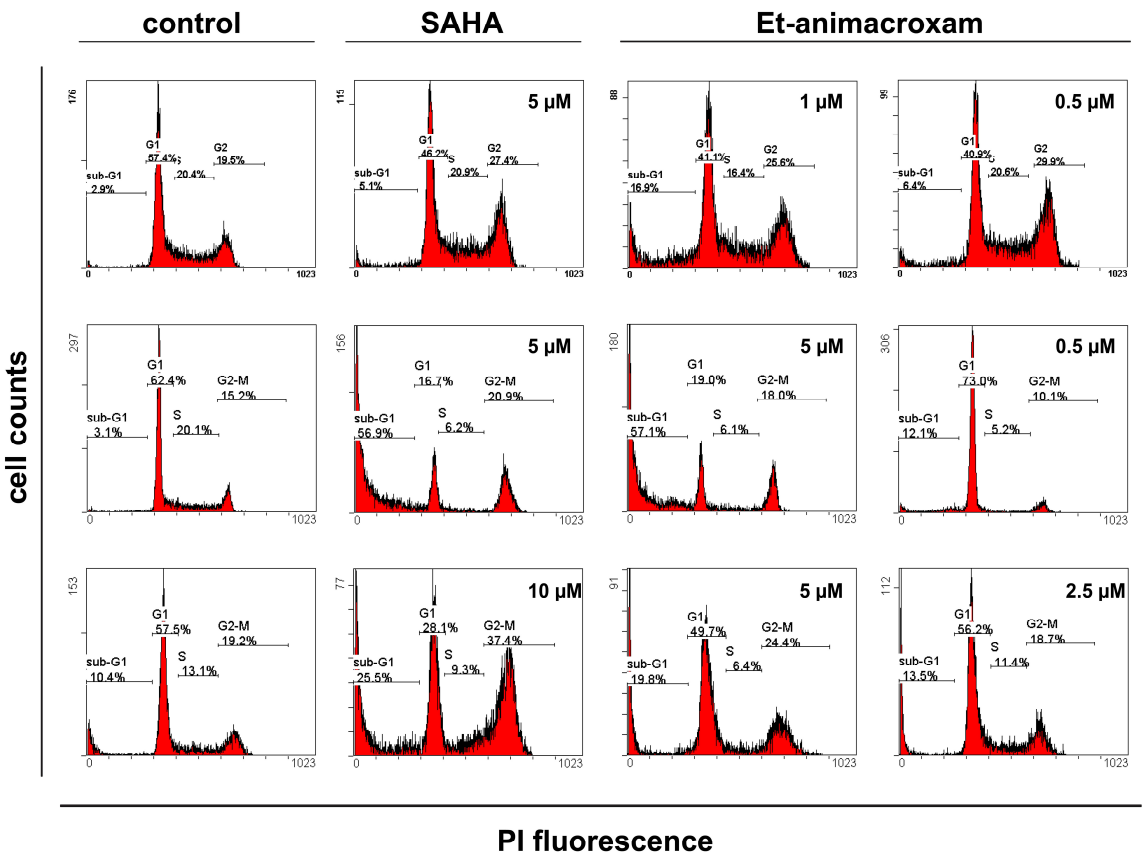

Fig. S2 – Cell line-specific effects on the cell cycle progression in cancer cell lines treated with SAHA or imidazole derivative 3 (Et-animacroxam). Flow cytometric analysis of the propidium iodide (PI)-stained DNA content in 518A2 melanoma (upper row), HT-29 colon carcinoma (middle row) or MCF-7/Topo (lower row) breast cancer cells after treatment with DMSO (control) or the indicated concentrations of Vorinostat (SAHA) or Etacrox **3** for 24 h and distribution (%) into G1, S and G2-M phase of the cell cycle as well as the content of sub-diploid (sub-G1, apoptotic) events. Values shown in the histograms are representative for at least two independent experiments.

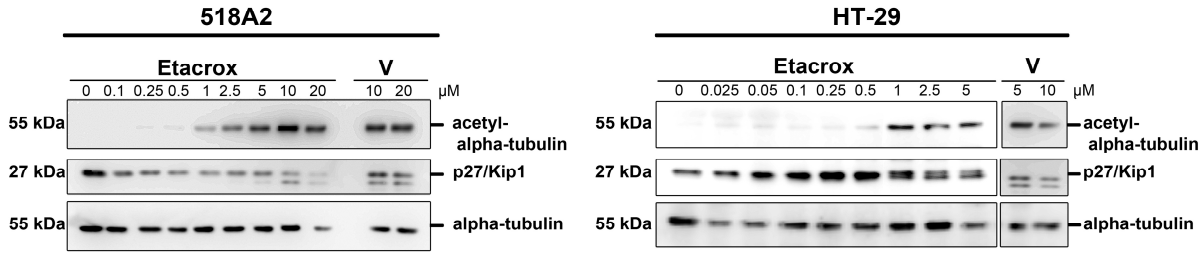

Fig. S3 – Immunoblot analyses of the effects of Etacrox 3 and Vorinostat on acetylated tubulin and p27/Kip1 level in cancer cells. Concentration-dependent (µM) increase in microtubule acetylation (acetyl-alpha-tubulin) with concomitant alterations in levels of cycle regulator p27/Kip1 (G1 marker, [9]) after treatment of cells with Etacrox **3** or Vorinostat (V) for 24h, alpha-tubulin was used as a loading control.

Western blot analyses of cell lysate fractions (cytosolic fraction)

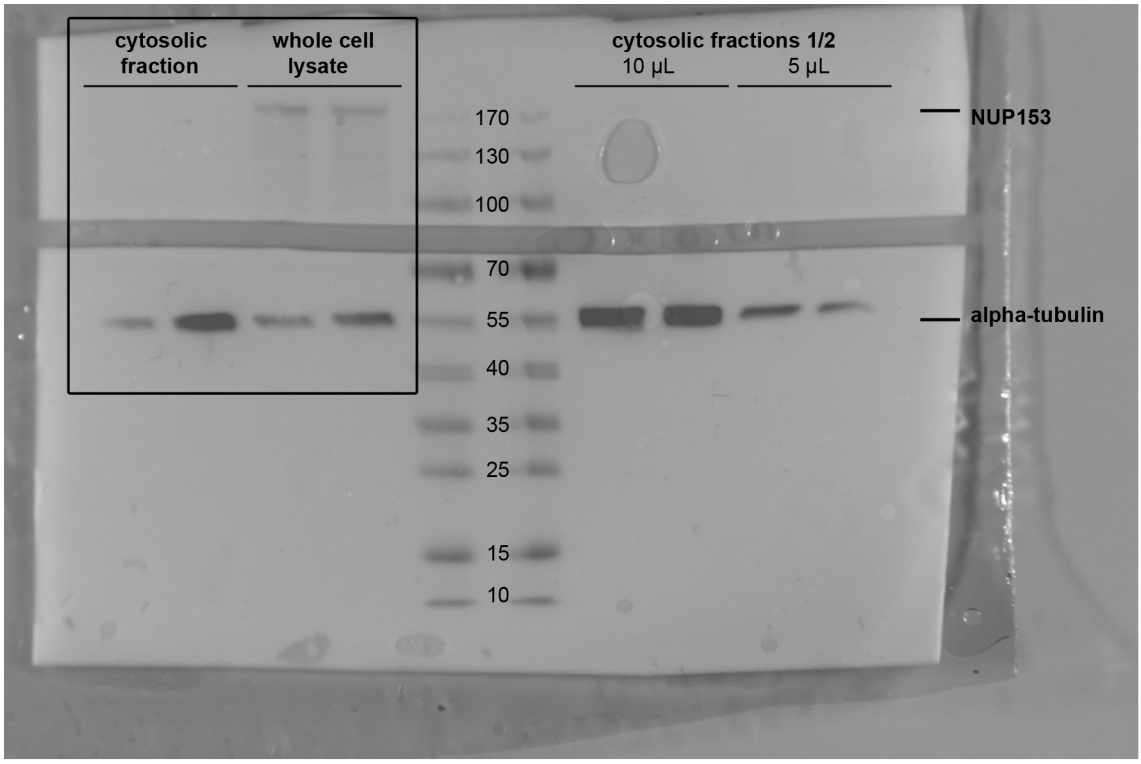

Fig. S4 – Original Western blot images of cell lysate fraction analyses. Determination of purity of cytosolic extracts from HeLa cells compared to total cell lysates. Overlay of brightfield and chemiluminescence images of PVDF membranes after incubation with alpha-tubulin (ca. 55 kDa, cytosolic marker) and nucleoporin-153 (NUP153, ca. 153 kDa, nuclear marker) primary antibodies. Images recorded with a LAS-3000 image reader (Fujifilm), molecular weight marker: PageRuler Prestained Protein Ladder (Fermentas/Thermo Scientific).

Western blot analyses of recombinant HDAC1 from transfected Hek-293 cultures

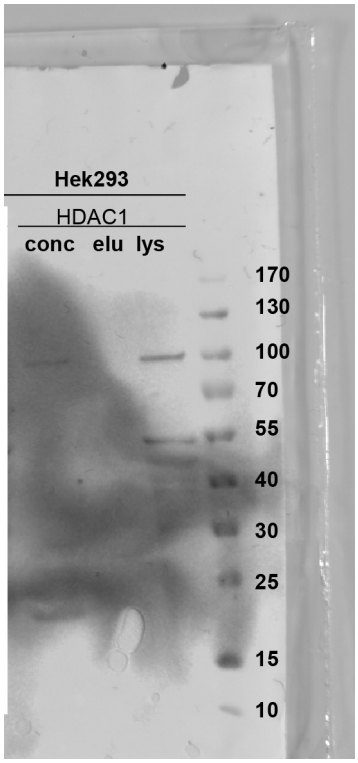

Fig. S5 – Original Western blot images of recombinant HDAC1 analyses. Overlay of brightfield and chemiluminescence images of the PVDF membrane after incubation with an anti-GST (glutathione S-transferase) tag primary antibody. Determination of the concentration of the recombinant human GST-TEV$_3$-HDAC1 fusion protein (85.7 kDa, iso-electric point 5.3) in cell lysates (lys) of transfected Hek-293 cells, in GSH (glutathione) elution buffer after GST-bead pulldown (elu) and in elution buffer concentrates (conc), 10 µL of each protein solution were loaded for SDS-PAGE. Images recorded with a LAS-3000 image reader (Fujifilm), molecular weight marker: PageRuler Prestained Protein Ladder (Fermentas/Thermo Scientific).

Original Western blot images pertinent to Figure 2A

A)

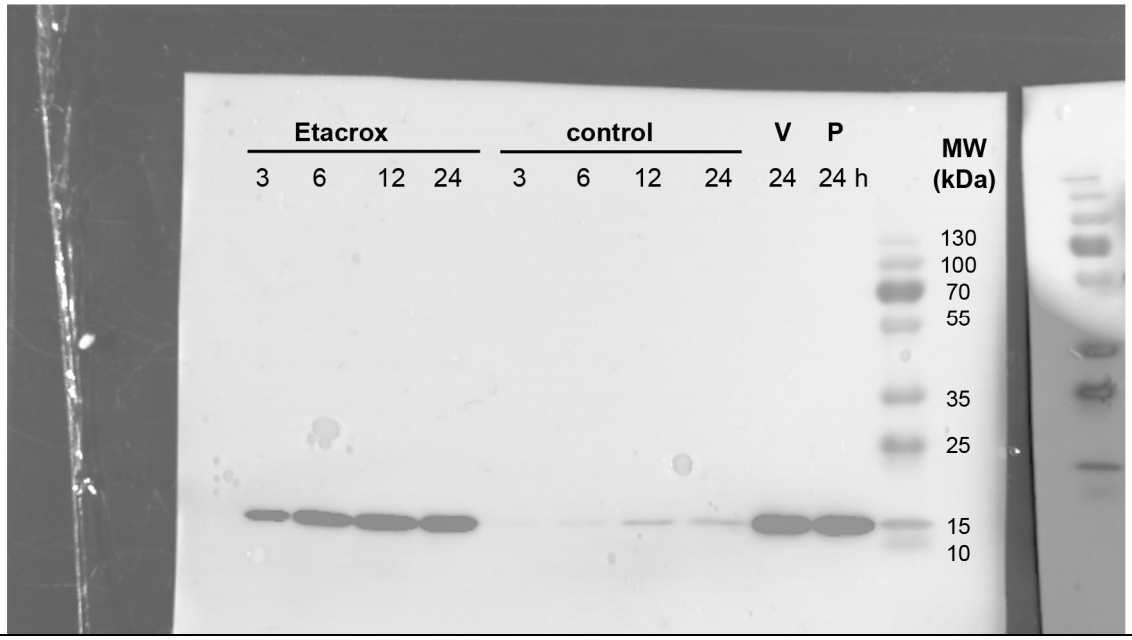

B)

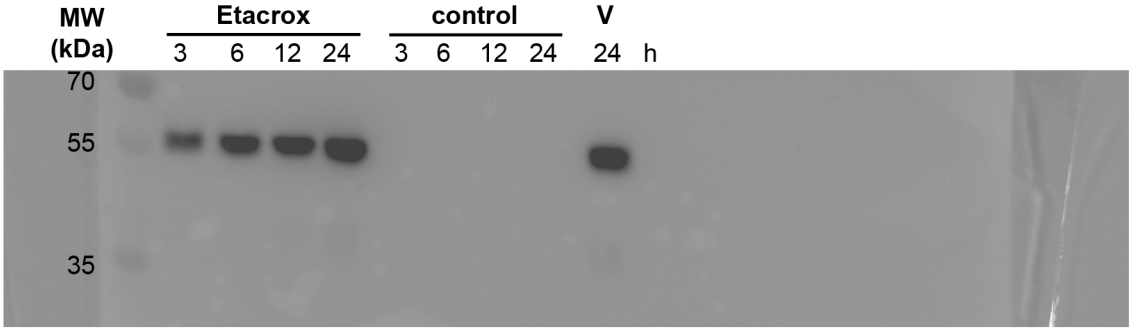

Fig. S6 – Original Western blot images of bands presented in Fig. 2A. Overlay of brightfield and chemiluminescence images of Western blot membranes after incubation with an (A) acetyl-histone H2B (ca. 17 kDa) primary antibody or (B) an acetyl-alpha-tubulin (ca. 55 kDa) primary antibody. 518A2 cells were treated with DMSO (control), Etacrox or Vorinostat (V) or Panobinostat (P) for the indicated time points (3-24 h). Equal volumes of cell lysates were subjected to SDS-PAGE with subsequent transfer to PVDF membranes and a standard procedure antibody staining. Images recorded with a LAS-3000 image reader (Fujifilm), molecular weight (MW) marker: PageRuler Prestained Protein Ladder Plus (Fermentas/Thermo Scientific).

A)

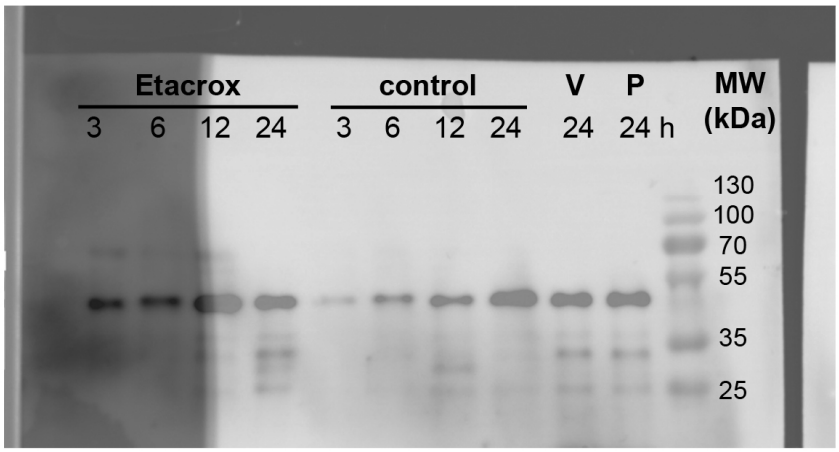

B)

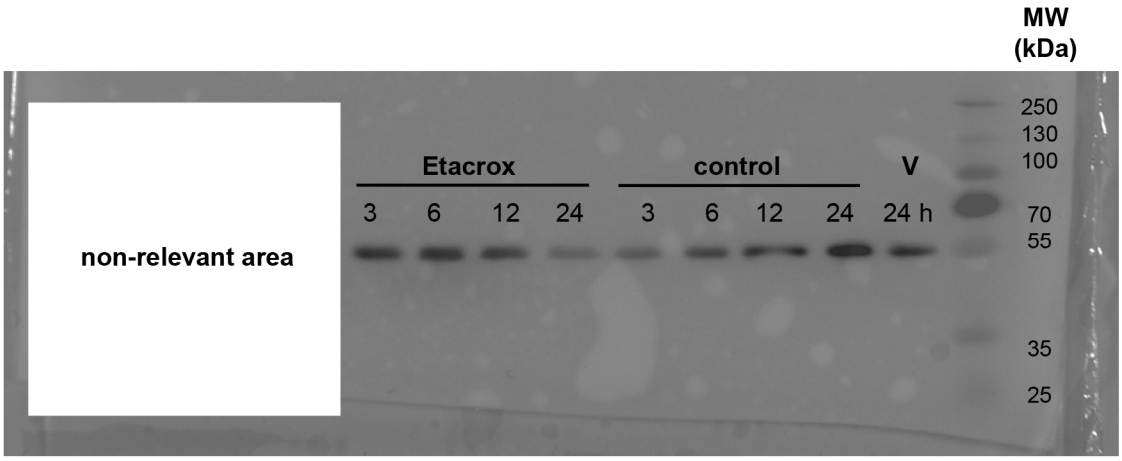

Fig. S7 – Original Western blot images of bands presented in Fig. 2A. Overlay of brightfield and chemiluminescence images of Western blot membranes after incubation with an (A) caspase-9 primary antibody [detection of full-length caspase-9 (ca. 45 kDa) and cleaved caspase fragments (> 35 kDa)] or (B) an alpha-tubulin (ca. 55 kDa) primary antibody (loading control). 518A2 cells were treated with DMSO (control), Etacrox or Vorinostat (V) or Panobinostat (P) for the indicated time points (3-24 h). Equal volumes of cell lysates were subjected to SDS-PAGE with subsequent transfer to PVDF membranes and a standard procedure antibody staining. Images recorded with a LAS-3000 image reader (Fujifilm), molecular weight (MW) marker: PageRuler Prestained Protein Ladder Plus (Fermentas/Thermo Scientific).

Original Western blot images pertinent to Figure 2B

A)

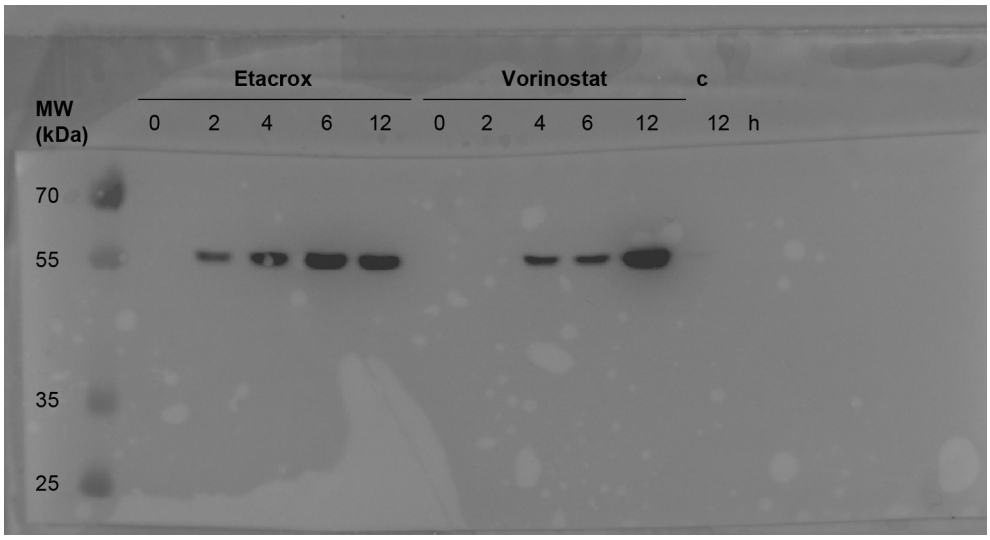

B)

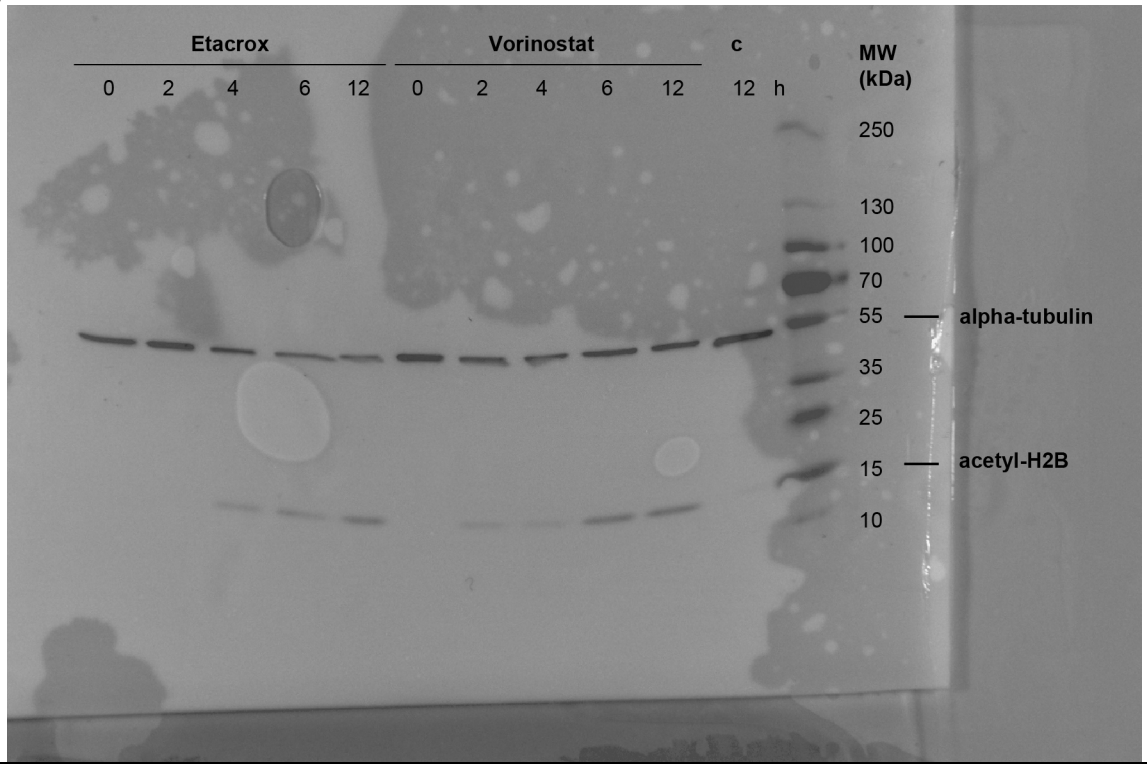

Fig. S8 – Original Western blot images of bands presented in Fig. 2B. Overlay of brightfield and chemiluminescence images of Western blot membranes after incubation with an (A) acetyl-alpha-tubulin (ca. 55 kDa) primary antibody or (B) an alpha-tubulin (loading control) and acetyl-histone H2B (ca. 14 kDa) primary antibody. HT-29 cells were treated with DMSO (control), Etacrox or Vorinostat for the indicated time points (2-12 h). Equal volumes of cell lysates were subjected to SDS-PAGE with subsequent transfer to PVDF membranes and a standard procedure antibody staining. Images recorded with a LAS-3000 image reader (Fujifilm), molecular weight (MW) marker: PageRuler Prestained Protein Ladder Plus (Fermentas/Thermo Scientific).

Original Western blot images pertinent to Figure 3

A)

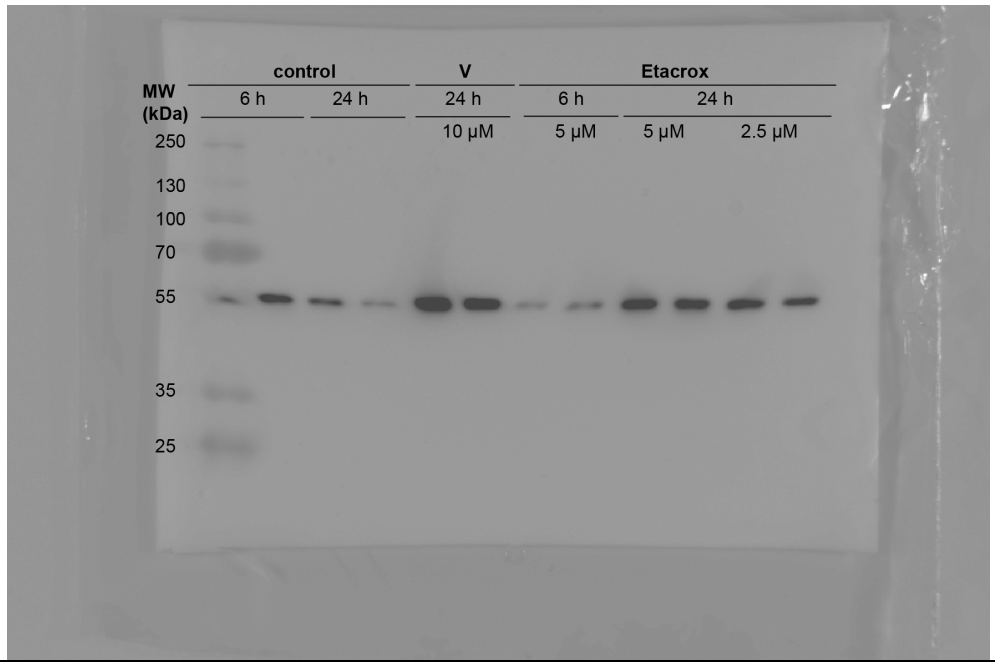

B)

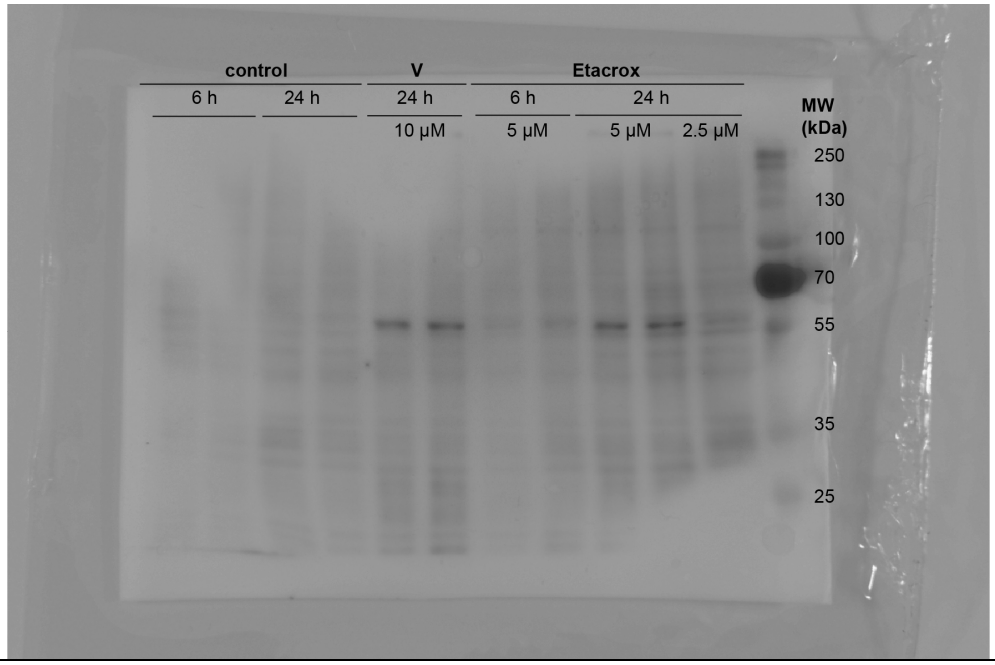

Fig. S9 – Original Western blot images of bands presented in Fig. 3. Overlay of brightfield and chemiluminescence images of Western blot membranes after incubation with an (A) alpha-tubulin (ca. 55 kDa) primary antibody or (B) an antibody for acetylated lysines (anti-acetylated lysines polyclonal antibody, broad-range lysine residue recognition). 518A2 cells were treated with DMSO (control), Etacrox or Vorinostat (V) for 6 h or 24 h. Equal volumes of fractionated cell lysates (detergent-insoluble fraction containing polymeric tubulin) were subjected to SDS-PAGE with subsequent transfer to PVDF membranes and a standard procedure antibody staining. Images recorded with a LAS-3000 image reader (Fujifilm), molecular weight (MW) marker: PageRuler Prestained Protein Ladder Plus (Fermentas/Thermo Scientific).

Original Western blot images pertinent to Figure 5

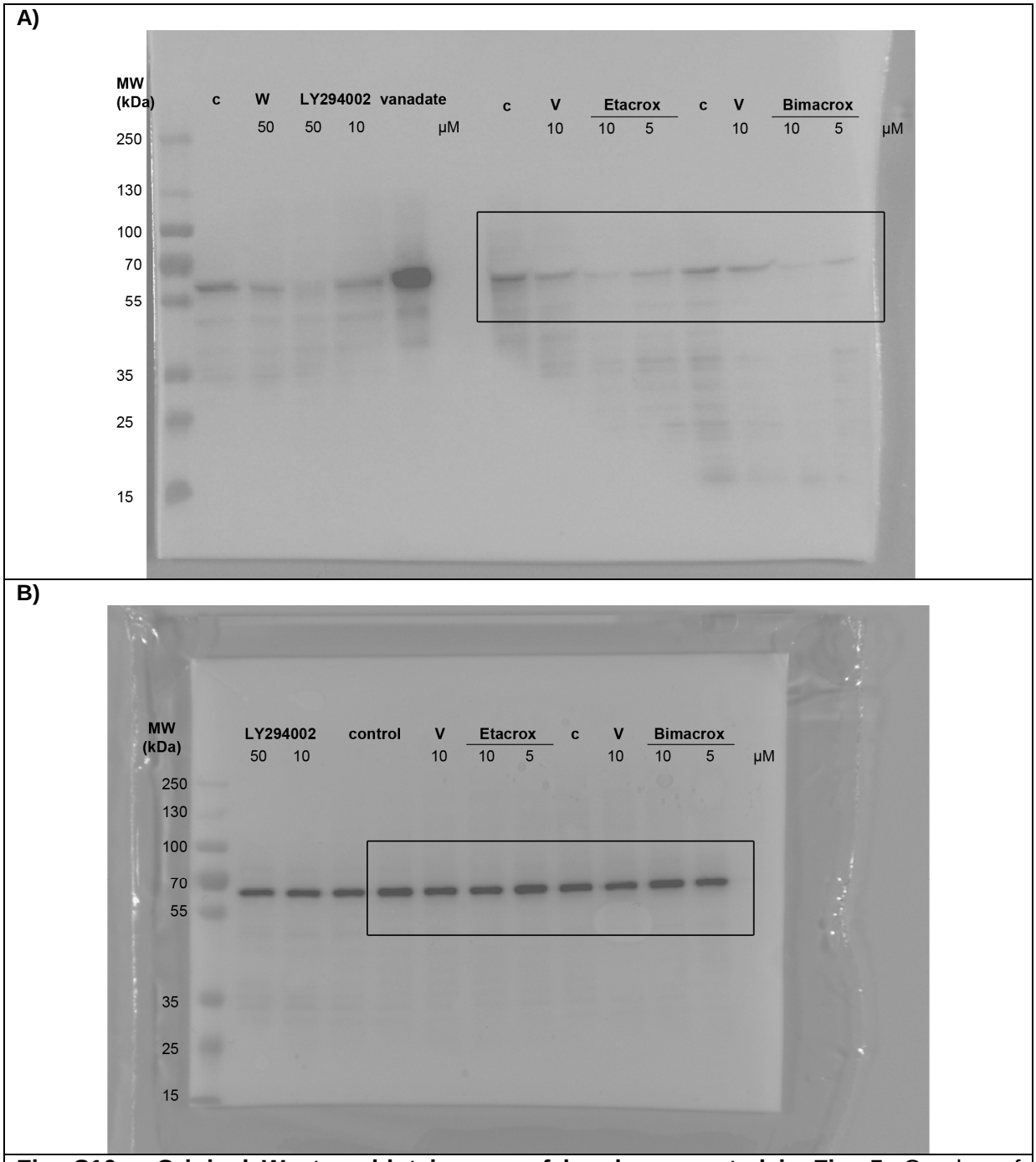

Fig. S10 – Original Western blot images of bands presented in Fig. 5. Overlay of brightfield and chemiluminescence images of Western blot membranes after incubation with an (A) phospho-Akt (ca. 60 kDa) primary antibody or (B) a pan-Akt (total Akt level, loading control) primary antibody. 518A2 cells were treated with DMSO (control), Etacrox, Bimacroxam (Bimacrox) or Vorinostat (V) or the PI3K inhibitors Wortmannin (W) or LY294002 for 6 h after EGF pre-incubation (2 h, 200 ng/mL). Equal volumes of cell lysates were subjected to SDS-PAGE with subsequent transfer to PVDF membranes and a standard procedure antibody staining. Images recorded with a LAS-3000 image reader (Fujifilm), vanadate: cells were treated with 100 µM ortho-vanadate/H_2O_2 for 10 min prior to cell lysis; molecular weight (MW) marker: PageRuler Prestained Protein Ladder Plus (Fermentas/Thermo Scientific).

Original images of gelatin zymograms

(Determination of MMP-2 and MMP-9 inhibition by gelatine zymography)

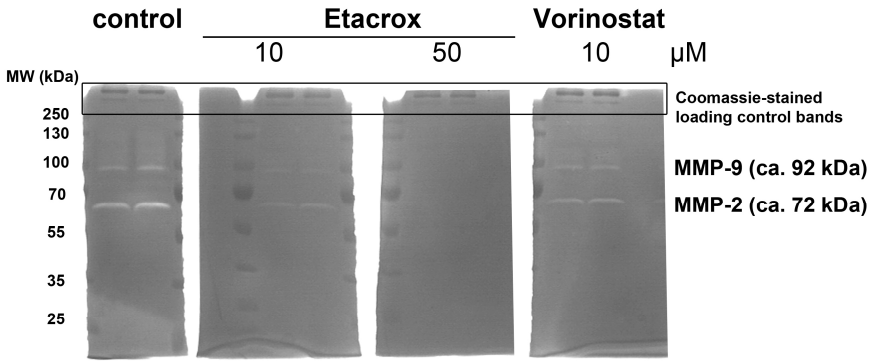

Fig. S11 – Original images of gelatin zymography-based detection of MMP inhibitors. A mixture of 2.5 µL non-reducing, denaturating 2X SDS-protein loading buffer and 2.5 µL conditioned DMEM (supernatant DMEM + 0.1% BSA + 200 KIU Aprotinin/mL from 518A2 melanoma cultures) was subjected to 10% SDS-Polyacrylamide gel electrophoresis with co-polymerised gelatin (0.1 mg/mL). Gels were cut into pieces containing to equal loaded lanes, washed (*cf.* Materials and Methods in the main manuscript for method description) and incubated with MMP activity-buffer containing Etacrox and Vorinostat at final concentrations as indicated. Gel slices were stained with coomassie brilliant blue and destained to detect concentrated MMP-9 and MMP-2 bands (white bands on dark background) and a high-molecular weight band that was used as an internal loading control (coomassie-stained protein band). Molecular weight standard: PageRuler Prestained Protein Ladder (Pierce/Thermo Scientific). Representative for three independent experiments.

Preliminary Animal Studies

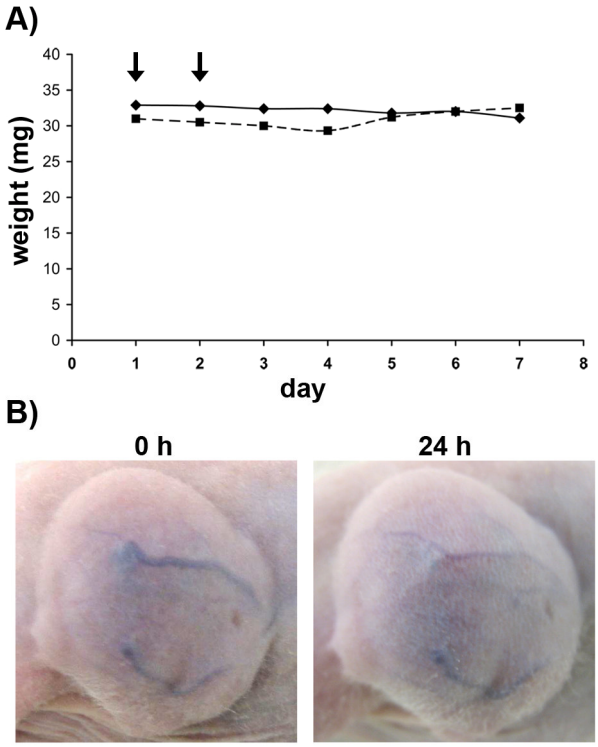

Fig. S12 – Outlook: Dose-toleration experiments with xenograft bearing mice. (A) Two doses of 150 mg/kg body weight of Etacrox **3** were given to two mice at day 1 and 2 (indicated by arrows). (B) Effects on highly-vascularised 1411HP germ cell tumours after 24 h representative for two experiments.

References

[1] M.V. Berridge, A.S. Tan, K.D. McCoy, R. Wang, The biochemical and cellular basis of cell proliferation assays that use tetrazolium salts, Biochemica. 4 (1996) 15–19.

[2] U. Michelsen, J. von Hagen, Chapter 19 Isolation of Subcellular Organelles and Structures, in: Methods Enzymol., Elsevier, 2009: pp. 305–328. http://linkinghub.elsevier.com/retrieve/pii/S0076687909630196 (accessed December 16, 2014).

[3] J.D. Dignam, R.M. Lebovitz, R.G. Roeder, Accurate transcription initiation by RNA polymerase II in a soluble extract from isolated mammalian nuclei, Nucleic Acids Res. 11 (1983) 1475–1489.

[4] K.S. Ullman, S. Shah, M.A. Powers, D.J. Forbes, The nucleoporin nup153 plays a critical role in multiple types of nuclear export, Mol. Biol. Cell. 10 (1999) 649–664.

[5] T.E. Shaiken, A.R. Opekun, Dissecting the cell to nucleus, perinucleus and cytosol, Sci. Rep. 4 (2014). doi:10.1038/srep04923.

[6] R. Schobert, B. Biersack, A. Dietrich, K. Effenberger, S. Knauer, T. Mueller, 4-(3-Halo/amino-4,5-dimethoxyphenyl)-5-aryloxazoles and - *N* -methylimidazoles That Are Cytotoxic against Combretastatin A Resistant Tumor Cells and Vascular Disrupting in a Cisplatin Resistant Germ Cell Tumor Model, J. Med. Chem. 53 (2010) 6595–6602. doi:10.1021/jm100345r.

[7] P. Di Fazio, S. Lingelbach, R. Schobert, B. Biersack, 4,5-Diaryl imidazoles with hydroxamic acid appendages as anti-hepatoma agents, Invest. New Drugs. (2014). doi:10.1007/s10637-014-0188-0.

[8] K. Mahal, S. Schruefer, F. Rausch, G. Steinemann, R. Schobert, M. Höpfner, et al., 4,5-diaryl imidazoles with hydroxamic acid appendages as new dual mode anticancer agents, Cancer Chemother. Pharmacol. (2015) *in press.*

[9] Z. Lu, T. Hunter, Ubiquitylation and proteasomal degradation of the p21 (Cip1), p27 (Kip1) and p57 (Kip2) CDK inhibitors, Cell Cycle. 9 (2010) 2342–2352.

5.2 Weitere Publikationen im Rahmen der Dissertation

2014

Activity of a Doxorubicin Menthol Conjugate Against Circulating Epithelial Tumor Cells of Cancer Patients.

Katharina Mahal, Erika Schill, Sandra Breyer, Ulrich Pachmann, Katharina Pachmann, Rainer Schobert, Bernhard Biersack.

Journal of Pharmaceutical Sciences and Pharmacology 1 (3), 233-236.

Article

Journal of Pharmaceutical Sciences and Pharmacology
Vol. 2, 1–4, 2014
www.aspbs.com/jpsp

Activity of a Doxorubicin Menthol Conjugate Against Circulating Epithelial Tumor Cells of Cancer Patients

Katharina Mahal[1], Erika Schill[2], Sandra Breyer[1], Ulrich Pachmann[2], Katharina Pachmann[2], Rainer Schobert[1], and Bernhard Biersack[1,*]

[1] *Organic Chemistry Laboratory, University of Bayreuth, Universitaetsstrasse 30, 95440 Bayreuth, Germany*
[2] *Transfusion Center Bayreuth, Kurpromenade 2, 95448 Bayreuth, Germany*

Circulating epithelial tumor cells have been established as predictive markers for the efficacy of anticancer drugs in patients while under therapy. An increase in the number of circulating epithelial tumor cells indicates the emergence of drug resistance eventually leading to an enhanced formation of metastases. We now tested two anthracycline derivatives, doxorubicin **1** and its menthol conjugate **2**, for their activity against circulating epithelial tumor cells that had been isolated from patients suffering from breast, tongue or prostate cancer. The menthol conjugate **2** led to a pronounced and rapid reduction of the circulating epithelial tumor cell numbers, exceeding the effect by the parent doxorubicin **1** even when applied at much lower concentrations. This shows that drug tests on circulating epithelial tumor cells from actual cancer patients do not only allow a real-time selection of the best possible personalized therapy but may also provide more meaningful information on the therapeutic impact of new anticancer drugs than tests on established age-old repository cell lines.

KEYWORDS: *Circulating Epithelial Tumor Cells, Doxorubicin, Menthol, Maintrac.*

2014

Ferrocene and (arene)ruthenium(II) complexes of the natural anticancer naphthoquinone plumbagin with enhanced efficacy against resistant cancer cells and a genuine mode of action.

Cornelia Spörlein-Güttler[1], Katharina Mahal[1], Rainer Schobert, Bernhard Biersack.
Journal of Inorganic Biochemistry 138, 64-72.

Journal of Inorganic Biochemistry 138 (2014) 64–72

Contents lists available at ScienceDirect

Journal of Inorganic Biochemistry

journal homepage: www.elsevier.com/locate/jinorgbio

Ferrocene and (arene)ruthenium(II) complexes of the natural anticancer naphthoquinone plumbagin with enhanced efficacy against resistant cancer cells and a genuine mode of action

Cornelia Spoerlein-Guettler [1], Katharina Mahal [1], Rainer Schobert, Bernhard Biersack *

Organic Chemistry Laboratory, University of Bayreuth, Universitätsstrasse 30, 95447, Bayreuth, Germany

Abstract

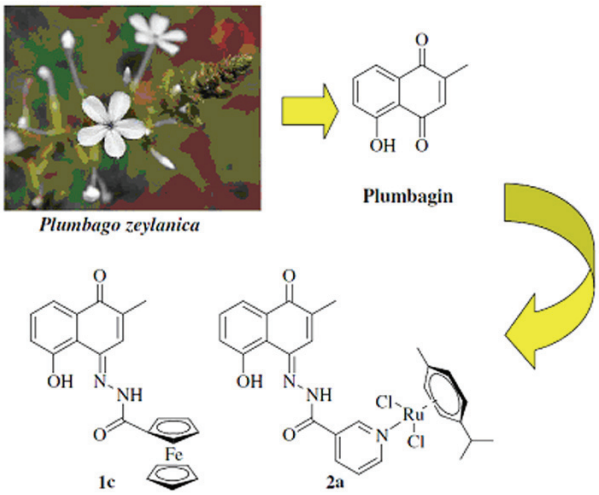

A series of ferrocene and (arene)ruthenium(II) complexes attached to the naturally occurring anticancer naphthoquinones plumbagin and juglone was tested for efficacy against various cancer cell lines and for alterations in the mode of action. The plumbagin ferrocene and (*p*-cymene)Ru(II) conjugates **1c** and **2a** overcame the multi-drug drug resistance of KB-V1/Vbl cervix carcinoma cells and showed IC_{50} (72 h) values around 1 µM in growth inhibition assays using 3-(4,5-dimethyl-2-yl)-2,5-diphenyl-tetrazolium bromide (MTT). They were further investigated for their influence on the cell cycle of KB-V1/Vbl and HCT-116 colon carcinoma cells, on the generation of reactive oxygen species (ROS) by the latter cell line, for their substrate character for the P-glycoprotein drug eflux pump via the calcein-AM efflux assays, and for DNA affinity by the electrophoretic mobility shift assay (EMSA). The derivatives **1c** and **2a** increased the number of dead cancer cells (sub-G0/G1 fraction) in a dose- and time-dependent manner. ROS levels were significantly increased upon treatment with **1c** and **2a**. These compounds also showed a greater affinity to linear DNA than plumbagin. While plumbagin did not affect calcein-AM transport by P-glycoprotein the derivatives **1c** and **2a** exhibited a 50% or 80% inhibition of the P-glycoprotein-mediated calcein-AM efflux relative to the clinically established sensitizer verapamil.
[Abstract and graphical abstract reprinted with permission from Elsevier]

2013

Effects of chrysin, apigenin, genistein and their homoleptic copper(II) complexes on the growth and metastatic potential of cancer cells.

Cornelia Spörlein, Katharina Mahal, Holger Schmidt, Rainer Schobert

Journal of Inorganic Biochemistry 127, 107-115.

Journal of Inorganic Biochemistry 127 (2013) 107–115

Contents lists available at ScienceDirect

Journal of Inorganic Biochemistry

journal homepage: www.elsevier.com/locate/jinorgbio

Effects of chrysin, apigenin, genistein and their homoleptic copper(II) complexes on the growth and metastatic potential of cancer cells

Cornelia Spoerlein [a], Katharina Mahal [a], Holger Schmidt [b], Rainer Schobert [a,*]

[a] Organic Chemistry Laboratory, University of Bayreuth, Universitätsstraße 30, 95447 Bayreuth, Germany
[b] Department of Plant Physiology, University of Bayreuth, Universitätsstraße 30, 95447 Bayreuth, Germany

Abstract

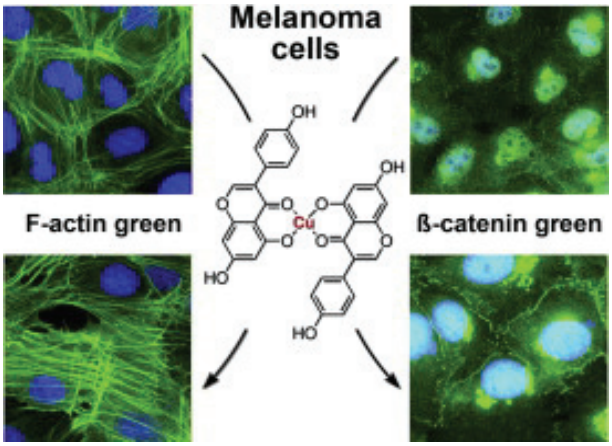

A series of ferrocene and (arene)ruthenium(II) The (iso-)flavonoids chrysin **1**, apigenin **2**, genistein **3** and their homoleptic copper(II) complexes **4**–**6** were compared for general cancer cell growth inhibition and for antimetastatic effects on rapidly proliferating and metastasizing 518A2 melanoma cells. The complexes **4**–**6** were three to five times more active than the free flavonoids in cytotoxicity assays with MTT [3-(4,5-dimethylthiazol-2-yl)-2,5-diphenyltetrazolium bromide] against 518A2melanoma, HCT-116 colon, KB-V1/Vbl cervix, andMCF-7/Topo breast carcinoma cells. This activity correlated with an arrest of the cell cycle of 518A2melanoma cells at the G2/M transition. The complexes also diminished the migration propensity of these cells in wound healing assays more distinctly than the flavonoid ligands. By fluorescent staining of F-actin and beta-catenin the antimetastatic effects of the Cu(II) genistein complex **6** were shown to originate from a remodeling of the actin cytoskeleton and an increase in cadherin–catenin complex formation, factors that favor cell-cell adhesion. Complex **6** also attenuated the expression and secretion of the metastasis relevant matrix metalloproteinases MMP-2 and MMP-9. In summary, coordination of apigenin and genistein to Cu(II) greatly enhances the antitumoral properties of these flavonoids and potentiates theirmechanistic diversity.

[Abstract and graphical abstract reprinted with permission from Elsevier]

2012

Gold(I)–NHC complexes of antitumoral diarylimidazoles: Structures, cellular uptake routes and anticancer activities.

Leonard Kaps, Bernhard Biersack, Helge Müller-Bunz, Katharina Mahal, Julienne Münzner, Matthias Tacke, Thomas Müller, Rainer Schobert.

Journal of Inorganic Biochemistry 106, 52-58.

Journal of Inorganic Biochemistry 106 (2012) 52–58

Contents lists available at SciVerse ScienceDirect

Journal of Inorganic Biochemistry

journal homepage: www.elsevier.com/locate/jinorgbio

Gold(I)–NHC complexes of antitumoral diarylimidazoles: Structures, cellular uptake routes and anticancer activities

Leonard Kaps [a], Bernhard Biersack [a], Helge Müller-Bunz [b], Katharina Mahal [a], Julienne Münzner [a], Matthias Tacke [b], Thomas Mueller [c], Rainer Schobert [a,*]

[a] Organic Chemistry Laboratory, University of Bayreuth, Universitätsstraße 30, 95440 Bayreuth, Germany
[b] School of Chemistry & Chemical Biology, UCD Science Centre, Belfield, Dublin 4, Ireland
[c] Department of Internal Medicine IV, Oncology/Hematology, Martin-Luther-University Halle-Wittenberg, 06120 Halle/Saale, Germany

Abstract

Five new heterocyclic gold carbene complexes were prepared, four chlorido-[1,3-dimethyl-4,5-diarylimidazol-2-ylidene]gold complexes **6a-d** and a chlorido-[1,3-dibenzylimidazol-2-ylidene]gold complex **11**, and three of them were characterised by X-ray single crystal analyses. They were tested for cytotoxicity against a panel of four human cancer cell lines and non-malignant fibroblasts, for tubulin interaction, and for the pathways of their uptake into 518A2 melanoma cells. All complexes showed cytotoxic activity in the micromolar IC_{50} range with distinct selectivities for certain cell lines. In stark contrast to related metal-free 1-methyl-4,5-diarylimidazoles, the complexes **6** and **11** did not noticeably inhibit the polymerisation of tubulin to give microtubules. The cellular uptake of complexes **6** occurred mainly via the copper transporter (Ctr1) and the organic cation transporters (OCT-1/2). Complex **11** was accumulated preferentially via the organic cation transporters and by Na^+/K^+-dependent endocytosis. The new gold carbene complexes seem to operate by a mechanism different from that of the parent 1-methylimidazolium ligands.

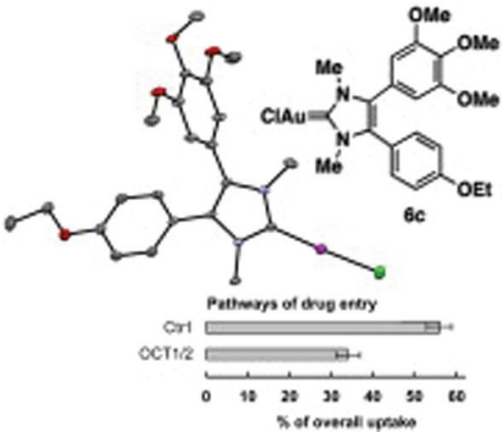

[Abstract and graphical abstract reprinted with permission from Elsevier]

2012

Modification of uptake and subcellular distribution of doxorubicin by N-acylhydrazone residues as visualised by intrinsic fluorescence.

Katharina Effenberger-Neidnicht, Sandra Breyer, Katharina Mahal, Florenz Sasse, Rainer Schobert.

Cancer Chemotherapy and Pharmacology 69, 85-90.

Cancer Chemother Pharmacol (2012) 69:85–90
DOI 10.1007/s00280-011-1675-z

ORIGINAL ARTICLE

Modification of uptake and subcellular distribution of doxorubicin by *N*-acylhydrazone residues as visualised by intrinsic fluorescence

Katharina Effenberger-Neidnicht · Sandra Breyer · Katharina Mahal · Florenz Sasse · Rainer Schobert

Received: 15 January 2011 / Accepted: 7 May 2011 / Published online: 24 May 2011

Abstract

Purpose: Doxorubicin (**1**) is commonly used in the treatment of a wide range of cancers. Some N-acylhydrazones of **1** were previously found to have an improved tumourand organ selectivity. In order to clarify the molecular basis for this effect, the cellular uptake into various cancer cells and the localisation in PtK2 potoroo kidney cells of **1** and its N-acylhydrazones derived from heptadecanoic acid (**2**) and 11-(menthoxycarbonyl)undecanoic acid (**3**) were studied drawing on their intrinsic fluorescence. Methods The uptake of compounds **1**–**3** into human cells of HL-60 leukaemia, 518A2 melanoma, HT-29 colon, and resistant KB-V1/Vbl and MCF-7/Topo breast carcinomas was determined fluorometrically from their residual amounts in the supernatant. Their time-dependent accumulation in PtK2 potoroo kidney cells was visualised by fluorescence microscopy.

Results: The uptake, though not the cytotoxicity, of **2** in multi-drug resistant MCF-7/Topo breast cancer cells was conspicuously greater than that of **1** and **3**, probably due to an attractive lipophilic interaction with the lipid-rich membranes of these cells. In non-malignant PtK2 cells, both **1** and **3** accumulated initially in the nuclei. Upon prolonged incubation, their fluorescent metabolites were visualised in lysosomes neighbouring the nuclei. In contrast, conjugate **2** was not observed in the nuclei at any time. After 2 h, it had accumulated in vesicles scattered all over the cells, and upon prolonged incubation, its fluorescent metabolites were concentrated in the cellular membrane.

Conclusions: Long unbranched fatty acyl residues when attached to doxorubicin via a hydrazone can act as lipophilic membrane anchors. This allows an increased uptake of such derivatives into lipid-rich membranes especially of multi-drug resistant cancer cells, a retarded release from there into the cytosol and the eventual storage of their metabolites again in the cell membrane rather than in lysosomes.

2011

Cancer Selective Metallocenedicarboxylates of the Fungal Cytotoxin Illudin M.

Rainer Schobert, Sebastian Seibt, Katharina Mahal, Aamir Ahmad, Bernhard Biersack, Katharina Effenberger-Neidnicht, Fazlul Sarkar, Thomas Müller.

Journal of Medicinal Chemistry 54, 6177-6182.

Journal of Medicinal Chemistry

ARTICLE

pubs.acs.org/jmc

Cancer Selective Metallocenedicarboxylates of the Fungal Cytotoxin Illudin M

Rainer Schobert,[*,†] Sebastian Seibt,[†] Katharina Mahal,[†] Aamir Ahmad,[‡] Bernhard Biersack,[†] Katharina Effenberger-Neidnicht,[†] Subhash Padhye,[‡,§] Fazlul H. Sarkar,[‡] and Thomas Mueller[*,∥]

[†]Organic Chemistry Laboratory, University Bayreuth, 95447 Bayreuth, Germany

[‡]Department for Pathology, Wayne State University School of Medicine and Barbara Ann Karmanos Cancer Institute, Detroit, Michigan 48201, United States

[§]Center for Drug Design and Molecular Medicine, Department of Environmental Sciences, University of Pune, Pune 411 007, India

[∥]Department of Internal Medicine IV, Oncology/Hematology, Martin-Luther-University Halle-Wittenberg, 06120 Halle, Germany

Abstract

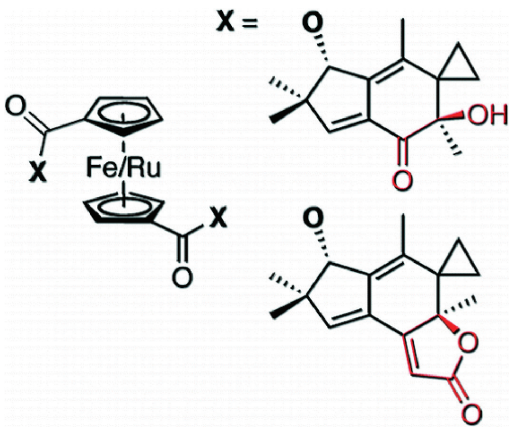

The diester **2a** obtained from 1,1′-ferrocenedicarboxylic acid and the highly and indiscriminately cytotoxic fungal metabolite illudin M (**1**) displayed antiproliferative activity at submicromolar IC_{50} (72 h) values against a panel of eight cancer cell lines. Compound **2a** was about 40 times less toxic than **1** to nonmalignant human foreskin fibroblasts (HF). The analogous bis(illudinyl M) 1,1′-ruthenocenedicarboxylate (**2b**) exhibited submicromolar IC_{50} (72 h) values only against MDA-MB-231 and MCF-7/Topo breast carcinoma and HL-60 leukemia cells. Cytotoxicity studies in the presence of inhibitors of c-Jun N-terminal kinase (JNK) or extracellular signal-regulated kinase (ERK) revealed that the high efficacy of **2a**, but not that of **2b**, against HCT-116 colon cancer cells depends on active JNK/ERK signaling. A new illudin M lactone **5** was of low anticancer activity, but its ruthenocene diester **6b** also reached single-digit micromolar IC_{50} (72 h) values in HCT-116, MCF-7, and HL-60 leukemia cells while not affecting HF. Compounds **2a** and **6b** were tolerated by mice symptom-free at single doses as high as 25 mg/kg body weight, which is evidence for them being chemically stable under physiological conditions. Compound **2a** displayed a manageable in vivo toxicity profile when given repeatedly in high doses.

[Abstract and graphical abstract reprinted with permission from 10.1021/jm200359n.]

2011

Cellular Localisation of Antitumoral 6-Alkyl Thymoquinones Revealed by an Alkyne-Azide Click Reaction and the Streptavidin-Biotin System.

Katharina Effenberger-Neidnicht, Sandra Breyer, Katharina Mahal, Randi Diestel, Florenz Sasse, Rainer Schobert.

ChemBioChem 12, 1237-1241.

FULL PAPERS

DOI: 10.1002/cbic.201000762

Cellular Localisation of Antitumoral 6-Alkyl Thymoquinones Revealed by an Alkyne–Azide Click Reaction and the Streptavidin–Biotin System

Katharina Effenberger-Neidnicht,[a] Sandra Breyer,[a] Katharina Mahal,[a] Randi Diestel,[b] Florenz Sasse,[b] and Rainer Schobert*[a]

[a] *K. Effenberger-Neidnicht, Dr. S. Breyer, K. Mahal, Prof. R. Schobert*
Organic Chemistry Laboratory, University Bayreuth
Universitaetsstrasse 30, 95440 Bayreuth (Germany)
Fax: (+49) 921-552671
E-mail: rainer.schobert@uni-bayreuth.de

[b] *Dr. R. Diestel, Dr. F. Sasse*
Helmholtz Centre for Infection Research (HZI)
Department of Chemical Biology
Inhoffenstrasse 7, 38124 Braunschweig (Germany)

Abstract

The subcellular distribution and accumulation of thymoquinone **1**, a natural anticancer agent, has hitherto been unknown. We prepared 6-(dec-9-ynyl)thymoquinone **3**, an alkyne-labelled derivative with anticancer activity similar to that of its parent compound **1**. Alkyne **3** was seen, after a Huisgen-type click reaction with 3-azido-7-hydroxycoumarin, to accumulate in distinct compartments of the nuclei of PtK_2 potoroo kidney cells, and in adjoining regions that were stained with an antibody specific for the Golgi apparatus. In contrast, a biotinlabelled thymoquinone **4** seemed to accumulate across the entire cell nucleus upon visualisation with streptavidin; but this was less easily traceable because of co-staining of other structures such as mitochondria. In conclusion, for small drug-like molecules, visualisation by alkyne–azide cycloaddition seems to be superior to conventional visualisation by the biotin–streptavidin system.

6 Liste der Publikationen und Tagungsbeiträge im Rahmen der Dissertation

Publikationen

(11) **Combretastatin A-4 derived imidazoles show cytotoxic, antivascular, and antimetastatic effects based on cytoskeletal reorganisation.**

Katharina Mahal, Bernhard Biersack, Henrike Caysa, Rainer Schobert, Thomas Mueller

Investigational New Drugs 33 (**2015**) 541-554.

(10) **Biological evaluation of 4,5-diaryl imidazoles with hydroxamic acid appendages as novel dual mode anticancer agents.**

Katharina Mahal, Sebastian Schrüfer, Gustav Steinemann, Franziska Rausch, Rainer Schobert, Bernhard Biersack, Michael Höpfner

Cancer Chemotherapy and Pharmacology 75 (**2015**) 691-700.

(9) **Activity of a Doxorubicin menthol conjugate against circulating epithelial tumor cells of cancer patients.**

Katharina Mahal, Erika Schill, Sandra Breyer, Ulrich Pachmann, Katharina Pachmann, Rainer Schobert, Bernhard Biersack

Journal of Pharmaceutical Sciences and Pharmacology 1 (**2014**) 233-236.

(8) **Ferrocene and (arene)ruthenium(II) complexes of the natural anticancer naphthoquinone plumbagin with enhanced efficacy against resistant cancer cells and a genuine mode of action.**

Cornelia Spörlein-Güttler[1], Katharina Mahal[1], Rainer Schobert, Bernhard Biersack

Journal of Inorganic Biochemistry 138 (**2014**) 64-72.

(7) **Effects of the tumor-vasculature-disrupting agent Verubulin and two heteroaryl analogues on cancer cells, endothelial cells, and blood vessels.**

Katharina Mahal, Marcus Resch, Ralf Ficner, Rainer Schobert, Bernhard Biersack, Thomas Müller

ChemMedChem 9 (**2014**) 847-854.

(6) **Effects of chrysin, apigenin, genistein and their homoleptic copper(II) complexes on the growth and metastatic potential of cancer cells.**

Cornelia Spörlein, Katharina Mahal, Holger Schmidt, Rainer Schobert

Journal of Inorganic Biochemistry 127 (**2013**) 107-115.

(5) **New oxazole-bridged combretastatin A-4 analogues as potential vascular-disrupting agents.**

Katharina Mahal, Bernhard Biersack, Rainer Schobert

International Journal of Clinical Pharmacology and Therapy 51 (**2013**) 41-43.

(4) **Gold(I)–NHC complexes of antitumoral diarylimidazoles: Structures, cellular uptake routes and anticancer activities.**

Leonard Kaps, Bernhard Biersack, Helge Müller-Bunz, Katharina Mahal, Julienne Münzner, Matthias Tacke, Thomas Müller, Rainer Schobert

Journal of Inorganic Biochemistry 106 (**2012**) 52-58.

(3) **Modification of uptake and subcellular distribution of doxorubicin by N-acylhydrazone residues as visualised by intrinsic fluorescence.**

Katharina Effenberger-Neidnicht, Sandra Breyer, Katharina Mahal, Florenz Sasse, Rainer Schobert

Cancer Chemotherapy and Pharmacology 69 (**2012**) 85-90.

(2) **Cancer selective metallocenedicarboxylates of the fungal cytotoxin illudin M.**

Rainer Schobert, Sebastian Seibt, Katharina Mahal, Aamir Ahmad, Bernhard Biersack, Katharina Effenberger-Neidnicht, Fazlul Sarkar, Thomas Müller

Journal of Medicinal Chemistry 54 (**2011**) 6177-6182.

(1) **Cellular localisation of antitumoral 6-alkyl thymoquinones revealed by an alkyne-azide click reaction and the streptavidin-biotin system.**

Katharina Effenberger-Neidnicht, Sandra Breyer, Katharina Mahal, Randi Diestel, Florenz Sasse, Rainer Schobert

ChemBioChem 12 (**2011**) 1237-1241.

Tagungsbeiträge

2014: **Jahrestagung der CESAR (Central European Society for Anticancer Drug Research), Bonn, DE**

Best Abstract Prize:

Posterbeitrag: **New antiangiogenic and antitumoral Histone Deacetylase (HDAC) inhibitors.**
K. Mahal, B. Biersack, T. Müller, R. Schobert

Vortrag: **First insights into the mode of action of new imidazole-based, antiangiogenic and antitumoral HDAC inhibitors.**

2013: **Second Whole Action Meeting of the COST (European Cooperation in Science and Technology) Action CM1105:**
Second International Symposium on Functional Metal Complexes that Bind to Biomolecules, Barcelona, ES

Posterbeitrag: **Anticancer effects of Ru(η^6-*p*-cymene)Cl_2 complexes bearing 3-halophenyl oxazole analogues of combretastatin A-4.**
K. Mahal, K. Effenberger-Neidnicht, B. Biersack, R. Schobert

GDCh-Wissenschaftsforum Chemie, Darmstadt, DE

Posterbeitrag: **Azacyclic combretastatin A-4 analogues as potential vascular-disrupting agents.**
K. Mahal, B. Biersack, R. Schobert

COST action CM1105 Working group #4 meeting, Metallodrugs II:
Design and Mechanism of Action, Olomouc, CZ

Vortrag: **Cancer selective metallocene dicarboxylates of the fungal toxin illudin M.**

2012: **Jahrestagung der CESAR, Essen, DE**

Posterbeitrag: **New oxazole-bridged combretastatin A-4 analogues as potential vascular-disrupting agents.**

K. Mahal, B. Biersack, R. Schobert

2011: **Jahrestagung der CESAR, Greifswald, DE**

Posterbeitrag: **New metallocene derivatives of the fungal cytotoxin illudin M with improved cancer selectivity and the contribution of MAPK signaling to their mode of action.**

K. Mahal, S. Seibt, K. Effenberger-Neidnicht, B. Biersack, R. Schobert

7 Danksagung

Besonderer Dank gilt Prof. Dr. Rainer Schobert für die Themenstellung und die wissenschaftlichen Freiheiten bei meiner Arbeit am Lehrstuhl Organische Chemie I. Darüber hinaus möchte ich mich bedanken für seine stete Diskussionsbereitschaft und Unterstützung, zahlreiche wissenschaftliche Anregungen sowie für die Möglichkeit, an einer Reihe interessanter wissenschaftlicher Tagungen und Konferenzen teilzunehmen.

Auch an Dr. Bernhard Biersack geht besonderer Dank für die vielen Diskussionen und Anregungen während meiner Promotion sowie die Unterstützung meiner Arbeit durch seine Ideen und die Synthese sämtlicher Verbindungen, die in der vorliegenden Arbeit dargestellt wurden.
Dr. Thomas Müller und PD Dr. Michael Höpfner sowie ihren Mitarbeitern möchte ich für die gute wissenschaftliche Zusammenarbeit und Unterstützung bei verschiedenen Projekten danken. Dies gilt auch für Dr. Marcus Resch und seine Ausarbeitung der *Docking*-Studien.
Dr. Florenz Sasse und seinem Team am HZI in Braunschweig möchte ich meinen Dank für die freundliche Aufnahme und die Unterstützung bei der Durchführung von Experimenten in ihrem Labor ausprechen.

Ein großes Dankeschön geht selbstverständlich an meine Kollegen der OCI:
Unseren „Räten“ Dr. Claus Hölzel und Dr. Thomas Schmalz sowie Frau Silvia Kastner, Frau Dr. Ulrike Lacher, Frau Kerstin Hannemann, Herrn Werner Kern und Herrn André Wetzel möchte ich für ihre Hilfsbereitschaft und Unterstützung bei den unterschiedlichsten organisatorischen, technischen, bürokratischen oder privaten Angelegenheiten danken.
Den aktuellen Doktoranden am Lehrstuhl – Matthias Göhl, Robert Haase, Marina Harras, Hussein Kalie, Karl Kempf, Anders Kroscky, David Linder, Sebastian Loscher, Julienne Münzner, Michael Ostermeier, Tobias Rehm, René Schmidt, Florian Schmitt, Mathias Schwedes, Cornelia Spörlein-Güttler, Julia Stöckl und Markus Winterer - möchte ich für die vielen wissenschaftlichen Anregungen und die freundschaftliche Atmosphäre am Lehrstuhl danken. Herzlicher Dank geht dabei besonders an meine ehemaligen und derzeitigen Biochemiker- und Biologen-Kollegen im „Bio-Labor“, Dr. Katharina Effenberger-Neidnicht, Dr. Sebastian Knauer, Julienne Münzner und Florian Schmitt für die gute Zusammenarbeit und Stimmung im Labor.

An dieser Stelle möchte ich mich auch bei allen meinen Grund-, Modul- und Forschungspraktikanten sowie meinen Bachelor- und Masterarbeitskandidaten, insbesondere bei Frau Julia Stich, Frau Carina Hagen und Herrn Sebastian Schrüfer bedanken, deren Arbeit mich unterstützt und weitergebracht hat.

Bedanken möchte ich mich auch bei Prof. Dr. Olaf Stemmann und seinen Mitarbeitern am Lehrstuhl für Genetik, insbesondere bei Herrn Markus Herrmann, für die Mitbenutzung sämtlicher Geräte, ohne die diese Arbeit nicht möglich gewesen wäre sowie für die fachliche Unterstützung und Hilfsbereitschaft.

Natürlich bedanke ich mich auch bei allen, die hier nicht namentlich erwähnt sind oder vergessen wurden, und dennoch während meiner (Labor-) Arbeit an der Universität Bayreuth eine wichtige Rolle gespielt haben.

Ein großes Dankeschön möchte ich außerdem an Frau Dr. Silke Kleinbölting, Alexander Bär, Anders Kroscky, Sebastian Loscher, Markus Petermichl und Mathias Schwedes richten, mit denen ich nicht nur anregende Diskussionen führen, sondern auch viele nette Feierabende an der Uni verbringen durfte.

Ein ganz herzliches Dankeschön möchte ich an dieser Stelle meinen Eltern aussprechen, die mich nicht nur während meines Studiums, sondern auch während meiner Promotion immer in allem unterstützt haben und für mich da waren. Herzlichen Dank möchte ich hiermit auch meinem Freund Philip sagen, der nicht nur ein guter und kritischer wissenschaftlicher Ratgeber war, sondern mich immer unterstützt und aufgebaut hat. Danke.

(§ 5 Nr. 4 PromO)

Hiermit erkläre ich, dass keine Tatsachen vorliegen, die mich nach den gesetzlichen Bestimmungen über die Führung akademischer Grade zur Führung eines Doktorgrades unwürdig erscheinen lassen.

(§ 8 S. 2 Nr. 5 PromO)

Hiermit erkläre ich mich damit einverstanden, dass die elektronische Fassung meiner Dissertation unter Wahrung meiner Urheberrechte und des Datenschutzes einer gesonderten Überprüfung hinsichtlich der eigenständigen Anfertigung der Dissertation unterzogen werden kann.

(§ 8 S. 2 Nr. 7 PromO)

Hiermit erkläre ich eidesstattlich, dass ich die Dissertation selbständig verfasst und keine anderen als die von mir angegebenen Quellen und Hilfsmittel benutzt habe.

(§ 8 S. 2 Nr. 8 PromO)

Ich habe die Dissertation nicht bereits zur Erlangung eines akademischen Grades anderweitig eingereicht und habe auch nicht bereits diese oder eine gleichartige Doktorprüfung endgültig nicht bestanden.

(§ 8 S. 2 Nr. 9 PromO)

Hiermit erkläre ich, dass ich keine Hilfe von gewerblichen Promotionsberatern bzw. -vermittlern in Anspruch genommen habe und auch künftig nicht nehmen werde.

…….

Ort, Datum, Unterschrift (Katharina Mahal)